CRISPR/Cas9-mediated genome editing of the cytochrome P450 system in the metabolically competent liver cell line HepaRG

Dissertation

der Mathematisch-Naturwissenschaftlichen Fakultät

der Eberhard Karls Universität Tübingen

zur Erlangung des Grades eines

Doktors der Naturwissenschaften

(Dr. rer. nat.)

vorgelegt von

Tamara Sonja Heintze, geb. Petrikat

aus Nagold

Tübingen

2021

Content

Abbreviations

MSMO	Methylsterolmonooxygenase
NAD(P)H	Nicotinamide adenine dinucleotide (phosphate)
NHEJ	Non-homologous end- joining
OAT	Organic anion transporter
OCT	Organic cation transporter
P/S	Penicilin/Streptomycin
PAM	Protospacer adjacent motifs
PHH	Primary human hepatocytes
POR	Cytochrom P450 Reductase
PORD	POR deficiency
PPAR	Peroxisome proliferator-activated receptor
PXR	Pregnane X receptor
qRT-PCR	Quantitative real-time PCR
RNAi	RNA interference
RNP	Ribonucleoprotein
rpm	Rounds per minute
RT	Room temperature
RXR	Retinoid X receptor
SC5DL	Sterol-C5-desaturase
SCD	Stearoyl-CoA-desaturase
SD	Standard deviation
sgRNA	Single guide RNA
shRNA	Small hairpin RNA
siRNA	Silencing RNA
SLC	Solute carrier familiy
SNP	Small nucleotide polymorphism
SpCas9	Cas9 derived from *Streptococcus pyogenes*
SQLE	Squalene monooxygenase
SREBF1	Sterol regulatory element binding transcription factor 1
STARD	Steroidogenic acute regulatory protein
SULT	Sulfotransferases
T7E1	T7 endonuclease 1
TALEN	Transcription activator-like effector nuclease
TCA	Taurocholic acid
TCDCA	Taurochenodesoxycholic acid
TM	Transmembrane domain
tracrRNA	Trans-activating CRISPR RNA
UGT	UDP-glucuronosyltransferases
WB	Western blot
ZFN	Zinc-finger nuclease

Summary

HepaRG cells are a suitable *in vitro* human liver model for absorption, distribution, metabolism, and excretion (ADME) research and toxicity studies, as they express multiple cytochrome P450 (CYP) isozymes and exhibit several regulatory pathways in a comparable level to primary human hepatocytes. CRISPR/Cas9-mediated genome editing of HepaRG cells could thus be a promising tool for new investigations regarding interindividual differences in ADME processes. However, application of CRISPR/Cas9 genome editing to HepaRG cells could be challenging because of their non-clonal origin and the required differentiation process to develop hepatic properties.

Due to their polyclonal origin, it was necessary to investigate whether differentiated clonal HepaRG cells have a hepatic phenotype comparable to the parental cell line. However, clonal selection of HepaRG cells resulted in a heterogenous mixture of individual cell clones where many of them lost their differentiation capability. Further single cell selection of clonal HepaRG cell lines resulted in a slight stabilization of phenotype but no completely homogenous phenotype was detectable which would be necessary for investigation of phenotype-genotype relations in genome-edited cell clones.

As HepaRG cells are hard to transfect several CRISPR/Cas9 delivery methods had to be tested. Two effective working protocols for CRISPR/Cas9-induced genome editing in HepaRG cells were established in this thesis. Lentiviral delivery of Cas9 and sgRNA was shown to be an effective approach for genome editing in HepaRG cells. This approach was used to create a HepaRG cell line that constitutively expresses Cas9 and that retains the ability to differentiate into hepatocyte-like cells with CYP expression and activity profiles that are highly similar to those of the parent cell line. Transfection of sgRNAs into these cells can now be used to study the influence of various genes on drug metabolism and other hepatic functions in a metabolically competent human hepatic cell line.

As a first target for CRISPR/Cas9-induced gene knockout in HepaRG cells the NADPH cytochrome P450 reductase (POR), a ubiquitous flavoprotein localized in the endoplasmatic reticulum, was chosen. POR is required for the two-electron transfer from NADPH to microsomal CYPs and is therefore essential for CYP-mediated drug metabolism as well as for other CYP dependent endogenous processes. Genetic knockout of *POR* resulted in differential, isozyme-dependent effects on CYP activities. The seemingly weak impact of POR knockdown on CYP2C8 activity led to the unveiling of a general role of CYB5 as alternative NADH-dependent electron donor in HepaRG cells, in particular for CYP2C8-dependent amodiaquine N-desethylation. This was confirmed by CRISPR/Cas9-mediated genetic *CYB5A* single and *POR/CYB5A* double-knockout using transfection of sgRNAS in Cas9 expressing HepaRG cells.

To further characterize the impact of POR knockdown on a more global level, drug metabolizing CYP protein expression, mRNA expression of a selected panel of genes and bile acid secretion were analyzed. POR knockdown influences the mRNA expression of several transcriptional regulators of hepatic CYP expression, bile acid and lipid homeostasis leading to decreased expression of various CYPs involved in drug as well as endogenous metabolism. The measured changes in bile acid homeostasis could be responsible for the observed gene expression patterns. Moreover, additional knockout experiments of CYP27A1 were performed to further analyze the involvement of POR and CYP27A1 in bile and lipid homeostasis.

Zusammenfassung

HepaRG-Zellen sind ein geeignetes humanes hepatisches *in vitro* Modell für die Erforschung von Absorptions-, Verteilungs-, Metabolismus- und Exkretions- (ADME) Prozessen sowie für Toxizitätsstudien, da sie eine Vielzahl an Cytochrom P450 (CYP) Isozymen exprimieren und mehrere Regulationssignalwege in einem vergleichbaren Ausmaß wie primäre menschliche Hepatozyten widerspiegeln. CRISPR/Cas9-vermittelte Genom Editierung von HepaRG-Zellen könnte daher eine vielversprechende Methode für neue Untersuchungen zu interindividuellen Unterschieden in ADME-Prozessen sein. Die Anwendung der CRISPR/Cas9 vermittelten Genom Editierung auf HepaRG-Zellen könnte sich jedoch aufgrund ihres nicht-klonalen Ursprungs und des erforderlichen Differenzierungsprozesses zur Entwicklung hepatischer Eigenschaften als herausfordernd darstellen.

Aufgrund ihres polyklonalen Ursprungs war es notwendig zu untersuchen, ob differenzierte klonale HepaRG-Zellen einen vergleichbaren hepatischen Phänotyp wie die elterliche Zelllinie aufweisen würden. Allerdings führte die klonale Selektion von HepaRG-Zellen jedoch zu einer heterogenen Mischung einzelner Zellklone, von denen viele ihre Differenzierungsfähigkeit verloren. Weitere Einzelzellselektion von klonalen HepaRG-Zelllinien führte zwar zu einer leichten Stabilisierung des Phänotyps, jedoch war kein vollständig homogener Phänotyp nachweisbar, der für die Untersuchung von Phänotyp-Genotyp-Beziehungen in genom-editierten Zellklonen notwendig wäre.

Da HepaRG-Zellen schwer zu transfizieren sind, mussten verschiedene CRISPR/Cas9-Transportmethoden getestet werden. Zwei effektive Arbeitsprotokolle für CRISPR/Cas9-induziertes Genome Editing in HepaRG-Zellen wurden in dieser Arbeit etabliert. Die lentivirale Applikation von Cas9 und sgRNA erwies sich als effektiver Ansatz für das Genome Editing in HepaRG-Zellen. Mit diesem Ansatz wurde eine HepaRG-Zelllinie erzeugt, die Cas9 konstitutiv exprimiert und die Fähigkeit behält, sich in hepatozytenähnliche Zellen mit CYP-Expressions- und Aktivitätsprofilen zu differenzieren, die denen der Elternzelllinie sehr ähnlich sind. Die Transfektion von sgRNAs in diese Zellen kann nun genutzt werden, um den Einfluss verschiedener Gene auf den Medikamentenstoffwechsel und andere Leberfunktionen in einer metabolisch kompetenten menschlichen Leberzelllinie zu untersuchen.

Als erstes Target für CRISPR/Cas9-induzierten Gen-Knockout in HepaRG-Zellen wurde die NADPH-Cytochrom-P450-Reduktase (POR), ein ubiquitäres Flavoprotein, das im endoplasmatischen Retikulum lokalisiert ist, ausgewählt. POR wird für den Zwei-Elektronen-Transfer von NADPH zu mikrosomalen CYPs benötigt und ist daher essentiell für den CYP-vermittelten Arzneimittelmetabolismus sowie für andere CYP-abhängige endogene Prozesse. Genetischer Knockout von *POR* führte zu differentiellen, isozyme-abhängigen Effekten auf CYP-Aktivitäten. Der scheinbar schwache Einfluss des POR-Knockdowns auf die CYP2C8-Aktivität führte zur Aufklärung einer allgemeinen Rolle von CYB5 als alternativer, NADH-abhängiger Elektronendonor in HepaRG-Zellen, insbesondere für die CYP2C8-abhängige Amodiaquin-N-Desethylierung. Dies wurde durch CRISPR/Cas9-vermittelten genetischen *CYB5A*-Einzel- und *POR/CYB5A*-Doppelknockout mittels Transfektion von sgRNAS in Cas9-exprimierenden HepaRG-Zellen bestätigt.

Um die Auswirkung des POR-Knockdowns auf einer globaleren Ebene weiter zu charakterisieren, wurden die Proteinexpression von medikamentenmetabolisierende CYPs, die mRNA-Expression einer ausgewählten Gruppe von Genen und die Gallensäuresekretion analysiert. Der POR-Knockdown beeinflusst die mRNA-Expression mehrerer transkriptioneller Regulatoren der hepatischen CYP-

Expression, der Gallensäure- und Lipid-Homöostase, was zu einer verminderten Expression verschiedener CYPs führt, die sowohl am Arzneimittel- als auch am endogenen Metabolismus beteiligt sind. Die gemessenen Veränderungen in der Gallensäure-Homöostase könnten für die beobachteten Genexpressionsmuster verantwortlich sein. Darüber hinaus wurden zusätzliche Knockout-Experimente von CYP27A1 durchgeführt, um die Beteiligung von POR und CYP27A1 an der Galle- und Lipid-Homöostase weiter zu analysieren.

1. Introduction

1.1. Drug metabolism in the liver

Many drugs and other xenobiotics have lipophilic properties which allow them to be easily absorbed into the body. However, for the subsequent elimination through the kidneys and bile metabolic modifications are needed to convert them into more hydrophilic substances (Anzenbacher and Zanger 2012). These absorption, distribution, metabolism, and excretion (ADME) processes of drugs are generally divided into three phases.

Phase I consists of several functionalization reactions, which are mostly oxidative. However, reductive and hydrolytic functionalizations are also known. Liver-expressed isozymes of the microsomal cytochrome P450 (CYP) families CYP1, CYP2 and CYP3 are responsible for the majority of phase I biotransformation processes (Aktories 2013). Other non-CYP oxidative enzymes like alcohol or aldehyde dehydrogenases, esterases and epoxide hydrolases are also involved in phase I drug metabolism.

Phase II drug metabolism includes conjugation reactions mediated by UDP-glucuronosyltransferases (UGT), glutathione S-transferases (GST), sulfotransferases (SULT) and many others. The conjugation of glucuronic acid, glutathione, sulfates, and other chemical groups results in increased hydrophilicity.

Phase III describes transport processes for renal and biliary excretion of the xenobiotic metabolites (Döring and Petzinger 2014). Transport proteins involved in these processes are the organic anion (OAT) and cation transporters (OCT) of the solute carrier (SLC) family as well as ATP-binding cassette (ABC) transporters.

The uptake of drugs and other xenobiotics by transporters is commonly termed phase 0 (Döring and Petzinger 2014).

1.1.1. Cytochrome P450 monooxygenases

CYP structure and reaction mechanism

CYP enzymes consist of a large family of membrane-bound hemoproteins of approximately 500 amino acids (45 to 55 kDa) with monooxygenase (also termed mixed-function oxidase) function. All CYPs harbor a specific signature sequence including a highly conserved cysteine residue, which serves as the axial ligand to the heme iron (Guengerich et al. 2016). This structural cysteine-thiolate feature is responsible for the unique spectral properties of CYPs, namely a characteristic absorption band at approximately 450 nm of the ferrous carbon monoxide complex (Omura and Sato 1962), hence the designation pigment (P)-450. The highly conserved cysteine is also a major structural distinctive feature of CYPs compared to hemoglobin, where the fifth heme iron ligand is a histidine.

CYPs generally catalyse the following reaction type consisting of the cleavage of molecular oxygen to incorporate one oxygen atom into a substrate molecule (R) and the other oxygen atom into water (Guengerich 2001; Guengerich et al. 2016):

$$\mathrm{NADPH} + \mathrm{H}^+ + \mathrm{O}_2 + \mathrm{R} \rightarrow \mathrm{NADP}^+ + \mathrm{H}_2\mathrm{O} + \mathrm{ROH}$$

CYPs do not only catalyse hydroxylations, but also other reactions including desaturations, C-C bond cleavages, aryl ring couplings, heteroatom dealkylations and oxygenations, ring formations, and rearrangements of oxygenated chemicals such as prostaglandins (Guengerich et al. 2016). The detailed steps of the catalytic cycle of CYP enzymes are depicted in Figure 1.
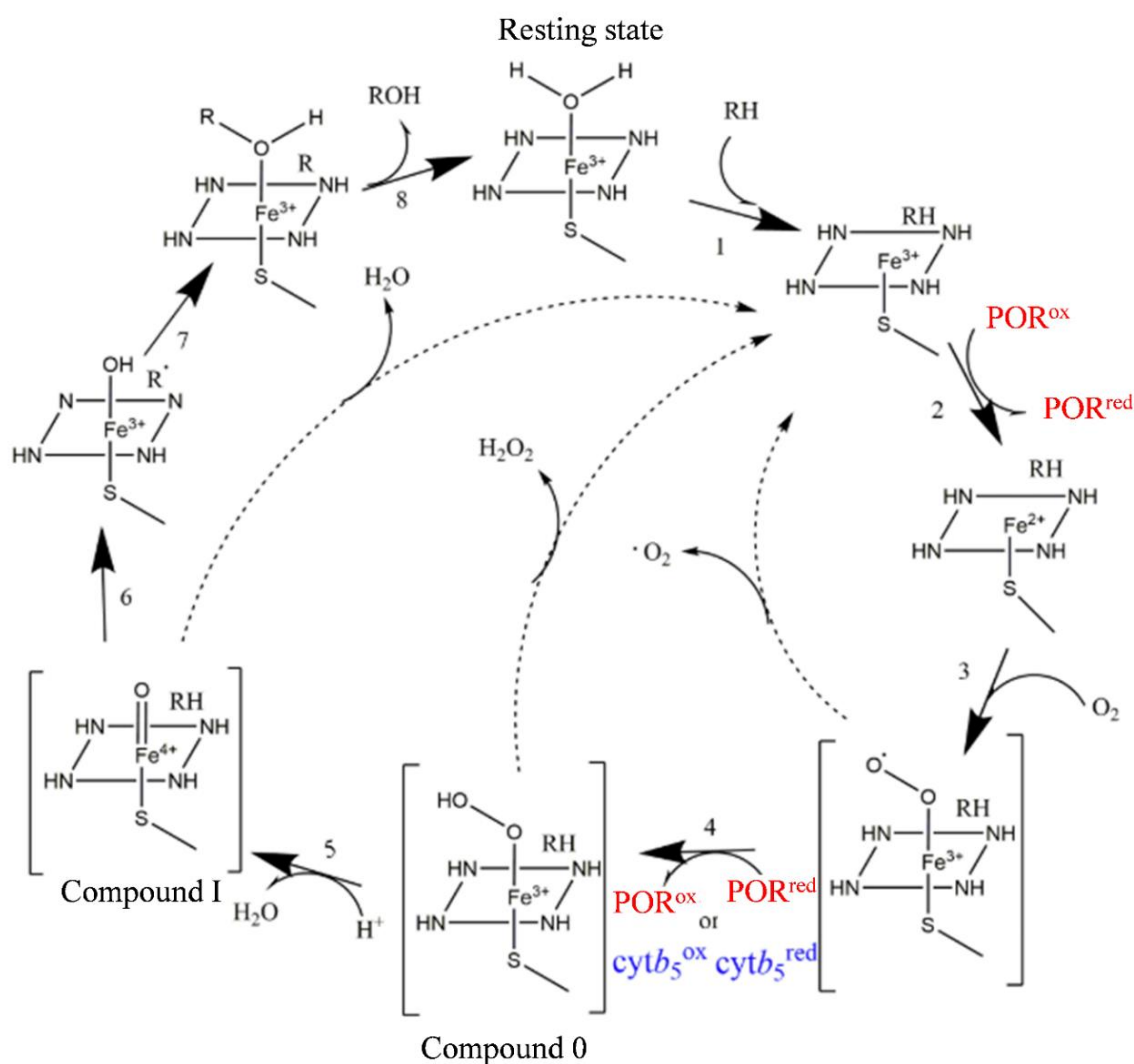
Figure 1: The catalytic cycle, structure, and redox partners of microsomal CYP enzymes. After substrate binding (R-H) (1) reduction of Fe^{3+} by one electron transfer from NADPH cytochrome P450 reductase (POR) is possible (2). Fe^{2+} binds O_2 in the next step (3) and further reduction (4) by either POR or cytochrome b5 (cytb5) leads to compound 0. Dehydroxylation of compound 0 forms the highly reactive compound I (5), which can transfer the oxygen atom to the substrate forming the hydroxyl group (ROH) (6,7). After product release (8) the resting state is achieved by binding of H_2O. Three uncoupling reactions and their products are marked with dashed lines (Nebert et al. 2013; Barnaba et al. 2017; Barnaba and Ramamoorthy 2018). Figure taken and adapted from Barnaba et al. 2017.

In the resting state the ferric heme iron (Fe^{3+}) is hexa-coordinated to heme and axially coordinated by cysteine thiolate (S) and a weakly bound water molecule. The first step of the catalytic cycle includes substrate binding in the vicinity of the distal region of the heme which displaces the water. This causes a decrease of the redox potential and allows the first reduction of Fe^{3+} by an electron delivered by POR (Barnaba et al. 2017). After binding of dioxygen to Fe^{2+}, the second reduction of the unstable ferric superoxo species by either POR or cytochrome b5 and protonation results in formation of the transient ferric hydroperoxo species (compound 0). Further protonation and dehydration leads to the highly reactive oxyferryl intermediate (compound I). Compound I abstracts a hydrogen from the substrate RH to produce a substrate radical. Rebinding of the hydroxyl-radical to the substrate to form a hydroxylated product (ROH) then restores the resting state of the CYP. The uncoupling of the CYP reaction cycle however, leads to reactive oxygen species production.

3

As CYPs are membrane-bound by a single hydrophobic N-terminal transmembrane anchor, it is also possible to classify CYP enzymes by their intracellular localization and thereby electron donor. CYP enzymes located in the mitochondria are termed "type I", whereas those found on the cytoplasmic side of the endoplasmatic reticulum (ER, microsomes) are termed "type II" (Nebert et al. 2013) (see Figure 2).
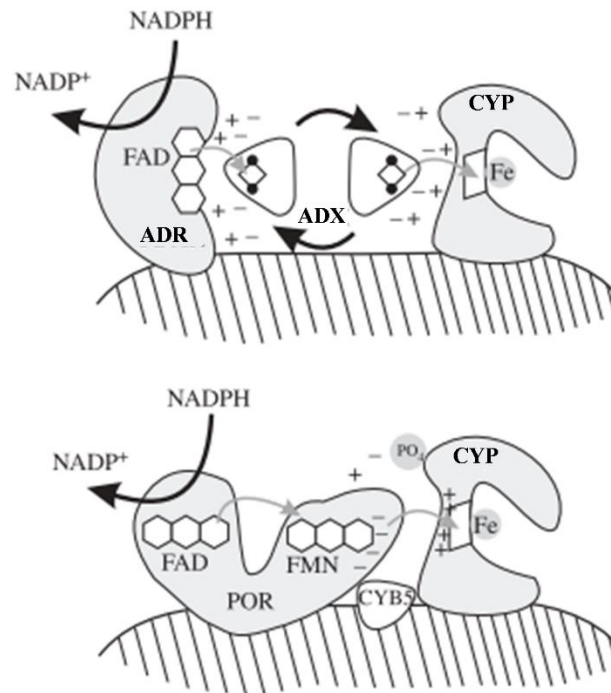
Figure 2: Two main CYP-redox partner systems. Upper panel: Type I (mitochondrial) enzymes, the two electrons from NADPH pass from the flavin (FAD) of adrenodoxin reductase (ADR) to the iron-sulfur adrenodoxin (ADX) and then to the heme of the CYP. Lower panel: Type II (microsomal) enzymes, the flavoprotein P450-oxidoreductase (POR) receives electrons from NADPH to its FAD moiety, transfers electrons to its FMN cofactor, and after a conformational rearrangement, directly transfers electrons from the FMN to the CYP. Figure taken and adapted from Nebert et al. 2013.

In the mitochrondria, electrons from NADPH are transferred by the membrane-bound flavoprotein adrenodoxin reductase to a soluble iron-sulfur protein adrenodoxin, which then transfers the electrons to type I CYPs (Nelson et al. 2008). NADPH cytochrome P450 reductase (POR), a ubiquitous flavoprotein localised in the ER, is required for the two-electron transfer from NADPH to microsomal CYPs. After NADPH binding, electrons are shuttled through the flavin adenine dinucleotide (FAD) cofactor to the flavin mononucleotide (FMN) cofactor, and subsequently to the heme group of the electron acceptor CYP (Guengerich 2001; Gentry et al. 2018).

Human CYP genes

The 57 human CYP-encoding genes are located over all autosomal chromosomes. Classification according to sequence similarity divides human CYPs into currently 18 families (indicated by an arabic numeral) and 44 subfamilies (indicated by a capital letter) (Nebert et al. 2013; Manikandan and Nagini 2018). In addition to protein-coding genes humans have more than 25 pseudogenes, which harbor mutations that prevent expression of functional proteins. All CYP proteins are considered to be intrinsically membrane-bound with the majority (50 proteins) located in the ER and the residual seven in the mitochondrial membranes (Guengerich et al. 2016). The drug-metabolizing CYP isozymes of the families CYP1 (three genes), CYP2 (19 genes), and CYP3 (four genes) are mostly expressed in the liver

4

and are characterized by a broad and overlapping substrate specificity which leads often to diverse reaction products. CYP isozymes of the families CYP4-CYP51 are responsible for the biotransformation of endogenous substances like steroid hormones, cholesterol, bile acids and many others.

CYPs in drug metabolism

Collectively, CYP isozymes of the families 1, 2 and 3 metabolize around 70-80 % of all hepatically cleared drugs, with CYP3A4 as one of the highest expressed isozymes being responsible for the metabolism of more than 30 % of all clinically prescribed drugs (Zanger et al. 2008; Zanger and Schwab 2013). The main physiological function of drug metabolizing CYPs is the detoxification of xenobiotica. However, some substances are converted to medically active drugs and others to toxic metabolites. Examples for clinically used prodrugs are the opiate codeine (CYP2D6), the anti-breastcancer drug tamoxifen (CYP2D6 and CYP3A4) or the anticancer drug cyclophosphamide (various CYPs) (Ortiz de Montellano 2013).

Toxification of xenobiotics is seen in multiple cases including aflatoxin B1 (CYP3A4) or benzo[a]pyrene (CYP1A1) (Guengerich 2008; Aktories 2013). While CYP isozymes of the families 4 to 51 play key roles in endogenous metabolism, drug-metabolizing CYP isozymes are also involved in cholesterol, steroid and bile acid biosynthesis, metabolism of polyunsaturated fatty acids such as arachidonic acid and prostaglandins, as well as activation of vitamins A and D3 to biologically active hormones (Estabrook 2003). Compared to CYP isozymes of the families 4 to 51, drug-metabolizing CYP enzymes have extremely high inter- and intraindividual variability of expression and function, which can lead to over-reactions, toxicity or lack of response to a certain drug in a considerable fraction of treated patients (Zanger et al. 2008).

Factors influencing drug metabolising CYP function

In a given population each CYP isozyme varies up to 100-fold due to a combination of (epi)genetic, non-genetic, as well as environmental mechanisms (Zanger et al. 2014). Genetic and epigenetic factors include polymorphisms (allelic frequency higher than 1 %) such as single nucleotide polymorphisms or copy number variations, rare mutations, DNA and histone modifications and non-coding RNAs (Zanger and Schwab 2013; Fisel et al. 2016). Genetic variations in CYP isozymes of the families CYP4-CYP51 are usually rare as they may cause inherited metabolic disorders. Non-genetic host factors include sex, age as well as disease state. Environmental factors, like drug-drug or drug-food interactions also play a role in influencing inter-and intraindividual variability. Consequently, individuals exhibit a constantly changing and unique CYP profile with important implications for therapeutic success. Understanding the interplay of all factors influencing drug-metabolising CYP function would enable the selection of a more personalized treatment regime.

Regulation in drug metabolism

Regulation of CYP expression in response to environmental stimuli often takes place by activation of a xeno-sensing receptor upon ligand binding. In most cases the activated receptor subsequently dimerizes with another protein to form a heterodimer, which then binds to a specific recognition sequence in the promoter region of a target CYP gene (Guengerich 2012). One example for this mechanism is the regulation of the CYP1 family by the aryl hydrocarbon receptor (AhR), which dimerizes after ligand binding (e.g., polycyclic aromates) with ARNT (AhR nuclear translocator). Other nuclear receptors are the constitutive androstane receptor (CAR, *NR1I3*) or the pregnane X receptor (PXR, *NR1I2*) which both dimerize with the retinoid X receptor (RXRα, *NR2B1*) to regulate predominantly the expression of the CYP2B, CYP2C and CYP3A subfamilies.

Ligands of CAR are chemically diverse and include steroids, certain drugs and also bilirubin. Ligands of PXR include certain endogenous or artificial steroids, certain macrolide antibiotics like rifampicin and many other drugs, noteworthy also hyperforin, an active component of St. John's wort (Offermanns and Rosenthal 2008; Guengerich 2012; Manikandan and Nagini 2018). An example of CYP regulation independent of xeno-sensing nuclear receptors is CYP2E1, which is mainly controlled by internally regulated signaling pathways, by hepatocyte nuclear factor 1α (HNF1α) and by the canonical Wnt/β-catenin pathway (Groll et al. 2016). In addition, other transcription factors including peroxisome proliferator-activated receptors (PPAR), the farnesoid X receptor (FXR), liver X receptor (LXR), HNF family members, glucocorticoid receptor (GR), and CCAAT/enhancer-binding proteins (C/EBPs) mediate CYP expression (Manikandan and Nagini 2018).

Direct inhibition of CYP enzymes

Direct CYP enzyme inhibition occurs principally via reversible or irreversible mechanisms mostly due to drug-drug or drug-food interactions and contributes to inter-and intraindividual CYP variability.

Reversible inhibition can occur by two mechanisms: the competitive inhibition of two substances for the active site or the allosteric inhibition by binding of the inhibitor to a site other than the active site (Manikandan and Nagini 2018). Irreversible mechanisms, based on suicide enzyme inhibition, happen when drugs are transformed by CYPs into reactive species that interact with moieties in the active site leading to enzyme inactivation. The inhibition of CYP3A4 by the metabolic intermediate of erythromycin is an example for mechanism-based inhibition (Manikandan and Nagini 2018). Food components are known to interfere with CYP activity, leading to drug-food interactions. Grapefruit juice, for example, contains CYP3A4 inhibitors (Offermanns and Rosenthal 2008).

1.1.2. NADPH cytochrome P450 reductase (POR)

POR is considered a further contributor to CYP variability, as it provides electrons mandatory for CYP function. It is expressed at 5-10 fold lower stoichiometric level in liver compared to total CYP content and the possibility that it may be a limiting factor for CYP activity has been discussed (Guengerich 2001; Hart et al. 2008; Gomes et al. 2009) .

POR structure

POR is a ubiquitous microsomal electron transport protein essential to cytochrome P450 (CYP)-mediated biosynthesis of endogenous substrates like sterols, bile acids and lipids as well as oxidative metabolism of xenobiotics. Moreover, POR plays a pivotal role for other important non-CYP enzymes such as heme oxygenase, squalene monooxygenase or cytochrome b5 (CYB5) (Porter 2012; Pandey and Flück 2013; Riddick et al. 2013) (see Figure 3).
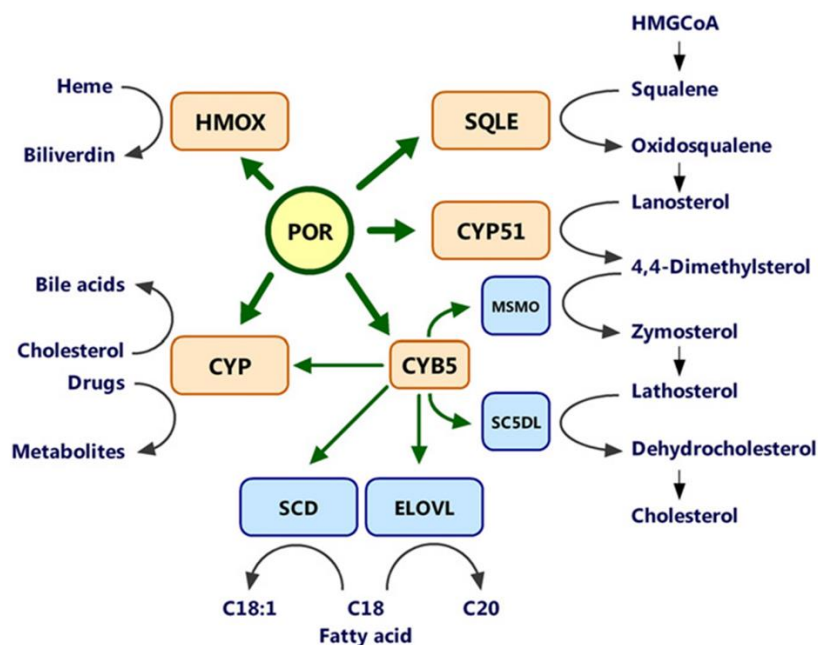
Figure 3: Redox partners of POR with corresponding metabolic pathways. HMOX: heme oxygenase (2 genes); SQLE: squalene monooxygenase; CYP: cytochrome P450 (51 microsomal forms); CYB5: cytochrome B5 (2 genes); MSMO: methylsterolmonooxygenase; SC5DL: sterol-C5-desaturase; SCD: stearoyl-CoA-desaturase (2 genes); ELOVL: fatty acid elongase (7 genes). Figure taken from Porter 2012.

In contrast to the multigenic mammalian *CYP* superfamily, *POR* is encoded by a single gene. The gene coding for human *POR* is located on chromosome 7q11.2 and consists of 15 coding and one untranslated exon (see Figure 15). It encodes a 82 kDa membrane-bound protein with 680 amino acids (Shephard et al. 1989; Yamano et al. 1989). The diflavin reductase POR consists of four major domains: the FAD binding domain, a linker domain, a FMN binding domain, and a hydrophobic N-terminal transmembrane domain (Wang et al. 1997; Gentry et al. 2018). Similar to microsomal CYP enzymes, POR is located on the cytoplasmic side of the ER using the N-terminal transmembrane domain as anchor (Pandey and Flück 2013).

As depicted in Figure 4, upon NADPH binding to POR, two electrons are transferred to FAD which triggers a conformational change in the hinge region. This causes the FAD and FMN domains to move

closer. The FMN domain interacts with CYPs and is therefore able to transfer the electrons to the CYP heme iron for the catalytic reaction.
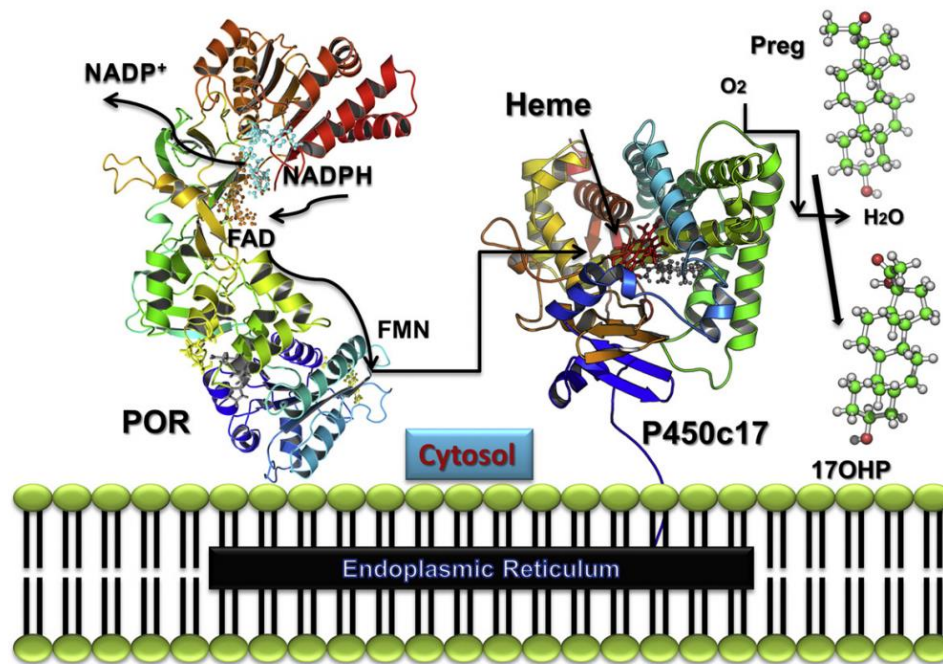
Figure 4: POR structure and electron transfer to microsomal CYPs. Two electrons from NAPDH are transferred over FAD to FMN, which can pass them over to the heme iron of microsomal CYP enzymes. The two electrons are essential for their mixed oxidase function. Figure taken from Pandey and Flück 2013.

As such, POR serves as intermediate between a dual electron donor (NADPH) and single electron acceptors (CYPs, heme oxygenase, cytochrome b5 etc.) (Pandey and Flück 2013). Thereby, the dynamic interplay between POR, CYPs and the ER membrane in protein-protein and protein-lipid complexes is important for CYP catalytic function and efficiency (Huang et al. 2015; Barnaba and Ramamoorthy 2018; Gentry et al. 2019). Limiting levels of redox partners like POR have been reported to influence CYP function by supporting the formation and stabilization of CYP-CYP multimers, which have been shown to exhibit differential substrate binding or kinetic properties compared to CYP monomers (Gut et al. 1982; Reed and Backes 2012, 2016).

POR knockout studies

Systemic deletion of *Por* in mice leads to embryonal death around day 13 due to severe disturbances in retinoid and cholesterol homeostasis, which is comparable to the phenotype in *Cyp26* (catabolism of all-trans-retinoic acid) knockout mice (Abu-Abed et al. 2001; Sakai et al. 2001). Thus, Por is essential for early-stage development (Shen et al. 2002; Otto et al. 2003; Schmidt et al. 2009). Conditional *Por* deletion in the mouse liver results in phenotypically normal and fertile mice with profoundly decreased hepatic microsomal Cyp function, reduced circulating cholesterol, triglyceride levels, and gallbladder bile volume, as well as hepatic lipidosis (Gu et al. 2003; Henderson et al. 2003; Wu et al. 2003; Finn et al. 2007). While mice show decreased hepatic Cyp activity, the Cyp protein amount is increased (Gu et al. 2003; Henderson et al. 2003). Effects of *Por* knockout in the liver on drug as well as endogenous metabolism were extensively studied in mouse models (Gu et al. 2003; Henderson et al. 2003; Weng et al. 2005; Wang et al. 2005; Finn et al. 2007; Cheng et al. 2014b).

There are several other studies that investigated diminished POR in cellular models. One example is the siRNA knockdown of POR in human and rat hepatocytes (Feidt et al. 2009; Porter et al. 2011). In more recent studies CRISPR/Cas9-induced genome editing was used in Hepa1c1c7 cells for *Por* knockout to investigate mechanisms of benzo[a]pyrene resistance (Sundberg and Hankinson 2019; Reed et al. 2019b). Moreover, CRISPR/Cas9 or zinc-finger induced knockout or small hairpin RNA (shRNA) knockdown of POR was used for the investigation of the role of POR as a predictive biomarker for hypoxia activated prodrug sensitivity (Su et al. 2013; Hunter et al. 2015; Rezende et al. 2017; Hunter et al. 2019).

PORD in humans

In humans certain *POR* mutations lead to deficient POR (PORD) characterized by disordered steroidogenesis. Patients with PORD patients show a broad spectrum of sympthoms including cortisol deficiency, altered sex steroid synthesis, disorders of sex development and skeletal malformations resembling the Antley-Bixler syndrome phenotype (Flück and Pandey 2011; Fukami and Ogata 2014; Miller 2018). Medical treatment of PORD patients consisting of glucocorticoid and sex steroid replacement therapy requires individually tailored dosing due to diminished CYP mediated hepatic drug-metabolism (Tomalik-Scharte et al. 2010; Miller et al. 2011). *In vitro* experiments showed variability in human drug metabolizing CYP activities caused by genetic variations in *POR* (Velazquez et al. 2019). Yet, no phenotypic changes of livers in PORD patients comparable to the lipidosis observed in mouse liver were reported up to this date (Miller 2018). However, translation of findings made in mouse models to the human system is limited, as mice show, for example, a different composition in CYP enzymes (Takahashi et al. 2016). This has effects on endogenous processes such as a changed bile acid pool (Li and Dawson 2019; Straniero et al. 2020). In order to improve the understanding of the role of POR in the human liver, studies in human cell models are needed.

Effects of POR on bile acid synthesis

Bile acid synthesis represents the dominant metabolic pathway of the catabolism of cholesterol and is a multi-step process mediated by the three POR-dependent CYP enzymes CYP7A1, 7B1, 8B1 and the mitochondrial, POR-independent CYP27A1 (Šarenac and Mikov 2018) (see Figure 5).
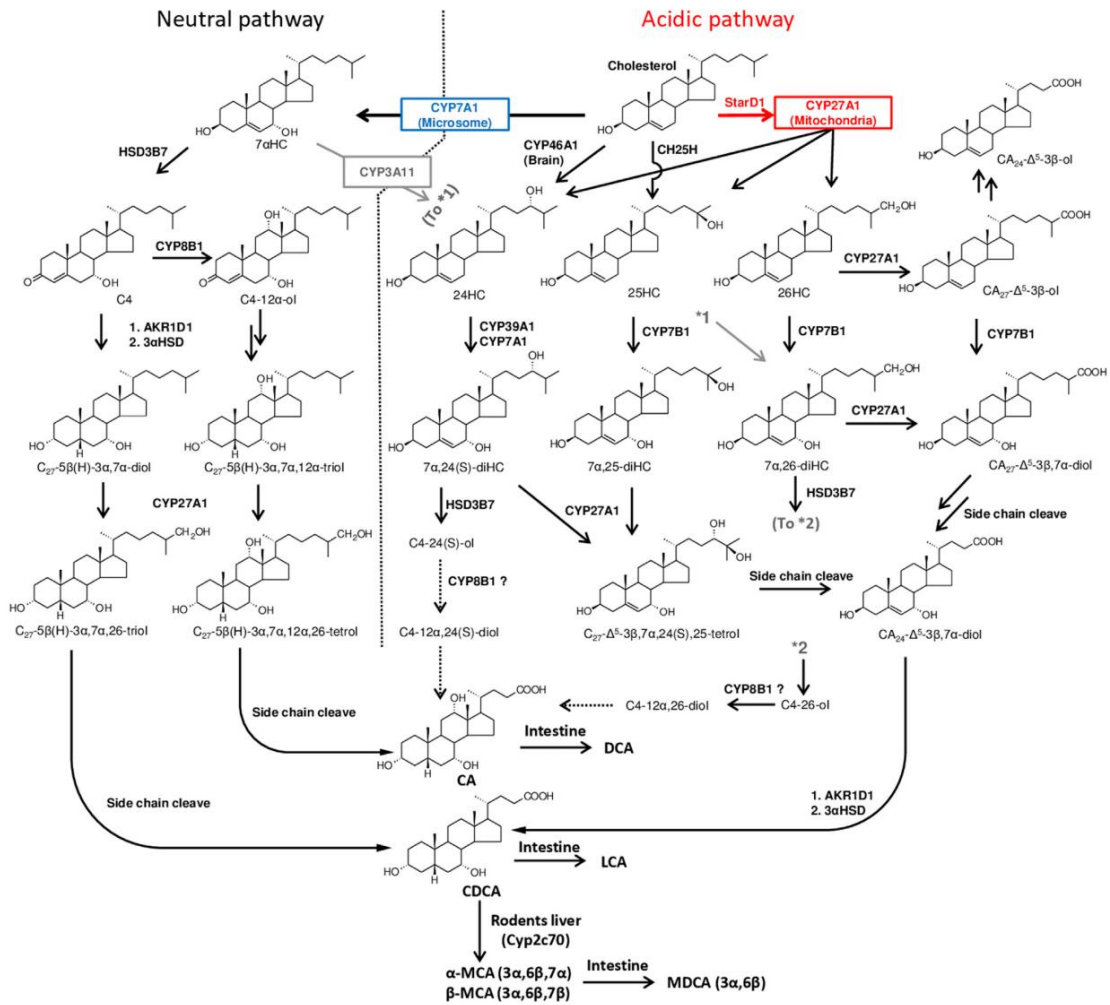
Figure 5: Overview of the mammalian neutral and acidic bile acid synthesis pathways, which is devided into the neutral and the acidic pathway. Figure taken from Pandak and Kakiyama 2019.

The classic neutral pathway is initiated by the rate-limiting step of the highly regulated microsomal CYP7A1. The alternative acidic pathway is initiated by mitochondrial CYP27A1. The rate-limiting step in this pathway is the transport of cholesterol into mitochondria and to CYP27A1 (sterol 27-hydroxylase) by steroidogenic acute regulatory protein (STARD1) (Pandak and Kakiyama 2019). The classical pathway leads to cholic acid (CA) as well as chenodesoxycholic acid (CDCA), while the alternative pathway leads predominantly to CDCA. Before secretion, primary bile acids are usually conjugated with taurine (~ 25 % in humans) or glycine (~ 75 % in humans) (Šarenac and Mikov 2018).

Effects of Por on bile acid synthesis were extensively analyzed in mouse models with liver-specific *Por* knockout. *Por* knockout revealed to have diverse effects on the composition of bile acid pools. While the total amount of bile acids in the liver was only slightly decreased, concentrations of CDCA and its gut microbial product lithocholic acid (LCA) were increased, which was hypothesized by Cheng et al. (2014b) to be due to induction of the alternative bile acid synthesis pathway.

Bile acids act as endogenous ligands for FXR, PXR and G protein-coupled bile acid receptor (TGR5 (Gpbar1)), which regulate homeostasis of xenobiotics and lipids, glucose, and energy metabolism (Pols et al. 2011; Chiang and Ferrell 2018). Differences in bile acid composition may thereby change signaling as indicated by gene expression analyzes of liver specific *Por* knockout mice (Wang et al. 2005; Weng

et al. 2005; Henderson et al. 2013; Mutch et al. 2007). One effect ascribed to changed bile acid signaling is the generally observed induction of drug metabolizing as well as bile acid synthesizing Cyp expression (Wang et al. 2005; Weng et al. 2005; Mutch et al. 2007; Henderson et al. 2013). Increased hepatic lipid accumulation as a result of impaired lipid secretion coupled with increased lipid uptake has also been attributed to changes in bile acid signaling (Weng et al. 2005; Mutch et al. 2007).

Alternative electron donors for CYPs

Cytochrome b5 (CYB5), a 17 kDa hemoprotein located on the cytoplasmic side of the ER, has been recognized early on of being capable of delivering the second electron in the catalytic cycle of CYP enzymes (Hildebrandt and Estabrook 1971; Porter 2002). In addition, CYB5 is known to stimulate CYP function by allosteric binding without electron transfer (Yamazaki et al. 1996; Porter 2002).

However, the delivery of the first electron by CYB5 is controversially discussed. Despite the fact that the redox gradient of the first reduction of CYP catalytic cycle is considered too high for CYB5 to overcome (Guengerich 2001; Barnaba et al. 2017), there is strong evidence that in some cases CYB5 can supply both electrons for CYP mediated catalysis (Pompon and Coon 1984; Porter 2002). Consequently, the CYB5/CYB5 reductase system has been studied over the years as alternative electron donor for human drug metabolism in many systems. Those included human liver microsomes (Yoo et al. 2019), reconstitution of recombinant enzymes (Yamazaki et al. 2002), structural interaction models (Zhang et al. 2007; Ahuja et al. 2013), and mouse models (Henderson et al. 2013; Henderson et al. 2014; Henderson et al. 2015). CYB5 shares partially overlapping but not identical binding sites on CYP with POR (Bridges et al. 1998; Zhang et al. 2005). As it is both substrate and enzyme specific and shows both stimulation and inhibition of CYP reactions, it has been found difficult to predict the contribution of CYB5 to xenobiotic metabolism (Gentry et al. 2018; Reed et al. 2019a).

In addition to CYB5, there are other enzymes discussed to be alternative electron donors for CYP enzymes. Several microsomal CYPs (CYP1A1, 2E1) have been found to be transported to the mitochondria where the electrons necessary for enzymatic activity are delivered by the mitochondrial electron transfer system (adrenodoxin and adrenodoxin reductase) (Addya et al. 1997; Neve and Ingelman-Sundberg 1999; Robin et al. 2001). However, studies of Knockaert et al. (2011) have indicated this to be predominantly associated with disease states like alcoholic liver disease with highly induced levels of CYP isozymes.

1.1.3. Liver models for drug metabolism

Liver, gut and kidney are the primary organs for all ADME processes (Almazroo et al. 2017). As the liver expresses a large amount of phase I- and II-related enzymes such as CYPs, GSTs, UGTs and SULTs, it plays a major role for drug metabolism. Therefore, *in vitro* hepatocyte models are essential for toxicological, pharmacological, and preclinical research. A suitable model should express a broad spectrum of genes involved in ADME processes, respond to enzyme inducers in a characteristic way and be capable of displaying a metabolic profile similar to the *in vivo* situation. Only few cell models reflect the needed liver characteristics. Among them are primary human hepatocytes (PHH), which are still regarded as "gold standard", despite their limited life span and rapidly dedifferentiation in culture. Additional disadvantages of PHH are restricted accessibility, a complex isolation protocol, difficulties in transfection and huge variability in functional activities – especially P450 levels – as well as in magnitude of P450 induction after treatment with prototypical inducers, reflecting large interindividual variability of ADME genes in the population (Madan et al. 2003; Guguen-Guillouzo and Guillouzo 2010).

Immortal cell lines isolated from human hepatoma or hepatoblastoma (eg. HepG2, Huh7) are easy to maintain, have a stable phenotype and show expression of liver specific proteins (Knowles et al. 1980; Nakabayashi et al. 1982; Castell et al. 2006; López-Terrada et al. 2009). However, as they usually only express CYP enzymes and liver specific transporters at very low levels (Castell et al. 2006; Westerink and Schoonen 2007; Guo et al. 2011; Jouan et al. 2016), immortal cell lines are suitable as hepatocyte models only to a limited degree.

The cell line HepaRG is an exception to those hepatoma cell lines. It is a bi-potent, polyclonal progenitor cell line isolated from a hepatocellular carcinoma of a female patient with the unique ability to differentiate into biliary- and hepatocyte-like cells (Gripon et al. 2002). These cells proliferate in their undifferentiated state, but demonstrate stable and functional expression of a broad range of liver-specific genes comparable to PHH (Rogue et al. 2012). This includes several CYP enzymes as well as phase II enzymes, drug transporters, and liver-specific transcription factors including ligand-activated nuclear receptors. As such, HepaRG cells are widely accepted as a highly useful model to study various aspects of drug metabolism, transport and its regulation (Kanebratt and Andersson 2008; Andersson et al. 2012; Rubin et al. 2015; Klein et al. 2015; Tolosa et al. 2016; Tanner et al. 2018; Kugler et al. 2020). Apart from *in vitro* ADME applications, HepaRG cells are used as a model for carbohydrate, bile acid and lipid metabolism (Madec et al. 2011; Samanez et al. 2012; Sharanek et al. 2014) as well as for disease states like cholestasis, steatosis and inflammation (Rogue et al. 2014; Klein et al. 2015; Tanner et al. 2018; Cuykx et al. 2019; Di Cocco et al. 2019; Lichtenstein et al. 2020).

However, transdifferentiation of HepaRG is a time-consuming process (Gripon et al. 2002; Cerec et al. 2007), which is one of the major disadvantages of HepaRG cells. Another limitation of differentiated HepaRG cells is the low efficiency of plasmid delivery using common transfection reagents or nucleofection (Laurent et al. 2010; Laurent et al. 2013; Demazeau et al. 2017).

The more recent developed "Upcyte Hepatocytes" present an additional hepatocyte model. Genetic modification of primary human hepatocytes resulted in expandable, non-cancerous human hepatocytes of various genetic backgrounds (Burkard et al. 2012; Levy et al. 2015). Comparable to HepaRG cells cultivation of "Upcyte Hepatocyte" requires a complex differentiation protocol, which is

albeit less time consuming. While HepaRG cells differentiate into a mixture of biliary- and hepatocyte-like cells (Gripon et al. 2002), differentiated "Upcyte Hepatocytes" only show hepatocyte-like phenotypes (Levy et al. 2015).

Differentiation of induced pluripotent stem cells (iPSC) is a further possibility to gain hepatocyte-like cells with many hepatocyte characteristics. They show lipid storage, albumin secretion, accumulation of glycogen, active uptake of low-density lipoproteins and synthesis of urea (Si-Tayeb et al. 2010; Corbett and Duncan 2019). CRISPR/Cas9 genome editing in patient-derived iPSC further has been reported to present a unique model system for investigation and treatment of rare liver diseases (Omer et al. 2017; Corbett and Duncan 2019). However, additional to complex differentiation procedures, most iPSC to hepatocyte protocols generate cells that are more similar to fetal or newborn hepatocytes with limited CYP expression and regulation (Baxter et al. 2015; Raju et al. 2018).

1.2.   Genome editing by CRISPR/Cas9-System

Genome editing is the targeted alteration (insertion, deletion, modification, or replacement) of the genome of a living organism. Until the first application of the clustered regularly interspaced short palindromic repeats/CRISPR associated protein 9 (CRISPR/Cas 9) system in mammalian cells in 2013 (Le Cong et al. 2013; Mali et al. 2013), transient genome editing was performed using RNA interference (RNAi) while non-transient methods consisted of engineered meganucleases, transcription activator-like effector nuclease (TALEN) or zinc-finger nuclease (ZFN) technologies.

RNAi is the RNA mediated post-transcriptional repression of protein translation. For this, single-stranded RNA molecules bind the mRNA of a certain target protein, which results either in degradation of the mRNA or in translational repression (Filipowicz et al. 2008). RNAi experiments are limited by variable knockdown efficiencies, off-target effects and the temporary limit of the knockdown to 2-7 days. However, it has still advantages in cases where permanent knockout is not feasible, for example when a permanent knockout leads to lethality or compensatory responses (Barrangou et al. 2015; Zimmer et al. 2019).

TALEN systems are fusion proteins of TALEs derived from the plant pathogen *Xanthomonas spp.* to the restriction endonuclease *Fok*I. The DNA binding domain of the TALE contains a series of 33-35 amino acid repeats, where two variant amino acids in each repeat specify the target DNA base pair. By modular assembly of these DNA binding domains, it is possible to target a certain DNA sequence. Fusion of TALE with repressors or activators enables influencing gene expression (Zhang et al. 2011; Le Cong et al. 2012). ZFN are also modular DNA recognition proteins generated by fusion of zinc finger-based DNA binding domains to an independent catalytic *Fok*I domain via a flexible linker. However, difficulties in protein design, synthesis and validation of engineered nucleases like TALEN or ZNF prevented a more widespread use. An example of interest for the use of ZNF mediated genome editing in clinical settings is the site-specific modification of CCR5, a major co-receptor for HIV in human CD4 T cell (Tebas et al. 2014).

In the field of ADME, only the ZNF technology was used for genome editing before the establishment of the CRISPR/Cas9 technology. Examples are the selective knockout of drug transporters in C2BBe1 cells (Pratt et al. 2012; Sampson et al. 2015), the knockout of endogenous canine transporters in MDCK II cells (Gartzke et al. 2015) and the knockout of PXR, BSEP and CAR in HepaRG (Li et al. 2015; Williamson et al. 2016; Qiu et al. 2016; Mackowiak et al. 2017).

CRISPR sequences were first discovered in 1987 in the genome of *E. coli* (Ishino et al. 1987) but their function as an adaptive form of immunity against hostile nucleotides originating from bacteriophages or plasmids was only elucidated in 2007 (Barrangou et al. 2007). In case of infection, the bacterium produces Cas proteins with endonucleolytic activity that can process foreign DNA, e.g., phage-derived double-stranded DNA to 20 bp long fragments. The fragments are integrated as spacers between palindromic repeats into the bacterial genome, building up the so-called CRISPR arrays. In case of reinfection, the bacterium then produces a 20 bp long RNA template complementary to the invading polynucleotides, called CRISPR RNA (crRNA), as well as the trans-activating CRISPR RNA (tracrRNA) (Deltcheva et al. 2011). These two RNA molecules are complexed with different Cas proteins and bind to the sequence homologues in the exogenous DNA, unwind it, and induce blunt end double-strand breaks (DSB) finally leading to the degradation of the hostile nucleic acids. Prerequisite for Cas binding

to the exogenous nucleic acids is a certain DNA sequence the so called protospacer adjacent motif (PAM).

CRISPR defense systems are found in 50 % of all sequenced bacterial and 95 % of all sequenced archaeal genomes, yet they show a huge variability regarding number and types of Cas proteins or PAM sequences. CRISPR systems have been classified into six distinct types (I-VI), where the Type II CRISPR system, consisting of the single Cas9 protein, was harnessed first for genome engineering. This achievement of Emmanuelle Charpentier and Jennifer A. Doudna was honored with the Nobel Prize in chemistry 2020 "for the development of a method for genome editing" – the CRISPR/Cas9 system.

For genome editing, a single guide RNA (sgRNA), the fusion of crRNA and tracrRNA, is designed homologous to a genomic region of interest. These molecules target Cas9 to the region of interest, where it introduces DSB into the DNA 3-4 bp upstream of the PAM. The only limitation in designing the sgRNA is in fact the choice of the PAM sequence (Mojica et al. 2009). In case of Cas9 derived from *Streptococcus pyogenes* (SpCas9) the sequence is 5ʹ-NGG-3ʹ. Due to the high occurrence of 5ʹ-NGG-3ʹ, e.g. in the human genome every eight bp (Le Cong et al. 2013), SpCas9 is widely used. More recent developments in engineered or alternative Cas9 enzymes made it possible to overcome the limitations of SpCas9 (Manghwar et al. 2019; Araldi et al. 2020). Additionally, alternative enzymes to SpCas9 are known, for example Cpf, which recognizes the PAM sequence 5ʹ-NTT-3ʹ(Zetsche et al. 2015).

After introduction of DSB, cellular repair mechanisms like error-prone non-homologous end-joining (NHEJ) or homology directed repair (HDR) with a DNA template lead to a diverse outcome of DNA alternations. NHEJ repair leads to insertion or deletion of bases (INDEL) that could result in gene knockout or disrupted translation due to frame shift mutations. This method is used for up to genome wide loss of function screens (Shalem et al. 2014; Liu and Li 2019). Addition of another sgRNA (multiplexing) allows deletion of a few bases (Dorr et al. 2017), genes (Simoff et al. 2016) or even chromosomes (Essletzbichler et al. 2014).

Multiplexing of sgRNAs does not only facilitate the deletion of multiple genes and increases the efficiency of editing a single locus (Campa et al. 2019), but also enables more complex applications in basic science, synthetic biology, and biotechnology (McCarty et al. 2020). An example for large-scale genome engineering in animals is the complete removal of all copies of porcine endogenous retrovirus using 62 sgRNAs in pig cells (Yang et al. 2015). Combinatorial mapping of genotype to phenotype is another application which benefits from multiplexed CRISPR technologies. By transfection of barcoded sgRNA pairs, genes involved in a certain pathway or cellular process can be identified (McCarty et al. 2020).

HDR with a DNA donor enables insertion of single nucleotides (Yin et al. 2016) as well as large pieces of DNA like genes (Yoshimi et al. 2016). Compared to NHEJ, HDR events happen less often and only in the S- and G2- phase of dividing cells (Iyama and Wilson 2013).

Despite all advantages of the CRISPR/Cas9 system, there are some drawbacks to be considered. DSB can occur at sites with as many as five mismatches and the rate of those off-target effects can be similar to those of gene editing at the target site (Fu et al. 2013; Hsu et al. 2013; Lin et al. 2014). Therefore, alterations in genes unrelated to the target gene are possible. In addition, the genome editing efficiency can vary depending on target sgRNA, cell line, delivery method and HDR/NHEJ approach (van Chu et al. 2015; Maruyama et al. 2015; Kosicki et al. 2017; Liu et al. 2019; Liu et al. 2020).

Current advances in protein engineering of Cas9 led to a large variety of CRISPR/Cas9 applications other than gene knockout or gene exchange. The basis of all those applications is a nuclease-inactivated Cas9 protein (dCas9) created by mutations in the nuclease domains RuvC and HNH (D10A and H840A) (Jinek et al. 2012). The fusion of transcriptional activators (CRISRPa) (Tanenbaum et al. 2014; Konermann et al. 2015; Chavez et al. 2015) or inactivators (CRISPRi) (Gilbert et al. 2013; Qi et al. 2013) has been shown to facilitate precise and robust gene expression modelling. For epigenome editing, dCas9 has been fused with epigenetic effector domains like DNA methylation or histone acetylation enzymes (Hilton et al. 2015; Vojta et al. 2016). Base editing, such as C>T editing, or even diverse point mutations has been performed by fusion of dCas9 or Cas9-nickases with cytidine deaminases (Komor et al. 2016; Hess et al. 2016). Following these approaches, introduction of precise substitutions or base edits was made possible without inducing double-strand breaks and thereby reducing INDELs. The labelling of dCas9 with fluorescent molecules (CRISPRainbow) was used for the dynamical tracking of DNA loci in living cells (Chen et al. 2013; Ma et al. 2016).

As shown by several authors CRISPR/Cas9 is not limited to genomic DNA, but may be applied to edit mitochondrial DNA as well as RNA (Jo et al. 2015) (Cox et al. 2017; Abudayyeh et al. 2017). Cleavage of single-stranded DNA by divergent CRISPR-Cas enzymes was also reported (Ma et al. 2015).

Both Cas9 and sgRNAs can be delivered in different ways to the target cells: Encoded on DNA expression plasmids, as RNA molecules or as ribonucleoproteins (RNP). Transfection is a mandatory procedure for each delivery form. While transfection using lipofection reagents is an uncomplicated and rapid procedure, it does not always result in high transfection efficiencies (Laurent et al. 2010). Viral transduction with either lenti- or adenoviral particles can increase transduction efficiency but introduction of additional mutations into the host DNA due to viral integration has been shown to make these methods not completely predictable (Araldi et al. 2020). The packaging capability of viral particles is an additional limitation of these delivery methods. Adenoviral particles have been found to have a packaging maximum of 4.7 kb, SpCas9 itself has 4.2 kb (Kennedy and Cullen 2015).

Transfection of expression vectors, or mRNA can result in a long expression period of Cas9, leading to off-target effects and adverse cellular responses (Kimberland et al. 2018; Araldi et al. 2020). This can be prevented using inducible expression systems (Zhang et al. 2019). Using RNPs has several advantages over plasmids or RNA. For once, it avoids possible problems regarding Cas9 protein folding. Additionally, it limits the exposition time of the cell towards Cas9 to a few hours, which reduces off-target cleaving, and integration of the transgene into to the host DNA is avoided, which could cause mutations (Araldi et al. 2020). Yet, adverse cellular reactions have been observed to not be excluded using RNPs, as their use may also trigger innate immune responses (Kimberland et al. 2018).

Application of genome editing using CRISPR/Cas9 technology to study human ADME processes has the major limitation that only few cell models reliably reflect relevant liver functions (Pankowicz et al. 2017; Karlgren et al. 2018; Chen 2020). One of the few recent examples is the modification of the *CYP3A5*3* loss-of-function allele to restore enzymatic activity in Huh7 cells (Dorr et al. 2017). Another example is the removal of endogenous P-gp background in the canine kidney cell line MDCK (Simoff et al. 2016; Karlgren et al. 2017; Chen et al. 2018).

Furthermore, genome editing approaches to study ADME related processes were performed in HepaRG cells. Currently there are 11 zinc-finger induced clonal knockout HepaRG cell lines available (Merck KGaA, Darmstadt, DE), including the transcriptional modulators AHR, CAR, PERK, and PXR, as

well as the transport proteins BCRP, BSEP, MDR1, MRD3, MRP2, MRP3, and OATP1B3. But only few research studies are published so far: Bile salt export pump (BSEP) knockout HepaRG cells were used to analyze responses on bile acid synthesis and hepatotoxicity of the antibiotic mithramycin (Qiu et al. 2016; Sissung et al. 2019). Studies of the CAR transcriptome and mechanisms of PXR activation by CITCO were performed in CAR knockout HepaRG cell lines (Li et al. 2015; Lin et al. 2020). Additionally, responses of CYP3A4 and CYP2B6 to prototypical inducers (e.g. CITCO, phenobarbital and rifampicin) were evaluated in HepaRG PXR knockout cells (Williamson et al. 2016). Furthermore, AhR, CAR and PXR knockout HepaRG cells were used to elucidate mechanisms behind triazole-mediated steatosis (Knebel et al. 2019).

The fact that CRISPR/Cas9-mediated genome editing in HepaRG was only reported in a few studies, highlights the difficulties accompanying the application of this method. One study used CRISPR/Cas9 to inhibit HBV DNA production in infected HepaRG cells (Kennedy et al. 2015). AhR-deficient HepaRG cells were used for investigation of non-alcoholic fatty liver disease progression induced by benzo[a]pyrene and ethanol co-exposure (Bucher et al. 2018). In the work of (Wei et al. 2020) CRISPR/dCas9-mediated modification of DNA methylation was used to verify a correlation between DNA methylation and drug induced liver injury. Moreover, the depletion of IKKβ in HepaRG cells was performed in a study on NF-κB signaling in virus control (Namineni et al. 2020).

2. Objectives

HepaRG cells are a widely used human hepatic cell model which expresses multiple CYP activities and reflects several regulatory pathways. Application of CRISPR/Cas9-mediated genome editing to HepaRG cells could thus be a promising way for new investigations. However, implementation of CRISPR/Cas9 genome editing to HepaRG cells is expected to be challenging because of their non-clonal origin and because differentiation is required to develop hepatic phenotype.

Therefore, the primary objective of this thesis was to establish a working protocol for CRISPR/Cas9 induced genome editing in HepaRG cells. As HepaRG cells are hard to transfect several CRISPR delivery methods had to be tested. At the same time it was necessary to investigate whether single cell selection is possible in case of HepaRG cells, as the parental cell line itself is not clonal.

As a first target for CRISPR/Cas9-induced gene knockout *POR* was chosen in order to investigate multiple POR functions in HepaRG cells. *POR* knockout is to be expected to reduce CYP activities, but it is unclear whether different CYP isozymes are equally affected. POR also exerts strong effects on several other cellular functions like bile acid and lipid homeostasis. Therefore, the effects of *POR* knockout in HepaRG cells had to be characterized thoroughly.

Furthermore, to develop a more generally applicable HepaRG-based genome editing system establishment of a stable Cas9-expressing HepaRG cell line was attempted. To elucidate the usefulness of the system other genes, especially *CYB5A* and *CYP27A1,* were targeted with CRISPR/Cas9. The resulting single- and double-knockouts were used for further investigations regarding CYB5 as an alternative electron donor to POR for CYPs and the role of POR and CYP27A1 in bile acid and lipid homeostasis.

3. Results

3.1. Generation of clonal HepaRG cell lines

HepaRG cells consist of a heterogeneous, non-clonal mixture of cells isolated from a hepatocellular carcinoma of a female patient. To study the effects of single cell selection on HepaRG cell growth rates, morphology and CYP activities were measured after clonal dilution and subsequent differentiation by dimethyl sulfoxide (DMSO). Furthermore, growth rates of the hepatoma cell lines HepG2 and the hepatocyte-like cells "Upcyte Hepatocytes" were investigated for comparison. The screening of the large amount of cell clones was performed using the CYP2C9 P450-Glo assay (Promega, Madison, USA). The CYP cocktail assay was applied for more detailed characterization of selected cell clones.

For elucidation of the phenotypic stability of clonal HepaRG cells as a prerequisite for CRISPR/Cas9 gene editing experiments, candidate F_1-clonal cell lines were diluted to single cells once more (see Figure 6 for experimental outline). The resulting F_2-clonal cell lines were characterized accordingly.

Heterogeneous parental HepaRG cell line (P)

↓

Clonal dilution (F_1 clones)

↓

Expansion and differentiation

↓

Characterisation:
- Growth rates
- Morphology
- CYP activity (2C9Glo, CYP mix)

↓

Selection of candidate clones

↓

Single cell sorting (FC) (F_2 clones)

↓

Expansion and differentiation

↓

Characterisation:
- Growth rates
- Morphology
- CYP activity (2C9Glo)
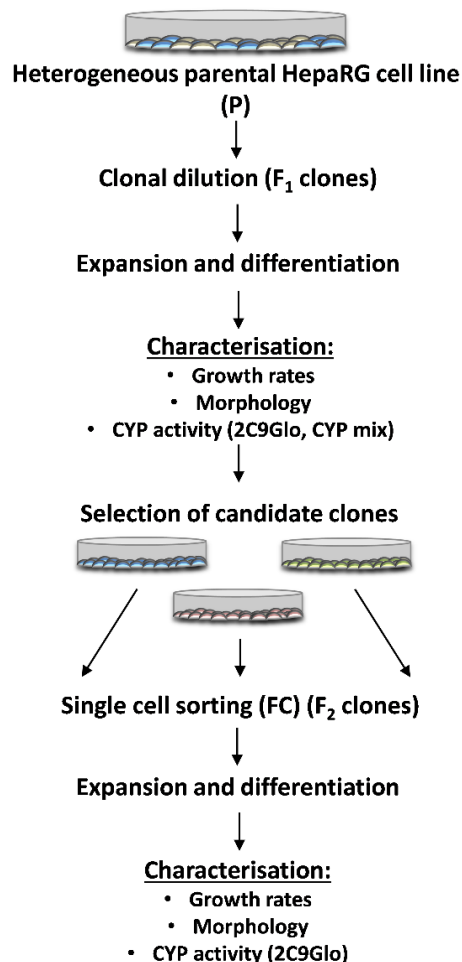
Figure 6: Experimental outline for generation and characterization of clonal HepaRG cell lines. Heterogeneous parental HepaRG cells were diluted to single cell F_1 clone populations, which were characterized after expansion and differentiation regarding growth rates, morphology and CYP activities (using the 2C9Glo- and the CYP cocktail assay). Selected candidate F_1 clones with high CYP activities were cloned to single cells once more using flow cytometry (FC). The resulting F_2 clones were characterized after expansion and differentiation regarding growth rates, morphology and CYP activities as well.

3.1.1. Growth characteristics and morphology of clonal hepatocyte cell lines

As some cell lines proliferate at low seeding density at a highly reduced rate, HepaRG, HepG2 and "Upcyte Hepatocyte" (batches 122-129-138 and 653-03) cells were seeded at decreasing starting cell densities (0.1 to 80 cells per well) in 96-well plates. Growth and numbers of cells were observed microscopically up to 25 days and counted manually (Figure 7). After curve fitting with a logistic growth model (seeding density and maximum cell count as fixed constraints), doubling times of the selected cell lines were calculated and compared with published data (see Table 2).
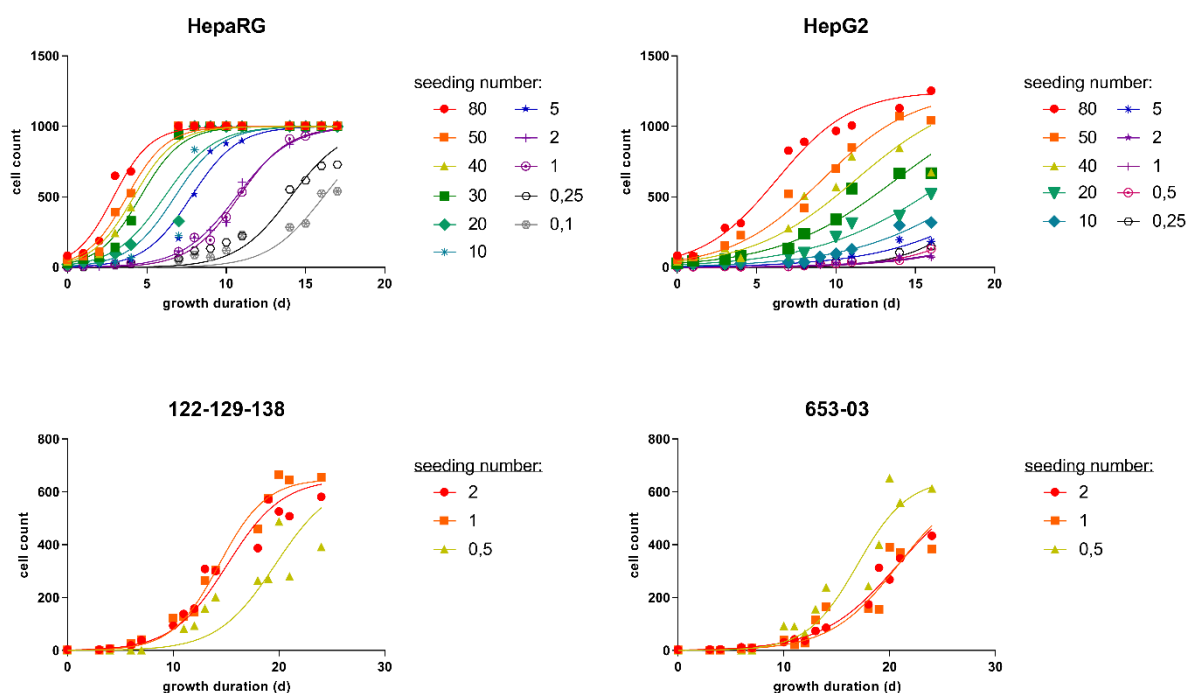
Figure 7: Growth curves of HepaRG, HepG2 and "Upcyte Hepatocytes" (batches: 122-129-138, 653-03) cells, seeded at different densities (0.1 to 80 cells per well). Cell number was counted manually in a size-defined field up to 25 days. Experiment was only performed once, curve fitting was performed with a logistic growth model (seeding density and maximum cell count as fixed constraints).

Table 2: Calculated and published doubling times of HepaRG, HepG2 and "Upcyte hepatocytes" (batches: 122-129-138 and 653-03) cell lines [95% confidence interval (CI)].

Cell line	Doubling time (calculated) [95% CI]		Doubling time (literature)
	1 cell/well	80 cells/well	
HepaRG	37 h [37 to 38]	28 h [25 to 32]	24 h[1]
HepG2	85 h [81 to 89]	46 h [52 to 62]	48 h[2]
122-129-138	61 h [51 to 71]		25 to 30 h[3]
653-03	73 h [53 to 89]		25 to 30 h[3]

[1] (Gripon et al. 2002), [2] (Wen-Sheng 2003), [3] (Schaefer et al. 2015)

HepaRG and HepG2 cell lines showed increasing lag times at lower seeding densities. Doubling times of around 28 h for 80 cells/well were calculated, which is in good agreement with published data (see Table 2). Doubling times of cells seeded at lower numbers seem to be slightly increased up to 37 h, which is marginally higher than published data.

HepG2 cells had in general lower growth rates than HepaRG cells. Doubling times of around 46 h for 80 cells/well were calculated, which is in line with published data (see Table 2). Doubling times of cells seeded at lower numbers were increased up to 85 h, which is higher than published data. For clones of both HepaRG and HepG2 cell lines no apparent morphological differences were seen in the undifferentiated state (data not shown), even though the HepaRG cell line is of polyclonal origin (Gripon et al. 2002).

Both "Upcyte Hepatocyte" batches were analyzed only at lower cell densities, showing that the doubling times for 1 cell/well was around 2 times higher than the published data. In contrast to the other cell lines striking differences in morphology between individual single-cell clone populations were observed (Figure 8).
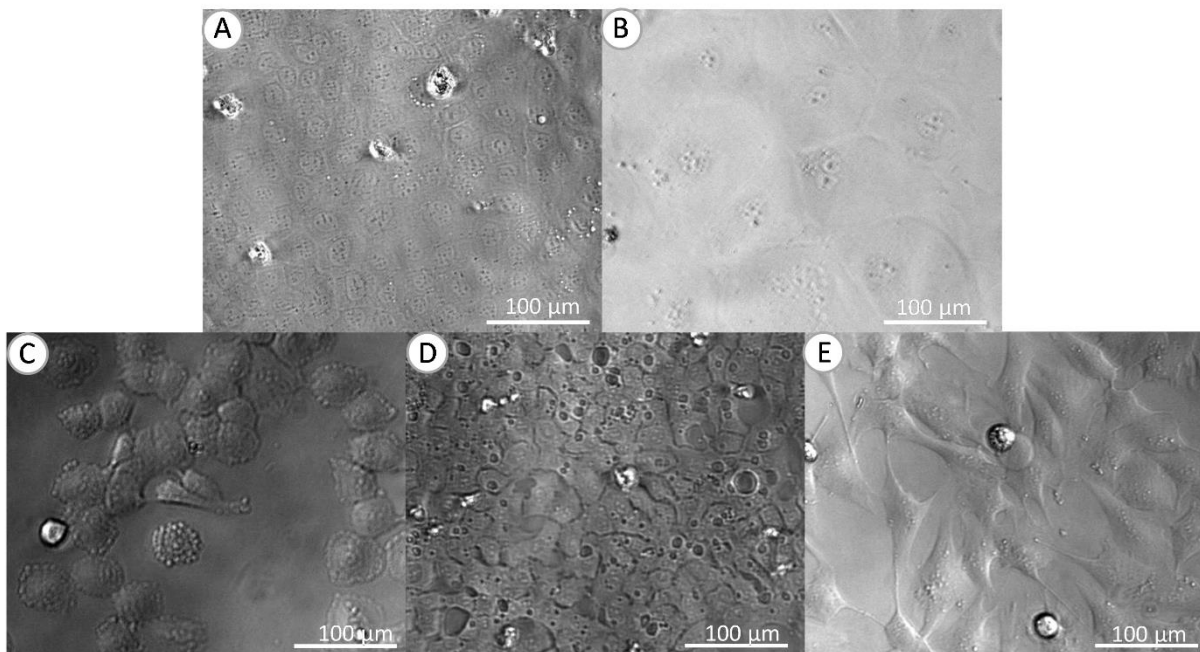
Figure 8: Morphology of selected "Upcyte hepatocyte" clones after clonal dilution. A, B: Exemplary pictures of single cell clones originating of "Upcyte Hepatocyte" batch 122-129-138. C-E: Exemplary pictures of single cell clones originating of "Upcyte Hepatocyte" batch 653-03. Scale: 100 µm.

Single-cell clone populations varied not only in cell size and quantity of nuclei (see Figure 8, A and B) but also in shape. For single cell populations of the "Upcyte Hepatocyte" batch 653-03 fibroblast-like populations (Figure 8, E) as well as cell populations with large vacuoles (Figure 8, D) and round shaped cells (Figure 8, C) were observed. This could be due to the heterogeneity of the polyclonal parental cell lines (Burkard et al. 2012). "Upcyte Hepatocytes" have a proliferative capacity for approximately 35 population doublings (Burkard et al. 2012; Schaefer et al. 2015) meaning that clonal cell lines of these cells are likely not suitable for long-term experiments.

Due to low cell growth rates after clonal dilution for both HepG2 and "Upcyte Hepatocytes" and strongly different morphologies in the case of "Upcyte Hepatocytes", these cell lines were not further evaluated.

3.1.2. Differentiation potential and CYP activities of F_1 clonal HepaRG cells

For further characterization of clonal HepaRG cells, 14 single cell clones (K1-14) created by limiting dilution were expanded to full confluence and differentiated with 2 % DMSO for 2 weeks. CYP activities of the differentiated F_1 clonal cell populations were assessed using the CYP cocktail assay and compared to activities measured in differentiated polyclonal HepaRG cells (Figure 9).
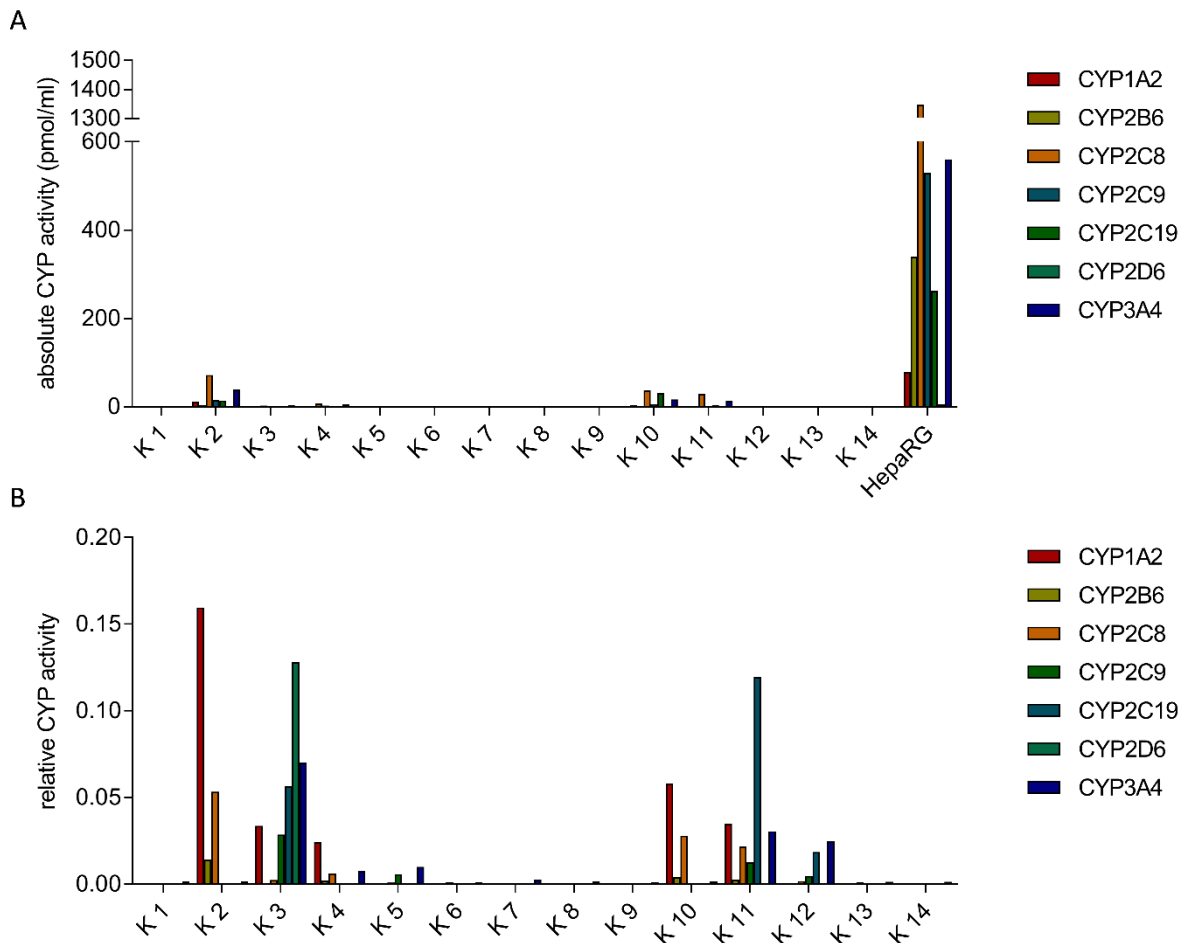
Figure 9: CYP activities in HepaRG single cell clones. CYP activities measured once in 14 HepaRG single cell clones and polyclonal HepaRG cells after differentiation with 2 % DMSO for 2 weeks. A: Absolute (pmol/ml) CYP activity levels. B: Relative CYP activity levels with corresponding CYP activity in polyclonal HepaRG set to 1.

The clonal cells showed much lower activities than parental HepaRG and only few clones (K2, K3, K10 and K11) showed detectable although strongly reduced CYP activities.

As there is a commercially available clonal HepaRG cell line (Li et al. 2015; Williamson et al. 2016), which shows CYP activities comparable to polyclonal HepaRG cells after differentiation (Brayman et al. 2014), it is reasonable to assume that out of a larger set of screened clones some clones with CYP activities comparable to parental HepaRG could possibly be isolated.

3.1.3. Generation and characterization of clonal HepaRG cell lines

As using the CYP cocktail assay to screen hundreds of cell clones was not practicable, the P450-Glo assay system from Promega (Madison, USA) was used to measure CYP2C9 activity as proxy to preselect clones of interest. A total of 98 clones created by limiting dilution and differentiated after reaching full confluence for 2 weeks in 2 % DMSO were screened for CYP2C9-Glo activity. In addition, the morphology of the differentiated clones as well as the number of cells were determined and documented microscopically (Figure 10).
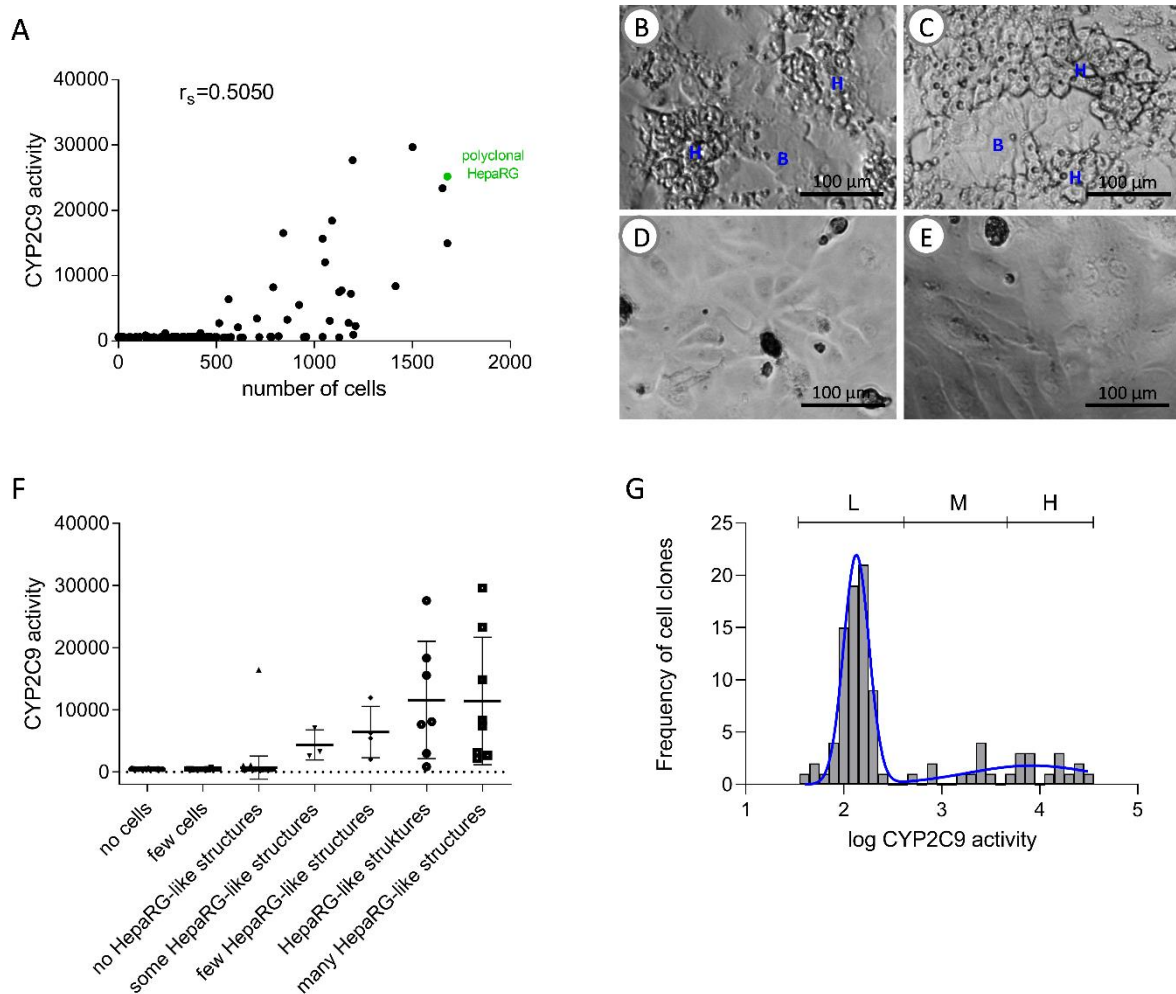
Figure 10: Characterization of HepaRG F_1 clones. A: Correlation of CYP2C9-Glo activity with cell count per well (in green: data for polyclonal HepaRG). B-E: Morphology of a selection of differentiated HepaRG single cell clones (H: hepatocyte-like cells, B: bile duct epithelial-like cells); scale: 100 μm. F: CYP2C9-Glo activity in HepaRG single cell clones depending on their morphology. G: Frequency distribution of CYP2C9-Glo activity in 98 confluent, differentiated HepaRG single cell clones, fitted with a "sum of two"-Gaussian model (L: low activities, M: medium activities, H: high activities).

Cell numbers below "500", as well as the morphology "no cells" or "few cells" indicated loss of confluency due to the differentiation process (Figure 10, A, F). Therefore, a huge proportion of clones were seemingly harmed by the DMSO conditions. By correlating measured CYP2C9-Glo activity and the corresponding cell number it was observed that the HepaRG single cell clones showed CYP2C9 activity only at higher cell densities (Figure 10, A). This is in accordance to the standard HepaRG differentiation protocol where differentiation is only achieved by treating HepaRG at full confluence with 2 % DMSO for 2 weeks (Aninat et al. 2006). CYP2C9 activities measured in differentiated single cell clone

populations were within the range of CYP2C9 activities measured in differentiated polyclonal HepaRG cells (Figure 10, A).

HepaRG cells have the unique ability to differentiate into two distinct cell types: biliary- and hepatocyte-like cells (Gripon et al. 2002; Cerec et al. 2007). These cell types have characteristic morphologies. Hepatocyte-like cells cluster together as piled-up 3D-structures with high contrast appearance. Biliary-like cells build up the spaces between the hepatocyte clusters appearing with low contrast (see Figure 36). Confluent differentiated single cell clones could be morphologically categorized into two distinct phenotypes: differentiated, "HepaRG-like" morphology with hepatocyte-like cells as well as bile duct epithelial-like cells (Figure 10, B and C) and cells with undifferentiated morphology (Figure 10, D and E). It is noted that cultures with a higher density of hepatocyte-like structures showed increased CYP2C9 activity (Figure 10, F).

The measured CYP2C9 activities of the confluent single cell clones were distributed in an apparent bimodal manner, with one major mode containing clones with low (L) activity level (values near to background level of 1 to 2.3) and a broader distributed mode of clones with varying CYP2C9 activities. For later analysis, this broad range was divided into two parts: clones with medium activity (M) and clones with high activity (H) (Figure 10, G). High activities were comparable to the activity of polyclonal HepaRG cells.

The percentage of single cell clones that have a differentiated morphology and high CYP2C9 activity, i.e., that seemed to regain their parental phenotype, was about 16 % of a total of 98 clones.

The present results, in addition to the previously measured CYP activities in clonal HepaRG (Figure 9), illustrate that single cell selection of polyclonal HepaRG cell line does not result in cell clones with a homogenous phenotype.

For further characterization in regard to CYP activities and morphology after differentiation, 18 clones out of all three activity ranges (L, M, H) were selected (high activities: H1-H8, medium activities: M1-M6, low activities: L1-L4) (Table 3).

Table 3: Overview of selected HepaRG single cell clones. In bold: characterized clones.

Clone	CYP2C9 activity	Morphology	Characterization
H1	27572	HepaRG-like	CYP activity measurements, cryo stocks
H2	11947	HepaRG-like	CYP activity measurements, cryo stocks
H3	14861	HepaRG-like	CYP activity measurements, cryo stocks
H4	16416	Flat cells, many dead	Growth arrest, no further characterization
H5	23276	HepaRG-like	CYP activity measurements, cryo stocks
H6	29572	HepaRG-like	CYP activity measurements, cryo stocks
H7	15563	Some HepaRG structures	CYP activity measurements, cryo stocks
H8	18324	Some HepaRG structures	Growth arrest, no further characterization
M1	2179	HepaRG-like	CYP activity measurements, cryo stocks
M2	7397	HepaRG-like	CYP activity measurements, cryo stocks
M3	8300	HepaRG-like	CYP activity measurements, cryo stocks
M4	1072	HepaRG-like	Growth arrest, no further characterization
M5	3308	Flat cells	Growth arrest, no further characterization
M6	2616	Flat cells	Growth arrest, no further characterization
L1	847	HepaRG-like	CYP activity measurements, cryo stocks
L2	557	Flat cells	Growth arrest, no further characterization
L3	557	Flat cells	Growth arrest, no further characterization
L4	545	Flat cells	Growth arrest, no further characterization

The clones H4, H8, M4, M5, M6, L2, L3 and L4 could not be characterized further because of cell growth arrest. Single-cell survival is highly cell line-dependent and may be increased by supplementation with additional serum or conditioned medium (Giuliano et al. 2019). While limiting dilution is considered to be a very gentle method compared to clonal dilution using flow cytometry, manual clonal colony picking methods have been shown to be able to increase single cell survival as the clonal colonies share growth factors (Gross et al. 2015).

The remaining clones were cultivated further, cryo-conserved, differentiated under standard conditions, and characterized regarding to their CYP activities measured with the CYP cocktail assay (Figure 11). The morphology of the differentiated cells was additionally documented microscopically (Figure 12).

A

B
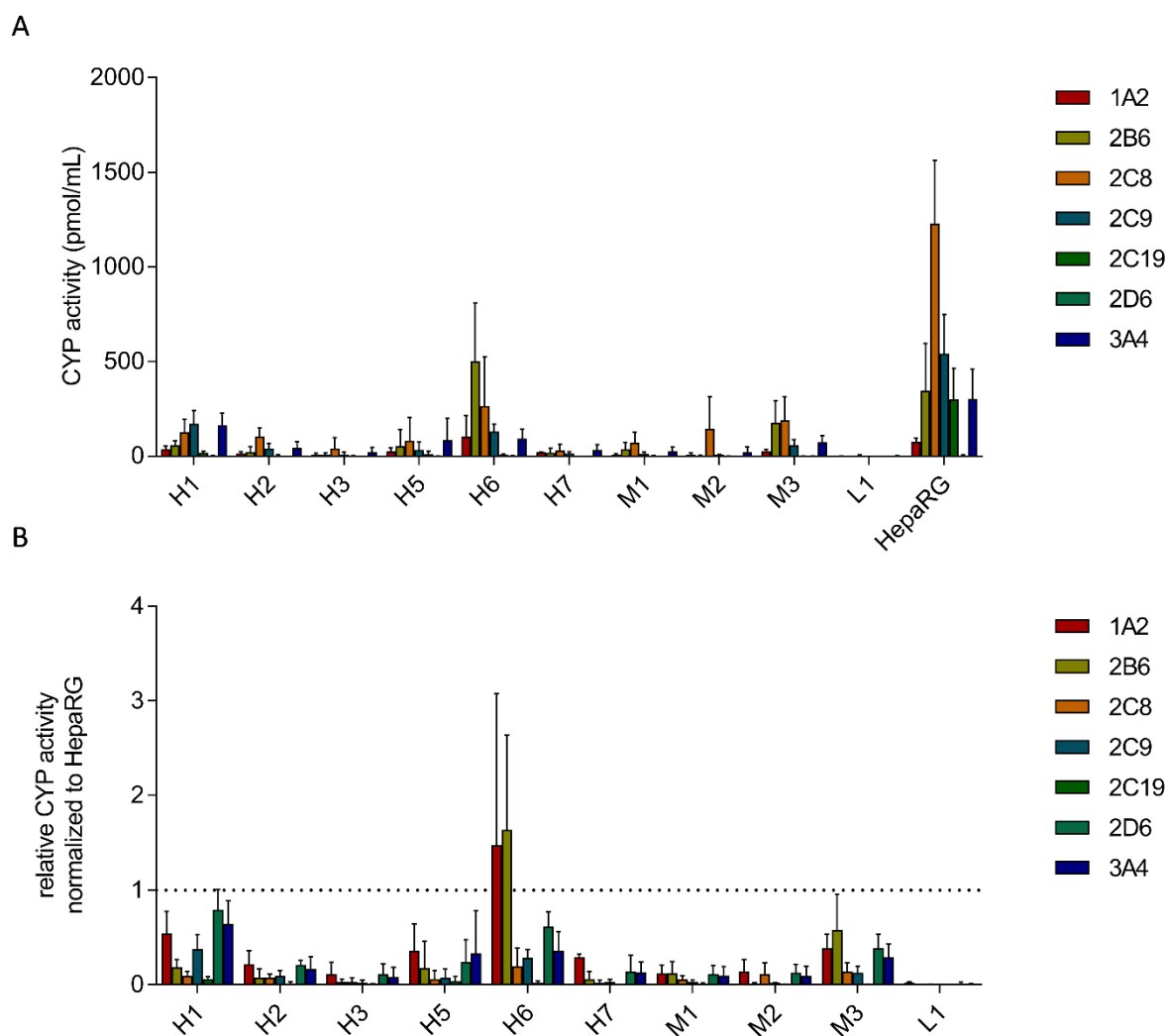
Figure 11: CYP activities in HepaRG F$_1$ clones. A: Absolute CYP activities (pmol/ml) measured with CYP cocktail assay of selected HepaRG single cell clones and HepaRG cells after differentiation with 2 % DMSO for 2 weeks. B: relative CYP-activities normalized to polyclonal HepaRG cells. Mean and SD of 3 batches of clones and 18 batches of HepaRG cells.

CYP activities in the selected single cell clones were in general lower than in polyclonal HepaRG cells. The clones showed a broad spectrum of activities, regardless of their similar morphologies (Figure 12, A). Several of them showed >20 % higher activities compared to the other clones (H1, H6 and M3). HepaRG clones L1 and H3 showed the lowest CYP activities.
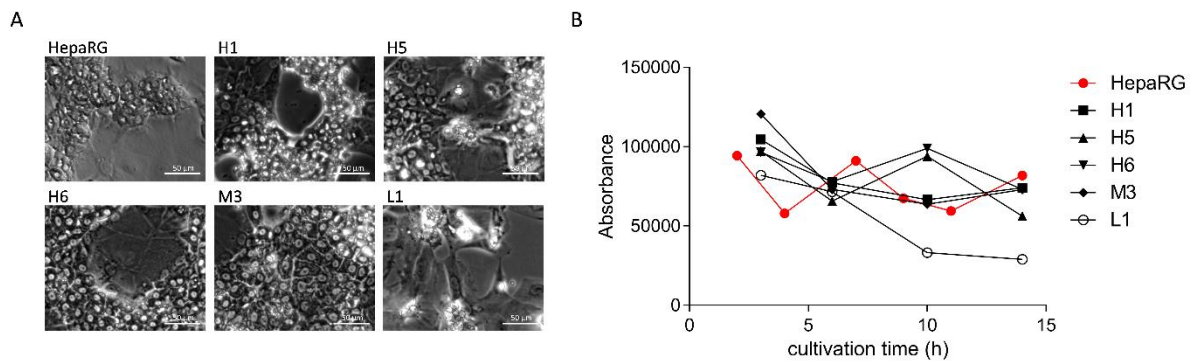
Figure 12: Morphological and viability analysis of selected HepaRG single cell clones. A: Morphologies of selected HepaRG single cell clones (H1, H5, H6, M3 and L1), scale: 50 µm. B: Viability measurement of selected HepaRG single cell clones (H1, H5, H6, M3 and L1) using the alamarBlue assay during 1 to 25 days of 2 % DMSO treatment.

Populations of H5, H6 and M3 single cell clones showed similar morphology as differentiated HepaRG cell with hepatocyte like cells and biliary cells (Figure 12). This contrasts with populations of single cell clones H1 and L1, which had large gaps in the cell layer. It is noted that the population of single cell clone B1 showed no differentiated cell morphology at all, but long fibroblast-like cells. A possible explanation for the cell layer gaps could be either decreasing cell size or increasing cell death during the differentiation process. Therefore, the viability of clonal HepaRG cells and the parental HepaRG cells during differentiation with 2 % DMSO (Figure 12, B) was examined using the alamarBlue assay. While viability of clonal HepaRG cell lines H1, H5, H6 and M3 were in the range of polyclonal HepaRG cells during differentiation, increased cell death was observed in the case of L1 cells.

Differentiation capability of the single cell clones (H1, H5, H6, M3 and L1) and parental HepaRG cells was analyzed by comparison of CYP activities pre-and post-2 % DMSO treatment (Figure 13).
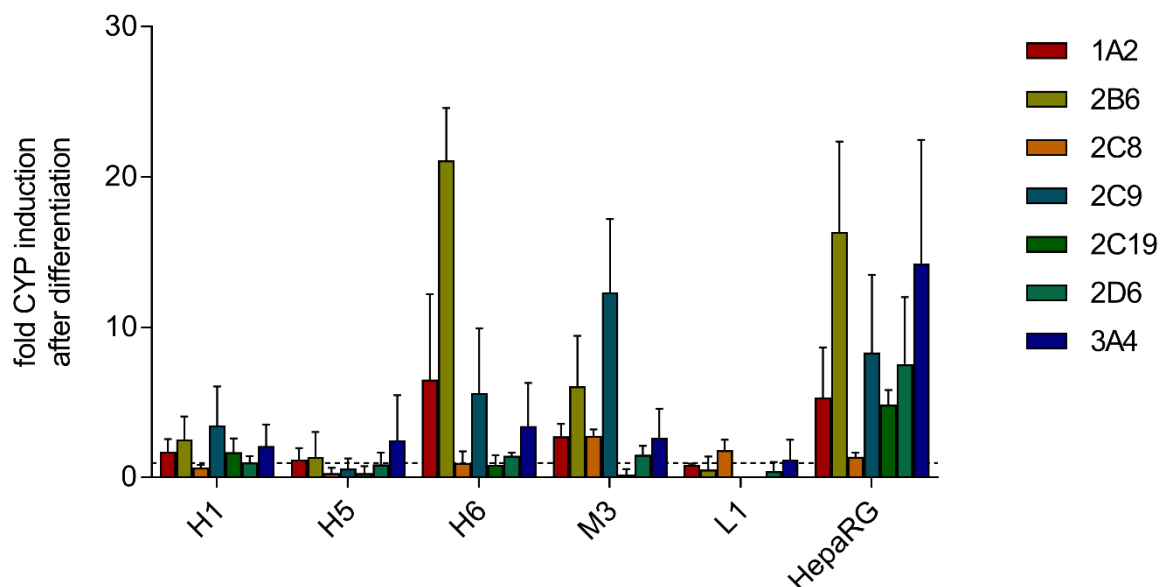
Figure 13: CYP activity induction in HepaRG single cell clones after 2% DMSO treatment for two weeks (H1, H5, H6, M3, L1) and HepaRG cells (mean/SD, n=3, for HepaRG n=4).

DMSO treatment had little effect on CYP activities of H1, H5 and L1. CYP2C8 activity remained unchanged during the differentiation process in both, single cell clones and in HepaRG cells. The strongest inducibility was seen for CYPs 2B6, 2C19 and 2C9, which is in agreement to the published induction in mRNA expression of these genes (Kanebratt and Andersson 2008). Differential CYP activity induction may be a consequence of different regulation pathways for the individual CYP isozymes. Furthermore, DMSO is known to induce individual regulatory pathways affecting CYPs in a differential manner (Cerec et al. 2007).

F_1 generation HepaRG single cell clones responded differently to the differentiation process. Only around 16 % of the clones retained their parental phenotype, characterized by the dual cell morphology and increased CYP activities after differentiation. However, the majority of clones (as example L1) seemed to have lost those properties. For these cells, DMSO treatment did not result in differentiation into hepatocyte-like and biliary cell types with increased CYP activities but was harmful to the cells. Measurements of additional hepatocyte markers such as CYP3A4 or albumin in a comparable setup could substantiate these findings.

3.1.4. Characterization of F_2 HepaRG clones

To elucidate whether single cell selection of clonal F_1 generation HepaRG cell lines does result in a homogeneous phenotype resembling F_1 clones, the clonal HepaRG F_1 cell lines H1, H6 and M3 were separated to single cells into two 96-well plates using flow cytometry. The resulting F_2 clones were then proliferated to full confluence and then differentiated for 2 weeks with 2 % DMSO. Afterwards, the fully confluent clones were screened for CYP2C9-Glo activities. In addition, morphology was documented before and after differentiation as well as viability and cell number after differentiation. For comparison of frequency distributions a normalization to the total sum of clones was performed. The differentiation capability of F_1 and F_2 clones was assessed only in populations with differentiated hepatocyte-like structures (see Figure 14). CYP2C9 activity from these populations were statistically compared using the Kruskal-Wallis test, as activity was not normal distributed.

A

	% of clones			
	F_1	F_2		
	HepaRG	H1	H6	M3
Surviving clones	62	44	24	53
HepaRG-like structures	23	33	33	51

B

C

Figure 14: Characterization of single cell clone populations. A: Percentage of surviving single cell clones and percentage of surviving clones with differentiated morphology. B: Frequency distribution of CYP2C9-Glo activity in confluent HepaRG F_1-clones, H1 and M3 F_2-clones, normalized to individual sum of clones, fitted with a "sum of two"-Gaussian model. C: Variation of CYP2C9-Glo activity in HepaRG F_1-clones, T1, T6 and M3 F_2-clones with differentiated hepatocyte-like morphology, mean of N = 22 (HepaRG), 33 (H1), 3 (H6), 57 (M3) with SD, significance was assessed by the Kruskal-Wallis test, as activity was not normal distributed (***$p < 0.001$, ****$p < 0.0001$).

As there were only a few F_2 clones originating of clonal HepaRG cell line H6 (37 in total and 3 with differentiated HepaRG-like structures), no meaningful analysis of the CYP2C9 activity distribution was possible for this cell line (see Figure 14, B).

F$_2$ clones originating from H1 and M3 had in general a higher percentage of clones with differentiated HepaRG-like morphologies than the clones of the parental cell line. Yet, the single cell survival was slightly decreased (Figure 14, A). This may be a property of clonal HepaRG cell lines but could also be due to the different single cell selection method, as F$_2$ clones were selected using flow cytometry in contrast to limiting dilution. As limiting dilution has low efficiency (empty wells or wells containing multiple cells) flow cytometry was used for F$_2$ clones.

Comparison of the frequency distribution of surviving clones from all three analyzed F$_1$ cell lines revealed a decreased amount of clones with low activities of around 2.6 (see Figure 14, B). The distribution shifted to higher activities and broader in shape. This observation fits to the higher percentage of clones with differentiated HepaRG-like morphology.

Analysis of clones with differentiated HepaRG-like morphology showed that F$_2$ clones originating of M3 had significantly lower CYP2C9 activities than clones originating from the parental F$_1$ cell line as well as those derived from H1. This could correspond to the parent medium high CYP2C9 activity of the F$_1$ M3 cell clone (marked by a red dot in Figure 14, C).

These results suggest a more pronounced ability of clonal F$_2$ HepaRG cells to differentiate, which means a slight stabilization of phenotype. Yet, at this stage, no homogeneous phenotype was detectable which allowed to investigate phenotype-genotype relations in genome-edited cell clones. It may be possible that a stable phenotype could be selected after several cloning generations. However, it is also possible that the unique ability of the HepaRG cell lines to differentiate into two distinct cell types always leads to clones with a broad distribution of phenotypes.

3.2. Genetic knockout of *POR* in HepaRG cells

To establish a working protocol for CRISPR/Cas9 induced genome editing in HepaRG cells, two major points had to be considered: The rational design of targeting sgRNAs and the proper delivery method. Clonal selection of HepaRG cells was shown to not result in cell clones with a homogenous phenotype as necessary for genome editing approaches (chapter 3.1). In addition, plasmid delivery into HepaRG cells using traditional transfection reagents is not very efficient. Therefore, other delivery methods with high efficiency had to be established. In the following chapters, RNP transfection, lentiviral transduction of Cas9 and sgRNA and transfection of sgRNAs in Cas9-expressing cells were evaluated for Cas9 and sgRNA delivery into HepaRG cells.

As a first target for CRISPR/Cas9-induced gene knockout *POR* was chosen in order to investigate multiple POR functions in hepatocytes. POR is considered to be a contributor to CYP variability, as it provides electrons essential for CYP function. Thus, *POR* knockout is to be expected to reduce CYP activities, but it is unclear whether different P450 isozymes are equally affected. POR also exerts strong effects on several other cellular functions like bile acid and lipid homeostasis. Therefore, those cells had to be characterized thoroughly.

The data presented in the following chapters 3.2.1, 3.2.2, 3.2.4 and 3.3 are summarized in the publication "Differential effects on human cytochromes P450 by CRISPR/Cas9-induced genetic knockout of cytochrome P450 reductase and cytochrome b5 in HepaRG cells" by Tamara Heintze, Kathrin Klein, Ute Hofmann and Ulrich M. Zanger (Heintze et al. 2021).

For this publication, scientific ideas were developed by Tamara Heintze, Kathrin Klein and Ulrich M. Zanger (80 %, 10 %, 10 %, respectively). Data generation from *in vitro* experiments was performed by Tamara Heintze; Ute Hofmann contributed the LC-MS/MS measurements. Analysis and interpretation of experiments were performed by Tamara Heintze. Paper writing was done by Tamara Heintze, Kathrin Klein and Ulrich M. Zanger (60 %, 10 %, 30 %, respectively).

3.2.1. Design of sgRNAs

A rational design of the sgRNA is essential for the success of CRISPR/Cas9-mediated genome editing. For gene knockout with one sgRNA there are several points including the PAM restriction to be taken into account. First, the sgRNA binding site should be located in an exon of the target gene to ensure frame shift after NHEJ of the introduced double-strand break. It is also reasonable to pinpoint the sgRNA near the 5ˈ- end or near a functionally important region of the gene to guarantee functional knockout. As sgRNAs have differential binding properties several sgRNAs should be chosen.

For the design of sgRNAs there are several online tools available. For this thesis the tools CRISPRdesign (http://crispr.mit.edu/) (no longer available) and CHOPCHOP (http://chopchop.cbu.uib.no/) (Labun et al. 2019) were chosen. Both tools rank possible sgRNAs regarding efficiency and predicted off-targets. While CRISPRdesign screens for sgRNAs in a region of 500 nucleotides of sequence, CHOPCHOP examines all possible exonic sgRNAs of the target gene. Table 4 lists the selected sgRNAs targeting *POR,* while Figure 15 visualizes the target sites of the individual sgRNA in the *POR* gene.

Table 4: Selected sgRNAs for genetic *POR* knockout

Name	Sequence	Target region
POR#1	5ˈ-TCGTGGGTCTCCTAACCTACTGG-3ˈ	Near 5ˈ-end in exon 2
POR#2	5ˈ-GGTCCACACCGACATAGATGCGG-3ˈ	5ˈ of FAD domain in exon 8; near binding site of zinc finger oligo published in (Su et al. 2013)
POR#3	5ˈ-TGGGACTTGCGCACGAACATGGG-3ˈ	5ˈ of NADPH binding site in exon 13
POR#4	5ˈ-CGTGTTCTACGGCTCCCAGACGG-3ˈ	Published in (Rezende et al. 2017), exon 4
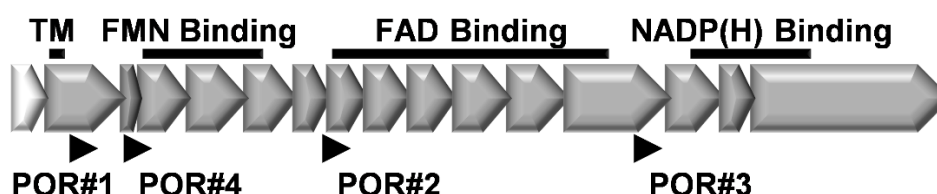
Figure 15: Location of *POR*-targeting sgRNAs relative to exon structure (gene chr7:75,899,200-75,986,855; GRCh38/hg38) indicating one 5'-untranslated exon (white) and 15 translated exons as well as binding regions (black) for FAD, FMN, and NADPH and the transmembrane domain (TM). The positions of for sgRNAs targeting exon 2 (POR#1), the FAD domain in exon 8 (POR#2), the NADPH binding site in exon 13 (POR#3) or the FMN binding site in exon 4 (POR#4) are indicated by arrows (adapted from Heintze et al. 2021).

For evaluation of the on-target efficiency, efficiency scores for the selected sgRNAs calculated by seven online available sgRNA design tools were compared (see Table 5). Except for the Horizon design tool, all others assign higher numbers to higher target efficiencies.

Table 5: Predicted on-target efficiency, highest predicted on-target score is marked in bold.

Name	POR#1	POR#2	POR#3	POR#4	Source
CHOPCHOP	51.77	**68.65**	47.35	57.49	(Labun et al. 2019)
Broad Institute GPP	5,163	**6,865**	4,896	5,749	(Sanson et al. 2019),
e-crisp	424,061	**677,194**	421,508	541,120	(Heigwer et al. 2014)
IDT	43	62	**70**	64	https://eu.idtdna.com/site/order/designtool/index/CRISPR_SEQUENCE
Synthego	0.516	**0.686**	0.473	0.575	https://www.synthego.com/products/bioinformatics/crispr-design-tool
Horizon	9.35	3.20	**3.05**	8.55	https://horizondiscovery.com/en/ordering-and-calculation-tools/crispr-design-tool
GuideScan	49	**69**	51	56	(Perez et al. 2017)

Most design tools predict sgRNA POR#2 to be most efficient, except for the design tools provided by Integrated DNA technologies (IDT, Coralville, USA) and Horizon Discovery (Waterbeach, UK).

3.2.2. sgRNA target sequencing and *POR* and *CYP* genotyping

Karyotyping of HepaRG cells showed exchanges between chromosome 12 and 22 and an additional remodeled chromosome 7 with a deletion between q11 and q21 and two inversions on q21 and q36 (Gripon et al. 2002). The deletions include the genomic region of *POR*, thus making it diploid in HepaRG cells. For further elucidation of the *POR* genotype, and to ensure that no mutations or polymorphisms interfere with sgRNA/Cas9 binding to the *POR* sgRNA target sites the entire *POR* gene including all exons and adjacent intron regions was sequenced in cellular DNA of HepaRG (see Supplemental table 1). No mutations at sgRNA binding sites were found.

For further characterization of *CYP* isozym genotypes in HepaRG whole gene sequencing of *CYP1A2* (see Supplemental table 2) and exon sequencing of *CYP2D6* (see Supplemental table 3) and *CYP2C8* (see Supplemental table 4) was performed. For *CYP2D6*, in addition to all coding exons, the area surrounding the 115 kb downstream enhancer SNPs enhancer SNPs (Wang et al. 2015; Wang et al. 2014) was sequenced. *POR* and *CYP* star allele annotation was done according to Pharmacogene Variation Consortium (PharmVar) guideline at www.PharmVar.org (Gaedigk et al. 2018; Gaedigk et al. 2019). Together with genotyping data for *CYP2B6, CYP2C9, CYP2C19, CYP3A4* and *CYP3A5* using OpenArray technology from preexisting studies done by Dr. Roman Tremmel (IKP, Stuttgart) the following genotypes for HepaRG cells were concluded (see Table 6).

Table 6: Genotypes of *POR, CYP1A2, CYP2B6, CYP2C8, CYP2C9, CYP2C19* and *CYP3A4* in HepaRG cells (adapted from Heintze et al. 2021)

Gene	Genoype	Phenotype of variant alleles	Method
POR	*1/*37	Not known (Gomes et al. 2009)	Sequencing
CYP1A2	*1/*1F	Higher inducibility	Sequencing
CYP2B6	*1/*6	Decreased function	OpenArray
CYP2C8	*3/*3	Increased *in vitro* function (Kaspera et al. 2011)	Sequencing
CYP2C9	*2/*2	Decreased function	OpenArray
CYP2C19	*1/*1	No variant allele detected	OpenArray
CYP2D6	*2/*9	Decreased function (*9*)	Sequencing
CYP3A4	Not *1B*, not *22*	No variant allele detected	OpenArray
CYP3A5	*3/*3	Splicing defect, severely decreased expression	OpenArray

Compared to the common allele *POR*28* (A503V), the rare allele (<1 %) *POR*37* (A503V + V631I) carries an additional mutation leading to a second amino acid change. While *POR*28* has been shown to influence CYP activities in diverse ways, *POR*37* has not been functionally characterized yet (www.PharmVar.org) (Gomes et al. 2009; Gaedigk et al. 2018; Gaedigk et al. 2019).

Genotyping of major drug metabolizing *CYP* isozymes confirmed previously described genotypes for CYPs *2C9* (*2/*2*), *2C19* (*1/*1*), *2D6* (*2/*9*) and *3A5* (*3/*3*) (Jackson et al. 2016). In addition, HepaRG cells were found to be homozygous for *CYP2C8*3* and heterozygous for *CYP2B6*6*.

3.2.3. Genetic knockout of *POR* in HepaRG cells via RNP complexes

One possibility to deliver Cas9 into cells is the transfection with RNP complexes consisting of SpCas9 and the targeting sgRNA. Using RNPs limits the exposure time of the cells towards Cas9 to a few hours, reducing off-target editing. However, as RNPs are delivered to the cells via transfection methods, the efficiency of this approach is dependent on the transfection rate. In this thesis the Alt-R CRISPR-Cas9 RNP System (Integrated DNA technologies, Coralville, USA) was tested to achieve the CRISPR/Cas9-induced knockout of *POR* in HepaRG. sgRNAs (sgRNA POR#1, #2, and #3) targeting different sites in the *POR* gene were used (see Figure 15). sgRNA POR#4 was excluded in the following experiment, as it has similar targeting sites to sgRNA POR#1. In addition, an established sgRNA targeting *HPRT1* (Hypoxanthine phosphoribosyltransferase 1) and a non-human targeting sgRNA were used as positive and negative controls, respectively. RNP complexes were transfected into undifferentiated HepaRG cells, as transfection efficiency in undifferentiated cells is described to be higher than in differentiated cells (Laurent et al. 2010). After transfection of undifferentiated HepaRG cells with the RNP complexes the success of Cas9 delivery was assessed via T7 endonuclease 1 (T7E1) mismatch digest with subsequent fragment analysis using the Agilent 2100 Bioanalyzer (Agilent Technologies) and POR expression in the transfected cells was measured by western blotting (see Figure 16). The T7E1 cleavage efficiency is calculated as the relation of the fragment band intensity to the sum of intensity of uncut and digest fragment bands.

sgRNA	Full legth fragment	Digest fragment 1	Digest fragment 2
Pos. control	1083 bp	827 bp	256 bp
POR#1	838 bp	402 bp	436 bp
POR#2	898 bp	412 bp	486 bp
POR#3	993 bp	508 bp	445 bp
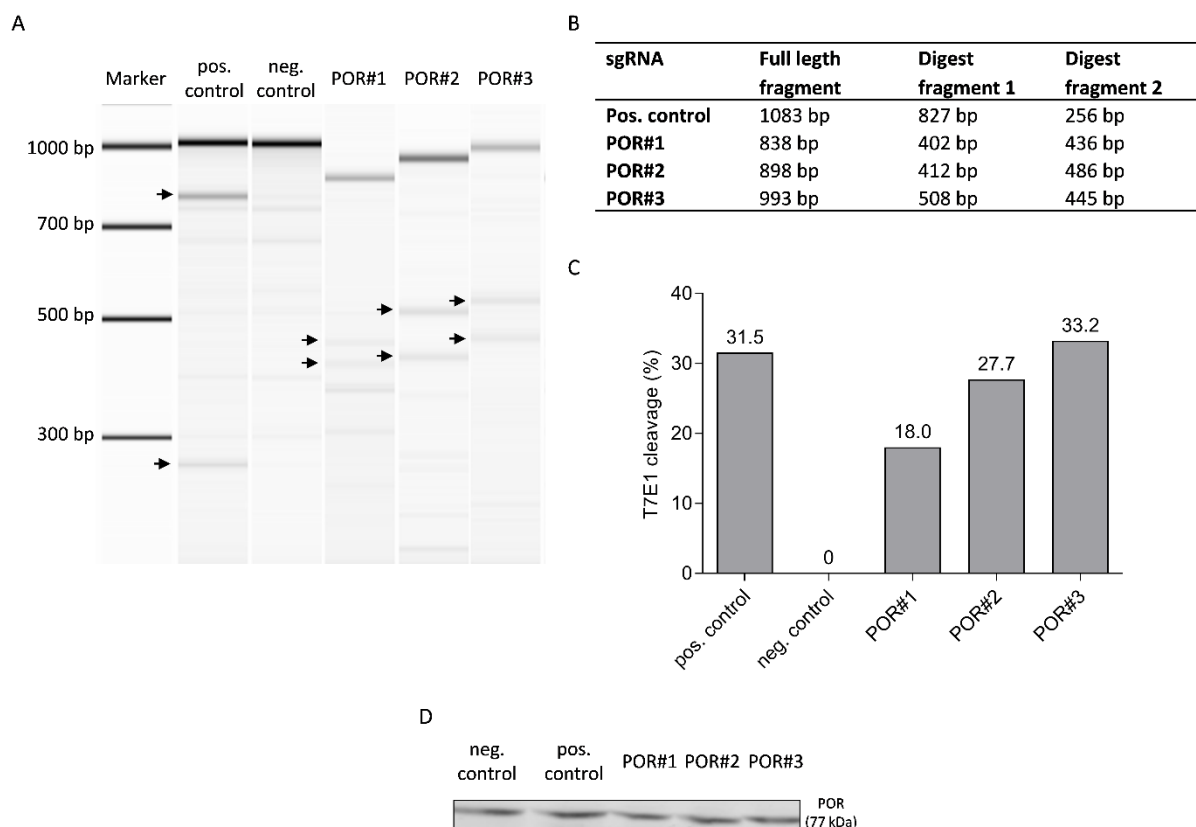
Figure 16: Analysis of RNP delivery in HepaRG cells. HepaRG cells were transfected with non-targeting RNP (neg. control) and RNPs targeting HPRT1 (pos. control), POR#1, POR#2, and POR#3. A: Fragment analysis using Agilent 2100 Bioanalyzer (Agilent Technologies) fragment analyzer after PCR amplification and following T7E1 digest of sgRNAs target regions; DNA marker: DNA 7500. Expected digestion products are marked by arrows. B: Expected fragment sizes after PCR amplification and following T7E1 digest of sgRNAs target regions. C: Calculated T7E1 cleavage efficiencies. D: POR protein expression analysis in transfected cells using western blotting.

Fragment analysis of the target sites confirmed Cas9-introduced mutations at the predicted target sites (Figure 16, A). The T7E1 cleavage efficiency was used to estimate the mutation rate at the target site. As seen in Figure 16, C, the highest mutation rates were seen in the cells transfected with RNPs targeting *HPRT1* (pos. controls) and *POR* exon 13 (POR#3).

For additional estimation of mutation frequency, the transfected cells were single cell selected using limiting dilution, and subsequently screened for Cas9-induced mutations with the T7E1 assay. Table 7 lists the frequency of mutated clones in comparison to the T7E1 cleavage efficiency.

Table 7: Estimation of mutation frequency in 35 RNP-transfected HepaRG cells.

	Pos. control	POR#1	POR#2	POR#3
T7E1 cleavage (%)	31	18	27	33
Mutation frequency (%)	31	16	9	25

The overall cleavage efficiency using RNP delivery in HepaRG cells was 13-33 %, with a slightly lower mutation frequency of 9-33 %. As the T7E1 assay underestimates the actual mutation frequency due to its inability to detect single nucleotide changes (Zischewski et al. 2017), this result appears plausible. Thus, RNPs targeting *HPRT1* (pos. control) and *POR* exon 13 (POR#3) appeared to be most efficient.

However, this mutation frequency did not result in a measurable effect on POR protein expression levels (Figure 16, D). The low mutation frequency is probably due to a low transfection efficiency of the RNPs into the HepaRG cells. Further quantification of the mutation rate may be enabled using next generation sequencing of the target region.

In summary, by RNP transfection genome editing at the predicted target sites in HepaRG cells was achieved. However, a mutation rate of 25 % was found to not result in a measurable effect on the protein expression level. As analysis of generated single cell clones would not result in meaningful results due to heterogeneous phenotype of clonal HepaRG cells (see chapter 3.1), this delivery method was not analyzed any further.

3.2.4. Genetic knockout of *POR* in HepaRG via lentiviral transduction

As single cell selection in HepaRG cannot be reliably used for phenotype-genotype relation analyzes and transfection of RNPs did not result in satisfactory transfection efficiency (see chapters 3.1 and 3.2.3), a Cas9 delivery method had to be applied which whould lead to a transfection efficiency close to 100 %. As HepaRG cells are hard to transfect by transfection reagents or nucleofection (Laurent et al. 2010), Cas9 and sgRNA delivery via lentiviral transduction into undifferentiated, proliferating HepaRG cells was tested as a potential more successful further option.

For the lentiviral approach, only two sgRNAs were used to reduce emerging cell characterization work in downstream steps. As on-target efficiencies of the previously described sgRNAs targeting diverse sites in *POR* were similiar, sgRNA POR#1 was chosen due to its target site near the 5'-end of exon 2 (Figure 15). As a second sgRNA, sgRNA POR#4, binding near the 5'-FMN binding site in exon 4 (Figure 15), was selected, as it was described in a previously published CRISPR/Cas9-mediated *POR* knockout study (Rezende et al. 2017) . Figure 17 visualizes the experimental setup.
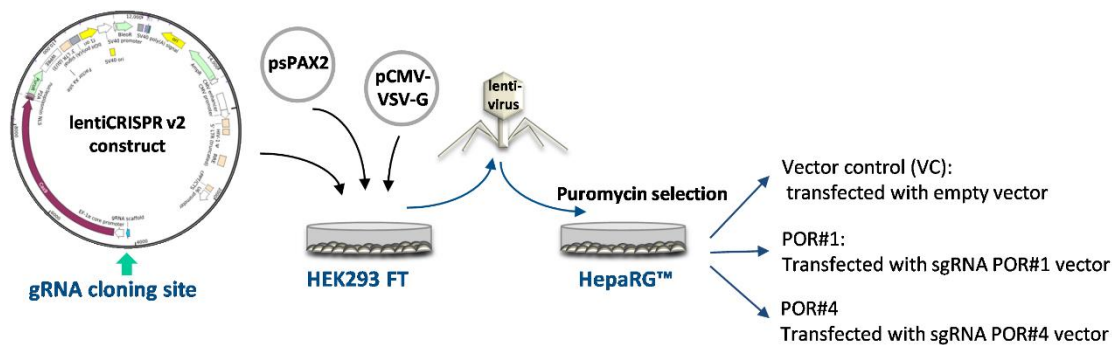
Figure 17: Scheme of lentiviral delivery of lentiCRISPRv2 constructs into HepaRG cells.

The lentiCRISPR v2 plasmid was chosen as it is a dual expression system for Cas9 and sgRNA which produces a high viral titer and provides expression of puromycin N-acetyl-transferase for antibiotic selection of transduced cells (Sanjana et al. 2014).

For the production of lentiviral particles HEK 293FT cells were transfected with the individual lentiCRIPSRv2 constructs and the lentiviral packaging and pseudotyping plasmids psPAX2 and pCMV-VSV-G, respectively. Resulting lentiviral particles were collected, and subsequently used to transduce undifferentiated HepaRG cells. Further selection with puromycin led to three individual edited HepaRG cell lines: 1) HepaRG[VC] cells transduced with the empty vector and expressing Cas9, 2) HepaRG[-POR#1] cells transduced with the empty vector and expressing Cas9 and sgRNA POR#1, and 3) HepaRG[-POR#4] cells transduced with the empty vector and expressing Cas9 and sgRNA POR#4.

Characterization of HepaRG *POR* knockout cells
After puromycin selection and growth to full confluence the transduced cells were differentiated for 2 weeks with 2 % DMSO. Subsequently, the cells were characterized regarding morphology and Cas9 expression (see Figure 18).
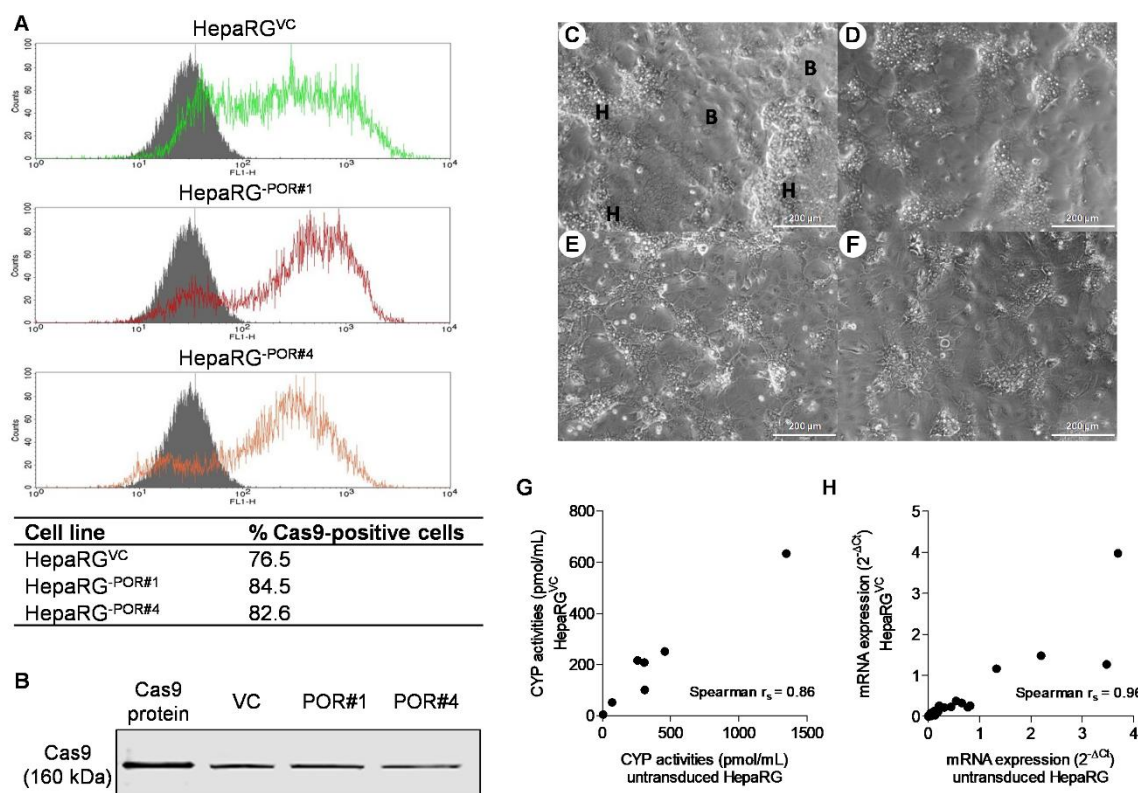
Figure 18: Characterization of transduced HepaRG cells. A: Flow cytometric analysis of undifferentiated HepaRG^{VC} (green), HepaRG$^{-POR\#1}$ (red) and HepaRG$^{-POR\#4}$ (orange) in comparison to untransduced HepaRG cells (grey). B: Western blot analysis of Cas9 expression in lysates of undifferentiated HepaRG^{VC}, HepaRG$^{-POR\#1}$ and HepaRG$^{-POR\#4}$, Cas9 protein as positive control (see Supplementary figure 1, for full blot). C-F: Morphology of untransduced, differentiated HepaRG cells compared to differentiated HepaRG^{VC} (D), HepaRG$^{-POR\#1}$, and HepaRG$^{-POR\#4}$ (F) (H: hepatocyte-like cells; B: biliary-like cells), scale: 200 μm. G: Correlation of sevem CYP activities in transduced vs. untransduced differentiated HepaRG cells. (h) Correlation of mRNA expression levels of 72 genes in transduced vs. untransduced differentiated HepaRG cells. Adapted from Heintze et al. 2021.

The high transduction efficiency of the lentiviral delivery coupled with puromycin selection led to a high proportion of HepaRG cells (~77 %) expressing Cas9 (see Figure 18, A and B). To elucidate whether transduced HepaRG^{VC} cells still have their differentiation potential, morphology as well as CYP activities and mRNA expression profiles after standard differentiation with DMSO for two weeks were compared to untransduced HepaRG cells. It was observed that HepaRG^{VC} cells showed differentiated hepatocyte-like as well as biliary cell types comparable to untransduced HepaRG cells (Figure 18, C-F).

Enzyme activities of seven simultaneously determined CYPs in HepaRG^{VC} cells correlated strongly (r_s=0.86) with those in untransduced HepaRG cells, although their absolute activity levels were observed to be reduced (see Figure 18, G). Expression levels of a set of 72 ADME-related genes were also slightly lower in HepaRG^{VC} cells compared to untransduced cells but confirmed the high correlation (r_s=0.94) (Figure 18, H).

These findings indicated that HepaRG^{VC} cells retain their differentiation potential with the most important characteristics of HepaRG cells and are therefore suitable for both, genome editing and as a control cell line.

For CRISPR/Cas9-mediated knockout of *POR* using lentiviral delivery sgRNAs POR#1 and POR#4 were chosen. For both sgRNAs comparable efficiency scores were predicted (see Table 5), with sgRNA POR#4 having three predicted off-targets.

A

Test region	Undigested Fragment	Fragment 1	Fragment 2
POR#1	642 bp	175 bp	467 bp
POR#4	481 bp	246 bp	235 bp

B
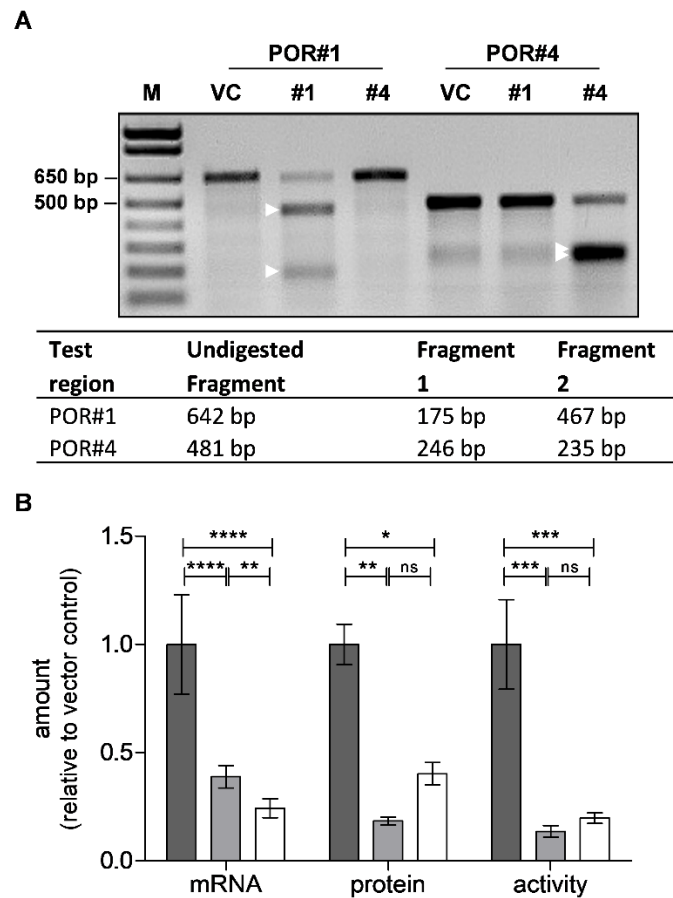
Figure 19: Validation of *POR* knockout in transduced HepaRG cells. A: T7E1 digest of DNA of transduced HepaRG cells. M: DNA marker (1 Kb Plus DNA Ladder, Thermo Fisher Scientific); lanes 2-4: digest products of test region POR#1; lanes 5-7: digest products of test region POR#4; VC: vector control; #1: sgRNA POR#1; #4: sgRNA POR#4. Digested fragments are marked with white arrows. The expected fragment sizes are summarized below. B: POR expression and cytochrome c reductase activity in transduced differentiated HepaRG cells. POR mRNA was quantified in cell lysates and POR protein and cytochrome c reductase activity were quantified in microsomal fractions. Mean levels ± SD are shown relative to vector control (VC) set at 1 (dark grey: VC, light grey: POR#1, white: POR#4). Statistical significance was assessed by unpaired t-test (*$p < 0.05$, **$p < 0.01$, ***$p < 0.001$, ****$p < 0.0001$; ns, not significant). Adapted from Heintze et al. 2021.

Using the T7E1 assay, CRISPR/Cas9 editing at the predicted target sites was confirmed for both sgRNAs (Figure 19, A) with T7E1 efficiencies of 72 % (POR#1) and 62 % (POR#4) and off-target gene editing of sgRNA POR#4 at the predicted sites was excluded.

Cas9 expression as well as differentiated HepaRG morphology were confirmed in both types of HepaRG[-POR] cells (see Figure 18).

Analysis of POR in differentiated HepaRG cells revealed that both sgRNAs were similarly effective and reduced POR mRNA and protein by 60 to 80 % (Figure 19, B). The minor differences in reduction of mRNA and protein between sgRNA POR#1 and POR#4 were not consistent and were considered as experimental variability. Determination of POR-mediated cytochrome c reductase activity in microsomal fractions of differentiated HepaRG cells revealed up to 90 % decrease for both sgRNAs. This is in good agreement with the effects at the mRNA and protein levels.

The residual POR expression and activity is the result of a mixture of individual cells with homozygous, heterozygous and no genetic knockout of *POR*. Therefore, the phenotype of these cells is a POR knockdown rather than a complete knockout.

For comparison, the difference in POR activity between microsomes form undifferentiated and differentiated HepaRG was 0.006 ± 0.0009 U/mg versus 0.029 ± 0.006 U/mg, respectively, and a similar value was obtained in a pool of human liver microsomal fractions (0.034 ± 0.004 U/mg).

Effect of POR knockdown on enzymatic activity of CYP isozymes

For the investigation of the effect of POR knockdown on the most important drug metabolizing CYP isozymes, microsomal fractions of differentiated HepaRG^{VC} and both types of HepaRG^{-POR} cells were used to measure enzyme activities of seven CYPs simultaneously with the CYP cocktail LC-MS/MS assay. For a more thorough characterization, kinetic experiments for CYP2C8, CYP2C9 and CYP3A4 were performed using the substrates amodiaquine, tolbutamide and atorvastatin, respectively, and midazolam as a second CYP3A4 substrate (Figure 20). Calculated kinetic parameters K_M and V_{max} are summarized in Table 8.
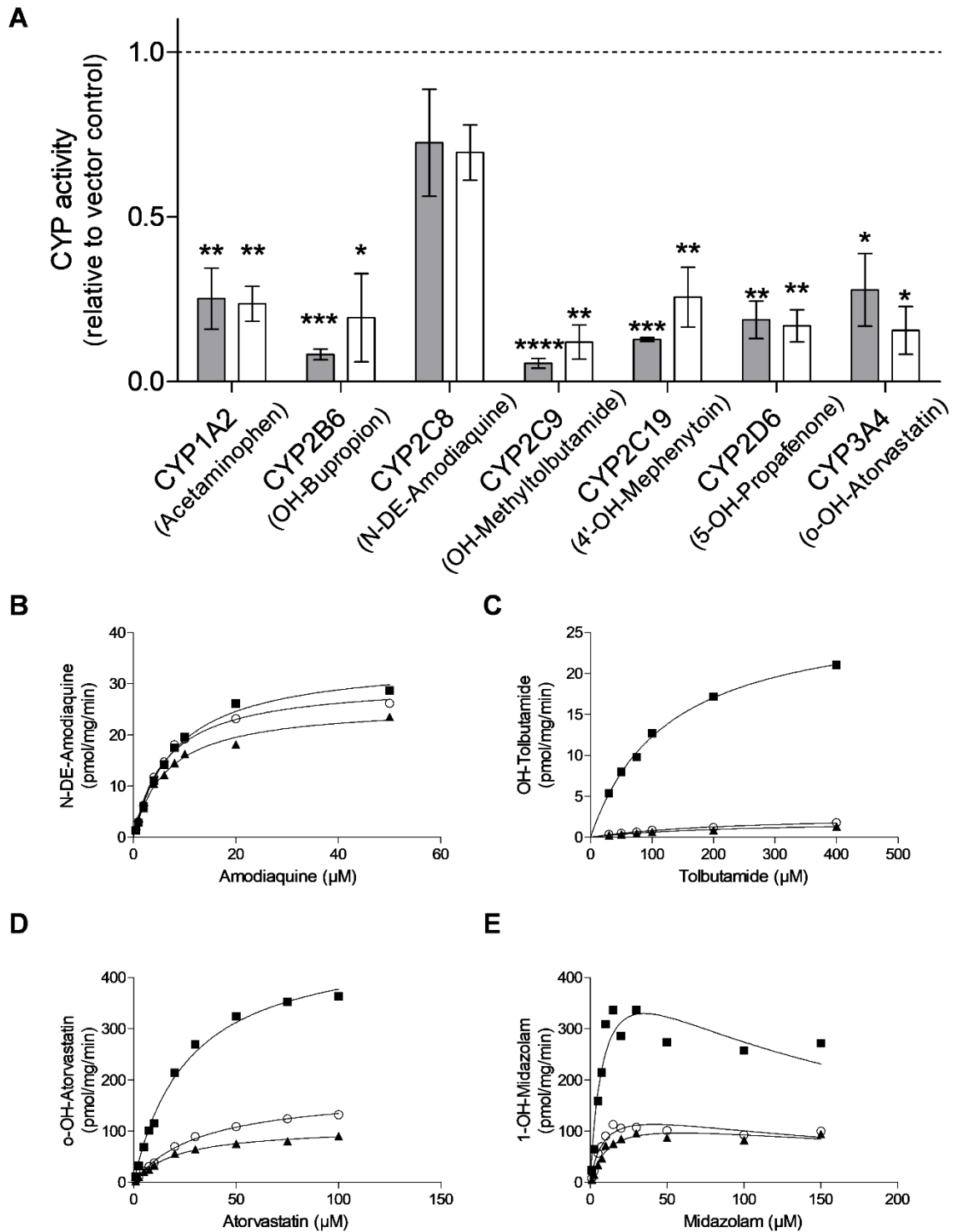
Figure 20: CYP activities in microsomal fractions of HepaRG^{-POR} cells. A: HepaRG cells transduced with sgRNA POR#1 (grey) or POR#4 (white) were differentiated for three weeks and harvested for microsome preparation. Enzyme activities of seven CYP enzymes were determined simultaneously by cocktail LC-MS/MS assay and given relative to HepaRG^{VC}. Results are shown as means ± SD of four independent experiments. Statistical significance was evaluated by unpaired t-test (*p < 0.05, **p < 0.01, ***p < 0.001, ****p < 0.0001). B-E: Kinetic analysis of selected substrate conversions in HepaRG microsomes. HepaRG cells transduced with vector control (VC, ■), sgRNAs POR#1 (▲) and POR#4 (○) were differentiated for three weeks and harvested for microsome preparation; (B) amodiaquine (CYP2C8); (C) tolbutamide (CYP2C9); (D) atorvastatin (CYP3A4); (E) midazolam (CYP3A4). Data were analyzed by Michaelis-Menten model (B-D) or by substrate inhibition model (E). Adapted from Heintze et al. 2021.

As shown in Figure 20 A, all CYP activities except for amodiaquine N-deethylation were negatively affected by both sgRNAs. While the effects on individual CYP isozymes differed substantially, the pattern was similar for both sgRNAs. Across all CYPs measured, 1.4- to 20-fold reductions were observed in enzyme activity. The strongest effect of POR knockdown was observed for CYP2C9 (85-95 % reduction of activity), while no significant reduction of CYP2C8 activity was seen. Compared to other CYP activities, CYP2C8-catalyzed amodiaquine N-deethylation thus appeared to be insensitive against variable POR levels.

Table 8: Calculated kinetic parameters of selected substrate conversions. Taken from Heintze et al. 2021.

|		V_{max} [95% CI] (pmol/mg/min)	K_M [95% CI] (µM)	K_i [95% CI] (µM)	Cl_{int} [95% CI]
Amodiaquine	VC	34.7 [31.5 to 37.9]	8.3 [6.3 to 10.2]		4.2 [3.7 to 5.0]
	POR#1	25.8 [23.7 to 27.9]	6.5 [5.0 to 7.9]		4.0 [3.5 to 4.7]
	POR#4	30.3 [27.8 to 32.9]	6.4 [4.9 to 7.8]		4.7 [4.2 to 5.7]
	CYP2C8 R	26.1 [23.4 to 28.8]	4.2 [2.7 to 5.8]		6.2 [5.0 to 8.7]
	CYP2C8 LR	2.0 [1.8 to 2.1]	3.5 [2.6 to 4.5]		0.57 [2.5 to 0.69]
Tolbutamide	VC	27.7 [25.6 to 29.8]	125 [104 to 148]		0.22 [0.20 to 0.25]
	POR#1	2.1 [1.5 to 2.7]	235 [106 to 364]		0.009 [0.007 to 0.014]
	POR#4	2.8 [2.2 to 3.3]	240 [147 to 332]		0.01 [0.001 to 0.015]
	CYP2C9 R	65.5 [39.4 to 91.7]	817 [381 to 1253]		0.08 [0.07 to 0.10]
	CYP2C9 LR	3.0 [2.6 to 3.3]	214 [170 to 258]		0.01 [0.013 to 0.015]
Atorvastatin	VC	476 [433 to 520]	26.3 [20.1 to 32.5]		18.1 [16.0 to 21.5]
	POR#1	108 [99.4 to 116]	21.4 [16.8 to 26.0]		5.0 [4.5 to 5.9]
	POR#4	179 [166 to 192]	33.1 [27.5 to 38.7]		5.4 [5.0 to 6.0]
	CYP3A4 R	5.7 [4.9 to 6.5]	34.4 [23.0 to 45.8]		0.17 [0.14 to 0.21]
	CYP3A4 LR	2.2 [1.9 to 2.5]	27.5 [17.8 to 37.2]		0.08 [0.07 to 0.11]
Midazolam	VC	499 [233 to 766]	9.0 [0.0 to 19.3]	137 [0 to 329]	55.4 [0 to 39.7]
	POR#1	136 [79.0 to 193]	12.1 [1.7 to 22.4]	286 [0 to 727]	11.2 [8.6 to 46.5]
	POR#4	162 [98.2 to 226]	9.0 [1.2 to 16.7]	191 [0 to 424]	18.0 [13.5 to 81.8]
	CYP3A4 R	1.2 [0.93 to 1.5]	2.7 [0.81 to 4.6]	231 [0 to 531]	0.44 [0.33 to 1.2]
	CYP3A4 LR	1.0 [0.68 to 1.4]	3.5 [0.43 to 6.6]	202 [0 to 511]	0.29 [0.21 to 1.4]

Substrates were incubated at different concentrations with microsomal fractions of HepaRG cells transduced with vector control (VC) or sgRNA POR#1, POR#4 or with bacterial membrane vesicles containing recombinant CYP2C8, CYP2C9 and CYP3A4 coexpressed with high (R) or low (LR) levels of POR. Following metabolite quantification by LC-MS/MS, kinetic parameters K_M and V_{max} were determined by Michaelis-Menten model or by substrate inhibition model, and K_i was determined by one site competition model. Internal clearance (Cl_{int}) was calculated using this equation: $Cl_{int} = \frac{V_{max}}{K_M}$. Results are shown with 95% CI (confidence interval) given in brackets. See Figure 20 for further details.

The effects of POR knockdown on kinetic parameters of amodiaquine N-deethylation were surprisingly small, reducing V_{max} by only 26 % (POR#1) and 13 % (POR#4), while substantial reductions in V_{max} were found for the other substrates (Table 8). Only for tolbutamide an increase in K_M (~ 2-fold) was observed, effectively reducing intrinsic clearance for CYP2C9 to about 5 % in HepaRG[-POR] compared to HepaRG[VC] cells. The kinetic measurements of the conversion of atorvastatin and midazolam by CYP3A4 both showed an approximately 4-fold decrease of V_{max} while K_M was not consistently affected.

To further investigate the insensitivity of amodiaquine N-deethylation towards POR knockdown, additional analyzes were made. Using the potent and specific CYP2C8 inhibitor montelukast (Walsky

et al. 2005) a similarly strong inhibition of amodiaquine N-deethylation in HepaRG[VC] and in both types of HepaRG[-POR] microsomes was found (Figure 21 with inhibition parameters summarized in Table 9), strongly supporting catalysis by CYP2C8. The phenomenon of increased IC_{50} at higher microsomal protein concentrations observed by Walsky et al. (2005) has been reproduced.
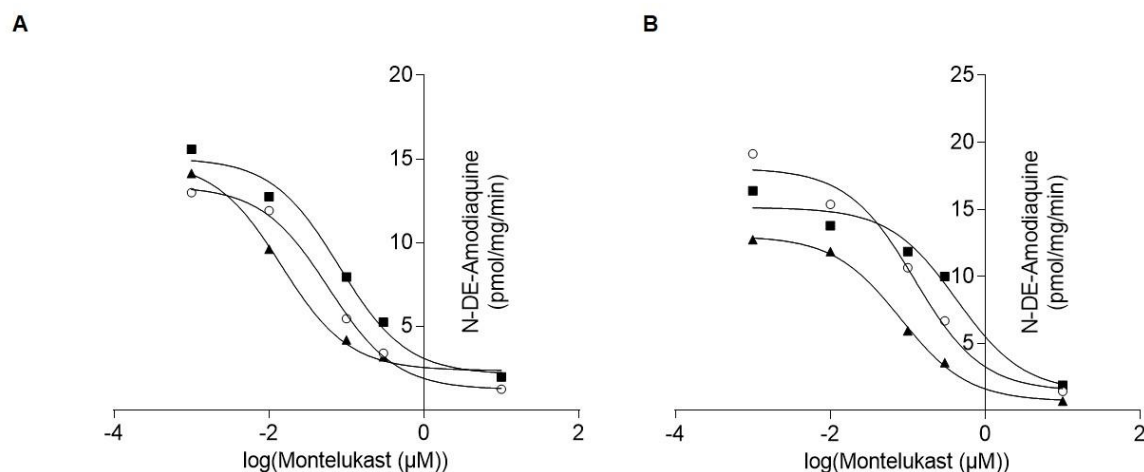
Figure 21: Inhibition of amodiaquine N-deethylation with montelukast in 2.5 µg (A) and 10 µg (B) of microsomal preparation. HepaRG cells transduced with vector control (VC, ■), sgRNAs POR#1 (▲) and POR#4 (○) were differentiated for three weeks and harvested for microsome preparation. Data were analyzed by one site competition model. Adapted from Heintze et al. 2021.

Table 9: Inhibition parameters of CYP2C8 mediated amodiaquine conversion by montelukast. Adapted from Heintze et al. 2021.

	VC	POR#1	POR#4	Liver microsomes (Walsky et al. 2005)
IC_{50} at 2.5 µM (µM) [95 % CI]	0.074 [0.043 to 0.127]	0.038 [0.012 to 0.124]	0.046 [0.029 to 0.073]	0.020 ± 0.002
IC_{50} at 10 µM (µM) [95 % CI]	0.393 [0,171 to 0,903]	0.084 [0.069 to 0.102]	0.103 [0,045 to 0.237]	0.072 ± 0.005
K_i at 2.5 µM (µM) [95 % CI]	0.057 [0.033 to 0.098]	0.030 [0.009 to 0.096]	0.036 [0.022 to 0.056]	0.014 ± 0.001
K_i at 10 µM (µM) [95 % CI]	0.178 [0.0775 to 0.410]	0.038 [0.031 to 0.046]	0.047 [0.020 to 0.107]	

As microsomal fractions of HepaRG cells contain multiple components that could influence CYP2C8 activity, a different system was chosen to test POR sensitivity of amodiaquine N-deethylation, namely commercially available bactosomes (Cypex Ltd.) which only express recombinant CYP2C8, CYP2C9 and CYP3A4 in combination with high or low levels of POR. For comparison to the HepaRG microsome system the same kinetic experiments as described above were performed (Figure 22).
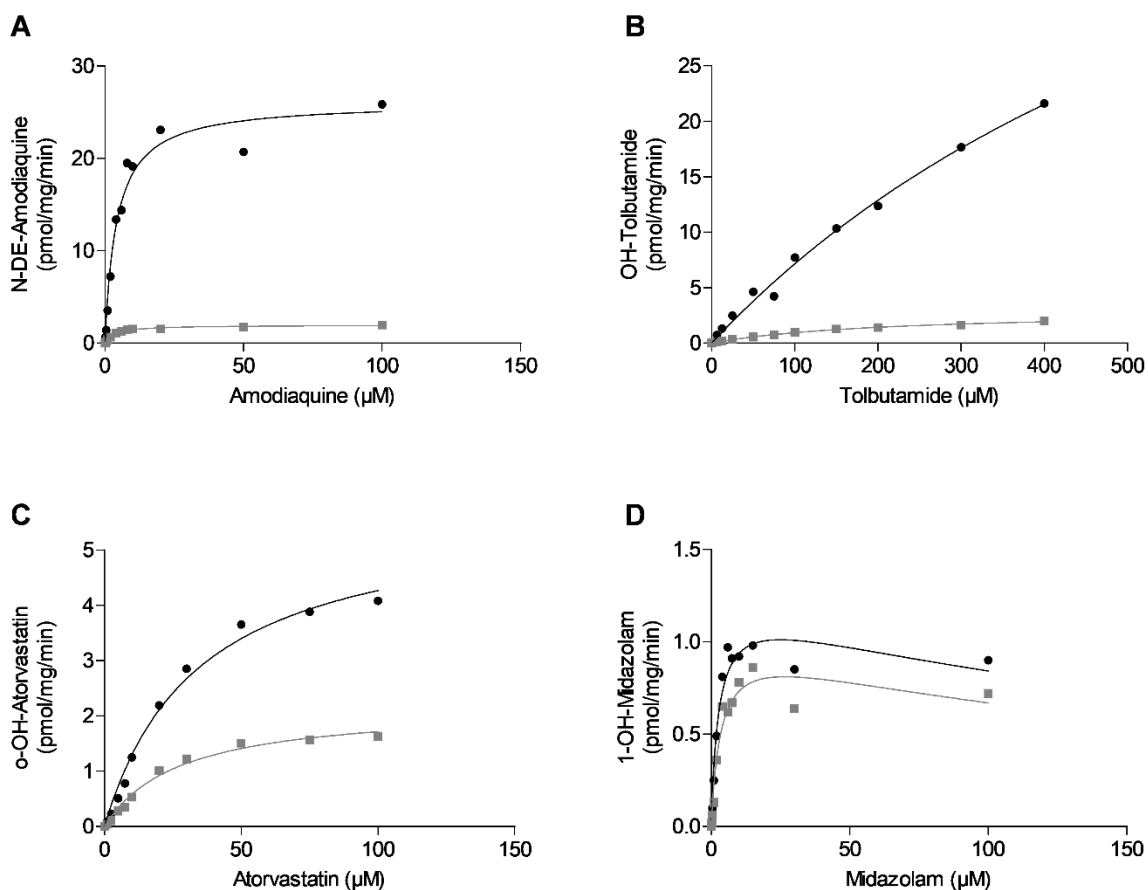
Figure 22: Kinetic analysis of selected substrate conversions in bactosomes containing recombinant CYP enzymes co-expressed with high (●) or low levels (■) of POR: (A) amodiaquine (CYP2C8); (B) tolbutamide (CYP2C9); (C) atorvastatin (CYP3A4); (D) midazolam (CYP3A4). Data were analyzed by Michaelis-Menten model (A-C) or by substrate inhibition model (D). Adapted from Heintze et al. 2021.

In this system amodiaquine N-deethylation was clearly POR-sensitive, suggesting that CYP2C8 may be supported by an alternative electron donor in HepaRG cells. The low sensitivity of midazolam conversion to the variable POR amount in this system is hypothesized to be due to its low conversion rate.

As a primary candidate for alternatively donating electrons to the CYPs the CYB5/CYB5 reductase system was obvious, which is lacking in the bacterial membrane vesicles but is expected to be expressed in HepaRG cells (Li et al. 2015). Leveraging the dependency of CYB5/CYB5 reductase on NADH rather than NADPH, comparative activity measurements in HepaRG[VC] and both types of HepaRG[-POR] microsomes by incubation with NADH, NADPH or both as cofactors were performed (see Figure 23).
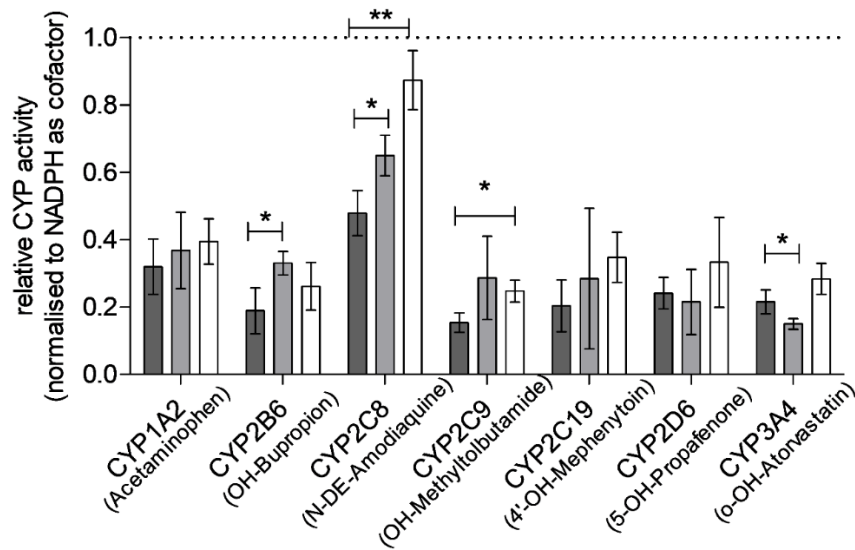
Figure 23: NAPDH/NADH dependent CYP-activities. Relative CYP-activities in microsomal preparations of differentiated HepaRG cells transduced with VC (dark grey), sgRNA POR#1 (light grey) and POR#4 (white) with either NADPH (set to 1.0) or NADH as cofactors. Results are means ± SD of 4 independent experiments. Statistical significance was assessed by unpaired t-test (*p < 0.05, **p < 0.01). Adapted from Heintze et al. 2021.

All seven CYP activities could be supported by NADH alone, albeit at a lower level (~15-50 % compared to NADPH; Figure 23). All differences of NADH- versus NADPH-supported activities were statistically significant (P < 0.05; two-way ANOVA with Bonferroni correction). Interestingly, CYP2C8 activity was least affected by the cofactor change (50 %) and in HepaRG^{-POR} microsomes NADH-dependent activity was significantly increased (POR#1, 65 %; POR#4, 87 %). Taken together these data suggest involvement of CYB5 in the various CYP activities, which seemed to be particularly strong for CYP2C8. To prove this assumption directly genetic *CYB5A* single- and *POR/CYB5A* double-knockout cells were created. These cells are described in chapter 3.3.

Effect of POR knockdown on CYP protein levels

The effects of POR knockdown on CYP protein expression quantified by western blotting in HepaRG[VC] as well as in both types of HepaRG[-POR] cells are summarized in Figure 24.
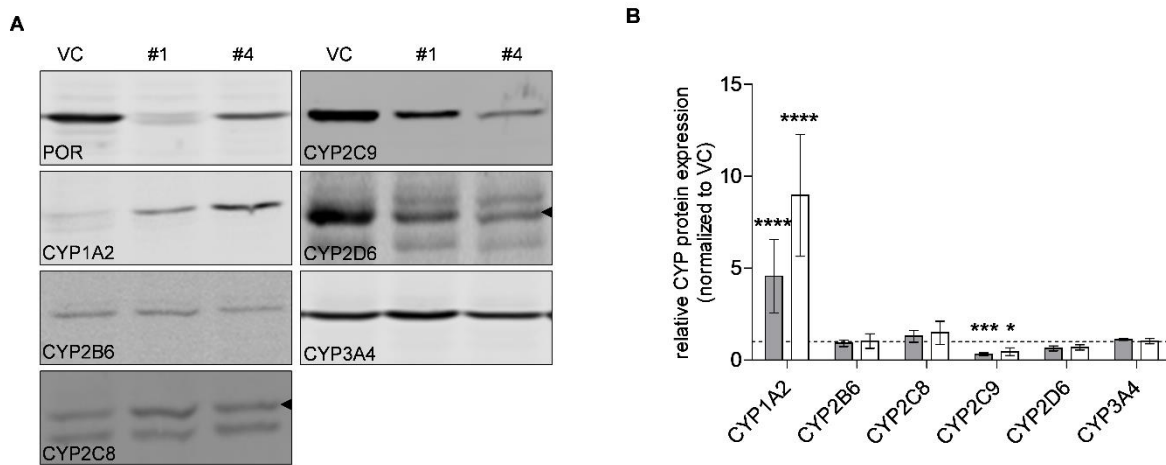
Figure 24: CYP protein expression analysis in HepaRG[-POR] microsomes. A: Exemplary western blots of microsomal fractions of HepaRG cells transduced with vector control (VC) or sgRNAs POR#1 or POR#4 after differentiation for three weeks (see Supplementary figure 2 for full blots). B: Protein expression data of CYP1A2, CYP2B6, CYP2C8, CYP2C9, CYP2D6 and CYP3A4 of 4 independent preparations (means ± SD) are shown relative to protein expression in VC (set to 1.0). Statistical significance was assessed by unpaired t-test. (*p < 0.05, **p < 0.01, ***p < 0.001, ****p < 0.0001). Adapted from Heintze et al. 2021.

CYP1A2 protein expression level was particulary strong increased by 4.5- and 9-fold for sgRNAs POR#1 and POR#4, respectively, while CYP2C9 and CYP2D6 were decreased by 50-70 % and 30-40 %, respectively. Protein expression of CYPs 2B6, 2C8 and 3A4 was not markedly changed by POR knockdown.

Effect of POR knockdown on gene expression

To investigate whether the differences on protein levels were due to mRNA expression changes, extended gene expression analysis was carried out using qRT-PCR on the Biomark HD System (Fluidigm). Figure 25 shows mRNA profiles of both types of HepaRG[-POR] cells in comparison to HepaRG[VC]. In addition to mRNA expression levels of the seven CYPs characterized by the LC-MS/MS cocktail assay, numerous other phase I and phase II drug/endogenous substrate metabolizing CYPs were analyzed for further characterization of the effect of POR knockdown in HepaRG cells.

CYPs and other Phase I Enzymes	POR#1	POR#4
POR	0.43***	0.23****
CYP1A1	3.48**	4.45*
CYP1A2	2.75*	3.13*
CYP1B1	0.99	0.99
CYP2A6	0.81	0.54**
CYP2B6	0.81	0.56**
CYP2B7	0.81	0.62*
CYP2C8	2.12	1.61
CYP2C9	0.70	0.37**
CYP2C19	1.02	0.86
CYP2D6	0.74	0.71*
CYP2E1	0.70*	0.32****
CYP3A4	1.05	0.91
CYP3A5	0.88*	0.60**
CYP3A7	1.07	0.56*
CYP4A11	0.91	0.57*
CYP7A1	0.83	0.28**
CYP8B1	0.69	0.38***
CYP27A1	1.13	1.00
CYP51	1.06	0.82*
DPYD	0.98	1.00

Phase II Enzymes	POR#1	POR#4
GSTA2	0.93	0.82
GSTM1	1.42	1.54
SULT1B1	0.85	0.78
SULT1E1	1.04	1.14
SULT2A1	0.77	0.84
UGT1A1	0.83	0.92
UGT1A3	0.89	0.86
UGT1A8	0.65	X
UGT1A9	0.89	0.88
UGT2B15	1.16	0.95
UGT2B4	1.16	0.57
UGT2B7	0.80	0.88

Transporters	POR#1	POR#4
MDR1	0.94	1.04
MRP2	0.83	0.89
MRP3	0.97	1.05
MRP4	0.88	1.13
OATP1B1	0.86	0.94
NPC2	1.00	1.01
NTCP	1.06	0.84
SLC22A7	0.69	0.46

Enzymes and Hemoproteins	POR#1	POR#4
ALDH3A1	1.01	1.02
CD36	0.99	0.62
CPT1A	0.85	1.01
CYB5A	1.14	0.68**
ELOVL6	1.06	0.92
FABP1	0.64	0.47
HMGCR	1.18	0.96
HMOX1	0.98	0.97
PGRMC1	1.07	0.87
PGRMC2	1.04	0.89
SCD	0.73*	0.49**

Fold Change: 1 2 3 4

Transcriptional Regulators	POR#1	POR#4
AHR	1.10	1.14
ARNT	1.03	0.99
CAR	0.69*	0.45**
Coup-TF1	1.11	0.94
Coup-TF2	1.19	0.78
CREBBP	0.95	0.90
EGR1	1.09	1.03
FOS	1.49	1.01
FOXO1	0.96	0.97
FXR	0.92	0.63***
GR	1.15	0.92
HNF1A	1.08	0.67
HNF4A	0.83	0.89
INSIG1	0.72	0.62
INSIG2	0.87	1.06
JUN	0.95	1.03
LRH-1	0.92*	0.69**
LXRa	0.93	0.64***
NUR77	1.07	1.28
PPARA	1.05	0.80*
PPARG	1.03	0.99
PXR	0.91*	0.57***
Rev-ErbAa	1.07	0.96
Rev-ErbAb	1.15	1.01
RXRA	1.02*	0.88*
SHP	0.84	1.18
SREBF1	0.82	0.63
SREBF2	1.01	1.02
VDR	1.22	1.22

Figure 25: Gene expression analysis in HepaRG^{-POR} cell lysates. Gene expression analysis of HepaRG cells transduced with sgRNAs POR#1 and POR#4 and vector control (VC) and differentiated for two weeks was performed by qPCR. The expression of the indicated genes of different classes is shown as fold-changes relative to VC and represented as heat map (colour code indicated below). Data of 6 independent experiments were normalized to the geometric mean of GAPDH, RPLP0 and ACTB. Statistical significance was assessed by paired t-test versus VC (*$p < 0.05$, **$p < 0.01$, ***$p < 0.001$, ****$p < 0.0001$).

Moreover, mRNA expression levels showed strongly CYP isozyme-dependent effects of POR knockdown. For CYPs 2B6 and 2C9 mRNA levels were decreased with generally stronger effects seen for sgRNA POR#4, in agreement with the CYP2C9 protein data. The strong induction of CYP1A2 protein expression was confirmed by an up to 3.13-fold increase of CYP1A2 mRNA level. Higher mRNA levels of CYP2C8 as well as unchanged levels of CYP3A4 mRNA were also in good agreement with the protein data.

For all additional measured drug-metabolizing CYP enzymes (CYP2A6, 2B7, 2E1, 3A5 and 3A7) a decrease in mRNA expression was observed with generally stronger effects seen for sgRNA#4. Increased mRNA expression among the phase I enzymes was only observed for CYP1A1 and CYP1A2. In addition to CYP2E1 and CYP2C9, the two CYP isozymes CYP7A1 and CYP8B1, involved in the bile acid synthesis, were among the four strongest decreased CYP enzymes. In contrast, mRNA expression of CYP27A1, which catalyses the first step of the alternative bile acid synthesis pathway, was not affected by POR knockdown. mRNA expression levels of two further important CYPs involved in lipid and cholesterol biosynthesis, CYP4A11 and CYP51, respectively, was also decreased, although only significantly in HepaRG$^{-POR\#4}$ cells.

Furthermore, the expression levels of a broad spectrum of other genes were determined in both types of HepaRG^{-POR} cells compared to HepaRG^{VC} cells. Generally, both sgRNAs influenced gene expression in the same direction, although somewhat stronger effects were seen in HepaRG$^{-POR\#4}$ cells. The

different target positions of sgRNAs POR#1 and POR#4 in the *POR* gene may be causal to this effect (Figure 15). Double-strand breaks induced by sgRNA POR#1 may therefore lead to 5' truncated but still active protein while genome editing using sgRNA POR#4 resulted in defect POR.

Phase II enzymes, as well as transporters were generally less strongly affected by POR knockdown compared to CYP genes and no significant effects were observed. In addition to CYP4A11, two genes involved in fatty acid processing, namely stearoyl-CoA desaturase (SCD) and cytochrome b5 (CYB5), which is a required cofactor for several fatty acid desaturase reactions were significantly downregulated. Furthermore, expression of the fatty acid binding protein (FABP1) was strongly reduced, but this difference was not statistically significant.

Additionally, several consistent patterns of expression changes for transcriptional regulators were observed. Thus, several regulators of hepatic CYP expression were consistently downregulated in both HepaRG^{-POR} cell lines, including CAR, FXR, LXRα, PPARα, PXR and RXR. By contrast, AHR/ARNT as transcriptional components of the Ah receptor pathway, which regulates CYPs 1A1/1A2, were not changed significantly. LRH-1 as regulator involved in sterol signaling was downregulated significantly. Sterol regulatory element binding transcription factor 1 (SREBF1), as another transcription factor involved in lipid homeostasis and sterol biosynthesis had a non-significantly decreased mRNA expression.

Effect of POR knockdown on bile acid synthesis

Essential steps of bile acid synthesis strongly depend on POR, particularly via the microsomal activities of CYPs 7A1, 7B1 and 8B1. As a strong decrease of CYP7A1 and CYP8B1 mRNA expression in HepaRG^{-}^{POR} cells was observed, changes in bile acid secretion to the culture medium were expected. Therefore, differentiated HepaRG^{VC} and both types of HepaRG^{-POR} cells were cultivated for 48 h without serum supplementation. Bile acids were quantified in the medium by ESI LC-MS/MS (Figure 26).
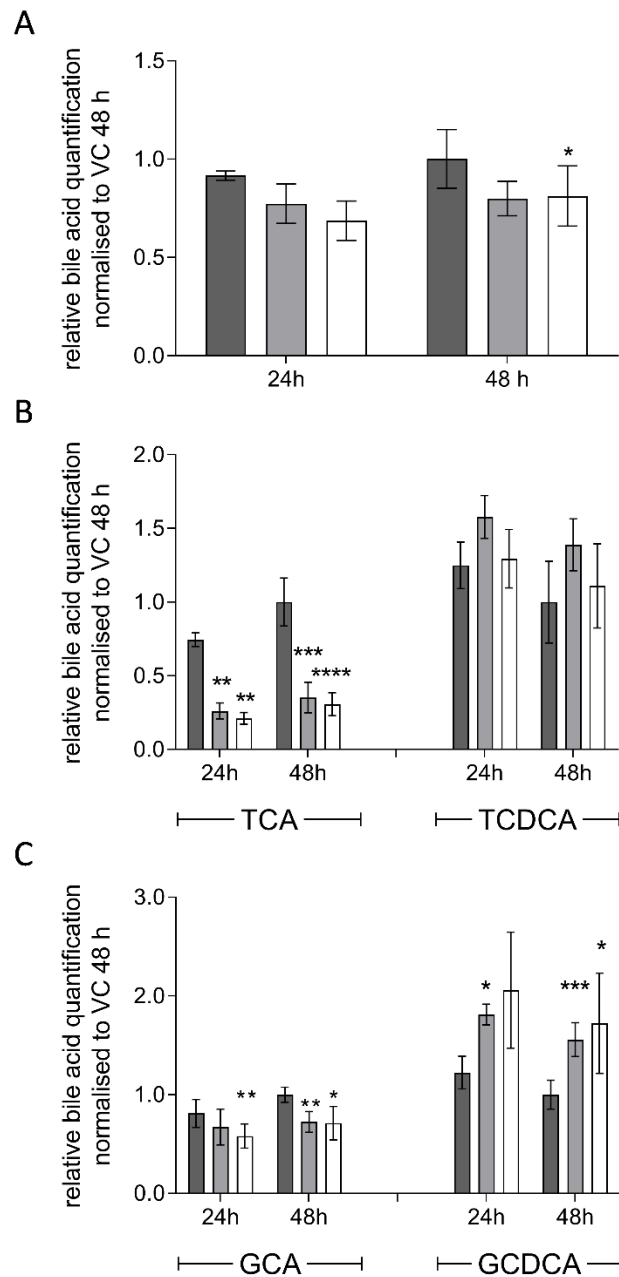
Figure 26: Bile acid secretion in HepaRG cells. Relative bile acid secretion into medium of HepaRG cells transduced with vector control (dark grey) or sgRNAs POR#1 (light grey) and POR#4 (white) and differentiated for two weeks was analyzed 24h and 48h after serum depletion by ESI LC-MS/MS. Respective bile acid amount secreted by HepaRG^{VC} cells at 48h was set to 1. A: Sum of all bile acids measured: cholic acid, chenodesoxycholic acid, taurocholic acid (TCA), glycocholic acid (GCA), taurochenodesoxycholic acid (TCDCA), glycochenodesoxycholic acid (GCDCA). B: Secretion of TCA and TCDCA; C: GCA and GCDCA. Means and SD of 3-7 independent measurements are shown. Statistical significance was assessed by Two-Way Anova with Bonferroni correction (*p < 0.05, **p < 0.01).

Indeed, global bile acid secretion into the culture medium was slightly decreased in both types of HepaRG^{-POR} cells compared to HepaRG^{VC} (Figure 26, A). More detailed analysis of the individual bile acids revealed a pronounced decrease of taurocholic acid (TCA) secretion by up to 70 % of both HepaRG^{-POR} cells (Figure 26, B). In contrast to HepaRG^{VC} cells, which further accumulated TCA in the medium (see values for 24 h and 48 h in Figure 26), no further increase was seen in the media of HepaRG^{-POR} cells. Taurochenodesoxycholic acid (TCDCA) secretion was not decreased by POR knockdown but seemed to be slightly increased, albeit not statistically significant.

In agreement with other reports (Burban et al. 2019), glycin-conjugated bile acids were found at much lower levels (glycin-conjugated bile acids: 4-6 pmol/ml, tauro-conjugated bile acids: 14-30 pmol/ml). While GCA secretion was not changed by POR knockdown, GCDCA secretion was significantly increased in both HepaRG^{-POR} cells (Figure 26, C).

3.2.5. Delivery of sgRNAs using lipofection

As the lentiviral delivery of CRISPR components (Cas9, tracrRNA and crRNAs) is very time consuming and the delivery via RNP complexes resulted in only ~25 % of mutated cells (see Table 7) a different delivery method was investigated. HepaRG cells are hard to transfect with plasmids (Laurent et al. 2010), but transfection of siRNAs by lipofection has been shown to be highly successful (Rieger et al. 2015; Kugler et al. 2020).

Therefore, transfection of sgRNAs consisting of complexed tracrRNA and crRNA in Cas9-expressing HepaRG cells is a promising strategy to achieve CRIPSR/Cas9-mediated genome editing. Atto550-labled tracrRNA (Integrated DNA technologies) was used for transfection in Cas9-expressing undiffernentiated HepaRG^{VC} cells, as the fluorescent marker allows monitoring of transfection efficiency. sgRNA POR#1 was used for optimization of reverse transfection conditions using 1.2 µl /500 µl Lipofectamine RNAiMax (Thermo Fisher Scientific) (Figure 27). The T7E1 assay was used to verify genome editing.
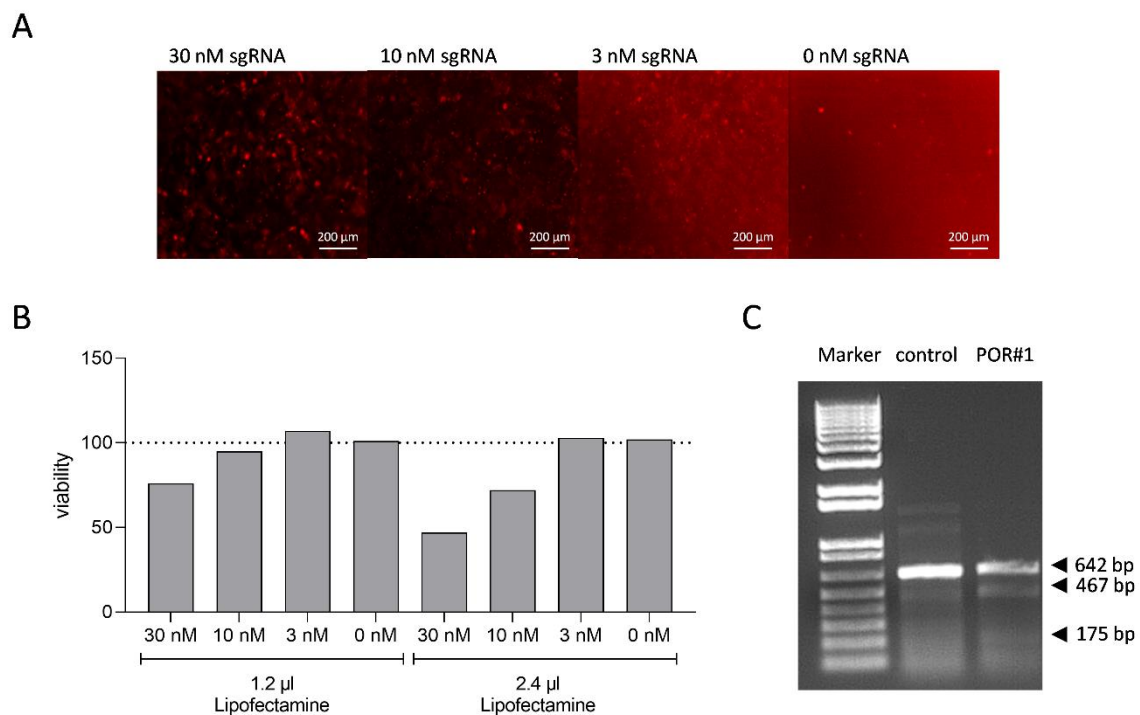
Figure 27: Optimization of transfection conditions. HepaRG^{VC} cells were reverse transfected with sgRNA POR#1 in a concentration range (0-30 nM) and two concentrations of lipofectamine RNAiMax (1.2 and 2.4 µl/500 µl) A: Fluorescent microscopic evaluation of transfection conditions using 1.2 µl/500 µl lipofectamine RNAiMax. Scale: 200 µm. B: Cell viability at 96 h post transfection using the alamarBlue assay (Thermo Fisher Scientific), n=1. C: T7E1 assay in HepaRG^{VC} cells. DNA Marker: 1 Kb Plus DNA Ladder (Thermo Fisher Scientific); control: untransfected HepaRG^{VC}; POR#1 transfected with 30 nM sgRNA POR#1 and 1.2 µl/500 µl lipofectamine RNAiMax.

Transfection efficiency correlated with amount of sgRNA used (Figure 27, A), while viability reversly correlated with concentration of sgRNA and Lipofectamine RNAiMax used (Figure 27, B). Concentration of 30 nM sgRNA at a Lipofectamine RNAiMax concentration of 1.2 µl /500 µl was found to be most efficient and not overly harmful to the cells. The T7E1 assay verified genome editing at the predicted target site (Figure 27, C).

For CRISPR/Cas9-mediated genome editing using sgRNA delivery at other target genes, several sgRNAs targeting *CYB5A*, *CYP2C8*, *CYP3A4*, and *CYP27A1* were designed using the online sgRNA design tool CHOPCHOP (Figure 28 and Table 10).
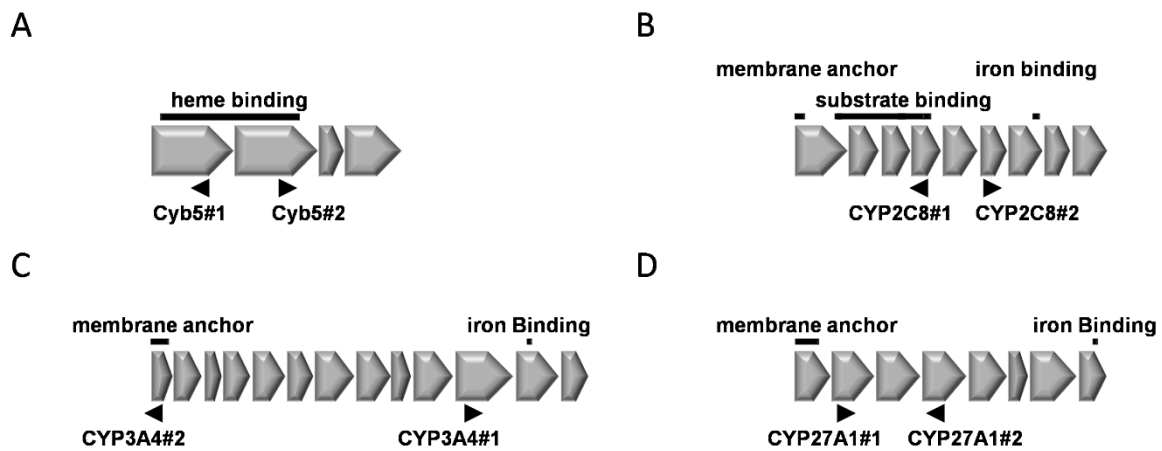

Figure 28: Location of sgRNAs relative to exon structures of *CYB5A, CYP2C8, CYP3A4* and *CYP27A1* A: *CYB5A* exon structure (gene chr18:74,250,846-74,292,016; GRCh38/hg38) indicating 4 translated exons as well as the binding region (black) for heme. B: *CYP2C8* exon structure (gene chr10:95,036,772-95,069,497; GRCh38/hg38) indicating 9 translated exons as well as the N-terminal transmembrane region and binding regions for substrates and iron (black) C: *CYP3A4* exon structure (chr7:99,756,960-99,784,248; GRCh38/hg38) indicating 13 translated exons as well as the N-terminal transmembrane region and iron binding region (black). D: *CYP27A1* exon structure (chr2:218,781,733-218,815,293; GRCh38/hg38) indicating 8 translated exons as well as the N-terminal transmembrane region and iron binding region (black). The positions of two sgRNAs per gene are indicated by arrows.

Table 10: sgRNAs targeting *CYB5A*, *CYP2C8*, *CYP3A4* and *CYP27A1* (PAM sequence in red).

Name	Sequenz	Rank CHOPCHOP (efficiency score)	Exon
Cyb5#1	5'- AATCGTACACCTTGTGGTGCAGG-3'	1 (46.71)	2
Cyb5#2	5'-TCGGGCACTCTACAGATGCCAGG-3'	4 (53.63)	1
CYP2C8#1	5'-CAAAATTCCGCAAGGTTGTGAGG-3'	1 (53.50)	4
CYP2C8#2	5'-TCTTACACGAAGTTACATTAGGG-3'	3 (50.04)	6
CYP3A4#1	5'-GATGTTCATTCCCAAAGGGGTGG-3'	3 (63.74)	11
CYP3A4#2	5'-AGGTTTCCATGGCCAAGTCTGGG-3'	11 (52.59)	1
CYP27A1#1	5'-GTACCCAGTACGGAACGACATGG-3'	1 (67.37)	2
CYP27A1#2	5'-TAACCCGATGGATCTGACGAAGG-3'	5 (71.13)	4

For further verification of the transfection protocol undifferentiated HepaRG^{VC} cells were transfected with sgRNAs CYP2C8#1 and #2 and CYP3A4#1 and #2 which were Atto550 labelled at the tracrRNA. 24 h after transfection, cells were analyzed using flow cytometry (see Figure 29). After additional 96 h cells were harvested for verification of genome editing using T7E1 assayas described in chapter 7.1.5. The specific primers are listed in Table 16 and Table 17.
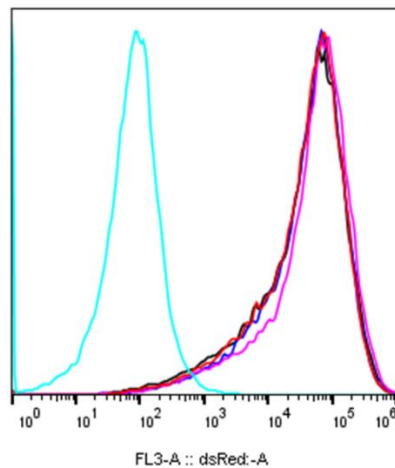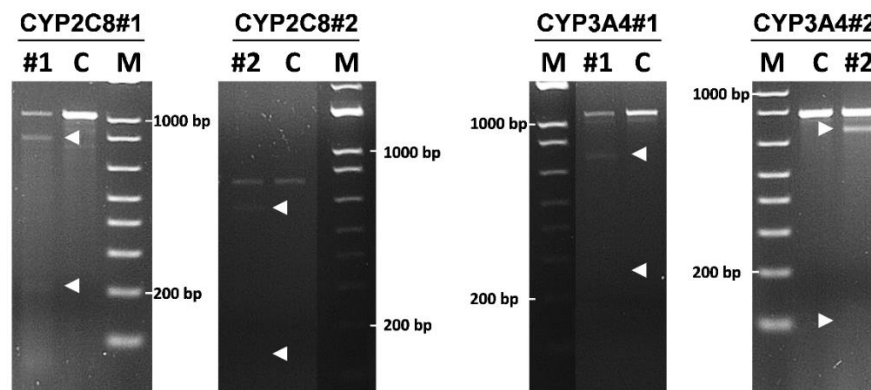
Figure 29: **Validation of sgRNA transfection protocol with new targets.** HepaRG[VC] cells were transfected with Atto550 labelled sgRNAs CYP2C8#1 and #2 and CYP3A4#1 and #2. A: Analysis of transfection efficiency using flow cytometry after 24 h, turquoise line: untransfected cells. B: T7E1 assay sgRNA target regions. Predicted fragments are indicated with white arrows. Lane #1 or #2 contain fragments of transfected cells, Lane C contains untransfected cells, lane M contains the 1 Kb Plus DNA Ladder (Thermo Fisher Scientific). Predicted fragment sizes are listed below the gel pictures.

Flow cytometric analysis of sgRNA transfection revealed rather high transfection efficiencies of over 95 % (Figure 29, A). Therefore, further sorting of fluorescent cells was not necessary any more. In addition, as shown in (Figure 29, B), genome editing is observed for all tested sgRNAs with the present transfection protocol. Thus, this novel protocol could be applied immediately and effectively to any target.

3.3. Genetic single and double knockout of *CYB5A* in HepaRG

The diverse CYP activity analyzes in POR knockdown HepaRG cells described in chapter 3.2.4 indicated an involvement of CYB5 in various CYP activities, especially in CYP2C8-catalyzed amodiaquine deethylation. In order to substantiate this conclusion, using the previously described protocol (chapter 3.2.5) genetic *CYB5A* single- and and *POR/CYB5A* double-knockout HepaRG cell lines were generated by transfecting HepaRG^{VC} and both types of HepaRG^{-POR} cells with a combination of two sgRNAs targeting *CYB5A* (see Table 10).

3.3.1. Characterization of genetic single- and double-knockout of *CYB5A*

Validation of the genetic *CYB5A* single and- and *POR/CYB5A* double-knockout was performed by mRNA and protein expression measurements (Figure 30).
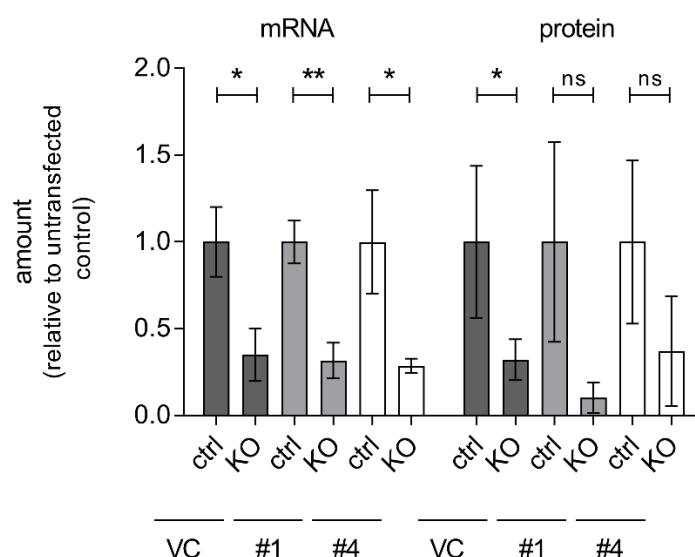
Figure 30: Genetic *CYB5A* single- and *POR/CYB5A* double-knockout in transduced HepaRG cells. CYB5 mRNA and protein expression in transduced differentiated HepaRG cells quantified in cell lysates (ctrl: untransfected control cells, KO: cells transfected with sgRNAs targeting *CYB5A*). Mean levels are shown relative to vector control (VC) set at 1 with SD bars (dark grey: VC, light grey: POR#1, white: POR#4). Results are means ± SD of three independent experiments. Statistical significance was assessed by unpaired t-test. Adapted from Heintze et al. 2021.

Characterization of genetic *CYB5A* knockout cells following differentiation revealed 50 % knockdown of CYB5 at the mRNA level and ~60 to 90 % knockdown at the protein level.

3.3.2. Impact of CYB5 knockdown on CYP activities

Effects of the CYB5 single- and POR/CYB5 double-knockdown on CYP activities in differentiated cells were measured using the LC-MS/MS CYP cocktail assay (Figure 31).
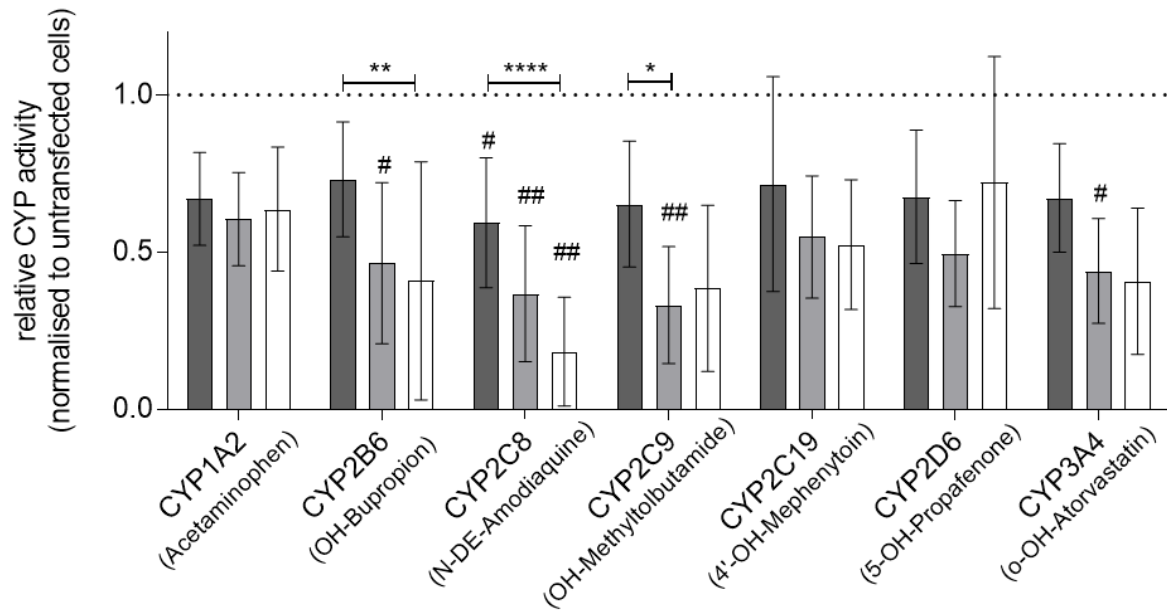
Figure 31: Effect of CYB5 knockdown on CYP activities. Enzyme activities of seven CYP enzymes were determined simultaneously by cocktail LC-MS/MS assay in CYB5/POR double-knockdown in VC (dark grey), sgRNA POR#1 (light grey) and POR#4 (white) cells. Results are means ± SD of three independent experiments. Statistical significance was assessed by repeated measurements ANOVA with Bonferroni correction (*/#$p < 0.05$, **/##$p < 0.01$, ***$p < 0.001$, ****$p < 0.0001$), # markers significant changes compared to untransfected HepaRG[VC] cells, * markers significant changes compared to HepaRG[VC] with CYB5 knockdown. Adapted from Heintze et al. 2021.

Although the CYB5 knockdown seemed to decrease all seven CYP activities by 20-40 %, only the strongest difference seen for CYP2C8-dependent amodiaquine N-deethylase activity was statistically significant. Most activities were further diminished in the double-knockdown cells, again most profoundly for CYP2C8 activity. Taken together, these and the former NADPH/NADH experiments (Figure 23) indicate that several of the human CYP enzyme activities tested for were markedly influenced by the CYB5 electron donor system and that amodiaquine N-deethylation showed a particularly strong dependence on CYB5 with accordingly less dependence on POR.

3.4. Genetic single- and double-knockout of *CYP27A1* in HepaRG

Analysis of secreted bile acids in HepaRG POR knockdown cells indicate an increase in alternative bile acid synthesis. As CYP27A1 catalyses the first step of the alternative bile acid synthesis, specific CRISPR/Cas9 mediated knockout of CYP27A1 could substantiate this. Therefore, using the previously described protocol (chapter 3.2.5) genetic *CYP27A1* single- and *POR/CYP27A1* double-knockout HepaRG cell lines were generated by transfecting undifferentiated HepaRG[VC] and both types of HepaRG[-POR] cells with a combination of two sgRNAs targeting *CYP27A1* (see Table 10).

3.4.1. Characterization of single- and double-knockout of *CYP27A1*

For verification of CRISPR/Cas9 induced double-strand breaks T7E1 digest was performed at sgRNA CYP27A1#1 and #2 target sites (Figure 32). The specific primers are listed in Table 18.

Test region	Undigested Fragment	Fragment 1	Fragment 2
CYP27A1#1	1050 bp	671 bp	379 bp
CYP27A1#2	815 bp	568 bp	247 bp
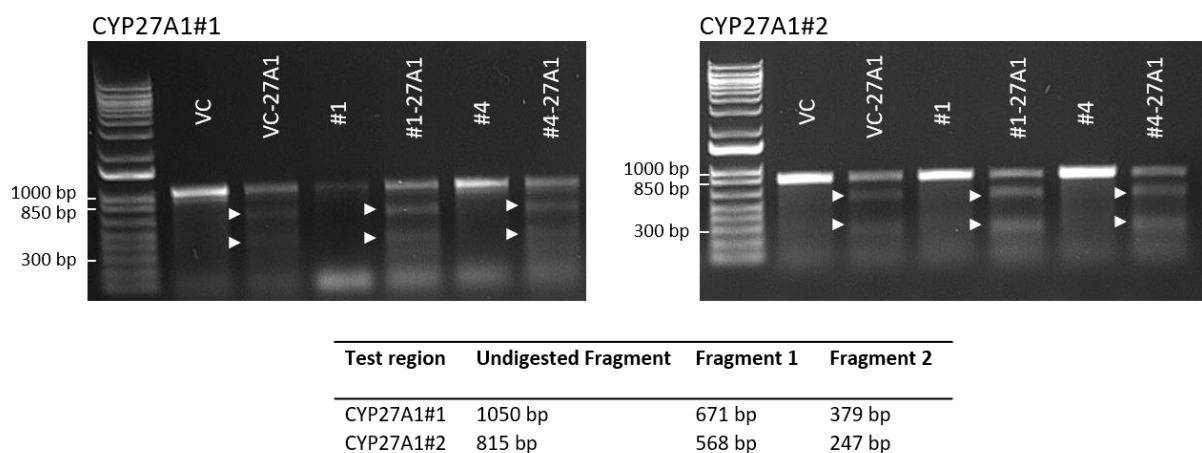
Figure 32: Verification of *CYP27A1* knockout in HepaRG cells. T7E1 digest of DNA of transduced HepaRG cells. CYP27A1#1: digest products of test region CYP27A1#1, CYP27A1#2: digest products of test region CYP27A1#2. Left lanes DNA marker (1 Kb Plus DNA Ladder, Thermo Fisher Scientific); VC: vector control; #1: sgRNA POR#1; #4: sgRNA POR#4; -27A1: transfected with sgRNAs targeting CYP27A1. Digested fragments are marked with white arrows. The expected fragment sizes are summarized below the gel pictures.

As despiced in Figure 32, DNA double-strand breaks could be detected for both sgRNAs in all transfected cell lines. Characterization of the resulting genetic *CYP27A1* single- and *POR/CYP27A1* double-knockout cells was done by mRNA expression measurement.
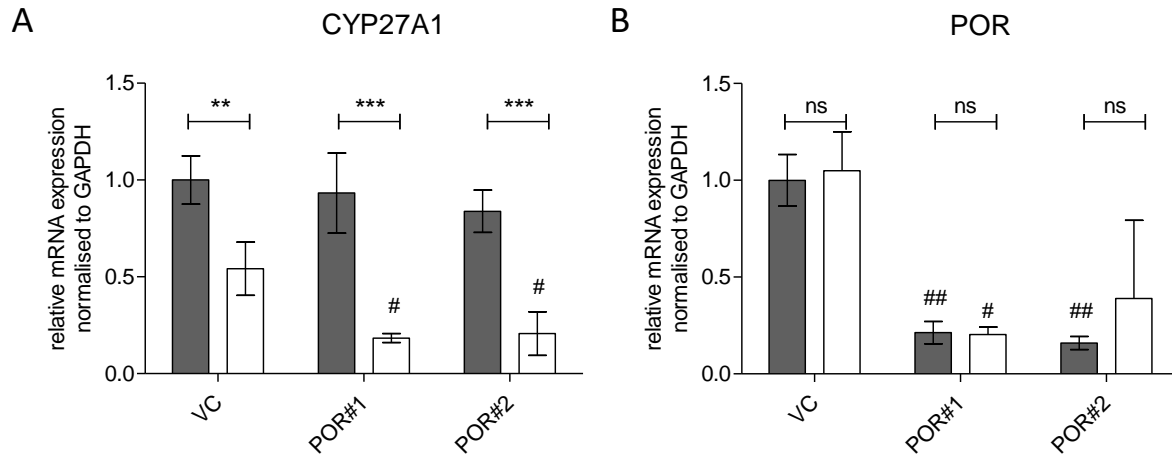
Figure 33: mRNA expression of CYP27A1 and POR in *CYP27A1* single- and *POR/CYP27A1* double-knockout HepaRG cells. CYP27A1 (A) and POR (B) mRNA expression measured in HepaRG[VC] and both types of HepaRG[-POR] cells transfected with two sgRNAs targeting CYP27A1. Untransfected cells are depicted as grey bars, CYP27A1 knockdown cells as white bars. Means and SD of 3 independent measurements are shown. Statistical significance was assessed by Two-Way Anova with Bonferroni correction (*/#$p < 0.05$, **/##$p < 0.01$); * describes differences to untransfected cells, # describes differences to HepaRG[VC].

Transfection of sgRNAs resulted in a significant knockdown of CYP27A1 mRNA expression of 50 % in HepaRG[VC] cells and up to 80 % in both types of HepaRG[-POR] cells (Figure 33, A). mRNA expression of POR was not influenced by CYP27A1 knockdown (Figure 33, B).

3.4.2. Impact of CYP27A1 knockdown on bile acid synthesis

The knockdown of CYP27A1 knockdown is expected severely affect bile homeostasis, as it catalyses the first step of the alternative bile acid synthesis. Secreted bile acids were quantified 48 h after serum depletion in the cell medium by ESI LC-MS/MS (Figure 34).
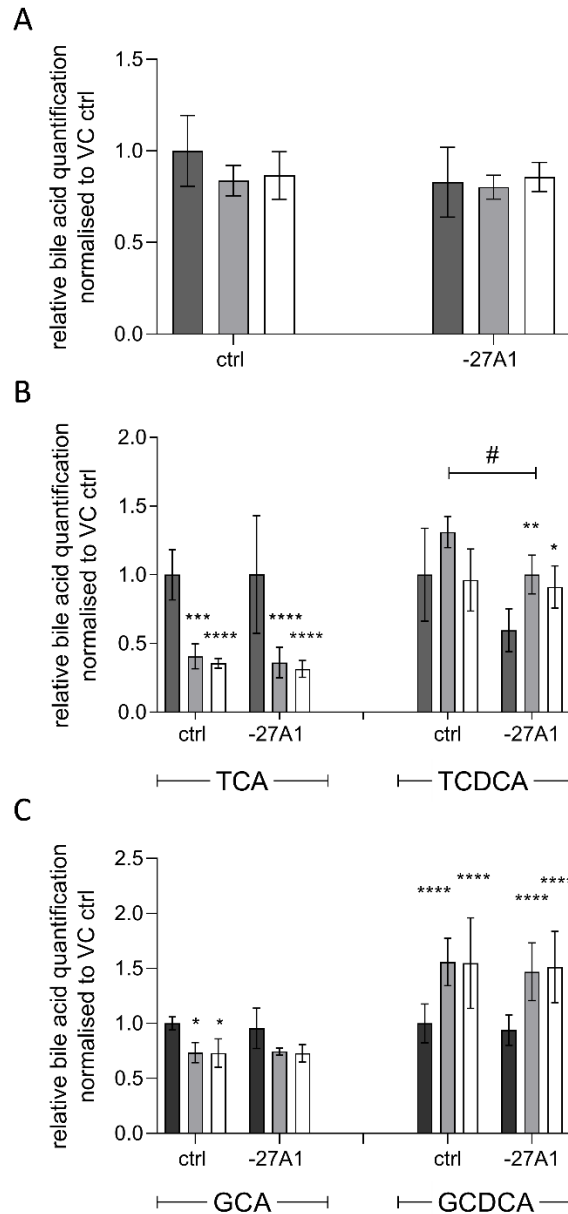
Figure 34: Effects of CYP27A1 single- and POR/CYP27A1 double-knockdown on bile homeostasis. Relative bile acid secretion into medium of differentiated HepaRG[VC] (dark grey) and both types of HepaRG[-POR] cells (light grey: POR#1, white POR#4) with or without transfection (ctrl) with sgRNAs targeting CYP27A1 (-27A1). Bile acids were quantified 48h after serum depletion by ESI LC-MS/MS. Respective bile acid amount secreted by HepaRG[VC] cells at 48h was set to 1. A: Sum of all bile acids measured: cholic acid, chenodesoxycholic acid, taurocholic acid (TCA), glycocholic acid (GCA), taurochenodesoxycholic acid (TCDCA), glycochenodesoxycholic acid (GCDCA). B: Secretion of TCA and TCDCA and C: GCA and GCDCA. Means and SD of 5 independent measurements are shown. Statistical significance was assessed by Two-Way Anova with Bonferroni correction (*p < 0.05, **p < 0.01). # describes differences to untransfected cells, * describes differences to HepaRGVC.

CYP27A1 knockdown had no significant effect on global bile acid synthesis. A more detailed analysis of individual single bile acids revealed no effects of CYP27A1 knockdown on CA derivates. However, significant effects were observed in HepaRG[-POR#1] cells for TCDCA.

Por knockout in mice leads to the hepatic accumulation of lipid droplets cells (Henderson et al. 2003; Gu et al. 2003; Porter et al. 2011). This was ascribed to various changes of bile acid homeostasis, with CDCA conjugates as most effective regulators (Porter et al. 2011; Chiang and Ferrell 2018). Therefore,

intracellular lipid droplet accumulation was assessed in CYP27A1 single- and POR/CYP27A1 double-knockdown cells by nile red staining after serum depletion for 48 h (Figure 35).
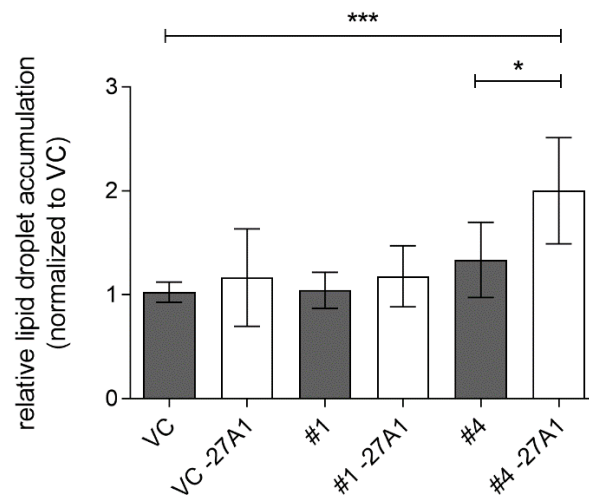
Figure 35: Effects of CYP27A1 single- and POR/CYP27A1 double-knockdown on lipid droplets. Relative lipid accumulation in differentiated HepaRG[VC] (dark grey) and both types of HepaRG[-POR] cells (light grey: POR#1, white POR#4) with or without transfection with sgRNAs targeting CYP27A1 (-27A1). Lipid accumulation stained with nile red after 48 h of serum depletion was set to 1. Means and SD of 5 independent measurements are shown. Statistical significance was assessed by One-Way Anova with Bonferroni correction (*p < 0.05, ***p < 0.001).

There was a slight increase of lipid droplets observable in HepaRG[-POR#4] cells, however, this effect was not statistically significant. Additional CYP27A1 knockdown significantly increased lipid droplet formation in these cells.

4. Discussion

The application of genome editing methods to study human ADME processes has been limited by the availability of only a few cell models that reliably reflect relevant liver functions. HepaRG cells are a suitable human model for ADME research and toxicity studies, as they express multiple CYP activities and reflect several regulatory pathways at levels and dynamic features comparable to primary human hepatocytes. In this thesis the requirements for CRISPR/Cas9-mediated genome editing in HepaRG cells were systematically investigated. Due to their non-clonal origin as well as the required differentiation process to develop hepatic properties, it was first necessary to study whether clonal HepaRG cells show a comparable phenotype to the parental non-clonal cells. For delivery of the CRISPR/Cas9 system in the hard to transfect cells, protocols uing RNPs, lentiviral particles and transfection of sgRNAs into Cas9 expressing HepaRG cells were then established and compared.

As a first target for CRISPR-induced gene knockout using a lentiviral delivery approach POR was chosen in order to investigate the influence of POR on drug and endogenous metabolism in the HepaRG cell model. Additional knockout experiments of CYB5 and CYP27A1 using transfection of sgRNAs into Cas9 expressing HepaRG cells were performed to further analyze the impact of CYB5 as alternative electron donor for POR and the involvement of POR and CYP27A1 in bile and lipid homeostasis.

4.1. Generation of clonal HepaRG cell lines

HepaRG cells consist of a heterogeneous, non-clonal mixture of cells isolated of a hepatocellular carcinoma of a female patient with the unique ability to differentiate into biliary- and hepatocyte-like cells (Gripon et al. 2002). While first studies about HepaRG concluded a clonal character due to a homogenous morphology after clonal selection (Parent et al. 2004), more recent publications using clonal HepaRG cells indicate the necessity of selection of a clonal HepaRG cell line with hepatocyte-specific properties (Brayman et al. 2014; Bucher et al. 2018).

Especially for application of genome editing methods like the CRISPR/Cas9 system, cell lines with a stable phenotype after clonal selection are needed. Therefore, a study was initiated to characterize the phenotype of clonal HepaRG cells (chapter 3.1).

Growth behavior and morphology of undifferentiated F_1 clonal HepaRG cells (Figure 7) were comparable to the parental cell line, initially confirming the findings of a homogenous morphology after selection as described in Parent et al. (2004). However, a more thorough analysis of morphology and CYP activities after differentiation revealed a more diverse picture. Only around 16 % of HepaRG F_1 clones retained their parental phenotype, characterized by the dual cell morphology and increased CYP2C9 activities after differentiation. The majority of clones seemed to have lost their differentiation potential. Standard differentiation conditions of 2 % DMSO treatment for two weeks did not result in differentiation into hepatocyte-like and biliary cell types with increased CYP activities, but was harmful to the cells. It is hypothesized, that changes in the differentiation protocol may result in differentiation for certain clones. The fact that the H6 clonal cell line needed an adapted freezing medium (40 % medium, 50 % FCS, 10 % DMSO) (data not shown) emphasizes this possibility.

Activity measurements of a panel of seven drug-metabolizing CYP enzymes by a LC-MS/MS cocktail assay additionally revealed that differentiated individual F_1 clones not only have different CYP activity

levels (Figure 11), but also differ in the CYP inducibility by DMSO (Figure 13). This highlights the need to characterize each F_1 clone thoroughly.

While previous publications using clonal HepaRG cells for genome editing methods also characterized selected F_1 clones regarding hepatocyte-specific properties before using them for clonal selection (Brayman et al. 2014; Bucher et al. 2018), they did not analyze whether clonal F_2 HepaRG cells would retain their differentiation potential. As a stable hepatic phenotype of the clonal F_2 HepaRG cells compared to the clonal F_1 cells is necessary for meaningful results in a genome editing experiment, this question has to be considered. Therefore, three clonal F_1 HepaRG cells were separated to single cells again and characterized with respect to CYP2C9 activity and morphology. Results indicated that F_2 clones had a higher percentage of clones with differentiated HepaRG-like morphologies compared to the clones of the parental cell line. This was mirrored by the decrease in the number of clones with low activities.

While no homogeneous phenotype was detectable in clonal F_2 cells, the results suggest at least a slight stabilization of phenotype. For the investigation of effects of genome editing in cell clones, the individual clones are required to display a stable phenotype, which only depends on the corresponding genotype. For clonal F_1 HepaRG cells this is not guaranteed. Although it is reasonable to expect a stable phenotype to be selectable after several cloning generations, the unique ability of HepaRG cell lines to differentiate into two distinct cell types may prohibit such selection by consistently leading to populations with a broad spectrum of phenotypes.

It was concluded that the clonal selection of mutated HepaRG clones (clonal F_1 or parental cells) after CRISPR/Cas9-induced genome editing is not a feasible approach, as the resulting phenotype cannot be guaranteed to be due to the genome editinig. Therefore, other non-clonal approaches should be selected.

4.2. Genetic knockout of *POR* in HepaRG cells

4.2.1. sgRNA design and delivery methods

To establish a working protocol for CRIPSR/Cas9 induced genome editing in HepaRG cells, two major points had to be considered: The rational design of targeting sgRNAs and the proper delivery method (chapters 3.2.1, 3.2.3, 3.2.4 and 3.2.5).

sgRNAs vary strongly in efficiency, which complicates efficiency predictions made by sgRNA design tools. Factors influencing target efficiency are for instance the position of specific nucleotides in the target sequence (e.g. GC content), the accessibility of the target site, or the sequence of its flanking regions (Labun et al. 2019). Folding stability of the sgRNA also correlates strongly with target efficiency (Xu et al. 2017). For the four selected sgRNAs targeting various sites in the *POR* gene sgRNA POR#2 was predicted by the online sgRNA design tool CHOPCHOP to exhibit the highest target efficiency. This was not reflected by the determined cleavage and mutation percentage, where POR#3 was found to be most efficient, as predicted by the remaining sgRNA design tools. Differences between predicted and actual efficiencies could have numerous reasons. By choosing a specific sgRNA design tool one also chooses certain efficiency prediction models. Those can lead to different efficiency ranking as illustrated in Table 5. The experimental setup could also lead to differences in efficiency, as slightly different transfection efficiencies could lead to varying amounts of RNPs in the cells. For efficient genome editing using CRISPR/Cas9 it is therefore considered best practice to test various sgRNAs or use a multiplex approach.

Delivery of Cas9 and sgRNAs is possible by various methods: Encoded on DNA expression plasmids, as RNA molecules or as ribonucleoproteins. For each delivery form transfection is mandatory to integrate the components into the cells. HepaRG cells are usually kept in a proliferative state and then differentiated to hepatocyte-like cells by DMSO (Gripon et al. 2002). All delivery methods were performed in proliferating HepaRG cells, due to two reasons. First, transfection using lipofection methods or even nucleofection methods in undifferentiated cells is more efficient than in differentiated cells (Laurent et al. 2010). Secondly, proliferating genome-edited cells can be easily expanded and stored for further research.

As a first method for targeting Cas9 and sgRNA delivery transfection of RNPs was tested (chapter 3.2.3). RNP delivery not only limits exposure time of the cells towards Cas9 to a few hours, reducing off-target editing, but also mitigates the problem of transgene integration into host DNA, which can cause mutations (Araldi et al. 2020). Transfection of RNPs targeting three different sites in *POR* resulted in 25 % mutated cell clones. However, this was not deemed sufficient to decrease POR protein expression in the cell pool markedly. Individual edited clones were not analyzed any further, as the phenotype of specifically selected clonal HepaRG cells had been shown to be not sufficiently stable for the investigation of phenotype-genotype relations.

Therefore, a different Cas9/sgRNA delivery method using lentiviral particles was examined (chapter 3.2.4). Lentiviral transduction itself resulted in high transduction efficiencies. Coupled with subsequent antibiotic selection using puromycin cell populations with over 75 % Cas9-positive cells were generated. The cells closely resemble original HepaRG cells in their ability to differentiate to the dual morphology of hepatocyte-like cells surrounded by biliary-like cells and in their CYP expression profile, portrayed by correlation of gene expression and CYP activity profiles (Figure 18). In HepaRG cells

transduced with sgRNAs targeting *POR*, this led to a decrease in POR expression of 60-80 % with 10 % residual enzymatic activity. Lentiviral delivery is therefore an effective delivery method for Cas9 and the targeting sgRNA into HepaRG cells. The use of several sgRNAs targeting the same gene simultaneously may further increase knockdown efficiency, as it increases the probability of loss-of-function mutation introduction.

Lentiviral delivery of expression cassettes coding for Cas9 and sgRNA leads to their integration into the host genome resulting in stable expression of Cas9 and sgRNAs. Especially the radom integration of the expression cassettes makes this approach not completely predictable, as it increases the risk of off-target editing and adverse cellular responses (Kimberland et al. 2018; Araldi et al. 2020). Editing of predicted off-targets were excluded in case of sgRNA POR#4 using the T7E1 assay, but no unbiased whole genome off-target screening was performed. Using inducible expression systems, prolonged Cas9 expression can be prevented if necessary (Zhang et al. 2019).

Lentiviral transduction is a very time-consuming process, as it requires complex plasmid preparations, cloning, isolation and titration of viral particles, leading to the transduction of the target cell line. Therefore, transfection of sgRNAs in Cas9 expressing HepaRG cells was tested as further delivery approach in this thesis (chapter 3.2.5). While HepaRG cells are hard to transfect with large plasmids (Laurent et al. 2010), the transfection of siRNAs by lipofection has been reported to be successful (Rieger et al. 2015; Kugler et al. 2020) and therefore, transfection of the small sgRNAs should also be possible. A fluorescently labeled tracrRNA was used for monitoring of transfection efficiency. Using reverse transfection, efficiencies of over 95 % were achieved, i.e. further sorting of cells using flow cytometry was unnecessary as this procedure would additionally decrease viability of cells. Transfection of two targeting sgRNAs simultaneously resulted in an overall knockdown efficiency of 60-80 %. Multiplexing additional sgRNAs in combination to increase knockdown efficiency is also possible in this case. However, the major limiting factor was the Cas9-expressing cell line, where only 75 % of the cells were shown to express Cas9. This limitation may be addressed in future studies by utilisation of an improved Cas9-expressing HepaRG cell line. A possible approach to achieve improvement would be the use of Cas9-expressing lentiviral vectors with one antibiotic selection marker and an additional fluorescent maker, following the work of Zafra et al. (2018) and Jin et al. (2020) and thereby increasing overall Cas9 expression by enabling a subsequent second selection step using flow cytometry.

In conclusion, two effective working protocols for CRISPR/Cas9-induced genome editing in HepaRG cells were established in this thesis. First, lentiviral delivery of Cas9 and sgRNA was shown to be an effective approach for genome editing in HepaRG cells. And second, transfection of sgRNAs into Cas9-expressing HepaRG[VC] cells was demonstrated to be a versatile tool to study the influence of diverse genes on drug metabolism and other hepatic functions in this metabolically competent human hepatic cell line, in single knockdown as well as double knockdown setup.

4.2.2. Effects of genetic *POR* knockout in HepaRG cells

As a first target for CRISPR-induced gene knockout in HepaRG cells *POR* was chosen in order to investigate multiple POR functions in a human hepatocyte model (chapter 3.2). Lentiviral delivery of Cas9 and either one of two sgRNAs targeting distinct sites in the *POR* gene resulted in a knockdown in POR expression of 60-80 % with 10 % residual activity. Residual POR expression and activity is considered to derive from cells with heterozygous or no knockout that escaped puromycin selection. In addition, N-terminally truncated target proteins or skipping of the edited exon were found to partially rescue target activity in CRISPR/Cas9-induced knockout cells (Smits et al. 2019). Knockdown efficiency of POR in HepaRG cells was in a comparable range with commonly achieved efficiencies of around 50 % up to 100 % depending on the technology used, as reported in several previous *POR* knockout or knockdown studies in mammalian cells (Feidt et al. 2009; Porter et al. 2011; Su et al. 2013; Hunter et al. 2015; Rezende et al. 2017; Sundberg and Hankinson 2019; Reed et al. 2019b; Hunter et al. 2019).

POR is required for the transfer of two electrons from NADPH to microsomal CYPs. Therefore, changes in POR levels are therefore expected to severely influence CYP activity. This has previously been characterized in hepatic *Por* knockout mice, showing severely decreased microsomal CYP activities (Gu et al. 2003; Henderson et al. 2003). In HepaRG cells, the reduction of POR has been observed to have diverse effects on the various CYP activities (chapter 3.2.4). CYP2C8-catalyzed amodiaquine N-deethylation was least affected while CYP2C9-catalyzed tolbutamide hydroxylation was the most affected (Figure 20). The assessment of this finding using kinetic measurements showed that the reduced CYP activities were generally attributable to reduced V_{max}.

Compared to the effect of POR knockdown on other CYP activities, the influence on tolbutamide hydroxylase activity was remarkably strong. This may be related to the significantly reduced protein expression of CYP2C9 in HepaRG^{-POR} microsomes (Figure 24). The decreased function allele *CYP2C9*2,* which was found to be homozygous in HepaRG cells, may additionally contribute to the strong effect of POR knockout as it has been described to have lower affinity towards POR (Crespi and Miller 1997).

Unexpectedly, amodiaquine N-deethylation was only reduced by 20 %. The possibility of an analytical artefact, e.g. via participation of another enzymatic activity, was excluded by inhibition experiments with the specific and potent CYP2C8 inhibitor montelukast, a leukotriene receptor antagonist used in the treatment of asthma (Walsky et al. 2005). In commercial bactosomes only expressing CYP2C8 with two different amounts of POR, a strong influence of POR on amodiaquine N-deethylation was observed. This indicated the participation of an alternative redox partner that can compensate for lacking POR in HepaRG cells.

CYB5 was a likely candidate since it has long been known to be able to deliver the second electron in the CYP catalytic cycle and shares overlapping binding sites on CYPs with POR (Bridges et al. 1998; Guengerich 2001; Zhang et al. 2005). The ER-bound CYB5 is regenerated by CYB5 reductase and uses NADH as cofactor (Porter 2002). Since POR exhibits only marginal NADH-dependent activity (Döhr et al. 2001), an involvement of CYB5 as electron donor in HepaRG cells was suggested by the observation that all seven CYP activities could be supported by NADH alone (15-50% for HepaRG^{VC}, chapter 3.3.2, Figure 23). These findings support and extend previous studies in other systems that indicate that CYB5 can act as sole electron donor for several mouse Cyps (Henderson et al. 2013) as well as for CYP1A1 in

humans (Stiborová et al. 2016). Furthermore, these findings are further evidence that CYB5 markedly influences the activity of several drug metabolism activities catalyzed by human CYPs (Yamazaki et al. 2002; Henderson et al. 2013; Henderson et al. 2014; Henderson et al. 2015).

CYP activity measurements in genetic *CYB5A* single- and *POR/CYB5A* double-knockout HepaRG cells directly confirmed the effect of CYB5 on some CYP activities and on amodiaquine N-deethylation in particular (Figure 31). With the possible exception of CYPs 1A2 and 2D6, the effect of CYB5 knockdown was even greater in the POR knockdown cells, suggesting that the CYB5/CYB5 reductase system compensates in part for lacking POR, probably due to unique but overlapping interaction sites for CYB5 and POR (Zhang et al. 2007; Waskell and Kim 2015). The CYB5 knockdown effect was most pronounced on amodiaquine N-deethylation, especially in the double-knockdown cells. This further demonstrated a particularly strong role of CYB5 for CYP2C8. The *CYP2C8* genotype found in HepaRG cells may contribute to this finding, as HepaRG cells are homozygous for *CYP2C8*3,* which is a relatively common variant reported to show altered interaction properties with POR and CYB5 *in vitro* (Kaspera et al. 2011; R Arnold et al. 2019).

While CYP activities in the liver-specific *Por* knockout mice were mostly decreased, Cyp expression was generally increased both on protein and mRNA level. This suggested some compensatory mechanisms ascribed to the activation of transcriptional regulators such as CAR, PXR, SREBP, PPARγ and Nrf1 and the repression of PPARα and FXR (Wang et al. 2005; Weng et al. 2005; Cheng et al. 2014a). Activation and inactivation of those transcriptional regulatos may lead to an increase in Cyp expression but also to an induction of alternative detoxification enzymes such as alcohol dehydrogenases or carboxylesterases in the liver and small intestine, which appear to partially compensate for the loss of microsomal P450 function (Cheng et al. 2014a). In addition, FXR inhibition leads to increased CYP7a1 and 8b1, two major CYP enzymes involved in bile acid synthesis, and a decrease of SHP mRNA expression. Alterations in PPARα and PPARγ target gene expression may be causative to a decrease in fatty acid oxidation but an increase in fatty acid uptake, which then accounts for the severe hepatic lipidosis (Weng et al. 2005). However, there are many regulatory pathways that potentially contribute to the effects of Por knockout but, to date, they have neither been clarified consistently nor have they been confirmed in a human cell culture system yet (Gu et al. 2003; Henderson et al. 2003). Expression profiling in HepaRG[-POR] cells in this study revealed changes in CYP mRNA and protein expression that considerably contrast mouse profiles with CYP1A2 being several-fold increased while CYP2C9 was several-fold decreased (Figure 24 and Figure 25).

Further analyses, to elucidate possible regulation mechanisms by mRNA expression profiling revealed the consistent decrease of mRNA expression of several transcriptional regulators of hepatic CYP expression, bile acid and lipid homeostasis in both HepaRG[-POR] cell lines (Figure 25). The observed downregulation of many CYP enzymes may therefore be a direct consequence. By contrast, AHR/ARNT as transcriptional components of the Ah receptor pathway which regulate CYPs 1A1 and 1A2 in particular, were not changed significantly. The induction of CYP1A1 and 1A2 highlights a possible compensation mechanism through regulation by AHR/ARNT. AHR has been shown to be induced by endogenous ligands like arachidonic acid derivates (Larigot et al. 2018). In addition, CDCA has been shown to increase mRNA expression of CYP1A in hepatoma cell lines (Ibrahim 2015).

Among the nuclear receptors downregulated in HepaRG[-POR] cells are members of the *NR1H* (LXR, FXR) and *NR1I* (PXR, CAR) subfamilies, which are involved in bile acid and xenobiotic metabolism regulation, respectively, by sensing the metabolic environment (Endo-Umeda and Makishima 2019). Furthermore,

the expression of other regulators involved in sterol and lipid homeostasis including PPARα, LRH-1 and SREBF1 was decreased. The main axis of bile acid regulation consists of FXR, SHP and LRH-1, which repress the rate-limiting enzyme for bile acid synthesis, CYP7A1. In cooperation with HNF4α they also repress also CYP8B1, another important CYP enzyme for bile acid synthesis (Shin and Wang 2019). FXR and LRH-1 are downregulated in HepaRG[-POR] cells suggesting deregulation of bile acid homeostasis. While FXR downregulation was also seen in liver specific *Por* knockout mice (Wang et al. 2005), FXR target gene expression (CYP8B1, 7A1) was decreased in HepaRG[-POR] cells suggesting FXR activation rather than inactivation. CYP7A1 and 8B1 as FXR targets were among the four phase I enzymes measured in HepaRG[-POR] cells with the strongest decrease, while expression of CYP27A1, involved in the alternative bile acid synthesis pathway, was not changed. In addition, deregulation of lipid and cholesterol biosynthesis was indicated by the decreased mRNA expression of other enzymes involved in these metabolic processes (CYP4A11, CYP51, SCD, CYB5, FABP1) which are also target genes for PPARα, LXRα and SREBF1 (Debeljak et al. 2000; Antoun et al. 2006; Paton and Ntambi 2009; Guzmán et al. 2013).

Taking the mRNA expression data as a basis, quantification of bile acids in HepaRG[-POR] cells was performed to test the hypotheses developed above (Figure 26). While the sum of all bile acids secreted by HepaRG[-POR] cells was only slightly decreased, individual bile acid species were very differently affected by POR knockout. As bile acid homeostasis was changed towards decreased levels of TCA but unchanged levels of TCDCA in these cells, the observed downregulation of nuclear receptors may be a possible response to this deregulation. Human FXR, which is not activated in hepatocytes under physiological conditions, is known to be triggered by higher levels of CDCA, with TCDCA as the most potent endogenous FXR agonist (Juřica et al. 2016; Chiang and Ferrell 2018). This may explain the decreases in CYP7A1 and 8B1 mRNA expression. Slightly increased CDCA conjugates in HepaRG[-POR] cells indicate increased bile acid synthesis via the acidic pathway (Figure 5) via the POR independent, mitochondrial CYP27A1 (Monte et al. 2009) as the acidic pathway leads predominantly to CDCA synthesis (Alnouti 2009; Pikuleva and Waterman 2013). Enhanced alternative bile acid synthesis was also reported in *Por* knockout mice, where *Por* knockout lead to an increase in CDCA and TCDCA in the liver (Cheng et al. 2014b). Moreover, increased CDCA levels could influence HNF4a target gene expression, as CDCA reduces the transactivation potential of HNF4a and was shown to inhibit the expression of endogenous OAT2 mRNA in Huh7 cells (Li et al. 2019). This was also seen in the mRNA expression analysis, albeit not statistically significant. The level of taurine-conjugates was higher compared to glycol-conjugates, as reported in other publications (Sharanek et al. 2015; Burban et al. 2019). Regarding bile acid composition, HepaRG cells seem to resemble hepatocytes originating from NASH or cholestatic patients (Trottier et al. 2012; Lake et al. 2013) rather than primary human hepatocytes (Sharanek et al. 2015).

As CYP27A1 catalyses the first step of the alternative bile acid synthesis (Figure 5), genetic *CYP27A1* single- and *POR/CYP27A1* double-knockout HepaRG cell lines were generated to further investigate a possibly enhanced alternative bile acid pathway (chapter 3.4). CYP27A1 knockdown had no significant effect on global bile acid as well as on the synthesis of CA derivates. The missing effect of CYP27A1 knockdown is expected, as the main synthesis pathway is not dependent on CYP27A1, even if there are studies reporting alternative CA synthesis (Pandak and Kakiyama 2019). The only significant effect was a slight decrease of TCDCA synthesis in HepaRG[-POR#1] cells. Residual CYP27A1 and POR expression may be causal to this result, as there are many crossways between the two bile acid pathways that could lead to a compensation (Chiang 2017).

Another effect of *Por* knockout in mice is the hepatic accumulation of lipid droplets (Henderson et al. 2003; Gu et al. 2003; Porter et al. 2011). This has been ascribed to various changes of bile acid homeostasis, with CDCA conjugates as most effective regulators (Li and Apte 2015). In addition, POR knockdown in HepaRG cells changed mRNA expression of several genes involved in lipid homeostasis (Figure 25). Thus, changes in lipid accumulation in HepaRG^{-POR} cells were expected. Therefore, intracellular lipid droplet accumulation was assessed in POR single- and POR/CYP27A1 double-knockdown cells by nile red staining after serum depletion for 48 h (Figure 35). However, only HepaRG$^{-POR\#4}$ cells slightly accumulated lipid droplets, an effect increasing with additional CYP27A1 knockdown. Lipidosis in *Por* knockout mice was ascribed to excessive loss of bile acids and thereby missing FXR stimulation, while CDCA administration inhibits lipid accumulation (Porter et al. 2011). As secreted CDCA levels were rather increased than decreased in HepaRG^{-POR} cells, this may explain the absence of additional lipid droplet formation. The alternative pathway, which provides CDCA, is more active in rodents than in humans (Li and Chiang 2014), therefore more pronounced effects on lipid droplet formation in a rodent system seems reasonable. Decreased expression levels of LXR/RXR may also contribute to the absence of lipid droplet formation as it is described that LXR/RXR agonists induce lipidosis in HepaRG cells (Lasch et al. 2020). Another explanation of the missing lipid accumulation may consist of the rather complex medium supplements of HepaRG cells. The medium supplement insulin may stimulate lipid accumulation that hides the effect of POR knockdown (Steneberg et al. 2015). Hydrocortison could further influence lipid metabolisms in the cells (Macfarlane et al. 2008).

In conclusion, while POR knockdown had a similar effect on bile acid composition as seen in *Por* knockout mice, the cellular response seen in the upregulation of CYP isozymes and increased lipid accumulation is not comparable to the mouse model. However, results regarding bile acid composition in HepaRG^{-POR} cells are hard to compare with results seen in *Por* knockout mice.

On the one hand, bile acid homeostasis is preserved by systemic regulation in a tight interplay between liver and intestine (Chiang 2017). In the liver specific *Por* knockout mouse this crosstalk has been observed to affect the magnitude of the *Por* knockout effects (Cheng et al. 2014b). In contrast, the HepaRG cell embodies a 2D cell model with hepatocyte-like and biliary-like cells. Changes in bile acid composition in HepaRG^{-POR} cells may thus not represent the liver-intestinal crosstalk.

On the other hand, bile acid homeostasis varies greatly between different species. Mice have an additional primary bile acid form, muricholic acid (MCA), a product of the microsomal Cyp2a70 (Takahashi et al. 2016). The taurine conjugates of MCA show FXR antagonistic features (Sayin et al. 2013; Li and Dawson 2019). Changes in bile acid composition could therefore lead to more pronounced effects on FXR. In certain disease states bile acid signaling also shows large species differences, as shown in case of cholestasis in humans, which is associated with suppressed bile acid synthesis, while rodents have increased bile acid synthesis (Straniero et al. 2020).

5. Conclusion and outlook

The application of CRISPR/Cas9-mediated genome editing has considerable potential as a convenient tool for ADME research. However, single cell selection of HepaRG cells did not result in clonal cells with a homogenous phenotype comparable to the parental cells. Moreover, the phenotype of clones originating of clonal HepaRG cells was quite heterogenous. Therefore, selection of single cell clones after genome editing is not a practical approach for HepaRG cells. Thus, Cas9 delivery methods had to be established in HepaRG cells, which result in high transfection and therefore mutation rates. Using lentiviral transduction, a HepaRG cell line was generated that constitutively expresses Cas9 and that retains the ability to differentiate into hepatocyte-like cells with cytochrome P450 expression and activity profiles that are highly similar to those of the parent cell line. This cell line allows simple transfection with any targeting sgRNAs for single but also double or even multiple knockdown of target genes. By optimizing this Cas9-expressing HepaRG cell line, even higher knockdown efficiencies than shown in this thesis could possibly be achieved.

Genetic knockout of *POR* and *CYB5A* in HepaRG cells resulted in differential, CYP isozyme-dependent effects on CYP expression and activities. These data support a general role of CYB5 as alternative electron donor for drug metabolizing CYPs in HepaRG cells as previously observed in other human drug metabolism systems. Besides these direct effects on CYP enzyme activities, POR knockdown seems to have numerous indirect influences on gene and protein expression, most likely as a coordinated response to changed endogenous metabolites like bile acids. To finally elucidate the regulatory processes behind these changes, additional analyses have to be performed. Targeted mRNA expression profiling revealed an impression on changes in expression of genes involved in several metabolic processes. Untargeted methods like proteomic or whole genome expression profiling could provide further insights in regulatory processes after POR knockdown. As POR is also involved in cholesterol biosynthesis, metabolomic analysis of this pathway may be used to further characterize the POR knockdown phenotype. Furthermore, a more detailed view on selected lipids via a lipidomic approach could result in more meaningful results than seen with the rather insensitive nile red lipid staining.

6. Material

6.1. Chemicals

Chemicals	Supplier
20X GE Sample Loading Reagent	Fluidigm, South San Francisco, USA
2X Assay Loading Reagent	Fluidigm, South San Francisco, USA
Acetonitril	Roth, Karlsruhe, DE
Acrylamide/Bis-acrylamide (30:0.8)	Bio-Rad Laboratories, Inc., Hercules, USA
Agarose	Merck KgaA, Darmstadt, DE
Ammoniumpersulfate (APS)	Merck KgaA, Darmstadt, DE
Amodiaquine	Toronto Research Chemicals Inc, Toronto, CA
Atorvastatin	Toronto Research Chemicals Inc, Toronto, CA
Bovine serum albumin (BSA)	Sigma-Aldrich, Steinheim, DE
Bromophenol blue	Sigma-Aldrich, Steinheim, DE
Bupropion hydrochloride	Chemical synthesis
Chameleon Duo Pre-stained Protein Ladder	LI-COR Biosciences, Bad Homburg, DE
Conditioning Medium	upcyte technologies GmbH, Hamburg, DE
Cytochrome C	Sigma-Aldrich, Steinheim, DE
Dimethyl sulfoxide (DMSO)	Sigma-Aldrich, Steinheim, DE
Dulbecco's phosphate buffered saline (DPBS)	GIBCO, Carlsbad, USA
Dulbecco's Modified Eagle Medium (DMEM)	GIBCO, Carlsbad, USA
Ethanol (100%)	Sigma-Aldrich, Steinheim, DE
Fetal calf serum (FCS)	Merck KgaA, Darmstadt, DE
Formic acid (250 mM)	Fluka, Buchs, Switzerland
Geneticin sulfate (G418)	Merck KgaA, Darmstadt, DE
Glucose-6-Phosphate	Sigma-Aldrich, Steinheim, DE
Glucose-6-Phosphate Dehydrogenase	Merck KgaA, Darmstadt, DE
Glycerol	Sigma-Aldrich, Steinheim, DE
Glycine	Serva, Heidelberg, GER
Growth Medium (HCM)	upcyte technologies GmbH, Hamburg, DE
Human insulin, Insuman Rapid (40 I.E.)	Sanofi, Frankfurt, DE
Hydrocortisone (50 mg/ml)	Pfizer, Karlsruhe, DE
L-Glutamine (200 mM)	GIBCO, Carlsbad, USA
Lipofectamine® RNAiMax	Life Technologies, Carlsbad, DE
Methanol	Roth, Karlsruhe, DE
$MgCl_2$	Sigma-Aldrich, Steinheim, DE
Midazolam	Gift from Ute Hofmann, IKP, Stuttgart
Montelukast	Gift from AG Nies, IKP, Stuttgart
NADH	Sigma-Aldrich, Steinheim, DE
$NADP^+$	Sigma-Aldrich, Steinheim, DE
NADPH	Sigma-Aldrich, Steinheim, DE
Nile red	Santa Cruz Biotechnology, Dallas, USA
Nuclease-free water	Ambion, Austin, USA
Opti-MEM	Life Technologies, Carlsbad, DE
Paraformaldehyde	Alfa Aesar, Haverhill, Massachusetts, USA
Passive Lysis Buffer (5X)	Promega, Madison, USA
Penicilin/Streptomycin (P/S) (10,000 U/ml, 10 mg/ml)	GIBCO, Carlsbad, USA
Phenacetine	Sigma-Aldrich, Steinheim, DE

Polybrene	Millipore, Billerica, USA
Ponceau S-solution	Sigma-Aldrich, Steinheim, DE
Potassium cyanide	Toronto Research Chemicals Inc, Toronto, CA
Pre-Culture Medium	upcyte technologies GmbH, Hamburg, DE
Propafenone	Knoll, Ludwigshafen, DE
Puromycin	Thermo Fisher Scientific, Waltham, USA
Skim milk powder	Sigma-Aldrich, Steinheim, DE
S-Mephenytoin	Toronto Research Chemicals Inc, Toronto, CA
Sodium dodecyl sulfate (SDS)	Sigma-Aldrich, Steinheim, DE
Sodium phosphate	Sigma-Aldrich, Steinheim, DE
TaqMan® PreAmp Master Mix	Applied Biosystems, Foster City, USA
Tetramethylethylenediamine (TEMED)	GIBCO, Carlsbad, USA
Tolbutamide	Toronto Research Chemicals Inc, Toronto, CA
Tris-HCl	Roth, Karlsruhe, DE
Trypsin-EDTA (0.25 %)	GIBCO, Carlsbad, USA
Tween20	Merck KgaA, Darmstadt, DE
William's E Medium (w/o l-glutamine, phenol red)	GIBCO, Carlsbad, USA
β-Mercaptoethanol	Sigma-Aldrich, Steinheim, DE
Lipofectamine® RNAiMax	Thermo Fisher Scientific, Waltham, USA
TurboFect	Thermo Fisher Scientific, Waltham, USA
1 Kb Plus DNA Ladder	Thermo Fisher Scientific, Waltham, USA

6.2. Equipment

Equipment	Supplier
6460 Triple quadrupole mass spectrometer	Agilent Technologies, Santa Clara, USA
Agilent 2100 Bioanalyzer	Agilent Technologies, Santa Clara, USA
Agilent 8453 UV-visible Spectroscopy System	Agilent Technologies, Santa Clara, USA
Beckmann Optima L-100XP; Rotor: SW28	Beckman Coulter, Brea, USA
Biofuge 22R/ Biofuge pico	Heraeus, Hanau, DE
Biomark® HD Reader	Fluidigm, San Francisco, USA
Centrifuge 5424 R	Eppendorf, Hamburg, DE
EnSpire® Multimode Plate Reader	PerkinElmer, Waltham, USA
FACSCalibur	Becton Dickinson, Franklin Lakes, USA
Fastblot B44 blotting chamber	Biometra GmbH, Goettingen, DE
FastPrep®-24	MP Biomedicals GmbH, Eschwege, DE
Heracell™ 240 incubator	Heraeus, Hanau, DE
IFC Controller MX	Fluidigm, San Francisco, USA
Millipore water purification system MilliQ	Millipore, Molsheim, France
NanoDrop™ 2000c	Thermo Fisher Scientific, Waltham, USA
Nucleofector™ 2b Device	Lonza, Basel, Switzerland
Odyssey CLx Infrared Imaging System	LI-COR Biosciences, Bad Homburg, DE
Olympus CKX 41 microscope	Olympus, Tokyo, Japan
OPTIMA MaxE ultracentrifuge	Beckman Coulter, Brea, Kalifornien, USA
PEQLAB Electrophoresis power supply EV231	PEQLAB Biotechnologie GmbH, DE
PROTEAN® II-/Mini-PROTEAN®-System	Bio-Rad Laboratories, Inc., Hercules, USA

ThermoMixer Comfort	Eppendorf, Hamburg, DE
TLA-55, MLA-80 ultracentrifuge rotor	Beckman Coulter, Brea, USA
Ultracentrifuce tubes, vials	Beckman Coulter, Brea, USA
Veriti 384-well Thermal Cycler	Applied Biosystems, Foster City, USA
Veriti 96-well Thermal Cycler	Applied Biosystems, Foster City, USA
Vortexer Reax control	Heidolph Instruments, Schwabach, DE
7900 HT Real Time PCR System	Applied Biosystems, Foster City, USA

6.3. Consumables

Consumables	Supplier
0.45 PVDF filter	Roth, Karlsruhe, DE
24 well plate, cell culture treated	Corning, Corning, USA
Amersham Protran Nitrocellulose Blotting Membrane (0.45 µm NC)	GE Healthcare Life Sciences, Freiburg, DE
C-Chip Counting chambers, Neubauer Imp.	NanoEnTek, Seoul, KR
Corning Axygen® P-96-450V-C Storage 96-Well Assay Microplate with V-Bottom Wells	Corning, Corning, USA
EASYstrainer™ cell strainer (40 µm)	Greiner Bio-One GmbH, Frickenhausen, DE
Falcon tube (15 and 50 ml)	Sarstedt, Nuembrecht, DE
Lysing Matrix D	MP Biomedicals GmbH, Eschwege, DE
Microplates (96-well)	Greiner Bio-One GmbH, Frickenhausen, DE
OptiPlate (96-well)	PerkinElmer, Waltham, USA
Rainin filter pipette tips (10, 20-200, 1000 µl)	Mettler-Toledo, Greifensee, CH
Rainin pipette	Mettler-Toledo, Greifensee, CH
Safe-Lock Tubes (0.5, 1.5, 2 ml)	Eppendorf, Hamburg, DE
Stripette® (2, 5, 10, 25 ml)	Corning, Corning, USA
Ultracentrifuge tubes: Ultra Clear #344058	Beckman Coulter, Brea, USA
VisiPlate-24 Black	PerkinElmer, Waltham, USA

6.4. Kits

Kit	Supplier
Agilent RNA 6000 Nano Kit	Agilent Technologies, Santa Clara, USA
Agilent DNA 7500 Kit	Agilent Technologies, Santa Clara, USA
Amaxa Cell line Nucleofector Kit V (VCA-1003)	Lonza, Basel, CH
DNeasy Blood & Tissue Kit	Qiagen, Hilden, USA
GENECLEAN Turbo Kit	MP Biomedicals, Santa Ana, USA
P450-Glo™ (CYP2C9, CYP3A4)	Promega, Madison, USA
Pierce® BCA Protein Assay Kit	Thermo Fisher Scientific, Waltham,USA
Pierce™ LDH Cytotoxicity Assay Kit	Thermo Fisher Scientific, Waltham,USA
PureYield™ Plasmid Midiprep System	Promega, Madison, USA
Qiaprep Spin Miniprep Kit	Qiagen, Hilden, USA
Rneasy Mini Kit	Qiagen, Hilden USA
alamarBlue	Thermo Fisher Scientific, Waltham,USA

6.5. Software

Software	Supplier
Agilent ChemStation	Agilent Technologies, Santa Clara, USA
BD CellQuest Pro Software	Becton Dickinson, Franklin Lakes, USA
CHOPCHOP	http://chopchop.cbu.uib.no/
Citavi 6	Swiss Academic Software, Wädenswil, CH
CRISPR design	http://crispr.mit.edu/
EnSpire™ Software 4.1	PerkinElmer, Waltham, USA
Fluidigm Real-Time CR analysis	Fluidigm, San Francisco, USA
Geneious 8.0.5	Biomatters Ltd, Auckland, NZ
GraphPad Prism 9	GraphPad Software, San Diego, USA
Image Studio™ Software v3.1	LI-COR Biosciences, Bad Homburg, DE
MS Office 2010	Microsoft, Redmond, USA
Genedata Profiler 13.0	Genedata, Basel, CH
Genotyper Software	Thermo Fisher Scientific, Waltham, USA
SDS version 2.3 TaqMan® software	Thermo Fisher Scientific, Waltham, USA
FlowJo 10.7.1	Becton Dickinson, Franklin Lakes, USA

6.6. Buffers and solutions

Buffer/solution	Substance	Amount
Collagen I-solution	Water (sterile)	49.21 ml
	Formic acid	57.5 µl
	Collagen Typ I (3,37 mg/ml)	732.5 µl
	Sterilie filtration	
TAE buffer (50x)	Acetic acid	57.1 ml
	EDTA (0,5 M, pH 8)	100 ml
	milliQ-H_2O	Ad 1,000 ml
DNA sample buffer (5x)	Ficoll (20 %)	874 µl
	Bromophenol blue (0,5 %)	87.4 µl
	EDTA (0,5 M, pH 8)	38 µl
APS (10 %)	Ammoniumpersulfate	1 g
	milliQ-H_2O	Ad 10 ml
Elektrophorese buffer	Tris-Base	150 g
	Glycine	720 g
	SDS (20 %)	250 ml
	milliQ-H_2O	Ad 5,000 ml
Lämmli buffer (5x)	SDS (20 %)	10 g
	1 M Tris-Buffer pH 6,8	30.6 ml
	2-Mercaptoethanol	25 ml
	Bromophenol blue	100 mg
	milliQ-H_2O	Ad 75 ml
	Glycerole	25 ml
SDS (20 %)	SDS	100 g
	milliQ-H_2O	Ad 500 ml
Skim milk solution (5%)	Skim milk powder	10 g
	milliQ-H_2O	Ad 200 ml

TBS (10x)	NaCl	400 g
	KCl	10 g
	Tris-Base	16.93 g
	Tris-HCl	175 g
	milliQ-H_2O	Ad 5,000 ml
TBST (1x)	TBS (10x)	500 ml
	VE-H_2O	4500 ml
	Tween20 (50%)	10 ml
Transfer buffer (WB)	Tris-Base	29 g
	Glycine	14.6 g
	SDS (20%)	9.25 ml
	Ethanol	1 l
	milliQ-H_2O	Ad 5,000 ml
Tris-HCL (0,5 M, pH 6.8)	Tris-Base	0.928 g
	Tris-HCl	38.19 g
	milliQ-H_2O	Ad 500 ml
Tris-HCL (1,5 M, pH 8.8)	Tris-Base	69.03 g
	Tris-HCl	28.40 g
	milliQ-H_2O	Ad 500 ml
Tris-HCL (1 M, pH 8.0)	Tris-HCl	7.878 g
	milliQ-H_2O	Ad 500 ml
	pH 8.0	
Tween20 (50%)	Tween20	250 ml
	milliQ-H_2O	250 ml
Homogenisation buffer	0.1 M potassium phosphate buffer, pH 7.4, 250 mM Sucrose	
Microsome buffer	0.1 M potassium phosphate buffer, pH 7.4, 10 % glycerol	
NADPH regenerating system (10x)	Glucose-6-Phosphat Dehydrogenase (500 U/ml)	20 µl
	$MgCl_2$	12.5 µl
	$NADP^+$	12.5 µl
	Glucose-6-phosphat	10 µl
	0.1 M potassium phosphate buffer, pH 7.4	195 µl
Stopping solution	50 % 250 mM formic acid + 50 % acetonitril	

## 6.7. Cell culture

Table 11: Cell line descriptions

Cell line (supplier)	Description
A549 (IKP, AG Aulizky)	Adherent, immortalised epithelial lung carcinoma cells of a male, 58 years old Caucasian.
HEK 293FT (Invitrogen, Carlsbad, USA)	Adherent, human embryonal kidney cells; expressing SV40 large T-antigen and allow DNA replication of episomal plasmids with SV40 origin of replication.
HepaRG (batch HPR101007, passage no. 12) (Biopredict International, Rennes, FR)	Adherent bipotent progenitor cells. Able to differentiate into hepatocyte-like cells as well as bile duct epithelial cells. Originate from a hepatocellular carcinoma of a woman.

HepG2 (ATCC, Manassas, USA)	Adherent, immortalised epithelial carcinoma cells of a male, 15 years old Caucasian.
"Upcyte Hepatocytes": Batches 122-129-138, 653-06 (upcyte technologies GmbH, Hamburg, DE)	"Upcyte Hepatocytes" retain proliferation capacity and certain hepatic functions and after transfection with oncostatin-M. They are available from different donors.
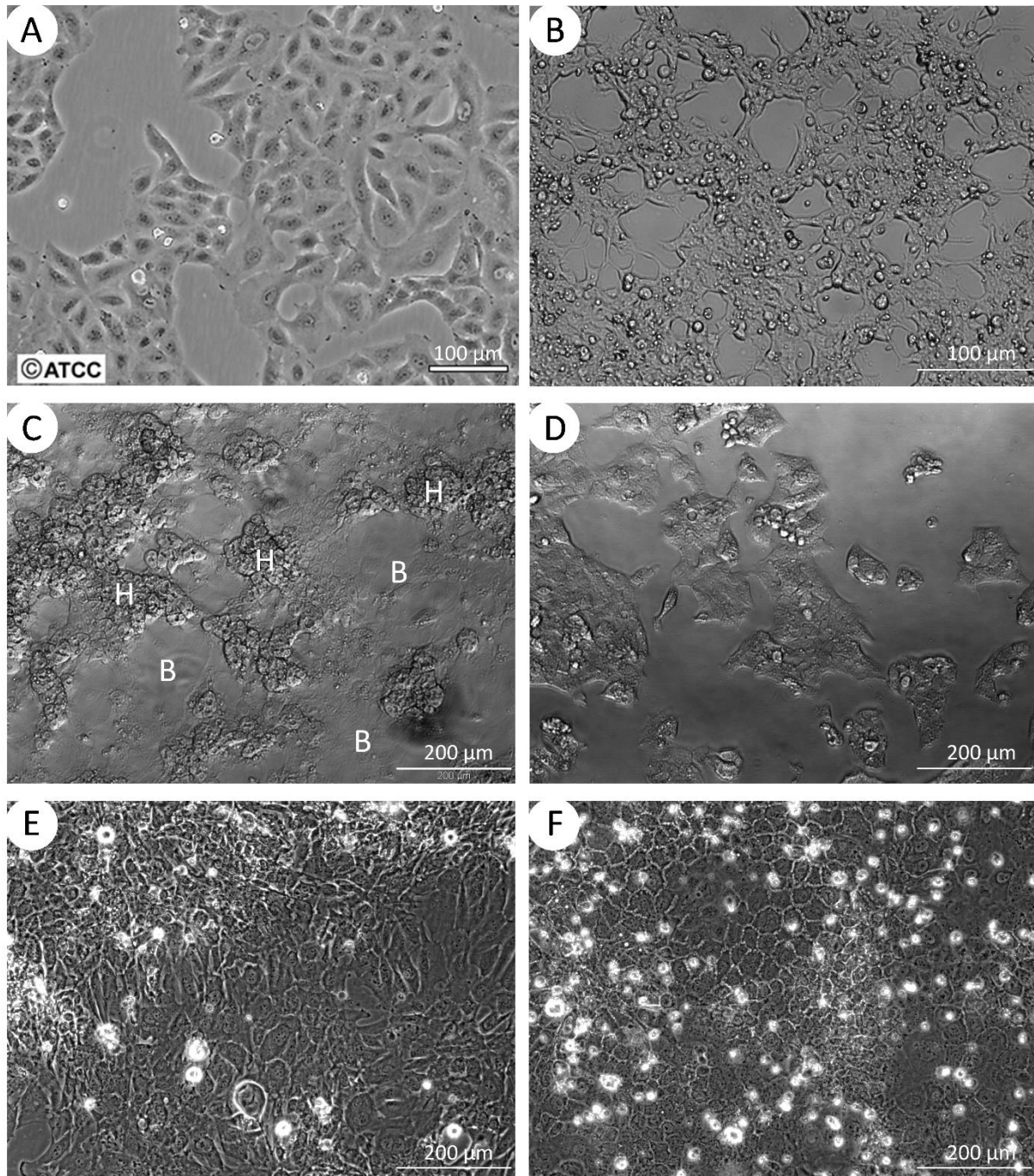
Figure 36: Used cell lines. A: A549 epithelial lung carcinoma cells (picture copyright ATCC, scale: 100 μm). B: HEK 293FT cells (scale: 100 μm). C: HepaRG cells (batch HPR101007), differentiated under standard conditions for 2 weeks under 2 % DMSO. H: hepatocyte-like cells, B: biliary-like cells (scale: 200 μm). D: HepG2 cells (scale: 200 μm). E: "Upcyte Hepatocytes" batch 653-03, day 10 under conditioning medium (scale: 200 μm). F: "Upcyte Hepatocytes" batch 122-129-138, day 8 under conditioning medium (scale: 200 μm)

Table 12: Medium composition for used cell lines

HepG2 and A549	
DMEM	500 ml
FCS	50 ml
P/S (10000 U/ml)	5 ml
Pyruvate 100 mM	5 ml
HEK 293FT	
DMEM	500 ml
FCS	50 ml
P/S (10000 U/ml)	5 ml
Pyruvat 100 mM	5 ml
L-Glutamine 600 mM	5ml
MEM Non-Essential Amino Acids (NEAA) 10 mM	5 ml
Geneticin sulfate (G418) 50 mg/ml	0.05 ml
HepaRG (lenti) cells	
William's E Medium	500 ml
FCS	50 ml
P/S (10000 U/ml)	5 ml
L-Glutamine 600 mM	5 ml
Insulin (Insuman Rapid; 40 I.E./ml)	2 ml
Hydrocortison 50 µg/ml	200 µl
Puromycin (10 mg/ml) (for HepaRG lenti)	250 µl
DMSO (for differentiation)	1 or 2%
"Upcyte Hepatocytes"	
Growth Medium (HCM)	
Pre-Culture Medium	(HCM + 0.5% DMSO)
Conditioning Medium	(HPM + 0.1% DMSO)

6.8. Oligonucleotides

Table 13: Oligonucleotides targeting POR

Name	Sequence 5'-3'	Use
POR ex2 2F	CTCTGTCTTCCAGGGACCCA	Sequencing POR Exon 2, PCR for T7E1 assay sgRNA POR#1
POR ex2 2R	AGCCTGGGCAATACAGTGAG	Sequencing POR Exon 2, PCR for T7E1 assay sgRNA POR#1
POR ex2 3F	GGATGTTCCAGCACACTGAGA	PCR for T7E1 assay sgRNA POR#1
POR ex2 3R	CCAAGAGTCACCCCAAAATGC	PCR for T7E1 assay sgRNA POR#1
por-ex2-f	CGTGACACCTGTGTCCCATGA	Sequencing POR Exon 3
por-ex2-r	CCAGCCGTCTGCTAGACTTGA	Sequencing POR Exon 3
por-ex3-f	CACCGGAGCCGTGGCTGA	Sequencing POR Exon 4
por-ex3-r	GACCTGCTCCCTGTCCTACC	Sequencin POR Exon 4
POR ex4 1F	TGTGTGAGATTGCCTTGGTGA	PCR for T7E1 assay sgRNA POR#4
POR ex4 1R	ACGGGAAGGCAACTTCCGA	PCR for T7E1 assay sgRNA POR#4
por-ex4-f	CGGGTTGAACCTTGAACAGGC	Sequencing POR Exon 5
por-ex4-r	GGGCTGCCTTTCAGATACATGG	Sequencing POR Exon 5
por-ex5-f	CCAGCAGCTCAGCCAGTGC	Sequencing POR Exon 6
por-ex5-r	CCTCACGTTCCACGGCCC	Sequencing POR Exon 6
por-ex6-f	CACCAGGTACCGTTGCCACAT	Sequencing POR Exon 7
por-ex6-r	GCTGCCCTCGGCACAGGA	Sequencing POR Exon 7
POR ex8 1F	GGCTCTGTGGCTAGGTTCAA	Sequencing POR Exon 8, PCR for T7E1 assay sgRNA POR#2
POR ex8 1R	CAGCTGGTCTTGGATGCAGT	Sequencing POR Exon 8, PCR for T7E1 assay sgRNA POR#2
por-ex8-f	CCTTGGAGACGGAGACTCAG	Sequencing POR Exon 9
por-ex8-r	GATGTGAGGCTCGGGAGG	Sequencing POR Exon 9
por-ex9-f	TGGGCCTCCTGACCTGGG	Sequencing POR Exon 10
por-ex9-r	CCTACAGGCCCAATCCCGC	Sequencing POR Exon 10
por-ex10-f	CAGAGCTGGCCCAAGGTGTCA	Sequencing POR Exon 11
por-ex10-r	GGCCCACGGAGCTCGGAAA	Sequencing POR Exon 11
por-ex11-f	TCCGGCGAGGGCAAGGTG	Sequencing POR Exon 12
por-ex11-r	CTGCTGTGAGCAGGGCTGG	Sequencing POR Exon 12
POR ex13 2F	CCATCGCCTCATCCTCCAAG	Sequencing POR Exon 13&14, PCR for T7E1 assay sgRNA POR#3
POR ex13 2R	TTAGCAGGTGCTGGACGTAG	Sequencing POR Exon 13&14, PCR for T7E1 assay sgRNA POR#3
por-ex14-f	TGAGGCTGGCAGGGCCAC	Sequencing POR Exon 15
por-ex14-r	CAACTGTGGCAGGCAGGGC	Sequencing POR Exon 15
por-ex15a-f	GACAAGGCCCTGCCTGCC	Sequencing POR Exon 16
por-ex15a-r	GGTGGACCTCACCTGGCCT	Sequencing POR Exon 16
por-ex15b-f	CTCCCTCCCGTAGTCTCCTG	Sequencing POR Exon 16
por-ex15b-r	CCACCACATGGGTTCCTGGG	Sequencing POR Exon 16

Table 14: Oligonucleotides targeting CYP2D6

Name	Sequence 5'-3'	Use
2D6ENH-E1F	ACCGCACCGAGGCCTTTTTGC	Amplifikation CYP2D6 enhancer fragment
2D6ENH-E1R	CGAGGCTGGCGGATCATTTGG	Amplifikation CYP2D6 enhancer fragment
2D6ENH-1F	TTTGACAAATGCCTCCCGGT	Sequencing CYP2D6 enhancer fragment
2D6ENH-1R	ACTGGAACTAGGGTGGTAATGTG	Sequencing CYP2D6 enhancer fragment
f1286	CTTTGCAGGCTTCAGGAGCTTGGA	Amplification CYP2D6 fragment A
2D6-r3874	AATCTCTGACGTGGATAGGAGG	Amplification CYP2D6 fragment A
F1382(1330)	AAGCAGGGGCAAGAACCTCTGGA	Amplification CYP2D6 fragment A nested
2D6-DH-3664-R	CTCGCCCTGCAGAGACTC	Amplification CYP2D6 fragment A nested
CYP2D6FragmentBfo	CCTTCATGGCCACGCGC	Amplification CYP2D6 fragment B
h-2D6	GGCTATCACCAGGTGCTGGTGCT	Amplification CYP2D6 fragment B
2D6-4574f	CCATCTGGGAAACAGTGCAG	Amplification CYP2D6 fragment C
2D6-k	ATTGTACATTAGAGCCTCTGGC	Amplification CYP2D6 fragment C
Upf	GCCTGGACAACTTGGAAGAACC	Amplification CYP2D6 promoter fragment
Upr1669	AGGAAGATGGCCACTATCAC	Amplification CYP2D6 promoter fragment
2222f	GCTGGGTCTCCTCCTTCCAC	Sequencing CYP2D6 fragment A nested
2D6-2803r	TGGCCCGCTGTCCCCACTC	Sequencing CYP2D6 fragment A nested
2D6-2803r	TGGCCCGCTGTCCCCACTC	Sequencing CYP2D6 fragment A nested
*35 nest for	TAAGGGAAGGGTCACGCGCT	Sequencing CYP2D6 fragment A nested
2D6-FORWARD3751	CCACTGTAAGAAGGGCCT	Sequencing CYP2D6 fragment B
2D6-FORWARD3751	CCACTGTAAGAAGGGCCT	Sequencing CYP2D6 fragment B
2D6-h for	AGCTCAGCACCAGCACCTGGTGA	Sequencing CYP2D6 fragment C
2D6-990r	GCACAGATCTCTTGTCCACT	Sequencing CYP2D6 promoter fragment
BtsVf	GTGCCGGGTCTGTATGTGTG	Sequencing CYP2D6 promoter fragment

Table 15: Oligonucleotides targeting CYP1A2 (Geng et al. 2016)

Name	Sequence 5'-3'	Use
1A2 Prom F	AATCGATATGGCAATCAAATGCAAA	Amplification/sequencing CYP1A2 Promoter
1A2 Prom R	CCCGTCTTTCTGTCCCCACT	Amplification/sequencing CYP1A2 Promoter
1A2 Ex1 F	TAGGCTCCCTACCCTGAACC	Amplification/sequencing CYP1A2 exon 1
1A2 Ex1 R	AACATGAACGCTGGCTCTCT	Amplification/sequencing CYP1A2 exon 1
1A2 Ex2.1 F	GTCACTGGGTAGGGGGAACT	Amplification/sequencing CYP1A2 exon 2
1A2 Ex2.1 R	AAGGTGTTGAGGGCATTCTG	Amplification/sequencing CYP1A2 exon 2
1A2 Ex2.2 F	CTGGCACTGTCAAGGATGAG	Amplification/sequencing CYP1A2 exon 2
1A2 Ex2.2 R	ATTGCAGGACTCTGCTAGGG	Amplification/sequencing CYP1A2 exon 2
1A2 Ex3 F	CAGGACTTTGACAAGGTGAGC	Amplification/sequencing CYP1A2 exon 3
1A2 Ex3 R	CATAGCCCAGGCTCAAACC	Amplification/sequencing CYP1A2 exon 3
1A2 Ex4 F	CCTGTTCAAGCACAGCAAGA	Amplification/sequencing CYP1A2 exon 4
1A2 Ex4 R	AACACAGAGGACAAGCAGAGC	Amplification/sequencing CYP1A2 exon 4
1A2 Ex5 F	CCTGTTATGTGCCTGCTGTG	Amplification/sequencing CYP1A2 exon 5
1A2 Ex5 R	GGGGATTCAGGCCTCTTACT	Amplification/sequencing CYP1A2 exon 5
1A2 Ex6 F	TCCCAGTGCCCTCTGTGCCA	Amplification/sequencing CYP1A2 exon 6
1A2 Ex6 R	GCCTTCCTGACTGCTGAACCTGC	Amplification/sequencing CYP1A2 exon 6

1A2 Int 6.1 F	AACAGCCAAGTGCGCAGCCA	Amplification/sequencing CYP1A2 intron 6
1A2 Int6.1 R	TCGCCTGAGGTACCCCACCT	Amplification/sequencing CYP1A2 intron 6
1A2 Int6.2 F	AGGTGGGGTACCTCAGGCGA	Amplification/sequencing CYP1A2 intron 6
1A2 Int6.2 R	GAGGTGCCTGGGGGAGGGAG	Amplification/sequencing CYP1A2 intron 6
1A2 Ex7.1 F	TTTGGTTCCTTCCCACCTACCCTT	Amplification/sequencing CYP1A2 exon 7
1A2 Ex7.1 R	GAAGAGAAACAAGGGCTGAGTCCCC	Amplification/sequencing CYP1A2 exon 7
1A2 Ex7.2 F	TGCTGTTTGGCATGGGCAAG	Amplification/sequencing CYP1A2 exon 7
1A2 Ex7.2 R	TCTGGTGATGGTTGCACAATTC	Amplification/sequencing CYP1A2 exon 7
1A2 3-UTR F	AGAATTGTGCAACCATCACCAGAA	Amplification/sequencing CYP1A2 3ʹ-UTR
1A2 3-UTR R	CCAGTCTCAGGACTCAAGCACCA	Amplification/sequencing CYP1A2 3ʹ-UTR

Table 16: Oligonucleotides targeting CYP2C8 (Yeo et al. 2011)

Name	Sequence 5ʹ-3ʹ	Use
2C8 5-UTR 1F	TGTCTTTAAATTATCTATGTTCCTTTT	Amplification/sequencing CYP2C8 5ʹ-UTR
2C8 5-UTR 2F	TGGTCAATTTAGAATAAAGGTAATC	Amplification/sequencing CYP2C8 5ʹ-UTR
2C8 5 UTR 3F	GGTGTCCTGTTCTCCCAGAG	Amplification/sequencing CYP2C8 5ʹ-UTR
2C8 5-UTR 1R	CCTTGCTCTGCTCCTTGTTT	Amplification/sequencing CYP2C8 5ʹ-UTR
2C8 5-UTR 2R	CAACTGGATTTATGAACATTACTAGA	Amplification/sequencing CYP2C8 5ʹ-UTR
2C8 5 UTR 3R	TTCATCATTAAAAGAGACTGGAG	Amplification/sequencing CYP2C8 5ʹ-UTR
2C8 5-UTR F	GGCAACACTAAAGTGAACTGTGG	Amplification/sequencing CYP2C8 5ʹ-UTR
2C8 5-UTR R	CAGCACCAGGACCACAAAAGGT	Amplification/sequencing CYP2C8 5ʹ-UTR
2C8 Ex2 F	TGCTGAATGTGTTGAAGTGAGG	Amplification/sequencing CYP2C8 exon 2/3
2C8 Ex2 R	GAGGGCTGACAACCAGGAT	Amplification/sequencing CYP2C8 exon 2/3
2C8 Ex4 F	CTGATTTTTTTTGGACACAT	Amplification/sequencing CYP2C8 exon 4
2C8 Ex4 R	TTTTCTTCACTCATACATCATTT	Amplification/sequencing CYP2C8 exon 4
2C8 Ex5 F	CAGGGCTTGGTGTAAGATACA	Amplification/sequencing CYP2C8 exon 5
2C8 Ex5 R	ACAGAAGGATTCGATGAATCAC	Amplification/sequencing CYP2C8 exon 5
2C8 Ex6 F	CTTCTGCTTTTATTTCTGGG	Amplification/sequencing CYP2C8 exon 6
2C8 Ex6 R	CAAGGTGGAGGATACTGGC	Amplification/sequencing CYP2C8 exon 6
2C8 Ex7 F	GGCTGGTTGTACTTCTGGAC	Amplification/sequencing CYP2C8 exon 7
2C8 Ex7 R	GGTTGGAACCAAACCAGCACT	Amplification/sequencing CYP2C8 exon 7
2C8 Ex8 F	CGTGATGTCCACTACTTCTCCT	Amplification/sequencing CYP2C8 exon 8
2C8 Ex8 R	ATGATGGTGTATTGTGAGGGTG	Amplification/sequencing CYP2C8 exon 8
2C8 Ex9 F	GTGCAAGTCACAAATGACTGT	Amplification/sequencing CYP2C8 exon 9
2C8 Ex9 R	CCTTGGAAAGTCTCAACAGA	Amplification/sequencing CYP2C8 exon 9
2C8 gRNA1 1F	AGGATGCGCAATGAAGACCT	PCR for T7E1 assay sgRNA CYP2C8#1
2C8 gRNA1 1R	GGGTAGTGGCCTCAAGGTG	PCR for T7E1 assay sgRNA CYP2C8#1
2C8 gRNA2 1F	TCAACCTCCAACTCCTTTGTGC	PCR for T7E1 assay sgRNA CYP2C8#2
2C8 gRNA2 1R	TTCAATCAGGGCTTGGTGTAAGA	PCR for T7E1 assay sgRNA CYP2C8#2

Table 17: Oligonucleotides targeting CYP3A4

Name	Sequence 5'-3'	Use
3A4 gRNA1 1F	TGATGGGACTGACTGATGGA	PCR for T7E1 assay sgRNA CYP3A4#1
3A4 gRNA1 1R	GATTTCAGTCCCTGGGGTGAG	PCR for T7E1 assay sgRNA CYP3A4#1
3A4 gRNA2 1F	GGCCTGATTAGCACCCCAAG	PCR for T7E1 assay sgRNA CYP3A4#2
3A4 gRNA2 1R	TCTGTTCAGGGAAACAGGCG	PCR for T7E1 assay sgRNA CYP3A4#2

Table 18: Oligonucleotides targeting CYP27A1

Name	Sequence 5'-3'	Use
CYP27A1 1F	AGTTCCACCAGACACGCATT	PCR for T7E1 assay CYP27A1#1
CYP27A1 1R	TCATGTCATAGGTGGCCTGG	PCR for T7E1 assay CYP27A1#1
CYP27A1 2F	TGTCGGACATGGCTCAACTC	PCR for T7E1 assay CYP27A1#2
CYP27A1 2R	CTTGGAGGGATGAAGGTCGG	PCR for T7E1 assay CYP27A1#2

6.9. Plasmids

| Name	Use	Source
pCMV-VSV-G	Lentiviral packaging plasmid	Addgene
psPAX2	Lentiviral packaging plasmid	Addgene
lentiCRISPR v2	Lentiviral Cas9 expression plasmid	Addgene
lentiCRISPR v2_#1	Lentiviral Cas9 expression plasmid, coexpressing sgRNA POR#1	Ligation 002
lentiCRISPR v2_#4	Lentiviral Cas9 expression plasmid, coexpressing sgRNA POR#1	Ligation 004
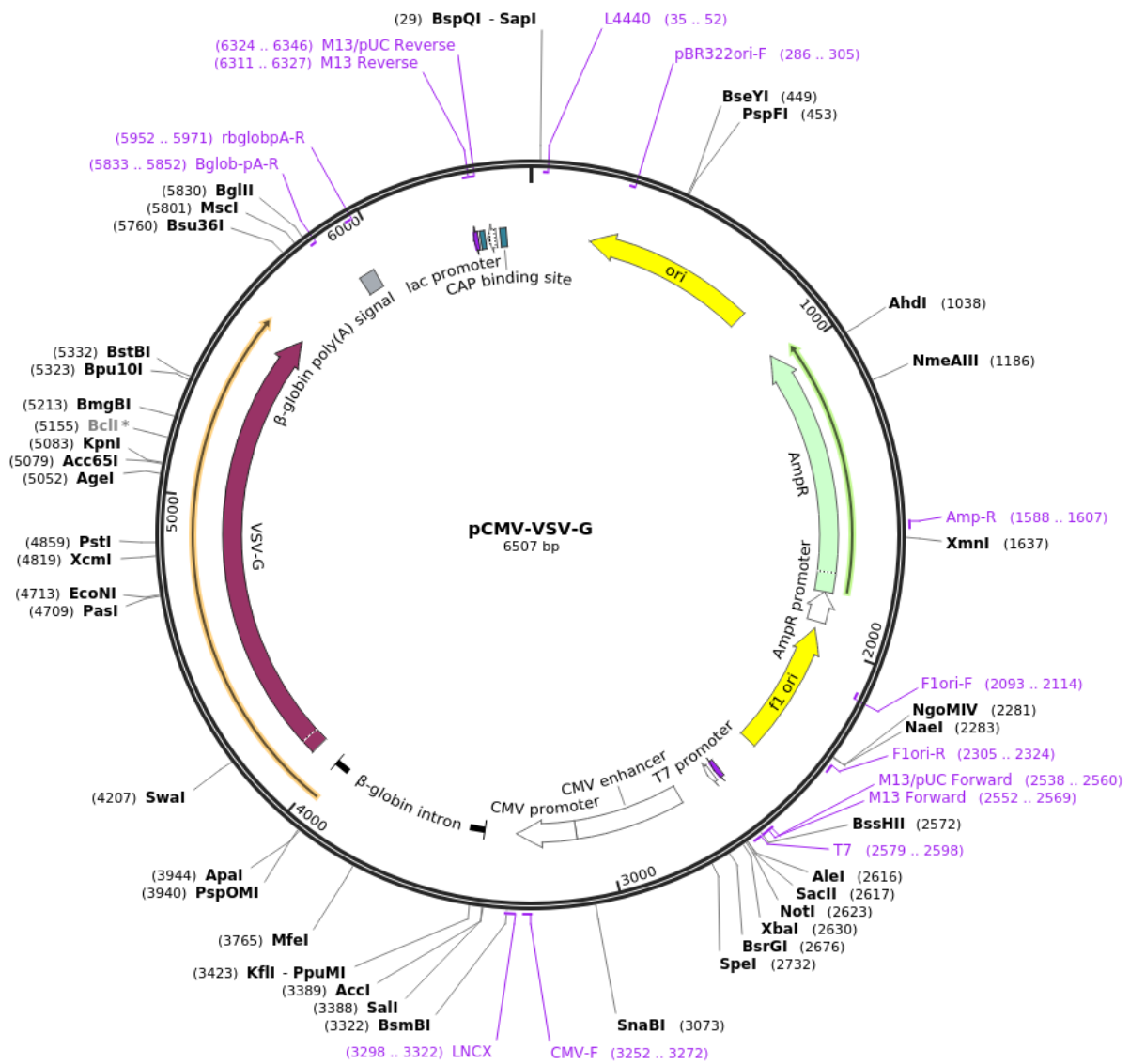
**Figure 37: pCMV-VSV-G full sequence map.** Figure taken from Addgene, Watertown, USA.
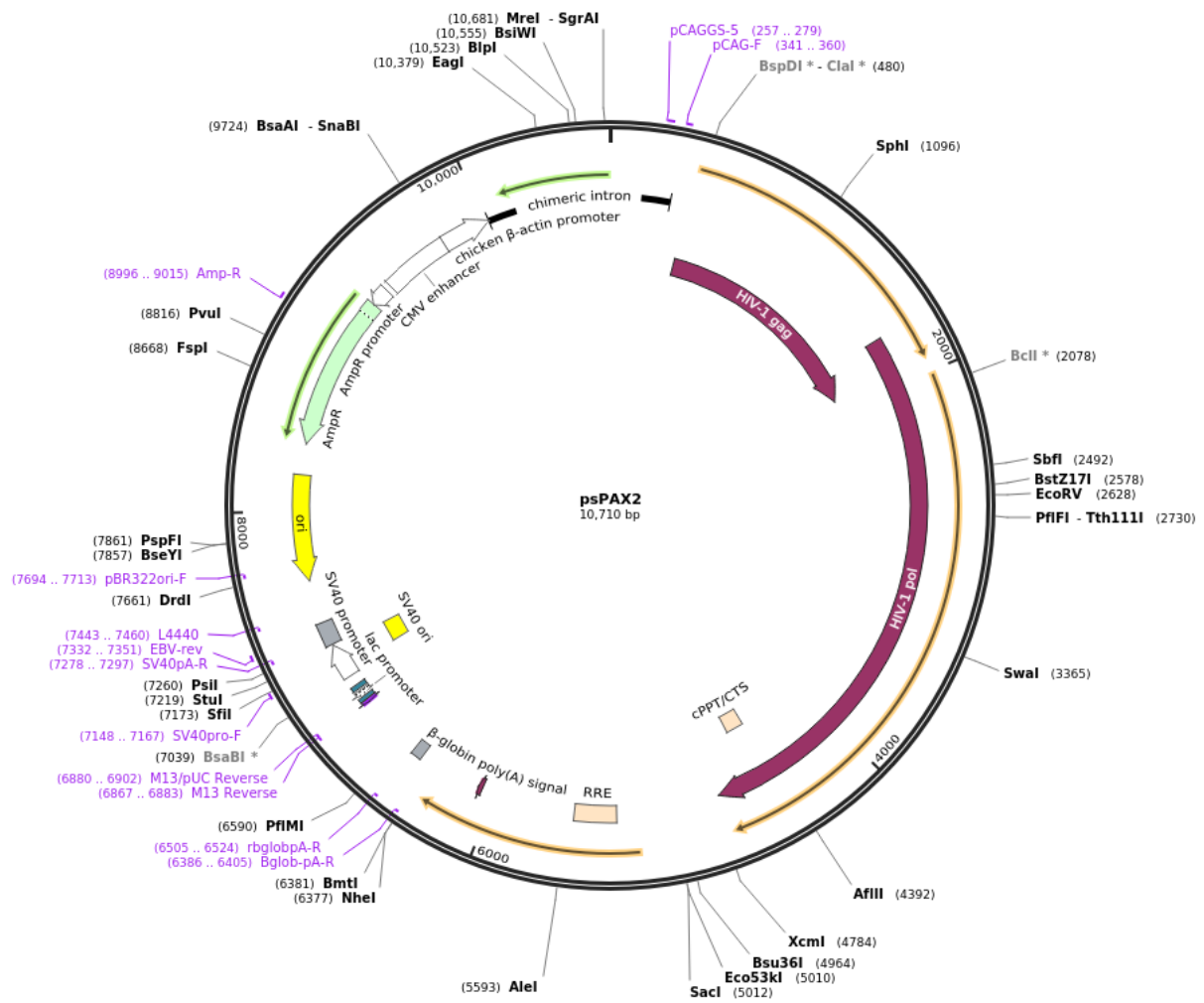
**Figure 38: spPAX2 full sequence map.** Figure taken from Addgene, Watertown, USA.
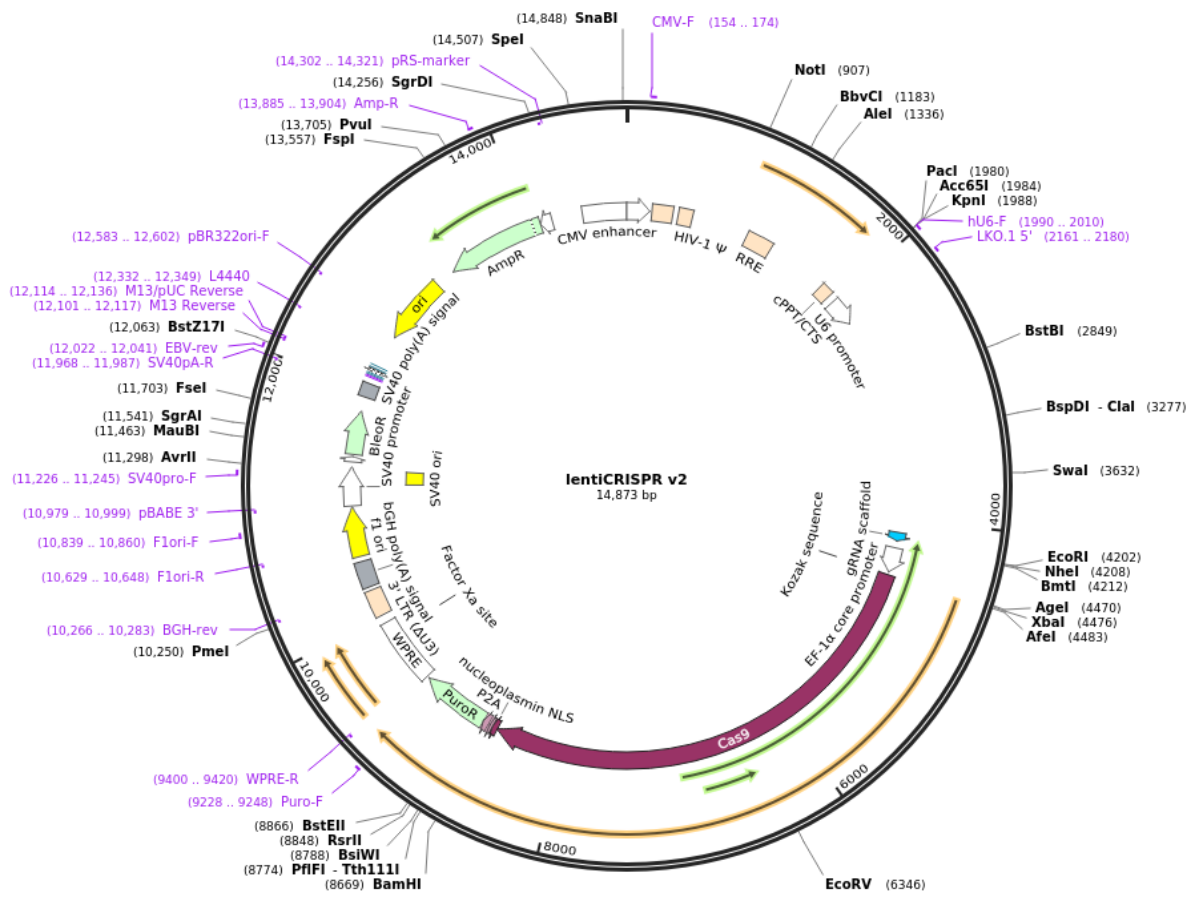
Figure 39: lentiCRISPRv2 full sequence map. Figure taken from Addgene, Watertown, USA.

6.10. TaqMan assays

Table 19: TaqMan Assays (Thermo Fisher Scientific, Waltham, USA)

Genname (protein)	Assay-ID
ABCB1 (ATP-dependent translocase)	Hs01067802_m1
ABCC2 (Canalicular multispecific organic anion transporter 1)	Hs00166123_m1
ABCC3 (Canalicular multispecific organic anion transporter 2)	Hs00978473_m1
ABCC4 (Multidrug resistance-associated protein 4)	Hs00988717_m1
ACTB (Actin, cytoplasmic 1)	Hs01060665_g1
AHR (Aryl hydrocarbon receptor)	Hs00169233_m1
AHSG (Alpha-2-HS-glycoprotein)	Hs00155659_m1
ALDH3A1 (Aldehyde dehydrogenase 3A1)	Hs00964880_m1
ARNT (Aryl hydrocarbon receptor nuclear translocator)	Hs01121918_m1
ASCL5 (Achaete-scute homolog 5)	Hs04334240_s1
CD36 (Platelet glycoprotein 4)	Hs01567185_m1
CPT1A (Carnitine O-palmitoyltransferase 1, liver isoform)	Hs00912671_m1
CREBBP (CREB-binding protein)	Hs00231733_m1
CYB5A (Cytochrome b5)	Hs04229876_g1
CYP1A1 (Cytochrome P450 1A1)	Hs00153120_m1
CYP1A1 (Cytochrome P450 1A1)	Hs00164383_m1
CYP1A2 (Cytochrome P450 1A2)	Hs01070374_m1
CYP27A1 (Sterol 26-hydroxylase, mitochondrial)	Hs01026016_m1
CYP2A6 (Cytochrome P450 2A6)	Hs00868409_s1
CYP2B6 (Cytochrome P450 2B6)	Hs03044634_m1
CYP2B7 (Cytochrome P450 2B7 isoform)	Hs00746388_s1
CYP2C19 (Cytochrome P450 2C19)	Hs00426380_m1
CYP2C8 (Cytochrome P450 2C8)	Hs00258314_m1
CYP2C9 (Cytochrome P450 2C9)	Hs00426397_m1
CYP2D6 (Cytochrome P450 2D6)	Hs00164385_m1
CYP2E1 (Cytochrome P450 2E1)	Hs00559368_m1
CYP3A4 (Cytochrome P450 3A4)	Hs00430021_m1
CYP3A5 (Cytochrome P450 3A5)	Hs01070905_m1
CYP3A7 (Cytochrome P450 3A7)	Hs00426361_m1
CYP4A11 (Cytochrome P450 4A11)	Hs04194779_g1
CYP51A1 (Lanosterol 14-alpha demethylase)	Hs00426415_m1
CYP7A1 (Cytochrome P450 7A1)	Hs00167982_m1
CYP8B1 (7-alpha-hydroxycholest-4-en-3-one 12-alpha-hydroxylase)	Hs00244754_s1
DPYD (Dihydropyrimidine dehydrogenase [NADP(+)])	Hs00559278_m1
EGR1 (Early growth response protein 1)	Hs00152928_m1
ELOVL6 (Elongation of very long chain fatty acids protein 6)	Hs00907564_m1
FABP1 (Fatty acid-binding protein, liver)	Hs00155026_m1
FOS (Proto-oncogene c-Fos)	Hs00170630_m1
FOXO1 (Forkhead box protein O1)	Hs00231106_m1
GAPDH (Glyceraldehyde-3-phosphate dehydrogenase)	Hs99999902_m1

GSTA2 (Glutathione S-transferase A2)	Hs00747232_mH
GSTM1 (Glutathione S-transferase Mu 1)	Hs01683722_gH
GSTP1 (Glutathione S-transferase P)	Hs00168310_m1
HMGCR (3-hydroxy-3-methylglutaryl-coenzyme A reductase)	Hs00168352_m1
HMOX1 (Heme oxygenase 1)	Hs00157965_m1
HNF1A (Hepatocyte nuclear factor 1-alpha)	Hs00167041_m1
HNF4A (Hepatocyte nuclear factor 4-alpha)	Hs01023298_m1
INSIG1 (Insulin-induced gene 1 protein)	Hs01650977_g1
INSIG2 (Insulin-induced gene 2 protein)	Hs00379223_m1
JUN (Transcription factor AP-1)	Hs00277190_s1
NPC2 (NPC intracellular cholesterol transporter 2)	Hs00197565_m1
NR0B2 (Nuclear receptor subfamily 0 group B member 2, SHP)	Hs00222677_m1
NR1D1 (Nuclear receptor subfamily 1 group D member 1, Rev-erbA-alpha)	Hs00253876_m1
NR1D2 (Nuclear receptor subfamily 1 group D member 2, Rev-erb-beta)	Hs00233309_m1
NR1H3 (Oxysterols receptor LXR-alpha)	Hs00172885_m1
NR1H4 (Bile acid receptor, FXR)	Hs00231968_m1
NR1I2 (Nuclear receptor subfamily 1 group I member 2, PXR)	Hs00243666_m1
NR1I3 (Nuclear receptor subfamily 1 group I member 3, CAR)	Hs00901571_m1
NR2F1 (COUP transcription factor 1)	Hs00818842_m1
NR2F2 (COUP transcription factor 2)	Hs01047078_m1
NR3C1 (Glucocorticoid receptor)	Hs00230818_m1
NR4A1 (Nuclear receptor subfamily 4 group A member 1, NUR77)	Hs00374226_m1
NR5A2 (Nuclear receptor subfamily 5 group A member 2, LRH-1)	Hs00187067_m1
PGRMC1 (Membrane-associated progesterone receptor component 1)	Hs00198499_m1
PGRMC2 (Membrane-associated progesterone receptor component 2)	Hs00175051_m1
POR (NADPH--cytochrome P450 reductase)	Hs00287016_m1
PPARA (Peroxisome proliferator-activated receptor alpha)	Hs00231882_m1
PPARG (Peroxisome proliferator-activated receptor gamma)	Hs01115513_m1
RPLP0 (60S acidic ribosomal protein P0)	Hs02758991_g1
RXRA (Retinoic acid receptor RXR-alpha)	Hs00172565_m1
SCD5 (Stearoyl-CoA desaturase 5)	Hs01682761_m1
SLC10A1 (Sodium/bile acid cotransporter, NTCP)	Hs00161820_m1
SLC22A7 (Solute carrier family 22 member 7, OAT2)	Hs00198527_m1
SLCO1B1 (Solute carrier organic anion transporter family member 1B1)	Hs00272374_m1
SREBF1 (Sterol regulatory element-binding protein 1)	Hs00231674_m1
SREBF2 (Sterol regulatory element-binding protein 2)	Hs00190237_m1
STAR (Steroidogenic acute regulatory protein)	Hs00986559_g1
SULT1A1 (Sulfotransferase 1A1)	Hs00738644_m1
SULT1B1 (Sulfotransferase family cytosolic 1B member 1)	Hs00234899_m1
SULT1E1 (Sulfotransferase 1E1)	Hs00960941_m1
SULT2A1 (Bile salt sulfotransferase)	Hs00234219_m1
UGT1A1 (UDP-glucuronosyltransferase 1A1)	Hs02511055_s1
UGT1A3 (UDP-glucuronosyltransferase 1A3)	Hs04194492_g1
UGT1A8 (UDP-glucuronosyltransferase 1A8)	Hs02557804_sH
UGT1A9 (UDP-glucuronosyltransferase 1A9)	Hs02516855_sH

UGT2B15 (UDP-glucuronosyltransferase 2B15)	Hs03008769_g1
UGT2B4 (UDP-glucuronosyltransferase 2B4)	Hs02383831_s1
UGT2B7 (UDP-glucuronosyltransferase 2B7)	Hs00426592_m1
VDR (Vitamin D3 receptor)	Hs01045840_m1

6.11. Bactosomes

Bactosome	Ordering ID (Cypex Ltd., Dundee, UK)
Human CYP2C8R EasyCYP Bactosomes	CYP/EZ017
Human CYP2C8LR EasyCYP Bactosomes	CYP/EZ047
Human CYP2C9R EasyCYP Bactosomes	CYP/EZ006
Human CYP2C9HR EasyCYP Bactosomes	CYP/EZ019
Human CYP3A4R EasyCYP Bactosomes	CYP/EZ002
HumanCYP3A4LR EasyCYP Bactosomes	CYP/EZ010

7. Methods

7.1. Molecular biological methods

7.1.1. mRNA expression analysis

RNA Isolation

For mRNA expression analysis mRNA was isolated using the RNeasy Mini Kit (Qiagen, Hilden, USA) according to manufacturer's instructions. RNA quantity and quality was determined using the NanoDrop™ spectrometer (PeqLab (VWR), Radnor, USA) or the Agilent 2100 Bioanalyzer (Agilent Technologies, Santa Clara, USA) for better estimation of RNA quality before storage of RNA samples at -80 °C or measurement of mRNA expression levels.

cDNA synthesis

For pre-mRNA expression analysis the isolated mRNA was reverse transcribed into cDNA using the TaqMan® Reverse Transcription Reagents Kit in 384-well plate format (see Table 20 for components). Synthesis of cDNA was performed on a Veriti 384-well Thermal Cycler (Veriti, Atlanta, USA) with the annealing step performed at 25 °C for 10 min, cDNA synthesis at 45 °C for 30 min and the inactivation of the reverse transcriptase at 95 °C for 5 min.

Table 20: Components for cDNA synthesis

Component	Final concentration	Volume per reaction (µl)
10 x TaqMan RT Buffer	1 x	1
MgCl2 (25 mM)	5.5 mM	2.2
dNTP-Mix	500 µM each	2
Random hexamers	2.5 µM	0.5
RNase Inhibitor	0.4 U/µl	0.2
Multiscribe RT (50 U/µl)	1.25 U/µl	0.25
RNA	100 ng	3.85
Total volume		10

Quantitative real-time PCR

Quantitative real-time PCR (qRT-PCR) with gene-specific TaqMan assays is a method for determining relative expression levels of certain genes. The TaqMan assay principal is explained in Figure 40.
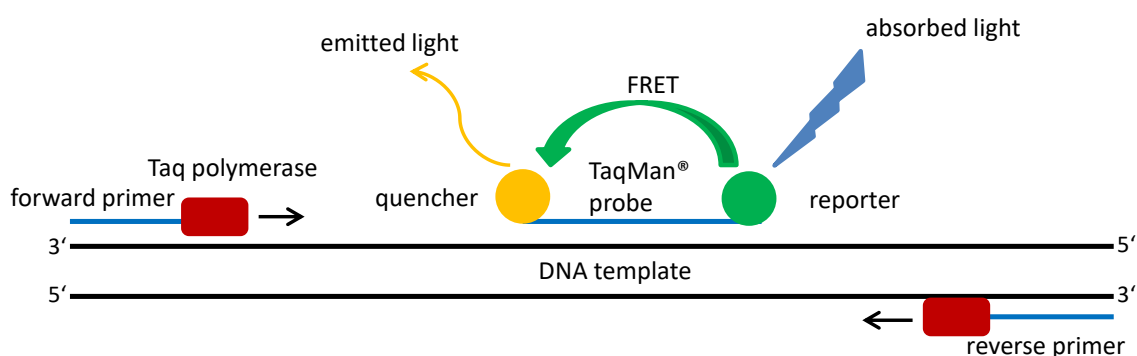

Figure 40: Scheme of a TaqMan-Probe.

In the amplification phase of the PCR the 5'-3' exonuclease activity of the Taq polymerase degrades the probe in 5' to 3' direction. This leads to separation of quencher and reporter and an increase of reporter fluorescence. The intensity of fluorescence is proportional to the amount of PCR product. For quantification of the amount of PCR product the cycle threshold value is determined. This value corresponds to the first cycle in which light intensity is doubled.

qRT-PCR was either performed on the Biomark HD System (Fluidigm) using microfluidic dynamic arrays (48.48 Dynamic Array™ IFC) or on the 7900 HT Real Time PCR System. The high-throughput gene expression platform Biomark HD was used for measuring large sample and gene sets simultaneously, while the 7900 PCR System was used for measuring fewer genes in small sample sets.

qRT-PCR using the Biomark HD System

Specific target amplification
As the microfluidic dynamic array (Fluidigm, San Francisco, USA) uses small volumes, detection of low-expressed genes is only possible after specific target preamplification, which increases concentration of the measured gene. By pooling gene expression assays containing gene-specific primer sets, up to 100 target genes can be preamplified simultaneously. One µl each of TaqMan assay (20x, listed in chapter 6.9) was diluted with DNA suspension buffer to a final concentration of 0.2x pooled assay mix. For preamplification the pooled assay mix was combined with PreAmp Master Mix and cDNA (see Table 21 for composition) and amplified in a Veriti 384-well Thermal Cycler (Veriti) under the conditions listed in Table 22.

Table 21: Reaction composition for Fluidigm preamplification

Substance	Volume per reaction
2x PreAmp Master Mix	2.5 µl
Pooled TaqMan assay mix (0.2x)	1.25 µl
cDNA	1.25 µl
Total volume	5 µl

Table 22: Thermal conditions for specific target amplification

Step	Temperature	Duration	Cycles
Enzyme activation	95 °C	10 min	1
Denaturation	95 °C	15 s	14
Annealing/Extension	60 °C	4 min	1

qRT-PCR on the Biomark HD System

For qRT-PCR on the Biomark HD System (Fluidigm) 10 X TaqMan® assays (see Table 23 for components) as well as the samples (see Table 24) were prepared in 96-well PCR plates. Both plates were sealed, vortexed, and centrifuged to avoid air bubbles.

Table 23: 10x TaqMan® assay mix for qRT-PCR on Biomark HD System.

Components	Amount for 1 reaction with overage
20 x TaqMan gene expression assay	3.5 µl
2 x Assay Loading Reagent	3.5 µl
Total volume	7 µl

Table 24: Sample pre-mix for qRT-PCR on Biomark HD System.

Components	Amount for 1 reaction with overage
2 x TaqMan Universal PCR Master Mix	3 µl
20 x GE Sample Loading Reagent	0.3 µl
cDNA	2.7 µl
Total volume	6 µl

After injection of the control line fluid into the 48.48 Dynamic Array IFC using a syringe, it was equilibrated on the integrated fluidic circuit (IFC) Controller HX for 15 min. Afterwards 5 µl of each assay and 5 µl of each sample (48 assays vs 48 samples) were transferred into the respective inlets on dynamic array chip and loaded using the IFC Controller HX. The GE 48x48 Standard v1 protocol was used for thermal cycling (see Table 25).

Table 25: Thermal protocol for qRT-PCR on the Biomark HD system (GE 48x48 Standard v1).

Step	Temperature	Duration	Cycles
Enzyme activation	95 °C	10 min	1
Denaturation	95 °C	15 s	40
Annealing/Elongation	60°C	1min	

qRT-PCR using 7900 HT Real Time PCR System

For qRT-PCR using the 7900 HT Real Time PCR System (Applied Biosystems, Foster City, USA) TaqMan assays (see chapter 6.9) were mixed with cDNA, water and TaqMan 2x PCR Master Mix (see Table 26).

Table 26: Compounds for qRT-PCR using 7900 HT Real Time PCR System

Compound	Amount
TaqMan 2X PCR MasterMix	5 µl
20x Assay	0.5 µl
water	2.5 µl
cDNA	2 µl
Total Volume	10 µl

The reaction mixes were transfered into a MicroAmp® optical 384-well reaction plate (Thermo Fisher Scientific, Waltham, USA). The qRT-PCR reaction took place under the following thermal cycling protocol (see Table 27).

Table 27: Thermal protocol for qRT-PCR using 7900 HT Real Time PCR System

Step	Temperature	Duration	Cycles
Enzyme activation	50 °C	2 min	1
Initial DNA denaturation	95°C	10 min	1
DNA denaturation	95 °C	15 s	50
Annealing/Extension	60°C	1min	

Data analysis

Data analysis was performed with Fluidigm Real-Time Analysis software (Fluidigm) or the SDS version 2.4 TaqMan® software (Thermo Fisher Scientific). Relative gene expression was quantified according to the $2^{-\Delta\Delta Ct}$ method (Livak and Schmittgen 2001). Gene expression was quantified in biological and technical multiplates and normalized for more accurate results to the geometric mean of the three housekeeping genes glyceraldehyde-3-phosphate dehydrogenase (GAPDH), ribosomal protein lateral stalk subunit P0 (RPLP0) and β-actin expression (Vandesompele et al. 2002).

7.1.2. Cloning of LentiCRISPR v2
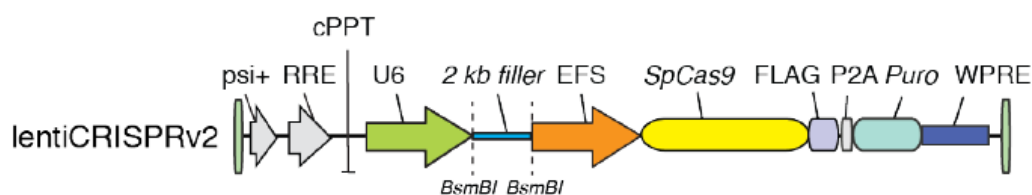
Figure 41: Scheme of lentiCRISPR v2 plasmid. Figure taken from (Sanjana et al. 2014).

The LentiCRISPR v2 plasmid (Addgene, Watertown, USA) was used for lentiviral knockout of POR in HepaRG cells. This plasmid contains two expression cassettes, human SpCas9 and the chimeric gRNA. Following digestion of the vector using *Bsm*BI, double-stranded oligonucleotides encoding the desired sgRNA can be cloned into the single guide RNA (sgRNA) scaffold. The single-stranded oligonucleotides are designed according to the following configurations:

Forward oligonucleotide: 5ˈ CACCG---20 bp Target --- 3ˈ

Reverse oligonucleotide: 5ˈ AAAC---20 bp Target ---C 3ˈ

The restriction digest of lentiCRISPR v2 using *Bsm*BI (see Table 28 for composition) was performed at 55 °C for 2 h with heat inactivation of the enzyme at 80 °C for 20 min.

Table 28: Components for BsmBI restriction digest

Substance	Amount
lentiCRISPR v2	2500 ng
10x buffer (3)	5 µl
***Bsm*B I (NEB)**	2.5 µl
Nuclease free H$_2$O	Add 50 µl

Afterwards the digestion products were loaded on a 1 % agarose gel and separated for 1 h at 80 V. The linearized plasmid (14 kb band) was extracted from the gel and cleaned using GENECLEAN Turbo Kit (Qbiogene, Carlsbad, USA) according to manufacturer's instructions. DNA concentration was quantified using NanoDrop™ (Peqlab).

In parallel, reannealing of oligonucleotides was performed (see Table 29 for composition) in a Veriti 96-well Thermal Cycler (Veriti) (Program: 5 min at 95 °C, slow cooling wit 0.1 °C/sec).

Table 29: Components for reannealing of oligonucleotides

Substance	Amount
Oligonucleotide F (100 µM)	1 µl
Oligonucleotide R (100 µM)	1 µl
10 x T4 ligation buffer	1 µl
Nuclease free H$_2$O	7 µl

The ligation of oligonucleotides to the linearized plasmid (see Table 30 for composition) was done at 4 °C overnight.

Table 30: Components for ligation

Substance	Amount
Linearized plasmid	50 ng
Oligos 1:200 diluted	2 µl
10 x T4 Ligation Buffer	1 µl
Nuclease free H_2O	Add 10 µl

+ 1 µl T4 Ligase

After ligation One Shot® Stbl3™ Chemically Competent *E. coli* (Thermo Fisher Scientific, Waltham, USA) were transformed with the ligated plasmid according to manufacturer's instructions (Invitrogen, Carlsbad, USA). 1-5 µl of DNA (10 pg to 100 ng) was added to one thawed vial of bacteria. Bacteria were then incubated for 30 min on ice with a following heat shock at 42 °C for 45 sec and cooling for 2 min on ice. Afterwards 250 ml S.O.C. medium (Invitrogen) was added at RT and the bacteria suspension was incubated at 37 °C for 1 h under shaking. Then 100 µl of the bacteria suspension was plated on LB-Ampicilin plates and incubated at 37 °C overnight. Afterwards bacteria colonies were proliferated for subsequent plasmid preparation.

7.1.3. Plasmid preparation

Mini- as well as midi-preparations of plasmids were carried out according to manufacturer's instructions (Qiaprep Spin Miniprep Kit (Qiagen) and PureYield™ Plasmid Midiprep System (Promega, Madison, USA). Plasmid concentrations were determined using NanoDrop™ (PeqLab).

7.1.4. DNA Isolation

DNA isolation was performed using the QIAamp DNA mini Kit (Qiagen) following the manufacturer's instructions. The DNA concentration was determined using NanoDrop™ (PeqLab).

7.1.5. T7 endonuclease 1 mismatch assay

There are several methods to detect CRISPR/Cas9 induced on-target mutations (see Figure 42). These include mismatch cleavage using a T7 endonuclease 1 (T7E1) or the surveyor™ nuclease, high resolution melt analysis or the heteroduplex mobility assay by PAGE. In this thesis the T7E1 mismatch was used because of its high sensitivity and simple application (Vouillot et al. 2015; Zischewski et al. 2017). Basis of this assay is the ability of T7E1 to cut DNA mismatches greater than 2 bp.
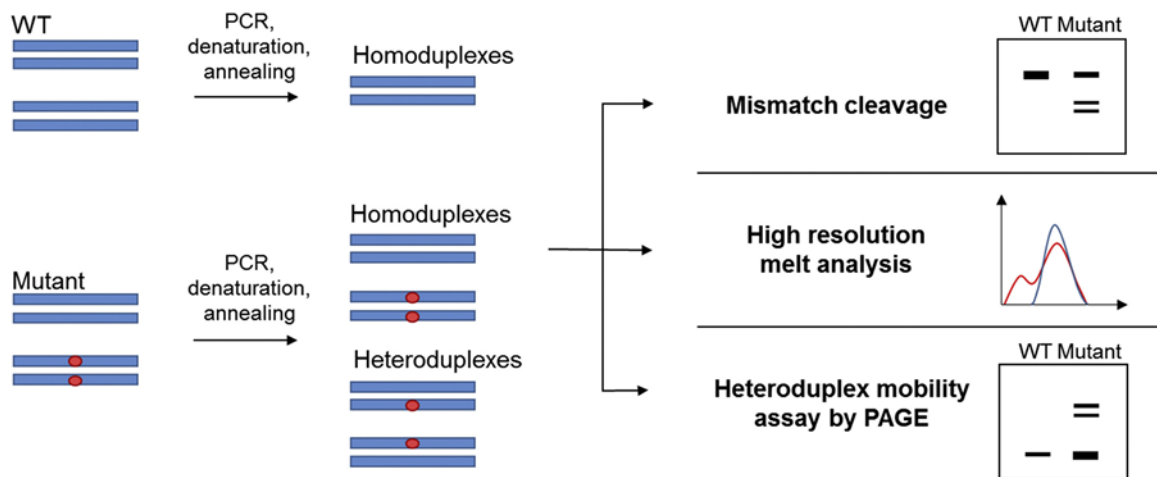
Figure 42: Mismatch-based assays for detection of mutations. Figure taken from (Zischewski et al. 2017).

For detection of Cas9-induced mutations the host DNA was isolated and the Cas9 target region (around 1 kb) was amplified via PCR. In chapter 6.8 all oligonucleotides used for PCR amplification for T7E1 digest are listed. Afterwards the PCR fragments were denatured and reannealed (see Table 31 for reaction composition) in a 96-well Thermal Cycler (Veriti) (denaturation conditions: 95 °C for 10 min, ramp down to 85 °C with -2 °C/s, ramp down to 25 °C with -0.3 °C/s) .

Table 31: Reaction composition for PCR denaturation and annealing pre T7E1 digest

Substance	Amount
PCR product	10 µl
10x NEBuffer 2 (NEB, Frankfurt a.M., DE)	1.5 µl
Nuclease free water	1.5 µl
Total volume	13 µl

Cas9-induced mutations will result in DNA heteroduplexes, which are recognized and cut by T7E1. For T7E1 digestion PCR heteroduplexes are mixed with T7E1 (NEB) (see Table 32 for conditions) and incubated for 1 h at 37 °C. The digestion fragments were analyzed by gel electrophoresis on a 1 % agarose gel (1h at 80 V) or using the Agilent 2100 Bioanalyzer (Agilent Technologies) fragment analyzer with the Agilent DNA7500 kit (Agilent Technologies).

Table 32: Components for T7E1 digestion

Substance	Amount
PCR heteroduplexes	13
T7E1 (1 U/µl)	2
Total volume	15

7.1.6. Sequencing and genotyping

Sanger sequencing was supplied by Microsynth AG (Göttingen, DE). Per reaction 720-1,200 ng plasmid or 18 ng per 100 bases DNA in a volume of 12 µl were mixed with 3 µl sequencing primers (see chapter 6.8) (10 pmol/µl) in a 1.5 ml reaction tube and sent to Microsynth. Delivered sequence data were analyzed with the Geneious 8.0.5 software.

Genotyping of the most important variants of *CYP2B6*, *2C9*, *2C19* and *3A4/5* was performend using OpenArray plates with a QuantStudio 12k flex system (Thermo Fisher Scientific) equipped with pre-desigend TaqMan assays (Thermo Fisher Scientific) (see Table 33) in cooperation with Dr. Roman Tremmel (IKP, Stuttgart). In brief, 3 µL DNA (50 ng/µL), mixed with OpenArray Genotyping MasterMix was applied on the OpenArray plate using the AccuFill Loader (Thermo Fisher Scientific). The plate was sealed within 90 s and placed into the real-time PCR machine. The PCR was performed using the genotyping mode. Genotypes were called using the Genotyper Software (Thermo Fisher Scientific).

Table 33: Pre-designed TaqMan assays for OpenArray genotyping

Target gene	Pre-designed TaqMan assay
CYP2B6	AHFBATH, C__60732328_20, AHABIR9
CYP2C9	C__27104892_10, C__25625805_10, C__30634132_70, C__27859817_40
CYP2C19	C____469857_10, C__25745302_30, C__30634136_10, C__30634130_30, C__25986767_70
	C__27861809_10, C__27861810_10, C__30634128_10, C__27531918_10
CYP3A4	C___1837671_50, C__59013445_10
CYP3A5	C__30203950_10, C__32287188_10, C__26201809_30

7.2. Protein biochemical methods

7.2.1. Protein quantification with BCA assay

Protein quantification was carried out using the Pierce™ BCA Protein Assay Kit (Thermo Fisher Scientific) following the manufacturer's instruction.

7.2.2. Flow cytometry

Protein expression analysis with flow cytometry

The expression of proteins in single cells of a certain population can be analyzed with flow cytometry. The target protein is fluorescence marked with antibodies allowing detection of the fluorescent marker in a rapid fluidic stream, where cells pass a laser detector individually. For antibody staining the separated cells were fixed in 4 % paraformaldehyde for 10 min at 37 °C and then permeabilized in 90 % methanol on ice for 30 min. After washing with incubation buffer (5 % BSA/PBS) the cells were stained with the primary antibody for 1 h at RT. An unstained control sample is treated in parallel with incubation buffer alone. After a second wash step the cells were incubated with the fluorescence labelled secondary antibody for 30 min at RT. For analysis with the flow cytometer (FACSCalibur, Becton Dickinson, Franklin Lakes, USA) the cells were suspended in PBS. Data analysis was done with the BD CellQuest Pro Software (Becton Dickinson). Table 34 lists all antibodies used for flow cytometry.

Table 34: Antibodies used for flow cytometry

Antigen	Type	Origin	Supplier	Article number	Dilution
Cas9 (s.p.)	Primary	Mouse monoclonal	abcam	Ab191468	1:200 in 5% BSA/PBS
Mouse IgG	Secondary	Goat polyclonal	Fisher Scientific GmbH	Ab150113	1:200 in 5% BSA/PBS

Clonal dilution of cells with FACS

A special application of flow cytometry is fluorescence-activated cell sorting. Here the cells are separated after laser detection via vibrations into single droplets containing single cells. The cell-containing droplets can then be sorted into different vessels like tubes or multiwell plates. Thereby sorting of special cell populations or even single cell sorting is possible. Cell sorting was done in cooperation with the flow cytometry core facility in Tübingen under kind supervision of Dr. Kristin Bieber using a BD FACS Aria cell sorter or at the Institute for Biochemistry and technical Biochemistry in Stuttgart under kind supervision of Dr. Pavel Bashtrykov using a Sony CellSorter SH800S. Because HepaRG cells tend to form cell aggregates, the cells had to be filtered through a cell strainer (40 µm) before sorting into 96-well plates.

7.2.3. Western Blotting

Sample preparation

For western blotting cells were lysed with 5x passive lysis buffer and stored at -80 °C until further used. Protein was quantified with the BCA assay. For protein detection with western blot 5x lämmli buffer and H_2O (1 part lämmli buffer, 4 parts protein/H_2O) was added to the thawed and centrifuged samples. The samples were stored at -20 °C.

SDS-PAGE

For electrophoretic separation of the different proteins the samples were loaded in appropriate amounts on a 10 % SDS-polyacrylamide gels. For the compositions and polymerisation conditions of the gel mixture see Table 35. As a marker the Chameleon Duo Pre-stained Protein Ladder (LI-COR Biosciences, Bad Homburg, DE) was used. The electrophoresis was conducted for protein stacking at 100 V for 30 min in a PROTEAN® II or Mini-PROTEAN® cell, then the voltage was increased for protein separation to 150 V.

Table 35: Gel compositions and polymerisation conditions for 10 % SDS-polyacrylamide gel

Substance	Separating gel (10 %)		Stacking gel (4 %)
H_2O	3 ml (12 ml)		1.535 ml (6.1 ml)
Acrylamid/Bis solution (30%)	2.5 ml (10 ml)		0.3375 ml (1.35 ml)
Tris-Buffer pH 8.8	1.875 ml (7.5 ml)	Tris-Buffer pH 6.8	0.625 ml (2.5 ml)
10 % SDS	0.075 ml (0.3 ml)		0.025 ml (0.1 ml)
TEMED	7.5 µl (30 µl)		2.5 µl (10 µl)
APS	0.075 ml (0.3 ml)		0.025 ml (0.1 ml)
	→Polymerisation for ~30 min		→ Polymerisation for ~60 min (or overnight)

Western blot

After SDS-PAGE the separated proteins in the gel were transferred to a nitrocellulose membrane for antibody detection. Therefore, filter papers, nitrocellulose membrane and the gel were soaked in transfer buffer before stacking them in a fast blotting chamber (Fastblot B44) (stacking order: 3 layers of filter, membrane, gel, 3 layers of filter). The semi-dry blotting was performed for 20 min at 100 mA (for small 7x9 cm gel). The transfer success was then verified by PonceauS staining for 5 min. Afterwards the membrane was blocked by incubation in 5 % skim milk for 1 h. This step was followed by primary and then secondary antibody staining, interrupted by a wash step with 1x TBST. Table 36 lists all antibodies and their usages. The blots were then analyzed in the Odyssey Infrared Imaging System using the Image Software.

Table 36: Antibodies used for western blotting

Antigen	Type	Origin	Supplier	Article number	Usage
Cas9 (s.p.)	Primary	Mouse monoclonal	abcam	ab191468	1:5000 in 1% MM-TBST
β-actin	Primary	Mouse monoclonal	Sigma Aldrich	SIGMA A5441	1:5000 in 1% MM-TBST
CYP1A2	Primary	Mouse monoclonal	Krasz/Bethesda	clone 26-7-5	1:2000 in 1% MM-TBST
CYP2B6	Primary	Mouse monoclonal	BDGentest	458326	1:2000 in 1% MM-TBST
CYP2C8	Primary	Rabbit polyclonal	Puracyp	Hu-A004	1:1000 in 5% MM-TBST
CYP2C9	Primary	Rabbit polyclonal	RDI	CYP2C9abr	1:1000 in 1% MM-TBST
CYP2D6	Primary	Mouse monoclonal	(Zanger et al. 2001)		1:1000 in 1% MM-TBST

CYP3A4	Primary	Rabbit polyclonal	BDGentest	458234	1:1000 in 1% MM-TBST
POR	Primary	Rabbit polyclonal	(Gomes et al. 2009)		1:1000 in 1% MM-TBST
Anti mouse IRD680/800	Secondary	Goat polyclonal	Licor GmbH	926-68070 /926-32210	1:5000-10.000 in 1% MM-TBST
Anti rabbit IRD680/800	Secondary	Goat polyclonal	Licor GmbH	926-68071 /926-32211	1:10.000 in 1% MM-TBST

7.2.4. Microsome preparation

Microsomes are artificial vesicles re-formed from the endoplasmic reticulum (ER) after cell disruption and differential centrifugation. They are used for analysis of ER bound proteins like CYPs or POR. For microsome preparation harvested cells were lysed using lysing matrix D 2 ml vials in homogenisation buffer (see chapter 6.6) with the FastPrep®-24 (MP Biomedicals GmbH, Eschwege, DE) 2 times for 10 sec at level 6 at 4 °C. The homogenate was then centrifuged with the Beckman Coulter OPTIMA MaxE ultracentrifuge (rotor MLA-80) for 30 min at 15,000 rpm (10,000 x g) at 10 °C. The supernatant was centrifuged a second time for 60 min at 45,000 rpm (100,000 x g) at 10 °C. The resulting supernatant is the cytosolic fraction and is to be stored; the pellet was resuspended in cold microsome buffer see (chapter 6.6) and transferred into a dounce homogenator. The microsomes were formed by 2-3 strokes with teflon pistils.

7.2.5. CYP activty measurements

CYP Cocktail assay

Activities of the most prominent liver CYP isozymes CYP1A2, CYP2B6, CYP2C8, CYP2C9, CYP2C19, CYP2D6 and CYP3A4 were determined with a liquid chromatography tandem mass spectrometry (LC-MS/MS) cocktail assay (Feidt et al. 2010). For analysis in cultured cells, seven specific substrates for the corresponding isozymes were supplemented to the medium (see Table 37 for the concentrations). After incubation for 3 h at 37 °C, 160 ml medium was harvested, mixed with 40 ml 250 mM formic acid and stored immediately at -20 °C.

Table 37: Composition of CYP cocktail

CYP isozyme	Substrate	Molecular weight [g/mol]	Stock concentration [mM]	Solvent	Final concentration [µM]
CYP1A2	Phenacetin	179	100	DMSO	50
CYP2B6	Bupropion	256	50	H2O	25
CYP2C8	Amodiaquine	465	10	H2O	5
CYP2C9	Tolbutamide	270	100	DMSO	100
CYP2C19	S-Mephentoin	218	100	ACN	100
CYP2D6	Propafenone	378	10	MeOH	5
CYP3A4	Atorvastatin	559	5	ACN/H2O	35

For absolute quantification of the metabolites formed during incubation time a calibration curve was prepared consisting of a series of standards and quality controls (see Table 38) in a 96-well plate.

Table 38: Calibration standards and quality controls for CYP cocktail assay (IS= internal standards, QC=quality control)

Name	Volume 250 mM formic acid (µl)	Volume HepaRG medium (µl)	Volume stock solutions (µl): EP0-EP8	
IS 0	10	40	-	ep0
IS 8	10	35	5	ep8
IS 7	10	35	5	ep7
IS 6	10	35	5	ep6
IS 5	10	35	5	ep5
IS 4	10	35	5	ep4
IS 3	10	35	5	ep3
IS 2	10	35	5	ep2
IS 1	10	35	5	ep1
QC 7	10	35	5	ep7
QC 5	10	35	5	ep5
QC 3	10	35	5	ep3

Afterwards 50 µl of each sample was added to the 96-well plate (Corning Axygen® P-96-450V-C Storage 96-Well Assay Microplate with V-Bottom Wells), followed by adding of 10 µl internal standard (deuterium labelled metabolite for each substrate) to all samples, standards and quality controls. The measurement was done with a 6460 triple quadrupole mass spectrometer coupled to a 1200 HPLC system by the analytic department.

CYP kinetic and inhibition measurements in microsomes

Kinetic measurements of conversion of amodiaquine, tolbutamide, atorvastatin and midazolam in HepaRG microsomes were performed for determination of kinetic parameter K_M and V_{max}. Before the kinetic experiments protein and time dependency experiments were performed to elucidate protein amounts and incubation times in the linear range. Microsome amounts, incubation times and substrate ranges of the kinetic experiments are listed in Table 39.

Table 39: Reaction conditions for kinetic measurements in microsomes

Substrate	Microsomes	Incubation time	Substrate concentrations (µM)
Amodiaquine	20 µg	15 min	50, 20, 10, 8, 6, 4, 2, 1, 0.5
Tolbutamide	20 µg	30 min	400, 200, 100, 75, 50, 30
Atorvastatin	10 µg	10 min	100, 75, 50, 30, 20, 10, 7.5, 5, 2.5, 1
Midazolam	10 µg	10 min	150, 100, 50, 30, 20, 15, 10, 7.5, 5, 2.5, 1

For microsomal kinetic experiments the individual substrate in a certain concentration was mixed with 0.1 N potassium phosphate buffer (pH 7.4) and 10x NADPH regenerating system (see chapter 6.6) and preincubated at 37 °C for 5 min. Reactions were started by addition of microsomes according to amounts listed in Table 39. The final reaction volume was 50 µl. After a certain incubation time (see Table 39) reaction was stopped by addition of 25 µl of stopping solution (see chapter 6.6) and kept on ice. For quantification of reaction products by liquid chromatography with tandem mass spectrometry (LC-MS/MS) method 10 µl of internal standard, a deuterium-labelled metabolite for each substrate, was added to each sample. The measurement was done with a 6460 triple quadrupole mass

spectrometer coupled to a 1200 HPLC system by the analytic department under supervision of Dr. Ute Hofmann (IKP, Stuttgart).

The same kinetic experiments were performed in bacterial membrane compartments called bactosomes (see chapter 6.11) (Cypex Ltd, Dundee, UK). They contain human CYP2C8, CYP2C9 and CYP3A4 and human POR in high (R) and low (LR) concentrations. Pre-kinetic experiments were performed to elucidate protein amounts in the linear range. Bactosome amounts, incubation times and substrate ranges of the kinetic experiments are listed in Table 40.

Table 40: Reaction conditions for kinetic measurements in bactosomes

Substrate	Bactosomes	Incubation time	Substrate concentrations (µM)
Amodiaquine (5 µM)	5 pmol	20 min	100, 50, 20, 10, 8, 6, 4, 2, 1, 0.5, 0.25, 0.125
Tolbutamide	5 pmol	20 min	400, 300, 200, 150, 100, 75, 50, 25, 12.5, 6.25
Atorvastatin	5 pmol	20 min	100, 75, 50, 30, 20, 10, 7.5, 5, 2.5, 1
Midazolam	5 pmol	20 min	100, 30, 15, 10, 7.5, 6, 4, 2, 1, 0.5, 0.25

For inhibition of conversion of amodiaquine by the CYP2C8 specific inhibitor montelukast. 10 µg of microsomes were incubated in 0.1 N potassium phosphate buffer (pH 7.4) and 10x NADPH regenerating system (see chapter 6.6) for 5 min at 37 °C. After addition of 1 µl montelukast (concentration range: 10, 3, 1, 0.3, 0.1, 0.03, 0.01, 0.001, 0.0001 µM) the reaction mix was incubated for additional 10 min at 37 °C. The reaction was started by addition of 10 µl amodiaquine and incubated for 30 min at 37 °C. The final reaction volume was 100 µl with a final amodiaquine concentration of 5 µM.   Addition of 50 µl stopping solution (see chapter 6.6) ended the reaction. Further procedures were according to the kinetic experiments.

For direct comparison of NADPH- and NADH-driven metabolism, 20 µg of microsomes were incubated in 0.1 N potassium phosphate buffer (pH 7.4) and 1 mM NADPH, NADH or NADPH + NADH for 6 min at 37 °C. After addition 5 µl of CYP substrate cocktail mix with final concentration as described above, the reaction mix was incubated for 20 min at 37 °C. Further procedures were according to the kinetic experiments.

Kinetic parameters K_M and V_{max} were determined by Michaelis-Menten model or in case of midazolam by substrate inhibition model. Inhibition parameters IC_{50} and K_i were determined by a one site competition model using Graphpad Prism V8 software (GraphPad, San Diego, USA). Internal clearance (Cl_{int}) was calculated using the following equation:

$$Cl_{int} = \frac{V_{max}}{K_M}$$

P450-Glo Assay

As the CYP cocktail assay is not suitable for screening of hundreds of cell clones, the P450-Glo assay system from Promega was selected for experiments where large sample sets must be screened for CYP activity. CYP2C9 was selected as proxy for global CYP activities. The assay is based on the specific conversion of Luciferin-H by CYP2C9 to a product which is detectable in a luminescence reaction (Figure 43).
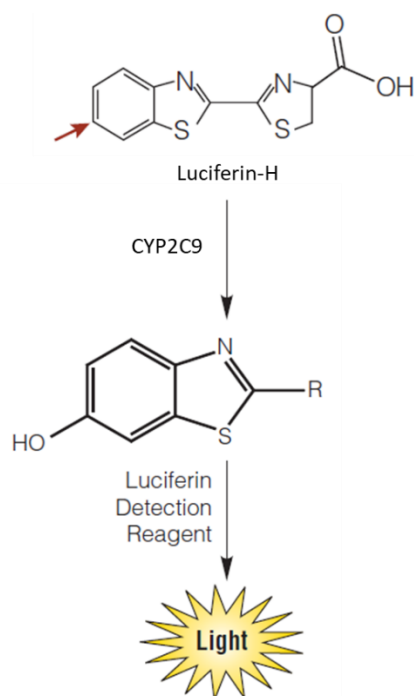
Figure 43: Conversion of the P450-Glo substrate Luciferin-H by CYP2C9 (figure taken and adapted from manufacturer's protocol, Promega, Madison, Wisconsin, USA)

The screened cells were treated with 1:50 in medium diluted substrate (Luciferin-H) and incubated for 4 h at 37°C. After incubation 25 ml of supernatant was transferred in a white OptiPlate (96-well) together with 25 µl luciferin detection reagent and incubated a second time for 20 min in the dark. Afterwards, luminescence was detected with the EnSpire Multimode Plate Reader.

7.2.6. Cytochrome C reduction assay

The cytochrome C reduction assay is the preferred assay for quantification of POR activity, as POR is also able to use cytochrome C as electron acceptor. This specific reaction is used as a model for CYP related POR activity in particular, as it requires two electrons that need to come from FMN through FAD (Pandey and Flück 2013). The reduced product is quantified photometrically at a wavelength of 550 nm. This assay was performed following a published protocol (Guengerich et al. 2009). In brief: after microsomal preparation, a certain amount of protein (15-30 µg) was added together with 10 µl of 4 mM cytochrome C solution, 10 µl of 100 mM KCN in 1 ml of 0.3 M sodiumphosphate buffer and measured as a blank at 550 nm. Following addition of 100 ml of 1 mM NADPH solution the reaction was started and the kinetics were measured for 3 min with the Agilent 8453 UV-visible Spectroscopy System (Agilent Technologies) and analyzed with the Agilent ChemStation Software (Agilent Technologies). POR activity was determined using the following formulas:

$$\text{Volume activity } \left(\frac{U}{ml}\right) = \frac{\Delta \text{ absorption} \cdot \text{dilution factor}}{\text{min} \cdot \varepsilon \cdot d}$$

$$\text{specific activity } \left(\frac{U}{mg}\right) = \frac{\text{Volume activity } (\frac{U}{ml})}{\text{protein concentration } (\frac{mg}{ml})}$$

$$\varepsilon \text{ (550nm)} = 21 \frac{1}{mM \cdot cm} \text{ ; extinction coefficient for reduced cytochrome C at 550 nm}$$

d = 1 cm; layer thickness of cuvette

The assay also detects activity of methionine synthase reductase (Olteanu and Banerjee 2001) (100-fold slower as POR), inducible NO-synthase (NOS2) (Newton et al. 1998) and NADPH dependent diflavin oxidoreductase (Paine et al. 2000), but at much lower catalytic efficiencies compared to POR.

7.2.7. Quantification of bile acids

Bile acid secretion into medium was measured after incubation of cells with serum free medium for 24 and 48 h. Concentrations of secreted cholic acids (GCA, TCA) as well as chenodeoxycholic acids (GCDCA, TCDCA) derivates were quantified in the medium by negative electrospray (ESI) LC-MS/MS in multiple-reaction-monitoring mode on an Agilent 6460 triple quadrupole mass spectrometer (Agilent, Waldbronn, Germany) coupled to an Agilent 1290 HPLC system (Ghallab et al. 2019; Haag et al. 2015). The analytical quantification of bile acid was performed in cooperation with Dr. Ute Hofmann (IKP, Stuttgart).

7.2.8. Quantification of lipid droplets

Nile red, 9-Diethylamino-2-hydroxy-5H-benz[a]phenoxazin-5-one, is used to localize and quantitate lipids, particularly neutral lipid droplets within cells due to its high specificity for staining lipids, as it is strongly fluorescent in hydrophobic environment but non fluorescent in water and other polar solvents. Moreover, staining with nile red does not dissolve the lipid droplet structures (Greenspan et al. 1985). The excitation maximum of nile red is about 554 nm (green) and the emission maximum is about 638 nm (red) ("Fluorescence SpectraViewer - Nile Red phospholipids", Thermo Fisher Scientific. Retrieved November 2020.)

Lipid droplet quantification by nile red staining was performed after incubation of HepaRG cells with serum free medium for 5 days. 15 µg/µl of nile red (Santa Cruz Biotechnology, Dallas, USA) were added to the cell medium for 20 min at 37 °C. Nile red fluorescence was analyzed at 580 nm using an EnSpire Mulitmode plate reader (PerkinElmer, Waltham, USA). For normalization cell vitality was assessed using the alamarBlue assay (Thermo Fisher Scientific) according to the manufacturer's instructions.

7.3.   Cell culture methods

7.3.1.   Cell culture

Standard cultivation

The cells were cultured in their respective medium (for medium composition see Table 12) in a 5 % CO_2 atmosphere at 37 °C in tissue culture flasks. Every three to four days when cells were at least 85 % confluent (checked by light-microscopy; Olympus CKX41) they were passaged. The medium was aspirated, and cell layers were washed with DPBS (Gibco). Then cells were incubated with 2 ml of 0.25 % trypsin-EDTA solution (Gibco) for 5 min at RT. Detached cells were resuspended using 10 ml medium (37 °C) and 20 to 30 % of the cells were seeded into a new flask. Cell numbers were determined using C-Chip Counting chambers, Neubauer Imp. (VWR).

Cultivation of HepaRG

For standard cultivation of HepaRG cells (Aninat et al. 2006) one cryo-conserved aliquot ($1.5*10^6$ cells) was thawed in HepaRG medium and cultivated in 25 cm^2 (T-25) cell culture flasks under refreshment of medium every 2-3 days. Afterwards the cells were passaged (washing with DPBS, incubation with 1 ml 0.25% trypsin-EDTA solution), seeded on 24 multiwell plates (50,000 cells per well) and cultivated two additional weeks until full confluency. After this period differentiation of HepaRG cells was started by adding 1 % DMSO to the medium for 2 days and for 12 additional days 2 % DMSO. By this point the cells showed a differentiated hepatocyte like morphology and liver specific functions. For cryo conservation HepaRG cells were stored in liquid nitrogen in HepaRG medium supplemented with 10 % DMSO.

Collagen coating of cell culture plates

For culturing "Upcyte Hepatocytes" additional coating of cell culture plates is needed for good attachment of cells. Therefore, the culture plates were incubated with collagen I solution for 30 min at 37 °C. Afterwards the plates were washed with DPBS and could be stored at 4 °C for up to 1 week.

Cultivation of "Upcyte Hepatocytes"

After thawing "Upcyte Hepatocytes" can be cultivated in growth phase up to 15 passages in Hepatocyte Culture Medium (HCM). For differentiation the cells were treated for 5 days in pre-culture medium (HCM + 0.5 % DMSO). Afterwards they were treated in the conditioning phase with hepatocyte high performance medium (HPM) + 0.1 % DMSO (conditioning medium). The conditioning phase can be extended up to 18 days; the maximum of CYP expression is expected on day 7 (Schaefer et al. 2015).

7.3.2.   Cell viability measurements

Resazurin assay

Resazurin is a redox indicator is used for vitality measurements of cells. Metabolically active cells convert it under NAD(P)H usage irreversibly to the pink, strongly fluorescent dye Resorufin (see Figure 44). Its fluorescence is measured at a wavelength of 550 nm.
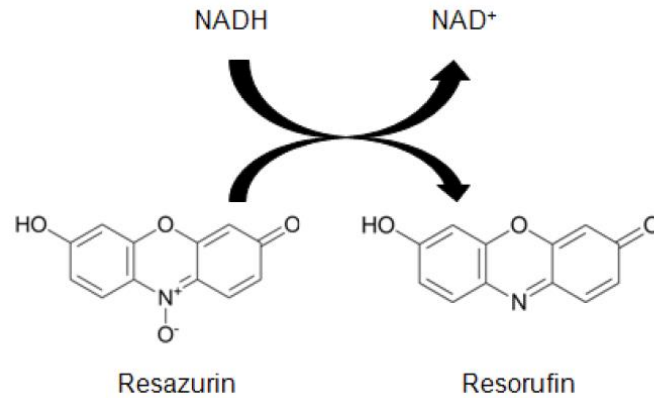
Figure 44: Formation of fluorescent resorufin through reduction of resazurin in living cells. Figure taken from (Riss et al. 2016)

For the measurement of cell viability with resazurin cells were treated with 0.15 mg/ml Resazurin in PBS in a dilution of 1:5. Depending on cell type fluorescence could be measured after an incubation of 1-4 h (for HepaRG 1.5 h) with the EnSpire Multimode Plate Reader (PerkinElmer, Waltham, USA).

LDH assay

The LDH assay is based on lactate release into culture medium of harmed cells. By adding lactate dehydrogenase (LDH) into the medium the lactate is converted under NAD^+ usage to Pyruvate. The resulting NADH can be detected through conversion of INT to the violet formazan.
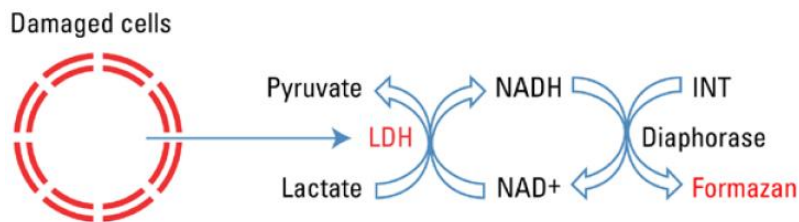
Figure 45: Principle of LDH Assay. Figure taken from supplier's information, Thermo Fisher Scientific Inc.

For the measurement of cell viability with the LDH assay the Pierce™ LDH Cytotoxicity Assay Kit (Thermo Fisher Scientific Inc.) was used following the manufacturer's instructions. 50 µl of medium was transferred to a 95 multiwell plate and mixed with additional 50 ml of reaction mixture. After 30 min incubation at RT the reaction is stopped by adding of 50 µl of stop solution. Afterwards the absorbance is measured at 490 and 680 nm with the EnSpire Multimode Plate Reader.

7.3.3. Cell transfection

Transfection of HepaRG cells with RNP complexes

One possibility to deliver Cas9 into cells is the transfection of the ribonucleoprotein sgRNA complexes (RNP complexes). In this thesis the Alt-R RNP System from IDT (Skokie, Illinois, USA) was used. For assembling the RNP complexes 100 µM of the RNA oligos (crRNA and tracrRNA) were equimolarly mixed, heated at 95°C and then cooled down slowly to RT. The sgRNA complexes (1 µM) were then mixed with 1 µM Cas9 nuclease in a total volume of 25 µl. After 5 min of incubation

at RT the RNP complexes were assembled and could be reverse transfected to cells in a 96-well format. For this purpose, 25 µl of RNP complex was mixed with 1.2 µl Lipofectamine® RNAiMAX transfection reagent and 23.8 ml Opti-MEM and incubated for 20 min at RT. After incubation 50 µl transfection complexes were added into a well of a 96-well cell culture plate together with 40,000 cells. 48 h after transfection cells could be harvested for DNA extraction or could be diluted to single cell clones with either limited dilution or with FACS.

Transfection of HepaRG^{VC} cells with Atto500 labled sgRNA

For genome editing with sgRNAs the complexes of tracrRNA and crRNA were delivered into Cas9 expressing cells. To monitor the transfection efficiency the red fluorescing tracrRNA atto500 was used. For assembling the sgRNA constructs 100 µM of the RNA oligos (crRNA and tracrRNA) were equimolarly mixed, heated at 95 °C and then cooled down slowly to RT. Afterwards the 150 µl of complexes (120 nM) were mixed with 4.8 µl lipofectamine RNAiMax and 45.2 µl Opti-MEM. After 20 min incubation at RT the transfection complexes were added into a well of a 24 well cell culture plate together with 400,000 cells. After 24 h cells were harvested for further analyzes or cultivated further.

7.3.4. Lentiviral transduction

Viral production in HEK 293FT cells

Lentiviral vectors are often used to integrate foreign nucleic acids into the genome of a target cell as they have the unique ability to infect even non dividing cells, which makes them a useful tool for gene delivery in hard to transfect cells. As HepaRG cells are known to be hard to transfect (Laurent et al. 2010) this method was chosen to deliver Cas9 and the sgRNAs into these cells.

The day before transfection HEK 293FT cells were seeded in T175 flasks ($1.6 * 10^7$). For transfection 20 µg lentiCRISPR v2 constructs, 10 µg pCMV-VSV-G (Addgene) and 15 µg psPAX2 (Addgene) were mixed with 70 µl TurboFect (Thermo Fisher Scientific Inc.) in 3.5 ml Opti-MEM. The transfection mix was incubated for 15-20 at RT and then added to the cells in 31 ml Opti-MEM (3.5 ml transfection mix per T-175 flask). The cells were incubated afterwards at 37 °C and 5 % CO_2.

Viral harvest

48 h after transfection the viral particles could be harvested. This work had to be be performed in a "Gentechnik"-S2 lab area. After sterile filtration (0.45 PVDF filter) medium was centrifugated (Beckmann Optima L-100XP in SW28) with 50,000 x g (16,651 rpm) for 90 min at 10 °C. The pellet containing the lentiviral particles was resuspended in 50 µl of 1 % BSA/PBS overnight at 4 °C and then stored at -80 °C until usage.

Relative viral titering with LDH assay

For determination of the optimal viral transduction concentration or MOI (multiplicity of infection) each charge of viral harvest has to be titered in a model cell line. Optimal cell lines for titering are those which are easy to infect, easy to kill by the selection drug and, easy to handle. We used A549 human lung carcinoma cells because they are well suited for titering vectors carrying a puromycin selection marker (see: Protocol: Relative Viral Titering with a Resazurin (alamarBlue) Cell Viability Assay, The Broad Institue, Sep 2015).

For titering, A549 cells in 96-well plates were treated with 10 µg/ml polybrene. The cells were then infected with 5 µl of lentiviral particles in decreasing dilutions (1:5, 1:10, 1:20, 1:40, 1:80, 1:160, 1:320). After 48 h incubation to the medium 1.5 µg/ml puromycin was added and after additional 72 h the puromycin resistance was assessed microscopically as well as with a LDH assay with readout in an EnSpire Multimode Plate Reader.

Transduction of target cells
Pre transduction medium of HepaRG cells was changed to a medium containing 10 µg/ml polybrene. Afterwards the viral particles were added in the appropriate dilution determined by titering. 48 h post transduction HepaRG cells were selected with 5 µg/ml Puromycin (Kennedy et al. 2015).

7.3.5. Statistical methods

All statistical analyzes were performed using Graphpad Prism V9 software (GraphPad Software, San Diego, USA) or Genedata Profiler 13.0 (Genedata, Basel, CH). Curve fitting of cellular growth was performed with a logistic growth model with seeding density and maximum cell count as fixed constraints. HepaRG single cell population analysis was fitted with a "sum of two"-Gaussian model. Spearman's correlation coefficients and corresponding tests were used to assess the associations between parental HepaRG and HepaRG[VC] on CYP activity and gene expression level. For statistical analysis of the experiments repeated measurements ANOVA with Bonferroni correction, Kruskal-Wallis test or appropriate paired/unpaired t-test statistics were applied, significance level was set to $p<0.05$. Results are shown as means ± standard deviation (SD). Kinetic parameters K_M and V_{max} were determined by a Michaelis-Menten model or by a substrate inhibition model. Inhibition parameters IC_{50} and K_i were determined by a one site competition model and shown with 95 % CI (confidence interval). Internal clearance (Cl_{int}) was calculated using the following equation: $Cl_{int} = \frac{V_{max}}{K_M}$

Publication bibliography

Abu-Abed, S.; Dollé, P.; Metzger, D.; Beckett, B.; Chambon, P.; Petkovich, M. (2001): The retinoic acid-metabolizing enzyme, CYP26A1, is essential for normal hindbrain patterning, vertebral identity, and development of posterior structures. In *Genes & development* 15 (2), pp. 226–240.

Abudayyeh, Omar O.; Gootenberg, Jonathan S.; Essletzbichler, Patrick; Han, Shuo; Joung, Julia; Belanto, Joseph J. et al. (2017): RNA targeting with CRISPR-Cas13. In *Nature* 550 (7675), pp. 280–284. DOI: 10.1038/nature24049.

Addya, S.; Anandatheerthavarada, H. K.; Biswas, G.; Bhagwat, S. V.; Mullick, J.; Avadhani, N. G. (1997): Targeting of NH2-terminal-processed microsomal protein to mitochondria. A novel pathway for the biogenesis of hepatic mitochondrial P450MT2. In *The Journal of cell biology* 139 (3), pp. 589–599.

Ahuja, Shivani; Jahr, Nicole; Im, Sang-Choul; Vivekanandan, Subramanian; Popovych, Nataliya; Le Clair, Stéphanie V. et al. (2013): A model of the membrane-bound cytochrome b5-cytochrome P450 complex from NMR and mutagenesis data. In *The Journal of Biological Chemistry* 288 (30), pp. 22080–22095. DOI: 10.1074/jbc.M112.448225.

Aktories, K. (Ed.) (2013): Allgemeine und spezielle Pharmakologie und Toxikologie. 11., überarbeitete Auflage. München: Urban & Fischer.

Almazroo, Omar Abdulhameed; Miah, Mohammad Kowser; Venkataramanan, Raman (2017): Drug Metabolism in the Liver. In *Clinics in liver disease* 21 (1), pp. 1–20. DOI: 10.1016/j.cld.2016.08.001.

Alnouti, Yazen (2009): Bile Acid sulfation: a pathway of bile acid elimination and detoxification. In *Toxicological sciences : an official journal of the Society of Toxicology* 108 (2), pp. 225–246. DOI: 10.1093/toxsci/kfn268.

Andersson, Tommy B.; Kanebratt, Kajsa P.; Kenna, John Gerry (2012): The HepaRG cell line: a unique in vitro tool for understanding drug metabolism and toxicology in human. In *Expert Opinion on Drug Metabolism & Toxicology* 8 (7), pp. 909–920. DOI: 10.1517/17425255.2012.685159.

Aninat, Caroline; Piton, Amélie; Glaise, Denise; Le Charpentier, Typhen; Langouët, Sophie; Morel, Fabrice et al. (2006): Expression of cytochromes P450, conjugating enzymes and nuclear receptors in human hepatoma HepaRG cells. In *Drug Metabolism and Disposition* 34 (1), pp. 75–83. DOI: 10.1124/dmd.105.006759.

Antoun, Joseph; Amet, Yolande; Simon, Brigitte; Dréano, Yvonne; Corlu, Anne; Corcos, Laurent et al. (2006): CYP4A11 is repressed by retinoic acid in human liver cells. In *FEBS letters* 580 (14), pp. 3361–3367. DOI: 10.1016/j.febslet.2006.05.006.

Anzenbacher, Pavel; Zanger, Ulrich M. (Eds.) (2012): Metabolism of Drugs and Other Xenobiotics // Metabolism of drugs and other xenobiotics. Weinheim, Chichester: John Wiley & Sons, Ltd; Wiley-VCH; John Wiley [distributor].

Araldi, Rodrigo Pinheiro; Khalil, Charbel; Grignet, Pedro Henrique; Teixeira, Michelli Ramires; Melo, Thatiana Correa de; Módolo, Diego Grando et al. (2020): Medical applications of clustered regularly interspaced short palindromic repeats (CRISPR/Cas) tool. A comprehensive overview. In *Gene* 745, p. 144636. DOI: 10.1016/j.gene.2020.144636.

Barnaba, Carlo; Gentry, Katherine; Sumangala, Nirupama; Ramamoorthy, Ayyalusamy (2017): The catalytic function of cytochrome P450 is entwined with its membrane-bound nature. In *F1000Research* 6, p. 662. DOI: 10.12688/f1000research.11015.1.

Barnaba, Carlo; Ramamoorthy, Ayyalusamy (2018): Picturing the Membrane-assisted Choreography of Cytochrome P450 with Lipid Nanodiscs. In *Chemphyschem : a European journal of chemical physics and physical chemistry* 19 (20), pp. 2603–2613. DOI: 10.1002/cphc.201800444.

Barrangou, Rodolphe; Birmingham, Amanda; Wiemann, Stefan; Beijersbergen, Roderick L.; Hornung, Veit; Smith, Anja van Brabant (2015): Advances in CRISPR-Cas9 genome engineering. Lessons learned from RNA interference. In *Nucleic Acids Research* 43 (7), pp. 3407–3419. DOI: 10.1093/nar/gkv226.

Barrangou, Rodolphe; Fremaux, Christophe; Deveau, Hélène; Richards, Melissa; Boyaval, Patrick; Moineau, Sylvain et al. (2007): CRISPR provides acquired resistance against viruses in prokaryotes. In *Science (New York, N.Y.)* 315 (5819), pp. 1709–1712. DOI: 10.1126/science.1138140.

Baxter, Melissa; Withey, Sarah; Harrison, Sean; Segeritz, Charis-Patricia; Zhang, Fang; Atkinson-Dell, Rebecca et al. (2015): Phenotypic and functional analyses show stem cell-derived hepatocyte-like cells better mimic fetal rather than adult hepatocytes. In *Journal of hepatology* 62 (3), pp. 581–589. DOI: 10.1016/j.jhep.2014.10.016.

Brayman, Tim; Xiao, Yongling; Bourner, Maureen; Blasberg, Jim; Angeles, Mark; Thompson, David (2014): HepaRG Clone 5F – A Highly Active Human Liver Cell Line for Drug Metabolism, Transporter, and Toxicology Studies. In.

Bridges, A.; Gruenke, L.; Chang, Y. T.; Vakser, I. A.; Loew, G.; Waskell, L. (1998): Identification of the binding site on cytochrome P450 2B4 for cytochrome b5 and cytochrome P450 reductase. In *The Journal of Biological Chemistry* 273 (27), pp. 17036–17049. DOI: 10.1074/jbc.273.27.17036.

Bucher, Simon; Le Guillou, Dounia; Allard, Julien; Pinon, Grégory; Begriche, Karima; Tête, Arnaud et al. (2018): Possible Involvement of Mitochondrial Dysfunction and Oxidative Stress in a Cellular Model of NAFLD Progression Induced by Benzoapyrene/Ethanol CoExposure. In *Oxidative medicine and cellular longevity* 2018, p. 4396403. DOI: 10.1155/2018/4396403.

Burban, Audrey; Sharanek, Ahmad; Humbert, Lydie; Eguether, Thibaut; Guguen-Guillouzo, Christiane; Rainteau, Dominique; Guillouzo, André (2019): Predictive Value of Cellular Accumulation of Hydrophobic Bile Acids As a Marker of Cholestatic Drug Potential. In *Toxicological sciences : an official journal of the Society of Toxicology* 168 (2), pp. 474–485. DOI: 10.1093/toxsci/kfz009.

Burkard, Alexandra; Dähn, Caroline; Heinz, Stefan; Zutavern, Anne; Sonntag-Buck, Vera; Maltman, Daniel et al. (2012): Generation of proliferating human hepatocytes using Upcyte® technology: characterisation and applications in induction and cytotoxicity assays. In *Xenobiotica; the Fate of Foreign Compounds in Biological Systems* 42 (10), pp. 939–956. DOI: 10.3109/00498254.2012.675093.

Campa, Carlo C.; Weisbach, Niels R.; Santinha, António J.; Incarnato, Danny; Platt, Randall J. (2019): Multiplexed genome engineering by Cas12a and CRISPR arrays encoded on single transcripts. In *Nature Methods* 16 (9), pp. 887–893. DOI: 10.1038/s41592-019-0508-6.

Castell, José V.; Jover, Ramiro; Martínez-Jiménez, Celia P.; Gómez-Lechón, María José (2006): Hepatocyte cell lines. Their use, scope and limitations in drug metabolism studies. In *Expert Opinion on Drug Metabolism & Toxicology* 2 (2), pp. 183–212. DOI: 10.1517/17425255.2.2.183.

Cerec, Virginie; Glaise, Denise; Garnier, Delphine; Morosan, Serban; Turlin, Bruno; Drenou, Bernard et al. (2007): Transdifferentiation of hepatocyte-like cells from the human hepatoma HepaRG cell line through bipotent progenitor. In *Hepatology (Baltimore, Md.)* 45 (4), pp. 957–967. DOI: 10.1002/hep.21536.

Chavez, Alejandro; Scheiman, Jonathan; Vora, Suhani; Pruitt, Benjamin W.; Tuttle, Marcelle; P R Iyer, Eswar et al. (2015): Highly efficient Cas9-mediated transcriptional programming. In *Nature Methods* 12 (4), pp. 326–328. DOI: 10.1038/nmeth.3312.

Chen, Baohui; Gilbert, Luke A.; Cimini, Beth A.; Schnitzbauer, Joerg; Zhang, Wei; Li, Gene-Wei et al. (2013): Dynamic imaging of genomic loci in living human cells by an optimized CRISPR/Cas system. In *Cell* 155 (7), pp. 1479–1491. DOI: 10.1016/j.cell.2013.12.001.

Chen, Eugene C.; Broccatelli, Fabio; Plise, Emile; Chen, Buyun; Liu, Liling; Cheong, Jonathan et al. (2018): Evaluating the Utility of Canine Mdr1 Knockout Madin-Darby Canine Kidney I Cells in Permeability Screening and Efflux Substrate Determination. In *Molecular Pharmaceutics* 15 (11), pp. 5103–5113. DOI: 10.1021/acs.molpharmaceut.8b00688.

Chen, Eugene Chia-Te (2020): Advances in CRISPR technologies enable novel in vitro tools for ADME studies. In Shuguang Ma, Swapan K. Chowdhury (Eds.): Identification and Quantification of Drugs, Metabolites, Drug Metabolizing Enzymes, and Transporters (Second Edition). Second Edition. Amsterdam: Elsevier, pp. 595–607. Available online at http://www.sciencedirect.com/science/article/pii/B9780128200186000211.

Cheng, Xingguo; Gu, Jun; Klaassen, Curtis D. (2014a): Adaptive hepatic and intestinal alterations in mice after deletion of NADPH-cytochrome P450 Oxidoreductase (Cpr) in hepatocytes. In *Drug Metabolism and Disposition: The Biological Fate of Chemicals* 42 (11), pp. 1826–1833. DOI: 10.1124/dmd.114.060053.

Cheng, Xingguo; Zhang, Youcai; Klaassen, Curtis D. (2014b): Decreased bile-acid synthesis in livers of hepatocyte-conditional NADPH-cytochrome P450 reductase-null mice results in increased bile acids in serum. In *The Journal of pharmacology and experimental therapeutics* 351 (1), pp. 105–113. DOI: 10.1124/jpet.114.216796.

Chiang, John Y. L.; Ferrell, Jessica M. (2018): Bile Acid Metabolism in Liver Pathobiology. In *Gene expression* 18 (2), pp. 71–87. DOI: 10.3727/105221618X15156018385515.

Chiang, John Yl (2017): Recent advances in understanding bile acid homeostasis. In *F1000Research* 6, p. 2029. DOI: 10.12688/f1000research.12449.1.

Corbett, James L.; Duncan, Stephen A. (2019): iPSC-Derived Hepatocytes as a Platform for Disease Modeling and Drug Discovery. In *Frontiers in medicine* 6, p. 265. DOI: 10.3389/fmed.2019.00265.

Cox, David B. T.; Gootenberg, Jonathan S.; Abudayyeh, Omar O.; Franklin, Brian; Kellner, Max J.; Joung, Julia; Zhang, Feng (2017): RNA editing with CRISPR-Cas13. In *Science (New York, N.Y.)* 358 (6366), pp. 1019–1027. DOI: 10.1126/science.aaq0180.

Crespi, C. L.; Miller, V. P. (1997): The R144C change in the CYP2C9*2 allele alters interaction of the cytochrome P450 with NADPH:cytochrome P450 oxidoreductase. In *Pharmacogenetics* 7 (3), pp. 203–210. DOI: 10.1097/00008571-199706000-00005.

Cuykx, Matthias; Beirnaert, Charlie; Rodrigues, Robim M.; Laukens, Kris; Vanhaecke, Tamara; Covaci, Adrian (2019): Untargeted liquid chromatography-mass spectrometry metabolomics to assess drug-induced cholestatic features in HepaRG® cells. In *Toxicology and applied pharmacology* 379, p. 114666. DOI: 10.1016/j.taap.2019.114666.

Debeljak, N.; Horvat, S.; Vouk, K.; Lee, M.; Rozman, D. (2000): Characterization of the mouse lanosterol 14alpha-demethylase (CYP51), a new member of the evolutionarily most conserved cytochrome P450 family. In *Archives of Biochemistry and Biophysics* 379 (1), pp. 37–45. DOI: 10.1006/abbi.2000.1859.

Deltcheva, Elitza; Chylinski, Krzysztof; Sharma, Cynthia M.; Gonzales, Karine; Chao, Yanjie; Pirzada, Zaid A. et al. (2011): CRISPR RNA maturation by trans-encoded small RNA and host factor RNase III. In *Nature* 471 (7340), pp. 602–607. DOI: 10.1038/nature09886.

Demazeau, Maxime; Quesnot, Nicolas; Ripoche, Nicolas; Rauch, Claudine; Jeftić, Jelena; Morel, Fabrice et al. (2017): Efficient transfection of Xenobiotic Responsive Element-biosensor plasmid using diether lipid and phosphatidylcholine liposomes in differentiated HepaRG cells. In *International journal of pharmaceutics* 524 (1-2), pp. 268–278. DOI: 10.1016/j.ijpharm.2017.03.080.

Di Cocco, Silvia; Belloni, Laura; Nunn, Abigail D. G.; Salerno, Debora; Piconese, Silvia; Levrero, Massimo; Pediconi, Natalia (2019): Inducing and Characterizing Vesicular Steatosis in Differentiated HepaRG Cells. In *Journal of visualized experiments : JoVE* (149). DOI: 10.3791/59843.

Döhr, O.; Paine, M. J.; Friedberg, T.; Roberts, G. C.; Wolf, C. R. (2001): Engineering of a functional human NADH-dependent cytochrome P450 system. In *Proceedings of the National Academy of Sciences of the United States of America* 98 (1), pp. 81–86. DOI: 10.1073/pnas.98.1.81.

Döring, Barbara; Petzinger, Ernst (2014): Phase 0 and phase III transport in various organs: combined concept of phases in xenobiotic transport and metabolism. In *Drug Metabolism Reviews* 46 (3), pp. 261–282. DOI: 10.3109/03602532.2014.882353.

Dorr, Casey R.; Remmel, Rory P.; Muthusamy, Amutha; Fisher, James; Moriarity, Branden S.; Yasuda, Kazuto et al. (2017): CRISPR/Cas9 Genetic Modification of CYP3A5 *3 in HuH-7 Human Hepatocyte Cell Line Leads to Cell Lines with Increased Midazolam and Tacrolimus Metabolism. In *Drug Metabolism and Disposition: The Biological Fate of Chemicals* 45 (8), pp. 957–965. DOI: 10.1124/dmd.117.076307.

Endo-Umeda, Kaori; Makishima, Makoto (2019): Liver X Receptors Regulate Cholesterol Metabolism and Immunity in Hepatic Nonparenchymal Cells. In *International Journal of Molecular Sciences* 20 (20). DOI: 10.3390/ijms20205045.

Essletzbichler, Patrick; Konopka, Tomasz; Santoro, Federica; Chen, Doris; Gapp, Bianca V.; Kralovics, Robert et al. (2014): Megabase-scale deletion using CRISPR/Cas9 to generate a fully haploid human cell line. In *Genome Research* 24 (12), pp. 2059–2065. DOI: 10.1101/gr.177220.114.

Estabrook, Ronald W. (2003): A passion for P450s (rememberances of the early history of research on cytochrome P450). In *Drug Metabolism and Disposition* 31 (12), pp. 1461–1473. DOI: 10.1124/dmd.31.12.1461.

Feidt, Diana M.; Klein, Kathrin; Hofmann, Ute; Riedmaier, Stephan; Knobeloch, Daniel; Thasler, Wolfgang E. et al. (2010): Profiling induction of cytochrome p450 enzyme activity by statins using a new liquid chromatography-tandem mass spectrometry cocktail assay in human hepatocytes. In *Drug Metabolism and Disposition: The Biological Fate of Chemicals* 38 (9), pp. 1589–1597. DOI: 10.1124/dmd.110.033886.

Feidt, Diana M.; Klein, Kathrin; Nüssler, Andreas; Zanger, Ulrich M. (2009): RNA-interference approach to study functions of NADPH. Cytochrome P450 oxidoreductase in human hepatocytes. In *Chemistry & Biodiversity* 6 (11), pp. 2084–2091. DOI: 10.1002/cbdv.200900135.

Filipowicz, Witold; Bhattacharyya, Suvendra N.; Sonenberg, Nahum (2008): Mechanisms of post-transcriptional regulation by microRNAs. Are the answers in sight? In *Nature Reviews. Genetics* 9 (2), pp. 102–114. DOI: 10.1038/nrg2290.

Finn, Robert D.; McLaren, Aileen W.; Carrie, Dianne; Henderson, Colin J.; Wolf, C. Roland (2007): Conditional deletion of cytochrome P450 oxidoreductase in the liver and gastrointestinal tract: a new model for studying the functions of the P450 system. In *The Journal of pharmacology and experimental therapeutics* 322 (1), pp. 40–47. DOI: 10.1124/jpet.107.121780.

Fisel, P.; Schaeffeler, E.; Schwab, M. (2016): DNA Methylation of ADME Genes. In *Clinical Pharmacology and Therapeutics* 99 (5), pp. 512–527. DOI: 10.1002/cpt.343.

Flück, Christa E.; Pandey, Amit V. (2011): Clinical and biochemical consequences of p450 oxidoreductase deficiency. In *Endocrine development* 20, pp. 63–79. DOI: 10.1159/000321221.

Fu, Yanfang; Foden, Jennifer A.; Khayter, Cyd; Maeder, Morgan L.; Reyon, Deepak; Joung, J. Keith; Sander, Jeffry D. (2013): High-frequency off-target mutagenesis induced by CRISPR-Cas nucleases in human cells. In *Nature Biotechnology* 31 (9), pp. 822–826. DOI: 10.1038/nbt.2623.

Fukami, Maki; Ogata, Tsutomu (2014): Cytochrome P450 oxidoreductase deficiency: rare congenital disorder leading to skeletal malformations and steroidogenic defects. In *Pediatrics international : official journal of the Japan Pediatric Society* 56 (6), pp. 805–808. DOI: 10.1111/ped.12518.

Gaedigk, Andrea; Ingelman-Sundberg, Magnus; Miller, Neil A.; Leeder, J. Steven; Whirl-Carrillo, Michelle; Klein, Teri E. (2018): The Pharmacogene Variation (PharmVar) Consortium. Incorporation of the Human Cytochrome P450 (CYP) Allele Nomenclature Database. In *Clinical Pharmacology and Therapeutics* 103 (3), pp. 399–401. DOI: 10.1002/cpt.910.

Gaedigk, Andrea; Sangkuhl, Katrin; Whirl-Carrillo, Michelle; Twist, Greyson P.; Klein, Teri E.; Miller, Neil A. (2019): The Evolution of PharmVar. In *Clinical Pharmacology and Therapeutics* 105 (1), pp. 29–32. DOI: 10.1002/cpt.1275.

Gartzke, Dominik; Delzer, Jürgen; Laplanche, Loic; Uchida, Yasuo; Hoshi, Yutaro; Tachikawa, Masanori et al. (2015): Genomic Knockout of Endogenous Canine P-Glycoprotein in Wild-Type, Human P-Glycoprotein and Human BCRP Transfected MDCKII Cell Lines by Zinc Finger Nucleases. In *Pharmaceutical Research* 32 (6), pp. 2060–2071. DOI: 10.1007/s11095-014-1599-5.

Geng, Tingting; Zhang, Xi Yang; Wang, Li; Wang, Huijuan; Shi, Xugang; Kang, Longli et al. (2016): Genetic polymorphism analysis of the drug-metabolizing enzyme CYP1A2 in a Uyghur Chinese population. A pilot study. In *Xenobiotica; the Fate of Foreign Compounds in Biological Systems* 46 (6), pp. 542–547. DOI: 10.3109/00498254.2015.1089367.

Gentry, Katherine A.; Anantharamaiah, G. M.; Ramamoorthy, Ayyalusamy (2019): Probing protein-protein and protein-substrate interactions in the dynamic membrane-associated ternary complex of cytochromes P450, b(5), and reductase. In *Chemical communications (Cambridge, England)* 55 (89), pp. 13422–13425. DOI: 10.1039/c9cc05904k.

Gentry, Katherine A.; Zhang, Meng; Im, Sang-Choul; Waskell, Lucy; Ramamoorthy, Ayyalusamy (2018): Substrate mediated redox partner selectivity of cytochrome P450. In *Chemical communications (Cambridge, England)* 54 (45), pp. 5780–5783. DOI: 10.1039/c8cc02525h.

Ghallab, Ahmed; Hofmann, Ute; Sezgin, Selahaddin; Vartak, Nachiket; Hassan, Reham; Zaza, Ayham et al. (2019): Bile Microinfarcts in Cholestasis Are Initiated by Rupture of the Apical Hepatocyte

Membrane and Cause Shunting of Bile to Sinusoidal Blood. In *Hepatology (Baltimore, Md.)* 69 (2), pp. 666–683. DOI: 10.1002/hep.30213.

Gilbert, Luke A.; Larson, Matthew H.; Morsut, Leonardo; Liu, Zairan; Brar, Gloria A.; Torres, Sandra E. et al. (2013): CRISPR-mediated modular RNA-guided regulation of transcription in eukaryotes. In *Cell* 154 (2), pp. 442–451. DOI: 10.1016/j.cell.2013.06.044.

Giuliano, Christopher J.; Lin, Ann; Girish, Vishruth; Sheltzer, Jason M. (2019): Generating Single Cell-Derived Knockout Clones in Mammalian Cells with CRISPR/Cas9. In *Current Protocols in Molecular Biology / Edited by Frederick M. Ausubel … [et Al.]* 128 (1), e100. DOI: 10.1002/cpmb.100.

Gomes, Ana M.; Winter, Stefan; Klein, Kathrin; Turpeinen, Miia; Schaeffeler, Elke; Schwab, Matthias; Zanger, Ulrich M. (2009): Pharmacogenomics of human liver cytochrome P450 oxidoreductase: multifactorial analysis and impact on microsomal drug oxidation. In *Pharmacogenomics* 10 (4), pp. 579–599. DOI: 10.2217/pgs.09.7.

Greenspan, P.; Mayer, E. P.; Fowler, S. D. (1985): Nile red: a selective fluorescent stain for intracellular lipid droplets. In *The Journal of cell biology* 100 (3), pp. 965–973. DOI: 10.1083/jcb.100.3.965.

Gripon, Philippe; Rumin, Sylvie; Urban, Stephan; Le Seyec, Jacques; Glaise, Denise; Cannie, Isabelle et al. (2002): Infection of a human hepatoma cell line by hepatitis B virus. In *Proceedings of the National Academy of Sciences of the United States of America* 99 (24), pp. 15655–15660. DOI: 10.1073/pnas.232137699.

Groll, Nicola; Petrikat, Tamara; Vetter, Silvia; Colnot, Sabine; Weiss, Frederik; Poetz, Oliver et al. (2016): Coordinate regulation of Cyp2e1 by β-catenin- and hepatocyte nuclear factor 1α-dependent signaling. In *Toxicology* 350-352, pp. 40–48. DOI: 10.1016/j.tox.2016.05.004.

Gross, Andre; Schoendube, Jonas; Zimmermann, Stefan; Steeb, Maximilian; Zengerle, Roland; Koltay, Peter (2015): Technologies for Single-Cell Isolation. In *International Journal of Molecular Sciences* 16 (8), pp. 16897–16919. DOI: 10.3390/ijms160816897.

Gu, Jun; Weng, Yan; Zhang, Qing-Yu; Cui, Huadong; Behr, Melissa; Wu, Lin et al. (2003): Liver-specific deletion of the NADPH-cytochrome P450 reductase gene: impact on plasma cholesterol homeostasis and the function and regulation of microsomal cytochrome P450 and heme oxygenase. In *The Journal of Biological Chemistry* 278 (28), pp. 25895–25901. DOI: 10.1074/jbc.M303125200.

Guengerich, F. P. (2001): Common and uncommon cytochrome P450 reactions related to metabolism and chemical toxicity. In *Chemical research in toxicology* 14 (6), pp. 611–650. DOI: 10.1021/tx0002583.

Guengerich, F. Peter (2008): Cytochrome p450 and chemical toxicology. In *Chemical research in toxicology* 21 (1), pp. 70–83. DOI: 10.1021/tx700079z.

Guengerich, F. Peter (2012): Cytochromes P450. In Pavel Anzenbacher, Ulrich M. Zanger (Eds.): Metabolism of Drugs and Other Xenobiotics // Metabolism of drugs and other xenobiotics, vol. 176. Weinheim, Chichester: John Wiley & Sons, Ltd; Wiley-VCH; John Wiley [distributor], pp. 27–66.

Guengerich, F. Peter; Martin, Martha V.; Sohl, Christal D.; Cheng, Qian (2009): Measurement of cytochrome P450 and NADPH-cytochrome P450 reductase. In *Nature Protocols* 4 (9), pp. 1245–1251. DOI: 10.1038/nprot.2009.121.

Guengerich, F. Peter; Waterman, Michael R.; Egli, Martin (2016): Recent Structural Insights into Cytochrome P450 Function. In *Trends in pharmacological sciences* 37 (8), pp. 625–640. DOI: 10.1016/j.tips.2016.05.006.

Guguen-Guillouzo, Christiane; Guillouzo, Andre (2010): General review on in vitro hepatocyte models and their applications. In *Methods in Molecular Biology (Clifton, N.J.)* 640, pp. 1–40. DOI: 10.1007/978-1-60761-688-7_1.

Guo, Lei; Dial, Stacey; Shi, Leming; Branham, William; Liu, Jie; Fang, Jia-Long et al. (2011): Similarities and Differences in the Expression of Drug-Metabolizing Enzymes between Human Hepatic Cell Lines and Primary Human Hepatocytes. In *Drug Metabolism and Disposition* 39 (3), pp. 528–538. DOI: 10.1124/dmd.110.035873.

Gut, J.; Richter, C.; Cherry, R. J.; Winterhalter, K. H.; Kawato, S. (1982): Rotation of cytochrome P-450. II. Specific interactions of cytochrome P-450 with NADPH-cytochrome P-450 reductase in phospholipid vesicles. In *The Journal of Biological Chemistry* 257 (12), pp. 7030–7036.

Guzmán, Carla; Benet, Marta; Pisonero-Vaquero, Sandra; Moya, Marta; García-Mediavilla, M. Victoria; Martínez-Chantar, M. Luz et al. (2013): The human liver fatty acid binding protein (FABP1) gene is activated by FOXA1 and PPARα; and repressed by C/EBPα: Implications in FABP1 down-regulation in nonalcoholic fatty liver disease. In *Biochimica et biophysica acta* 1831 (4), pp. 803–818. DOI: 10.1016/j.bbalip.2012.12.014.

Haag, Mathias; Hofmann, Ute; Mürdter, Thomas E.; Heinkele, Georg; Leuthold, Patrick; Blank, Antje et al. (2015): Quantitative bile acid profiling by liquid chromatography quadrupole time-of-flight mass spectrometry: monitoring hepatitis B therapy by a novel Na(+)-taurocholate cotransporting polypeptide inhibitor. In *Analytical and Bioanalytical Chemistry* 407 (22), pp. 6815–6825. DOI: 10.1007/s00216-015-8853-5.

Hart, Steven N.; Wang, Shuang; Nakamoto, Kaori; Wesselman, Christopher; Li, Ye; Zhong, Xiao-Bo (2008): Genetic polymorphisms in cytochrome P450 oxidoreductase influence microsomal P450-catalyzed drug metabolism. In *Pharmacogenetics and Genomics* 18 (1), pp. 11–24. DOI: 10.1097/FPC.0b013e3282f2f121.

Heigwer, Florian; Kerr, Grainne; Boutros, Michael (2014): E-CRISP: fast CRISPR target site identification. In *Nature Methods* 11 (2), pp. 122–123. DOI: 10.1038/nmeth.2812.

Heintze, Tamara; Klein, Kathrin; Hofmann, Ute; Zanger, Ulrich M. (2021): Differential effects on human cytochromes P450 by CRISPR/Cas9-induced genetic knockout of cytochrome P450 reductase and cytochrome b5 in HepaRG cells. In *Scientific Reports* 11 (1), p. 1000. DOI: 10.1038/s41598-020-79952-1.

Henderson, Colin J.; McLaughlin, Lesley A.; Finn, Robert D.; Ronseaux, Sebastien; Kapelyukh, Yury; Wolf, C. Roland (2014): A role for cytochrome b5 in the In vivo disposition of anticancer and cytochrome P450 probe drugs in mice. In *Drug Metabolism and Disposition: The Biological Fate of Chemicals* 42 (1), pp. 70–77. DOI: 10.1124/dmd.113.055277.

Henderson, Colin J.; McLaughlin, Lesley A.; Scheer, Nico; Stanley, Lesley A.; Wolf, C. Roland (2015): Cytochrome b5 is a major determinant of human cytochrome P450 CYP2D6 and CYP3A4 activity in vivo. In *Molecular Pharmacology* 87 (4), pp. 733–739. DOI: 10.1124/mol.114.097394.

Henderson, Colin J.; McLaughlin, Lesley A.; Wolf, C. Roland (2013): Evidence that cytochrome b5 and cytochrome b5 reductase can act as sole electron donors to the hepatic cytochrome P450 system. In *Molecular Pharmacology* 83 (6), pp. 1209–1217. DOI: 10.1124/mol.112.084616.

Henderson, Colin J.; Otto, Diana M. E.; Carrie, Dianne; Magnuson, Mark A.; McLaren, Aileen W.; Rosewell, Ian; Wolf, C. Roland (2003): Inactivation of the hepatic cytochrome P450 system by conditional deletion of hepatic cytochrome P450 reductase. In *The Journal of Biological Chemistry* 278 (15), pp. 13480–13486. DOI: 10.1074/jbc.M212087200.

Hess, Gaelen T.; Frésard, Laure; Han, Kyuho; Lee, Cameron H.; Li, Amy; Cimprich, Karlene A. et al. (2016): Directed evolution using dCas9-targeted somatic hypermutation in mammalian cells. In *Nature Methods* 13 (12), pp. 1036–1042. DOI: 10.1038/nmeth.4038.

Hildebrandt, Alfred; Estabrook, Ronald W. (1971): Evidence for the participation of cytochrome b5 in hepatic microsomal mixed-function oxidation reactions. In *Archives of Biochemistry and Biophysics* 143 (1), pp. 66–79. DOI: 10.1016/0003-9861(71)90186-X.

Hilton, Isaac B.; D'Ippolito, Anthony M.; Vockley, Christopher M.; Thakore, Pratiksha I.; Crawford, Gregory E.; Reddy, Timothy E.; Gersbach, Charles A. (2015): Epigenome editing by a CRISPR-Cas9-based acetyltransferase activates genes from promoters and enhancers. In *Nature Biotechnology* 33 (5), pp. 510–517. DOI: 10.1038/nbt.3199.

Hsu, Patrick D.; Scott, David A.; Weinstein, Joshua A.; Ran, F. Ann; Konermann, Silvana; Agarwala, Vineeta et al. (2013): DNA targeting specificity of RNA-guided Cas9 nucleases. In *Nature Biotechnology* 31 (9), pp. 827–832. DOI: 10.1038/nbt.2647.

Huang, Rui; Zhang, Meng; Rwere, Freeborn; Waskell, Lucy; Ramamoorthy, Ayyalusamy (2015): Kinetic and structural characterization of the interaction between the FMN binding domain of cytochrome P450 reductase and cytochrome c. In *The Journal of Biological Chemistry* 290 (8), pp. 4843–4855. DOI: 10.1074/jbc.M114.582700.

Hunter, Francis W.; Devaux, Jules B. L.; Meng, Fanying; Hong, Cho Rong; Khan, Aziza; Tsai, Peter et al. (2019): Functional CRISPR and shRNA Screens Identify Involvement of Mitochondrial Electron Transport in the Activation of Evofosfamide. In *Molecular Pharmacology* 95 (6), pp. 638–651. DOI: 10.1124/mol.118.115196.

Hunter, Francis W.; Young, Richard J.; Shalev, Zvi; Vellanki, Ravi N.; Wang, Jingli; Gu, Yongchuan et al. (2015): Identification of P450 Oxidoreductase as a Major Determinant of Sensitivity to Hypoxia-Activated Prodrugs. In *Cancer research* 75 (19), pp. 4211–4223. DOI: 10.1158/0008-5472.CAN-15-1107.

Ibrahim, Zein Shaban (2015): Chenodeoxycholic acid increases the induction of CYP1A1 in HepG2 and H4IIE cells. In *Exp Ther Med* 10 (5), pp. 1976–1982. DOI: 10.3892/etm.2015.2719.

Ishino, Y.; Shinagawa, H.; Makino, K.; Amemura, M.; Nakata, A. (1987): Nucleotide sequence of the iap gene, responsible for alkaline phosphatase isozyme conversion in Escherichia coli, and identification of the gene product. In *Journal of Bacteriology* 169 (12), pp. 5429–5433.

Iyama, Teruaki; Wilson, David M. (2013): DNA repair mechanisms in dividing and non-dividing cells. In *DNA repair* 12 (8), pp. 620–636. DOI: 10.1016/j.dnarep.2013.04.015.

Jackson, J. P.; Li, L.; Chamberlain, E. D.; Wang, H.; Ferguson, S. S. (2016): Contextualizing Hepatocyte Functionality of Cryopreserved HepaRG Cell Cultures. In *Drug Metabolism and Disposition* 44 (9), pp. 1463–1479. DOI: 10.1124/dmd.116.069831.

Jin, Jiankang; Xu, Yan; Huo, Longfei; Ma, Lang; Scott, Ailing W.; Pizzi, Melissa Pool et al. (2020): An improved strategy for CRISPR/Cas9 gene knockout and subsequent wildtype and mutant gene rescue. In *PLoS ONE* 15 (2), e0228910. DOI: 10.1371/journal.pone.0228910.

Jinek, Martin; Chylinski, Krzysztof; Fonfara, Ines; Hauer, Michael; Doudna, Jennifer A.; Charpentier, Emmanuelle (2012): A Programmable Dual-RNA-Guided DNA Endonuclease in Adaptive Bacterial Immunity. In *Science (New York, N.Y.)* 337 (6096), pp. 816–821. DOI: 10.1126/science.1225829.

Jo, Areum; Ham, Sangwoo; Lee, Gum Hwa; Lee, Yun-Il; Kim, SangSeong; Lee, Yun-Song et al. (2015): Efficient Mitochondrial Genome Editing by CRISPR/Cas9. In *BioMed Research International* 2015, p. 305716. DOI: 10.1155/2015/305716.

Jouan, Elodie; Le Vée, Marc; Denizot, Claire; Parmentier, Yannick; Fardel, Olivier (2016): Drug Transporter Expression and Activity in Human Hepatoma HuH-7 Cells. In *Pharmaceutics* 9 (1). DOI: 10.3390/pharmaceutics9010003.

Juřica, J.; Dovrtělová, G.; Nosková, K.; Zendulka, O. (2016): Bile acids, nuclear receptors and cytochrome P450. In *Physiological research* 65 (Suppl 4), S427-S440. DOI: 10.33549/physiolres.933512.

Kanebratt, Kajsa P.; Andersson, Tommy B. (2008): Evaluation of HepaRG cells as an in vitro model for human drug metabolism studies. In *Drug Metabolism and Disposition* 36 (7), pp. 1444–1452. DOI: 10.1124/dmd.107.020016.

Karlgren, M.; Simoff, I.; Keiser, M.; Oswald, S.; Artursson, P. (2018): CRISPR-Cas9. A New Addition to the Drug Metabolism and Disposition Tool Box. In *Drug Metabolism and Disposition: The Biological Fate of Chemicals* 46 (11), pp. 1776–1786. DOI: 10.1124/dmd.118.082842.

Karlgren, Maria; Simoff, Ivailo; Backlund, Maria; Wegler, Christine; Keiser, Markus; Handin, Niklas et al. (2017): A CRISPR-Cas9 generated MDCK-hMDR1 cell line without endogenous cMDR1 (cABCB1) - an improved tool for drug efflux studies. In *Journal of Pharmaceutical Sciences*. DOI: 10.1016/j.xphs.2017.04.018.

Kaspera, Rüdiger; Naraharisetti, Suresh B.; Evangelista, Eric A.; Marciante, Kristin D.; Psaty, Bruce M.; Totah, Rheem A. (2011): Drug metabolism by CYP2C8.3 is determined by substrate dependent interactions with cytochrome P450 reductase and cytochrome b5. In *Biochemical Pharmacology* 82 (6), pp. 681–691. DOI: 10.1016/j.bcp.2011.06.027.

Kennedy, Edward M.; Bassit, Leda C.; Mueller, Henrik; Kornepati, Anand V.R.; Bogerd, Hal P.; Nie, Ting et al. (2015): Suppression of hepatitis B virus DNA accumulation in chronically infected cells using a bacterial CRISPR/Cas RNA-guided DNA endonuclease. In *Virology* 476, pp. 196–205. DOI: 10.1016/j.virol.2014.12.001.

Kennedy, Edward M.; Cullen, Bryan R. (2015): Bacterial CRISPR/Cas DNA endonucleases. A revolutionary technology that could dramatically impact viral research and treatment. In *Virology* 479-480, pp. 213–220. DOI: 10.1016/j.virol.2015.02.024.

Kimberland, Michelle L.; Hou, Wangfang; Alfonso-Pecchio, Adolfo; Wilson, Stephen; Rao, Yanhua; Zhang, Shu; Lu, Quinn (2018): Strategies for controlling CRISPR/Cas9 off-target effects and biological

variations in mammalian genome editing experiments. In *Journal of biotechnology* 284, pp. 91–101. DOI: 10.1016/j.jbiotec.2018.08.007.

Klein, Marcus; Thomas, Maria; Hofmann, Ute; Seehofer, Daniel; Damm, Georg; Zanger, Ulrich M. (2015): A systematic comparison of the impact of inflammatory signaling on absorption, distribution, metabolism, and excretion gene expression and activity in primary human hepatocytes and HepaRG cells. In *Drug Metabolism and Disposition: The Biological Fate of Chemicals* 43 (2), pp. 273–283. DOI: 10.1124/dmd.114.060962.

Knebel, Constanze; Buhrke, Thorsten; Süssmuth, Roderich; Lampen, Alfonso; Marx-Stoelting, Philip; Braeuning, Albert (2019): Pregnane X receptor mediates steatotic effects of propiconazole and tebuconazole in human liver cell lines. In *Archives of Toxicology* 93 (5), pp. 1311–1322. DOI: 10.1007/s00204-019-02445-2.

Knockaert, Laetitia; Fromenty, Bernard; Robin, Marie-Anne (2011): Mechanisms of mitochondrial targeting of cytochrome P450 2E1. Physiopathological role in liver injury and obesity. In *The FEBS journal* 278 (22), pp. 4252–4260. DOI: 10.1111/j.1742-4658.2011.08357.x.

Knowles, B. B.; Howe, C. C.; Aden, D. P. (1980): Human hepatocellular carcinoma cell lines secrete the major plasma proteins and hepatitis B surface antigen. In *Science* 209 (4455), pp. 497–499. DOI: 10.1126/science.6248960.

Komor, Alexis C.; Kim, Yongjoo B.; Packer, Michael S.; Zuris, John A.; Liu, David R. (2016): Programmable editing of a target base in genomic DNA without double-stranded DNA cleavage. In *Nature* 533 (7603), pp. 420–424. DOI: 10.1038/nature17946.

Konermann, Silvana; Brigham, Mark D.; Trevino, Alexandro E.; Joung, Julia; Abudayyeh, Omar O.; Barcena, Clea et al. (2015): Genome-scale transcriptional activation by an engineered CRISPR-Cas9 complex. In *Nature* 517 (7536), pp. 583–588. DOI: 10.1038/nature14136.

Kosicki, Michael; Rajan, Sandeep S.; Lorenzetti, Flaminia C.; Wandall, Hans H.; Narimatsu, Yoshiki; Metzakopian, Emmanouil; Bennett, Eric P. (2017): Dynamics of Indel Profiles Induced by Various CRISPR/Cas9 Delivery Methods. In *Progress in molecular biology and translational science* 152, pp. 49–67. DOI: 10.1016/bs.pmbts.2017.09.003.

Kugler, Nicole; Klein, Kathrin; Zanger, Ulrich M. (2020): MiR-155 and other microRNAs downregulate drug metabolizing cytochromes P450 in inflammation. In *Biochemical Pharmacology* 171, p. 113725. DOI: 10.1016/j.bcp.2019.113725.

Labun, Kornel; Montague, Tessa G.; Krause, Maximilian; Torres Cleuren, Yamila N.; Tjeldnes, Håkon; Valen, Eivind (2019): CHOPCHOP v3. Expanding the CRISPR web toolbox beyond genome editing. In *Nucleic Acids Research* 47 (W1), W171-W174. DOI: 10.1093/nar/gkz365.

Lake, April D.; Novak, Petr; Shipkova, Petia; Aranibar, Nelly; Robertson, Donald; Reily, Michael D. et al. (2013): Decreased hepatotoxic bile acid composition and altered synthesis in progressive human nonalcoholic fatty liver disease. In *Toxicology and applied pharmacology* 268 (2), pp. 132–140. DOI: 10.1016/j.taap.2013.01.022.

Larigot, Lucie; Juricek, Ludmila; Dairou, Julien; Coumoul, Xavier (2018): AhR signaling pathways and regulatory functions. In *Biochimie open* 7, pp. 1–9. DOI: 10.1016/j.biopen.2018.05.001.

Lasch, Alexandra; Alarcan, Jimmy; Lampen, Alfonso; Braeuning, Albert; Lichtenstein, Dajana (2020): Combinations of LXR and RXR agonists induce triglyceride accumulation in human HepaRG cells in a synergistic manner. In *Archives of Toxicology*. DOI: 10.1007/s00204-020-02685-7.

Laurent, Veronique; Fraix, Aurore; Montier, Tristan; Cammas-Marion, Sandrine; Ribault, Catherine; Benvegnu, Thierry et al. (2010): Highly efficient gene transfer into hepatocyte-like HepaRG cells. New means for drug metabolism and toxicity studies. In *Biotechnology journal* 5 (3), pp. 314–320. DOI: 10.1002/biot.200900255.

Laurent, Véronique; Glaise, Denise; Nübel, Tobias; Gilot, David; Corlu, Anne; Loyer, Pascal (2013): Highly efficient SiRNA and gene transfer into hepatocyte-like HepaRG cells and primary human hepatocytes. New means for drug metabolism and toxicity studies. In *Methods in Molecular Biology (Clifton, N.J.)* 987, pp. 295–314. DOI: 10.1007/978-1-62703-321-3_25.

Le Cong; Ran, F. Ann; Cox, David; Lin, Shuailiang; Barretto, Robert; Habib, Naomi et al. (2013): Multiplex genome engineering using CRISPR/Cas systems. In *Science (New York, N.Y.)* 339 (6121), pp. 819–823. DOI: 10.1126/science.1231143.

Le Cong; Zhou, Ruhong; Kuo, Yu-Chi; Cunniff, Margaret; Zhang, Feng (2012): Comprehensive interrogation of natural TALE DNA-binding modules and transcriptional repressor domains. In *Nature Communications* 3, p. 968. DOI: 10.1038/ncomms1962.

Levy, Gahl; Bomze, David; Heinz, Stefan; Ramachandran, Sarada Devi; Noerenberg, Astrid; Cohen, Merav et al. (2015): Long-term culture and expansion of primary human hepatocytes. In *Nature Biotechnology* 33 (12), pp. 1264–1271. DOI: 10.1038/nbt.3377.

Li, Daochuan; Mackowiak, Bryan; Brayman, Timothy G.; Mitchell, Michael; Zhang, Lei; Huang, Shiew-Mei; Wang, Hongbing (2015): Genome-wide analysis of human constitutive androstane receptor (CAR) transcriptome in wild-type and CAR-knockout HepaRG cells. In *Biochemical Pharmacology* 98 (1), pp. 190–202. DOI: 10.1016/j.bcp.2015.08.087.

Li, Jianing; Dawson, Paul A. (2019): Animal models to study bile acid metabolism. In *Biochimica et biophysica acta. Molecular basis of disease* 1865 (5), pp. 895–911. DOI: 10.1016/j.bbadis.2018.05.011.

Li, Tiangang; Apte, Udayan (2015): Bile Acid Metabolism and Signaling in Cholestasis, Inflammation, and Cancer. In *Advances in pharmacology (San Diego, Calif.)* 74, pp. 263–302. DOI: 10.1016/bs.apha.2015.04.003.

Li, Tiangang; Chiang, John Y. L. (2014): Bile acid signaling in metabolic disease and drug therapy. In *Pharmacological reviews* 66 (4), pp. 948–983. DOI: 10.1124/pr.113.008201.

Li, Ting-Ting; An, Jia-Xing; Xu, Jing-Yu; Tuo, Bi-Guang (2019): Overview of organic anion transporters and organic anion transporter polypeptides and their roles in the liver. In *World journal of clinical cases* 7 (23), pp. 3915–3933. DOI: 10.12998/wjcc.v7.i23.3915.

Lichtenstein, Dajana; Mentz, Almut; Schmidt, Felix F.; Luckert, Claudia; Buhrke, Thorsten; Marx-Stoelting, Philip et al. (2020): Transcript and protein marker patterns for the identification of steatotic compounds in human HepaRG cells. In *Food and chemical toxicology : an international journal published for the British Industrial Biological Research Association* 145, p. 111690. DOI: 10.1016/j.fct.2020.111690.

Lin, Wenwei; Bwayi, Monicah; Wu, Jing; Li, Yongtao; Chai, Sergio C.; Huber, Andrew D.; Chen, Taosheng (2020): CITCO Directly Binds to and Activates Human Pregnane X Receptor. In *Molecular Pharmacology* 97 (3), pp. 180–190. DOI: 10.1124/mol.119.118513.

Lin, Yanni; Cradick, Thomas J.; Brown, Matthew T.; Deshmukh, Harshavardhan; Ranjan, Piyush; Sarode, Neha et al. (2014): CRISPR/Cas9 systems have off-target activity with insertions or deletions between target DNA and guide RNA sequences. In *Nucleic Acids Research* 42 (11), pp. 7473–7485. DOI: 10.1093/nar/gku402.

Liu, Guanqing; Zhang, Yong; Zhang, Tao (2020): Computational approaches for effective CRISPR guide RNA design and evaluation. In *Computational and structural biotechnology journal* 18, pp. 35–44. DOI: 10.1016/j.csbj.2019.11.006.

Liu, Jia-qing; Li, Tao (2019): CRISPR-Cas9-mediated loss-of-function screens. In *Frontiers in Life Science* 12 (1), pp. 1–13. DOI: 10.1080/21553769.2019.1670739.

Liu, Qiao; Di He; Xie, Lei (2019): Prediction of off-target specificity and cell-specific fitness of CRISPR-Cas System using attention boosted deep learning and network-based gene feature. In *PLoS computational biology* 15 (10), e1007480. DOI: 10.1371/journal.pcbi.1007480.

Livak, K. J.; Schmittgen, T. D. (2001): Analysis of relative gene expression data using real-time quantitative PCR and the 2(-Delta Delta C(T)) Method. In *Methods (San Diego, Calif.)* 25 (4), pp. 402–408. DOI: 10.1006/meth.2001.1262.

López-Terrada, Dolores; Cheung, Sau Wai; Finegold, Milton J.; Knowles, Barbara B. (2009): Hep G2 is a hepatoblastoma-derived cell line. In *Human pathology* 40 (10), pp. 1512–1515. DOI: 10.1016/j.humpath.2009.07.003.

Ma, Enbo; Harrington, Lucas B.; O'Connell, Mitchell R.; Zhou, Kaihong; Doudna, Jennifer A. (2015): Single-Stranded DNA Cleavage by Divergent CRISPR-Cas9 Enzymes. In *Molecular Cell* 60 (3), pp. 398–407. DOI: 10.1016/j.molcel.2015.10.030.

Ma, Hanhui; Tu, Li-Chun; Naseri, Ardalan; Huisman, Maximiliaan; Zhang, Shaojie; Grunwald, David; Pederson, Thoru (2016): Multiplexed labeling of genomic loci with dCas9 and engineered sgRNAs using CRISPRainbow. In *Nature Biotechnology* 34 (5), pp. 528–530. DOI: 10.1038/nbt.3526.

Macfarlane, David P.; Forbes, Shareen; Walker, Brian R. (2008): Glucocorticoids and fatty acid metabolism in humans: fuelling fat redistribution in the metabolic syndrome. In *The Journal of endocrinology* 197 (2), pp. 189–204. DOI: 10.1677/JOE-08-0054.

Mackowiak, Bryan; Li, Linhao; Welch, Matthew A.; Li, Daochuan; Jones, Jace W.; Heyward, Scott et al. (2017): Molecular basis of metabolism-mediated conversion of PK11195 from an antagonist to an agonist of the constitutive androstane receptor. In *Molecular Pharmacology*. DOI: 10.1124/mol.117.108621.

Madan, Ajay; Graham, Richard A.; Carroll, Kathleen M.; Mudra, Daniel R.; Burton, L. Alayne; Krueger, Linda A. et al. (2003): Effects of prototypical microsomal enzyme inducers on cytochrome P450 expression in cultured human hepatocytes. In *Drug Metabolism and Disposition* 31 (4), pp. 421–431. DOI: 10.1124/dmd.31.4.421.

Madec, Stéphanie; Cerec, Virginie; Plée-Gautier, Emmanuelle; Antoun, Joseph; Glaise, Denise; Salaun, Jean-Pierre et al. (2011): CYP4F3B expression is associated with differentiation of HepaRG human

hepatocytes and unaffected by fatty acid overload. In *Drug Metabolism and Disposition* 39 (10), pp. 1987–1996. DOI: 10.1124/dmd.110.036848.

Mali, Prashant; Yang, Luhan; Esvelt, Kevin M.; Aach, John; Guell, Marc; DiCarlo, James E. et al. (2013): RNA-guided human genome engineering via Cas9. In *Science (New York, N.Y.)* 339 (6121), pp. 823–826. DOI: 10.1126/science.1232033.

Manghwar, Hakim; Lindsey, Keith; Zhang, Xianlong; Jin, Shuangxia (2019): CRISPR/Cas System: Recent Advances and Future Prospects for Genome Editing. In *Trends in plant science* 24 (12), pp. 1102–1125. DOI: 10.1016/j.tplants.2019.09.006.

Manikandan, Palrasu; Nagini, Siddavaram (2018): Cytochrome P450 Structure, Function and Clinical Significance: A Review. In *Current drug targets* 19 (1), pp. 38–54. DOI: 10.2174/1389450118666170125144557.

Maruyama, Takeshi; Dougan, Stephanie K.; Truttmann, Matthias C.; Bilate, Angelina M.; Ingram, Jessica R.; Ploegh, Hidde L. (2015): Increasing the efficiency of precise genome editing with CRISPR-Cas9 by inhibition of nonhomologous end joining. In *Nature Biotechnology* 33 (5), pp. 538–542. DOI: 10.1038/nbt.3190.

McCarty, Nicholas S.; Graham, Alicia E.; Studená, Lucie; Ledesma-Amaro, Rodrigo (2020): Multiplexed CRISPR technologies for gene editing and transcriptional regulation. In *Nature Communications* 11 (1), p. 1281. DOI: 10.1038/s41467-020-15053-x.

Miller, Walter L. (2018): MECHANISMS IN ENDOCRINOLOGY: Rare defects in adrenal steroidogenesis. In *European journal of endocrinology* 179 (3), R125-R141. DOI: 10.1530/EJE-18-0279.

Miller, Walter L.; Agrawal, Vishal; Sandee, Duanpen; Tee, Meng Kian; Huang, Ningwu; Choi, Ji Ha et al. (2011): Consequences of POR mutations and polymorphisms. In *Molecular and cellular endocrinology* 336 (1-2), pp. 174–179. DOI: 10.1016/j.mce.2010.10.022.

Mojica, F. J. M.; Díez-Villaseñor, C.; García-Martínez, J.; Almendros, C. (2009): Short motif sequences determine the targets of the prokaryotic CRISPR defence system. In *Microbiology (Reading, England)* 155 (Pt 3), pp. 733–740. DOI: 10.1099/mic.0.023960-0.

Monte, Maria J.; Marin, Jose J. G.; Antelo, Alvaro; Vazquez-Tato, Jose (2009): Bile acids: chemistry, physiology, and pathophysiology. In *World journal of gastroenterology* 15 (7), pp. 804–816. DOI: 10.3748/wjg.15.804.

Mutch, David M.; Klocke, Bernward; Morrison, Peter; Murray, Carol A.; Henderson, Colin J.; Seifert, Martin; Williamson, Gary (2007): The disruption of hepatic cytochrome p450 reductase alters mouse lipid metabolism. In *Journal of proteome research* 6 (10), pp. 3976–3984. DOI: 10.1021/pr0700448.

Nakabayashi, H.; Taketa, K.; Miyano, K.; Yamane, T.; Sato, J. (1982): Growth of human hepatoma cells lines with differentiated functions in chemically defined medium. In *Cancer research* 42 (9), pp. 3858–3863.

Namineni, Sukumar; O'Connor, Tracy; Faure-Dupuy, Suzanne; Johansen, Pål; Riedl, Tobias; Liu, Kaijing et al. (2020): A dual role for hepatocyte-intrinsic canonical NF-κB signaling in virus control. In *Journal of hepatology* 72 (5), pp. 960–975. DOI: 10.1016/j.jhep.2019.12.019.

Nebert, Daniel W.; Wikvall, Kjell; Miller, Walter L. (2013): Human cytochromes P450 in health and disease. In *Philosophical transactions of the Royal Society of London. Series B, Biological sciences* 368 (1612), p. 20120431. DOI: 10.1098/rstb.2012.0431.

Nelson, D.; Heldmaier, G.; Häcker, B.; Cox, M.; Held, A.; Maxam, G. et al. (2008): Lehninger Biochemie: Springer Berlin Heidelberg (Springer-Lehrbuch). Available online at https://books.google.de/books?id=jJt-cgAACAAJ.

Neve, E. P.; Ingelman-Sundberg, M. (1999): A soluble NH(2)-terminally truncated catalytically active form of rat cytochrome P450 2E1 targeted to liver mitochondria(1). In *FEBS letters* 460 (2), pp. 309–314.

Newton, D. C.; Montgomery, H. J.; Guillemette, J. G. (1998): The reductase domain of the human inducible nitric oxide synthase is fully active in the absence of bound calmodulin. In *Archives of Biochemistry and Biophysics* 359 (2), pp. 249–257.

Offermanns, Stefan; Rosenthal, Walter (2008): Encyclopedia of Molecular Pharmacology. Berlin, Heidelberg: Springer Berlin Heidelberg.

Olteanu, H.; Banerjee, R. (2001): Human methionine synthase reductase, a soluble P-450 reductase-like dual flavoprotein, is sufficient for NADPH-dependent methionine synthase activation. In *The Journal of Biological Chemistry* 276 (38), pp. 35558–35563. DOI: 10.1074/jbc.M103707200.

Omer, Linda; Hudson, Elizabeth A.; Zheng, Shirong; Hoying, James B.; Shan, Yuan; Boyd, Nolan L. (2017): CRISPR Correction of a Homozygous Low-Density Lipoprotein Receptor Mutation in Familial Hypercholesterolemia Induced Pluripotent Stem Cells. In *Hepatology communications* 1 (9), pp. 886–898. DOI: 10.1002/hep4.1110.

Omura, T.; Sato, R. (1962): A new cytochrome in liver microsomes. In *The Journal of Biological Chemistry* 237, pp. 1375–1376.

Ortiz de Montellano, Paul R. (2013): Cytochrome P450-activated prodrugs. In *Future medicinal chemistry* 5 (2), pp. 213–228. DOI: 10.4155/fmc.12.197.

Otto, Diana M. E.; Henderson, Colin J.; Carrie, Dianne; Davey, Megan; Gundersen, Thomas E.; Blomhoff, Rune et al. (2003): Identification of novel roles of the cytochrome p450 system in early embryogenesis: effects on vasculogenesis and retinoic Acid homeostasis. In *Molecular and Cellular Biology* 23 (17), pp. 6103–6116. Available online at http://www.ncbi.nlm.nih.gov/pubmed/12917333, checked on 1/6/2012.

Paine, M. J.; Garner, A. P.; Powell, D.; Sibbald, J.; Sales, M.; Pratt, N. et al. (2000): Cloning and characterization of a novel human dual flavin reductase. In *The Journal of Biological Chemistry* 275 (2), pp. 1471–1478.

Pandak, William M.; Kakiyama, Genta (2019): The acidic pathway of bile acid synthesis: Not just an alternative pathway☆. In *Liver research* 3 (2), pp. 88–98. DOI: 10.1016/j.livres.2019.05.001.

Pandey, Amit V.; Flück, Christa E. (2013): NADPH P450 oxidoreductase. Structure, function, and pathology of diseases. In *Pharmacology & Therapeutics* 138 (2), pp. 229–254. DOI: 10.1016/j.pharmthera.2013.01.010.

Pankowicz, Francis P.; Jarrett, Kelsey E.; Lagor, William R.; Bissig, Karl-Dimiter (2017): CRISPR/Cas9: at the cutting edge of hepatology. In *Gut*. DOI: 10.1136/gutjnl-2016-313565.

Parent, Romain; Marion, Marie-Jeanne; Furio, Laetitia; Trépo, Christian; Petit, Marie-Anne (2004): Origin and characterization of a human bipotent liver progenitor cell line☆. In *Gastroenterology* 126 (4), pp. 1147–1156. DOI: 10.1053/j.gastro.2004.01.002.

Paton, Chad M.; Ntambi, James M. (2009): Biochemical and physiological function of stearoyl-CoA desaturase. In *American journal of physiology. Endocrinology and metabolism* 297 (1), E28-37. DOI: 10.1152/ajpendo.90897.2008.

Perez, Alexendar R.; Pritykin, Yuri; Vidigal, Joana A.; Chhangawala, Sagar; Zamparo, Lee; Leslie, Christina S.; Ventura, Andrea (2017): GuideScan software for improved single and paired CRISPR guide RNA design. In *Nature Biotechnology* 35 (4), pp. 347–349. DOI: 10.1038/nbt.3804.

Pikuleva, Irina A.; Waterman, Michael R. (2013): Cytochromes p450: roles in diseases. In *The Journal of Biological Chemistry* 288 (24), pp. 17091–17098. DOI: 10.1074/jbc.R112.431916.

Pols, Thijs W. H.; Noriega, Lilia G.; Nomura, Mitsunori; Auwerx, Johan; Schoonjans, Kristina (2011): The bile acid membrane receptor TGR5. A valuable metabolic target. In *Digestive diseases (Basel, Switzerland)* 29 (1), pp. 37–44. DOI: 10.1159/000324126.

Pompon, D.; Coon, M. J. (1984): On the mechanism of action of cytochrome P-450. Oxidation and reduction of the ferrous dioxygen complex of liver microsomal cytochrome P-450 by cytochrome b5. In *The Journal of Biological Chemistry* 259 (24), pp. 15377–15385.

Porter, Todd D. (2002): The roles of cytochrome b5 in cytochrome P450 reactions. In *Journal of biochemical and molecular toxicology* 16 (6), pp. 311–316. DOI: 10.1002/jbt.10052.

Porter, Todd D. (2012): New insights into the role of cytochrome P450 reductase (POR) in microsomal redox biology. In *Acta Pharmaceutica Sinica B* 2 (2), pp. 102–106. DOI: 10.1016/j.apsb.2012.02.002.

Porter, Todd D.; Banerjee, Subhashis; Stolarczyk, Elzbieta I.; Zou, Ling (2011): Suppression of Cytochrome P450 Reductase (POR) Expression in Hepatoma Cells Replicates the Hepatic Lipidosis Observed in Hepatic POR-Null Mice. In *Drug Metabolism and Disposition* 39 (6), pp. 966–973. DOI: 10.1124/dmd.111.038562.

Pratt, Jennifer; Venkatraman, Neetu; Brinker, Amanda; Xiao, Yongling; Blasberg, Jim; Thompson, David C.; Bourner, Maureen (2012): Use of zinc finger nuclease technology to knock out efflux transporters in C2BBe1 cells. In *Current protocols in toxicology* Chapter 23, Unit 23.2. DOI: 10.1002/0471140856.tx2302s52.

Qi, Lei S.; Larson, Matthew H.; Gilbert, Luke A.; Doudna, Jennifer A.; Weissman, Jonathan S.; Arkin, Adam P.; Lim, Wendell A. (2013): Repurposing CRISPR as an RNA-guided platform for sequence-specific control of gene expression. In *Cell* 152 (5), pp. 1173–1183. DOI: 10.1016/j.cell.2013.02.022.

Qiu, Xi; Zhang, Yueping; Liu, Tongtong; Shen, Hong; Xiao, Yongling; Bourner, Maureen J. et al. (2016): Disruption of BSEP Function in HepaRG Cells Alters Bile Acid Disposition and Is a Susceptive Factor to Drug-Induced Cholestatic Injury. In *Molecular Pharmaceutics* 13 (4), pp. 1206–1216. DOI: 10.1021/acs.molpharmaceut.5b00659.

R Arnold, William; Zelasko, Susan; D Meling, Daryl; Sam, Kimberly; Das, Aditi (2019): Polymorphisms of CYP2C8 Alter First-Electron Transfer Kinetics and Increase Catalytic Uncoupling. In *International Journal of Molecular Sciences* 20 (18). DOI: 10.3390/ijms20184626.

Raju, Ravali; Chau, David; Notelaers, Tineke; Myers, Chad L.; Verfaillie, Catherine M.; Hu, Wei-Shou (2018): In Vitro Pluripotent Stem Cell Differentiation to Hepatocyte Ceases Further Maturation at an Equivalent Stage of E15 in Mouse Embryonic Liver Development. In *Stem cells and development* 27 (13), pp. 910–921. DOI: 10.1089/scd.2017.0270.

Reed, James R.; Backes, Wayne L. (2012): Formation of P450 · P450 complexes and their effect on P450 function. In *Pharmacology & Therapeutics* 133 (3), pp. 299–310. DOI: 10.1016/j.pharmthera.2011.11.009.

Reed, James R.; Backes, Wayne L. (2016): The functional effects of physical interactions involving cytochromes P450: putative mechanisms of action and the extent of these effects in biological membranes. In *Drug Metabolism Reviews* 48 (3), pp. 453–469. DOI: 10.1080/03602532.2016.1221961.

Reed, Lindsay; Indra, Radek; Mrizova, Iveta; Moserova, Michaela; Schmeiser, Heinz H.; Wolf, C. Roland et al. (2019a): Application of hepatic cytochrome b5/P450 reductase null (HBRN) mice to study the role of cytochrome b5 in the cytochrome P450-mediated bioactivation of the anticancer drug ellipticine. In *Toxicology and applied pharmacology* 366, pp. 64–74. DOI: 10.1016/j.taap.2019.01.020.

Reed, Lindsay; Jarvis, Ian W. H.; Phillips, David H.; Arlt, Volker M. (2019b): Deletion of cytochrome P450 oxidoreductase enhances metabolism and DNA adduct formation of benzoapyrene in Hepa1c1c7 cells. In *Mutagenesis*. DOI: 10.1093/mutage/gez033.

Rezende, Flávia; Prior, Kim-Kristin; Löwe, Oliver; Wittig, Ilka; Strecker, Valentina; Moll, Franziska et al. (2017): Cytochrome P450 enzymes but not NADPH oxidases are the source of the NADPH-dependent lucigenin chemiluminescence in membrane assays. In *Free Radical Biology and Medicine* 102, pp. 57–66. DOI: 10.1016/j.freeradbiomed.2016.11.019.

Riddick, David S.; Ding, Xinxin; Wolf, C. Roland; Porter, Todd D.; Pandey, Amit V.; Zhang, Qing-Yu et al. (2013): NADPH–Cytochrome P450 Oxidoreductase: Roles in Physiology, Pharmacology, and Toxicology. In *Drug Metabolism and Disposition* 41 (1), pp. 12–23. DOI: 10.1124/dmd.112.048991.

Rieger, Jessica K.; Reutter, Sandra; Hofmann, Ute; Schwab, Matthias; Zanger, Ulrich M. (2015): Inflammation-associated microRNA-130b down-regulates cytochrome P450 activities and directly targets CYP2C9. In *Drug Metabolism and Disposition* 43 (6), pp. 884–888. DOI: 10.1124/dmd.114.062844.

Riss, Terry L.; Moravec, Richard A.; Niles, Andrew L.; Duellman, Sarah; Benink, Hélène A.; Worzella, Tracy J.; Minor, Lisa (2016): Cell Viability Assays: Eli Lilly & Company and the National Center for Advancing Translational Sciences.

Robin, M. A.; Anandatheerthavarada, H. K.; Fang, J. K.; Cudic, M.; Otvos, L.; Avadhani, N. G. (2001): Mitochondrial targeted cytochrome P450 2E1 (P450 MT5) contains an intact N terminus and requires mitochondrial specific electron transfer proteins for activity. In *The Journal of Biological Chemistry* 276 (27), pp. 24680–24689. DOI: 10.1074/jbc.M100363200.

Rogue, Alexandra; Anthérieu, Sébastien; Vluggens, Aurore; Umbdenstock, Thierry; Claude, Nancy; La Moureyre-Spire, Catherine de et al. (2014): PPAR agonists reduce steatosis in oleic acid-overloaded HepaRG cells. In *Toxicology and applied pharmacology* 276 (1), pp. 73–81. DOI: 10.1016/j.taap.2014.02.001.

Rogue, Alexandra; Lambert, Carine; Spire, Catherine; Claude, Nancy; Guillouzo, André (2012): Interindividual variability in gene expression profiles in human hepatocytes and comparison with

HepaRG cells. In *Drug Metabolism and Disposition: The Biological Fate of Chemicals* 40 (1), pp. 151–158. DOI: 10.1124/dmd.111.042028.

Rubin, Katarina; Janefeldt, Annika; Andersson, Linda; Berke, Zsofia; Grime, Ken; Andersson, Tommy B. (2015): HepaRG cells as human-relevant in vitro model to study the effects of inflammatory stimuli on cytochrome P450 isoenzymes. In *Drug Metabolism and Disposition* 43 (1), pp. 119–125. DOI: 10.1124/dmd.114.059246.

Sakai, Y.; Meno, C.; Fujii, H.; Nishino, J.; Shiratori, H.; Saijoh, Y. et al. (2001): The retinoic acid-inactivating enzyme CYP26 is essential for establishing an uneven distribution of retinoic acid along the anterio-posterior axis within the mouse embryo. In *Genes & development* 15 (2), pp. 213–225.

Samanez, Carolina Huaman; Caron, Sandrine; Briand, Olivier; Dehondt, Hélène; Duplan, Isabelle; Kuipers, Folkert et al. (2012): The human hepatocyte cell lines IHH and HepaRG. Models to study glucose, lipid and lipoprotein metabolism. In *Archives of physiology and biochemistry* 118 (3), pp. 102–111. DOI: 10.3109/13813455.2012.683442.

Sampson, Kathleen E.; Brinker, Amanda; Pratt, Jennifer; Venkatraman, Neetu; Xiao, Yongling; Blasberg, Jim et al. (2015): Zinc finger nuclease-mediated gene knockout results in loss of transport activity for P-glycoprotein, BCRP, and MRP2 in Caco-2 cells. In *Drug Metabolism and Disposition: The Biological Fate of Chemicals* 43 (2), pp. 199–207. DOI: 10.1124/dmd.114.057216.

Sanjana, Neville E.; Shalem, Ophir; Zhang, Feng (2014): Improved vectors and genome-wide libraries for CRISPR screening. In *Nature Methods* 11 (8), pp. 783–784. DOI: 10.1038/nmeth.3047.

Sanson, Kendall R.; DeWeirdt, Peter C.; Sangree, Annabel K.; Hanna, Ruth E.; Hegde, Mudra; Teng, Teng et al. (2019): Optimization of AsCas12a for combinatorial genetic screens in human cells. In *bioRxiv*. DOI: 10.1101/747170.

Šarenac, Tanja M.; Mikov, Momir (2018): Bile Acid Synthesis. From Nature to the Chemical Modification and Synthesis and Their Applications as Drugs and Nutrients. In *Frontiers in Pharmacology* 9, p. 939. DOI: 10.3389/fphar.2018.00939.

Sayin, Sama I.; Wahlström, Annika; Felin, Jenny; Jäntti, Sirkku; Marschall, Hanns-Ulrich; Bamberg, Krister et al. (2013): Gut microbiota regulates bile acid metabolism by reducing the levels of tauro-beta-muricholic acid, a naturally occurring FXR antagonist. In *Cell metabolism* 17 (2), pp. 225–235. DOI: 10.1016/j.cmet.2013.01.003.

Schaefer, Michelle; Schanzle, Gerhard; Bischoff, Daniel; Sussmuth, Roderich D. (2015): Upcyte® Human Hepatocytes: a Potent In Vitro Tool for the Prediction of Hepatic Clearance of Metabolically Stable Compounds. In *Drug Metabolism and Disposition*. DOI: 10.1124/dmd.115.067348.

Schmidt, Katy; Hughes, Catherine; Chudek, J. A.; Goodyear, Simon R.; Aspden, Richard M.; Talbot, Richard et al. (2009): Cholesterol metabolism: the main pathway acting downstream of cytochrome P450 oxidoreductase in skeletal development of the limb. In *Molecular and Cellular Biology* 29 (10), pp. 2716–2729. DOI: 10.1128/MCB.01638-08.

Shalem, Ophir; Sanjana, Neville E.; Hartenian, Ella; Shi, Xi; Scott, David A.; Mikkelson, Tarjei et al. (2014): Genome-Scale CRISPR-Cas9 Knockout Screening in Human Cells. In *Science (New York, N.Y.)* 343 (6166), pp. 84–87. DOI: 10.1126/science.1247005.

Sharanek, Ahmad; Azzi, Pamela Bachour-El; Al-Attrache, Houssein; Savary, Camille C.; Humbert, Lydie; Rainteau, Dominique et al. (2014): Different dose-dependent mechanisms are involved in early

cyclosporine a-induced cholestatic effects in hepaRG cells. In *Toxicological sciences : an official journal of the Society of Toxicology* 141 (1), pp. 244–253. DOI: 10.1093/toxsci/kfu122.

Sharanek, Ahmad; Burban, Audrey; Humbert, Lydie; Bachour-El Azzi, Pamela; Felix-Gomes, Neuza; Rainteau, Dominique; Guillouzo, Andre (2015): Cellular Accumulation and Toxic Effects of Bile Acids in Cyclosporine A-Treated HepaRG Hepatocytes. In *Toxicological sciences : an official journal of the Society of Toxicology* 147 (2), pp. 573–587. DOI: 10.1093/toxsci/kfv155.

Shen, Anna L.; O'Leary, Kathleen A.; Kasper, Charles B. (2002): Association of multiple developmental defects and embryonic lethality with loss of microsomal NADPH-cytochrome P450 oxidoreductase. In *The Journal of Biological Chemistry* 277 (8), pp. 6536–6541. DOI: 10.1074/jbc.M111408200.

Shephard, E. A.; Phillips, I. R.; Santisteban, I.; West, L. F.; Palmer, C. N.; Ashworth, A.; Povey, S. (1989): Isolation of a human cytochrome P-450 reductase cDNA clone and localization of the corresponding gene to chromosome 7q11.2. In *Annals of human genetics* 53 (4), pp. 291–301. DOI: 10.1111/j.1469-1809.1989.tb01798.x.

Shin, Dong-Ju; Wang, Li (2019): Bile Acid-Activated Receptors. A Review on FXR and Other Nuclear Receptors. In *Handbook of experimental pharmacology* 256, pp. 51–72. DOI: 10.1007/164_2019_236.

Simoff, Ivailo; Karlgren, Maria; Backlund, Maria; Lindström, Anne-Christine; Gaugaz, Fabienne Z.; Matsson, Pär; Artursson, Per (2016): Complete Knockout of Endogenous Mdr1 (Abcb1) in MDCK Cells by CRISPR-Cas9. In *Journal of Pharmaceutical Sciences* 105 (2), pp. 1017–1021. DOI: 10.1016/S0022-3549(15)00171-9.

Sissung, Tristan M.; Huang, Phoebe A.; Hauke, Ralph J.; McCrea, Edel M.; Peer, Cody J.; Barbier, Roberto H. et al. (2019): Severe Hepatotoxicity of Mithramycin Therapy Caused by Altered Expression of Hepatocellular Bile Transporters. In *Molecular Pharmacology* 96 (2), pp. 158–167. DOI: 10.1124/mol.118.114827.

Si-Tayeb, Karim; Noto, Fallon K.; Nagaoka, Masato; Li, Jixuan; Battle, Michele A.; Duris, Christine et al. (2010): Highly efficient generation of human hepatocyte-like cells from induced pluripotent stem cells. In *Hepatology (Baltimore, Md.)* 51 (1), pp. 297–305. DOI: 10.1002/hep.23354.

Smits, Arne H.; Ziebell, Frederik; Joberty, Gerard; Zinn, Nico; Mueller, William F.; Clauder-Münster, Sandra et al. (2019): Biological plasticity rescues target activity in CRISPR knock outs. In *Nature Methods* 16 (11), pp. 1087–1093. DOI: 10.1038/s41592-019-0614-5.

Steneberg, Pär; Sykaras, Alexandros G.; Backlund, Fredrik; Straseviciene, Jurate; Söderström, Ingegerd; Edlund, Helena (2015): Hyperinsulinemia Enhances Hepatic Expression of the Fatty Acid Transporter Cd36 and Provokes Hepatosteatosis and Hepatic Insulin Resistance. In *The Journal of Biological Chemistry* 290 (31), pp. 19034–19043. DOI: 10.1074/jbc.M115.640292.

Stiborová, Marie; Indra, Radek; Moserová, Michaela; Šulc, Miroslav; Hodek, Petr; Frei, Eva et al. (2016): NADPH- and NADH-dependent metabolism of and DNA adduct formation by benzoapyrene catalyzed with rat hepatic microsomes and cytochrome P450 1A1. In *Monatshefte fur chemie* 147, pp. 847–855. DOI: 10.1007/s00706-016-1713-y.

Straniero, Sara; Laskar, Amit; Savva, Christina; Härdfeldt, Jennifer; Angelin, Bo; Rudling, Mats (2020): Of mice and men: murine bile acids explain species differences in the regulation of bile acid and cholesterol metabolism. In *Journal of lipid research* 61 (4), pp. 480–491. DOI: 10.1194/jlr.RA119000307.

Su, Jiechuang; Gu, Yongchuan; Pruijn, Frederik B.; Smaill, Jeff B.; Patterson, Adam V.; Guise, Christopher P.; Wilson, William R. (2013): Zinc Finger Nuclease Knock-out of NADPH:Cytochrome P450 Oxidoreductase (POR) in Human Tumor Cell Lines Demonstrates That Hypoxia-activated Prodrugs Differ in POR Dependence. In *The Journal of Biological Chemistry* 288 (52), pp. 37138–37153. DOI: 10.1074/jbc.M113.505222.

Sundberg, Christopher D.; Hankinson, Oliver (2019): A CRISPR/Cas9 Whole-Genome Screen Identifies Genes Required for Aryl Hydrocarbon Receptor-Dependent Induction of Functional CYP1A1. In *Toxicological sciences : an official journal of the Society of Toxicology* 170 (2), pp. 310–319. DOI: 10.1093/toxsci/kfz111.

Takahashi, Shogo; Fukami, Tatsuki; Masuo, Yusuke; Brocker, Chad N.; Xie, Cen; Krausz, Kristopher W. et al. (2016): Cyp2c70 is responsible for the species difference in bile acid metabolism between mice and humans. In *Journal of lipid research* 57 (12), pp. 2130–2137. DOI: 10.1194/jlr.M071183.

Tanenbaum, Marvin E.; Gilbert, Luke A.; Qi, Lei S.; Weissman, Jonathan S.; Vale, Ronald D. (2014): A protein-tagging system for signal amplification in gene expression and fluorescence imaging. In *Cell* 159 (3), pp. 635–646. DOI: 10.1016/j.cell.2014.09.039.

Tanner, Norman; Kubik, Lisa; Luckert, Claudia; Thomas, Maria; Hofmann, Ute; Zanger, Ulrich M. et al. (2018): Regulation of Drug Metabolism by the Interplay of Inflammatory Signaling, Steatosis, and Xeno-Sensing Receptors in HepaRG Cells. In *Drug Metabolism and Disposition* 46 (4), pp. 326–335. DOI: 10.1124/dmd.117.078675.

Tebas, Pablo; Stein, David; Tang, Winson W.; Frank, Ian; Wang, Shelley Q.; Lee, Gary et al. (2014): Gene editing of CCR5 in autologous CD4 T cells of persons infected with HIV. In *The New England Journal of Medicine* 370 (10), pp. 901–910. DOI: 10.1056/NEJMoa1300662.

Tolosa, Laia; Gómez-Lechón, M. José; Jiménez, Nuria; Hervás, David; Jover, Ramiro; Donato, M. Teresa (2016): Advantageous use of HepaRG cells for the screening and mechanistic study of drug-induced steatosis. In *Toxicology and applied pharmacology* 302, pp. 1–9. DOI: 10.1016/j.taap.2016.04.007.

Tomalik-Scharte, Dorota; Maiter, Dominique; Kirchheiner, Julia; Ivison, Hannah E.; Fuhr, Uwe; Arlt, Wiebke (2010): Impaired hepatic drug and steroid metabolism in congenital adrenal hyperplasia due to P450 oxidoreductase deficiency. In *European journal of endocrinology* 163 (6), pp. 919–924. DOI: 10.1530/EJE-10-0764.

Trottier, Jocelyn; Białek, Andrzej; Caron, Patrick; Straka, Robert J.; Heathcote, Jenny; Milkiewicz, Piotr; Barbier, Olivier (2012): Metabolomic profiling of 17 bile acids in serum from patients with primary biliary cirrhosis and primary sclerosing cholangitis: a pilot study. In *Digestive and liver disease : official journal of the Italian Society of Gastroenterology and the Italian Association for the Study of the Liver* 44 (4), pp. 303–310. DOI: 10.1016/j.dld.2011.10.025.

van Chu, Trung; Weber, Timm; Wefers, Benedikt; Wurst, Wolfgang; Sander, Sandrine; Rajewsky, Klaus; Kühn, Ralf (2015): Increasing the efficiency of homology-directed repair for CRISPR-Cas9-induced precise gene editing in mammalian cells. In *Nature Biotechnology* 33 (5), pp. 543–548. DOI: 10.1038/nbt.3198.

Vandesompele, Jo; Preter, Katleen de; Pattyn, Filip; Poppe, Bruce; van Roy, Nadine; Paepe, Anne de; Speleman, Frank (2002): Accurate normalization of real-time quantitative RT-PCR data by geometric averaging of multiple internal control genes. In *Genome Biology* 3 (7), RESEARCH0034. DOI: 10.1186/gb-2002-3-7-research0034.

Velazquez, Maria Natalia Rojas; Parween, Shaheena; Udhane, Sameer S.; Pandey, Amit V. (2019): Variability in human drug metabolizing cytochrome P450 CYP2C9, CYP2C19 and CYP3A5 activities caused by genetic variations in cytochrome P450 oxidoreductase. In *Biochemical and biophysical research communications* 515 (1), pp. 133–138. DOI: 10.1016/j.bbrc.2019.05.127.

Vojta, Aleksandar; Dobrinić, Paula; Tadić, Vanja; Bočkor, Luka; Korać, Petra; Julg, Boris et al. (2016): Repurposing the CRISPR-Cas9 system for targeted DNA methylation. In *Nucleic Acids Research* 44 (12), pp. 5615–5628. DOI: 10.1093/nar/gkw159.

Vouillot, Léna; Thélie, Aurore; Pollet, Nicolas (2015): Comparison of T7E1 and surveyor mismatch cleavage assays to detect mutations triggered by engineered nucleases. In *G3 (Bethesda, Md.)* 5 (3), pp. 407–415. DOI: 10.1534/g3.114.015834.

Walsky, Robert L.; Obach, R. Scott; Gaman, Emily A.; Gleeson, Jean-Paul R.; Proctor, William R. (2005): Selective inhibition of human cytochrome P4502C8 by montelukast. In *Drug Metabolism and Disposition: The Biological Fate of Chemicals* 33 (3), pp. 413–418. DOI: 10.1124/dmd.104.002766.

Wang, Danxin; Papp, Audrey C.; Sun, Xiaochun (2015): Functional characterization of CYP2D6 enhancer polymorphisms. In *Human Molecular Genetics* 24 (6), pp. 1556–1562. DOI: 10.1093/hmg/ddu566.

Wang, Danxin; Poi, Ming J.; Sun, Xiaochun; Gaedigk, Andrea; Leeder, J. Steven; Sadee, Wolfgang (2014): Common CYP2D6 polymorphisms affecting alternative splicing and transcription: long-range haplotypes with two regulatory variants modulate CYP2D6 activity. In *Human Molecular Genetics* 23 (1), pp. 268–278. DOI: 10.1093/hmg/ddt417.

Wang, M.; Roberts, D. L.; Paschke, R.; Shea, T. M.; Masters, B. S.; Kim, J. J. (1997): Three-dimensional structure of NADPH-cytochrome P450 reductase: prototype for FMN- and FAD-containing enzymes. In *Proceedings of the National Academy of Sciences of the United States of America* 94 (16), pp. 8411–8416. DOI: 10.1073/pnas.94.16.8411.

Wang, Xiu Jun; Chamberlain, Mark; Vassieva, Olga; Henderson, Colin J.; Wolf, C. Roland (2005): Relationship between hepatic phenotype and changes in gene expression in cytochrome P450 reductase (POR) null mice. In *The Biochemical journal* 388 (Pt 3), pp. 857–867. DOI: 10.1042/BJ20042087.

Waskell, Lucy; Kim, Jung-Ja P. (2015): Electron Transfer Partners of Cytochrome P450. In Paul R. Ortiz de Montellano (Ed.): Cytochrome P450. Cham: Springer International Publishing, pp. 33–68.

Wei, Yuqi; Huai, Cong; Zhou, Chenxi; Gao, Yaqi; Chen, Luan; Zhou, Wei et al. (2020): A methylation functional detection hepatic cell system validates correlation between DNA methylation and drug-induced liver injury. In *The Pharmacogenomics Journal*. DOI: 10.1038/s41397-020-0160-7.

Weng, Yan; DiRusso, Concetta C.; Reilly, Andrew A.; Black, Paul N.; Ding, Xinxin (2005): Hepatic gene expression changes in mouse models with liver-specific deletion or global suppression of the NADPH-cytochrome P450 reductase gene. Mechanistic implications for the regulation of microsomal cytochrome P450 and the fatty liver phenotype. In *The Journal of Biological Chemistry* 280 (36), pp. 31686–31698. DOI: 10.1074/jbc.M504447200.

Wen-Sheng, Wu (2003): ERK signaling pathway is involved in p15INK4b/p16INK4a expression and HepG2 growth inhibition triggered by TPA and Saikosaponin a. In *Oncogene* 22 (7), pp. 955–963. DOI: 10.1038/sj.onc.1206237.

Westerink, Walter M. A.; Schoonen, Willem G. E. J. (2007): Phase II enzyme levels in HepG2 cells and cryopreserved primary human hepatocytes and their induction in HepG2 cells. In *Toxicology in vitro : an international journal published in association with BIBRA* 21 (8), pp. 1592–1602. DOI: 10.1016/j.tiv.2007.06.017.

Williamson, Beth; Lorbeer, Mathias; Mitchell, Michael D.; Brayman, Timothy G.; Riley, Robert J. (2016): Evaluation of a novel PXR-knockout in HepaRG(™) cells. In *Pharmacology Research & Perspectives* 4 (5), e00264. DOI: 10.1002/prp2.264.

Wu, Lin; Gu, Jun; Weng, Yan; Kluetzman, Kerri; Swiatek, Pam; Behr, Melissa et al. (2003): Conditional knockout of the mouse NADPH-cytochrome p450 reductase gene. In *Genesis (New York, N.Y. : 2000)* 36 (4), pp. 177–181. DOI: 10.1002/gene.10214.

Xu, Xiaojun; Duan, Dongsheng; Chen, Shi-Jie (2017): CRISPR-Cas9 cleavage efficiency correlates strongly with target-sgRNA folding stability: from physical mechanism to off-target assessment. In *Scientific Reports* 7 (1), p. 143. DOI: 10.1038/s41598-017-00180-1.

Yamano, S.; Aoyama, T.; McBride, O. W.; Hardwick, J. P.; Gelboin, H. V.; Gonzalez, F. J. (1989): Human NADPH-P450 oxidoreductase: complementary DNA cloning, sequence and vaccinia virus-mediated expression and localization of the CYPOR gene to chromosome 7. In *Molecular Pharmacology* 36 (1), pp. 83–88.

Yamazaki, H.; Johnson, W. W.; Ueng, Y. F.; Shimada, T.; Guengerich, F. P. (1996): Lack of electron transfer from cytochrome b5 in stimulation of catalytic activities of cytochrome P450 3A4. Characterization of a reconstituted cytochrome P450 3A4/NADPH-cytochrome P450 reductase system and studies with apo-cytochrome b5. In *The Journal of Biological Chemistry* 271 (44), pp. 27438–27444. DOI: 10.1074/jbc.271.44.27438.

Yamazaki, Hiroshi; Nakamura, Mami; Komatsu, Tomoko; Ohyama, Katsuhiro; Hatanaka, Naoya; Asahi, Satoru et al. (2002): Roles of NADPH-P450 reductase and apo- and holo-cytochrome b5 on xenobiotic oxidations catalyzed by 12 recombinant human cytochrome P450s expressed in membranes of Escherichia coli. In *Protein expression and purification* 24 (3), pp. 329–337. DOI: 10.1006/prep.2001.1578.

Yang, Luhan; Güell, Marc; Niu, Dong; George, Haydy; Lesha, Emal; Grishin, Dennis et al. (2015): Genome-wide inactivation of porcine endogenous retroviruses (PERVs). In *Science* 350 (6264), pp. 1101–1104. DOI: 10.1126/science.aad1191.

Yeo, Chang-Woo; Lee, Su-Jun; Lee, Sang Seop; Bae, Soo Kyung; Kim, Eun-Young; Shon, Ji-Hong et al. (2011): Discovery of a novel allelic variant of CYP2C8, CYP2C8*11, in Asian populations and its clinical effect on the rosiglitazone disposition in vivo. In *Drug Metabolism and Disposition: The Biological Fate of Chemicals* 39 (4), pp. 711–716. DOI: 10.1124/dmd.110.035899.

Yin, Hao; Song, Chun-Qing; Dorkin, Joseph R.; Zhu, Lihua J.; Li, Yingxiang; Wu, Qiongqiong et al. (2016): Therapeutic genome editing by combined viral and non-viral delivery of CRISPR system components in vivo. In *Nature Biotechnology* 34 (3), pp. 328–333. DOI: 10.1038/nbt.3471.

Yoo, Sung-Eun; Yi, MyeongJin; Kim, Woo-Young; Cho, Sun-Ah; Lee, Sang Seop; Lee, Su-Jun; Shin, Jae-Gook (2019): Influences of cytochrome b5 expression and its genetic variant on the activity of CYP2C9, CYP2C19 and CYP3A4. In *Drug metabolism and pharmacokinetics* 34 (3), pp. 201–208. DOI: 10.1016/j.dmpk.2019.03.001.

Yoshimi, Kazuto; Kunihiro, Yayoi; Kaneko, Takehito; Nagahora, Hitoshi; Voigt, Birger; Mashimo, Tomoji (2016): ssODN-mediated knock-in with CRISPR-Cas for large genomic regions in zygotes. In *Nature Communications* 7, p. 10431. DOI: 10.1038/ncomms10431.

Zafra, Maria Paz; Schatoff, Emma M.; Katti, Alyna; Foronda, Miguel; Breinig, Marco; Schweitzer, Anabel Y. et al. (2018): Optimized base editors enable efficient editing in cells, organoids and mice. In *Nature Biotechnology* 36 (9), pp. 888–893. DOI: 10.1038/nbt.4194.

Zanger, U. M.; Fischer, J.; Raimundo, S.; Stüven, T.; Evert, B. O.; Schwab, M.; Eichelbaum, M. (2001): Comprehensive analysis of the genetic factors determining expression and function of hepatic CYP2D6. In *Pharmacogenetics* 11 (7), pp. 573–585. DOI: 10.1097/00008571-200110000-00004.

Zanger, U. M.; Klein, K.; Thomas, M.; Rieger, J. K.; Tremmel, R.; Kandel, B. A. et al. (2014): Genetics, epigenetics, and regulation of drug-metabolizing cytochrome p450 enzymes. In *Clin Pharmacol Ther* 95 (3), pp. 258–261. DOI: 10.1038/clpt.2013.220.

Zanger, Ulrich M.; Schwab, Matthias (2013): Cytochrome P450 enzymes in drug metabolism: regulation of gene expression, enzyme activities, and impact of genetic variation. In *Pharmacology & Therapeutics* 138 (1), pp. 103–141. DOI: 10.1016/j.pharmthera.2012.12.007.

Zanger, Ulrich M.; Turpeinen, Miia; Klein, Kathrin; Schwab, Matthias (2008): Functional pharmacogenetics/genomics of human cytochromes P450 involved in drug biotransformation. In *Analytical and Bioanalytical Chemistry* 392 (6), pp. 1093–1108. DOI: 10.1007/s00216-008-2291-6.

Zetsche, Bernd; Gootenberg, Jonathan S.; Abudayyeh, Omar O.; Slaymaker, Ian M.; Makarova, Kira S.; Essletzbichler, Patrick et al. (2015): Cpf1 Is a Single RNA-Guided Endonuclease of a Class 2 CRISPR-Cas System. In *Cell* 163 (3), pp. 759–771. DOI: 10.1016/j.cell.2015.09.038.

Zhang, Feng; Le Cong; Lodato, Simona; Kosuri, Sriram; Church, George M.; Arlotta, Paola (2011): Efficient construction of sequence-specific TAL effectors for modulating mammalian transcription. In *Nature Biotechnology* 29 (2), pp. 149–153. DOI: 10.1038/nbt.1775.

Zhang, Haoming; Im, Sang-Choul; Waskell, Lucy (2007): Cytochrome b5 increases the rate of product formation by cytochrome P450 2B4 and competes with cytochrome P450 reductase for a binding site on cytochrome P450 2B4. In *The Journal of Biological Chemistry* 282 (41), pp. 29766–29776. DOI: 10.1074/jbc.M703845200.

Zhang, Haoming; Myshkin, Eugene; Waskell, Lucy (2005): Role of cytochrome b5 in catalysis by cytochrome P450 2B4. In *Biochemical and biophysical research communications* 338 (1), pp. 499–506. DOI: 10.1016/j.bbrc.2005.09.022.

Zhang, Jingfang; Li Chen; Zhang, Ju; Wang, Yu (2019): Drug Inducible CRISPR/Cas Systems. In *Computational and structural biotechnology journal* 17, pp. 1171–1177. DOI: 10.1016/j.csbj.2019.07.015.

Zimmer, Alex M.; Pan, Yihang K.; Chandrapalan, Theanuga; Kwong, Raymond W. M.; Perry, Steve F. (2019): Loss-of-function approaches in comparative physiology. Is there a future for knockdown experiments in the era of genome editing? In *The Journal of experimental biology* 222 (Pt 7). DOI: 10.1242/jeb.175737.

Zischewski, Julia; Fischer, Rainer; Bortesi, Luisa (2017): Detection of on-target and off-target mutations generated by CRISPR/Cas9 and other sequence-specific nucleases. In *Biotechnology advances* 35 (1), pp. 95–104. DOI: 10.1016/j.biotechadv.2016.12.003.

Figures

Tables

Danksagung

Zuallererst möchte ich mich ganz herzlich bei meinen beiden Betreuern Prof. Ulrich Zanger und Prof. Peter Ruth für ihre Unterstützung während meiner Promotion bedanken.

Besonderen Dank geht dabei an Uli, nicht nur für die ausgezeichnete fachliche Unterstützung während meiner Zeit als Doktorandin, sondern auch für die Möglichkeit mich am IKP wissenschaftlich in einem sehr spannendem Umfeld frei zu entfalten. Besonders während meiner Schwangerschaft und Babypause hat Uli mir immer den Rückhalt und die Unterstützung gegeben, die ich brauchte um die Doktorarbeit fertig zu stellen.

Herrn Prof. Dr. Peter Ruth danke ich für die Bereitschaft meine externe Doktorarbeit von Seiten der Universität Tübingen zu betreuen und zu begutachten.

Viel Dank gebürt auch Herrn Prof. Dr. Matthias Schwab, dass er es mir ermöglichte meine Arbeit am Dr. Margarete Fischer-Bosch Institut für klinische Pharmakologie (IKP) in Stuttgart durchzuführen.

Besonderen Dank möchte ich auch Dr. Kathrin Klein ausprechen. Als lange Bürogefährtin hat sie mir stets in allen Fragen und Unklarheiten beigestanden. Kathrin hatte immer ein offenes Ohr für alle Probleme und stand mir stets mit Rat und Tat bei Seite.

Bei den restlichen aktuellen und ehemaligen Kollegen in der AG Zanger: Dr. Ryoichi Fujiwara, Dr. Nicole Kugler, Britta Klumpp, Igor Liebermann, Dr. Kyoko Momoi, Dr. Chang Ryu, Dr. Maria Thomas möchte ich mich auch für ein sehr tolles Arbeitsklima am IKP bedanken. Besonders Britta und Igor haben mir bei vielen praktischen Arbeiten beigestanden.

Einen weiteren wichtigen Beitrag zu meiner Doktorarbeit haben Dr. Ute Hofmann, Markus König, und Ralf Barnaba am IKP geleistet. Vielen lieben Dank für die Messung und Analyse der CYP-Aktivitäten sowie der Gallensäuren.

Für die Unterstützung bei meinen Arbeiten mit dem FACS möchte ich mich bei Dr. Kristin Bieber (FACS core facility, Tübingen) sowie bei Dr. Pavel Bashtrykov (Institut für Biochemie und technische Biochemie, Stuttgart) bedanken.

Ich hatte viele kleine und große Helfer rund um das IKP und in meinem Familien- und Freundeskreis, die mir stets den Rückhalt gegegeben haben, den ich brauchte. Ohne sie würde diese Arbeit nicht stehen. Besonderen Dank gilt dabei meinem Mann, der gerade in der Endphase meiner Doktorarbeit mir viel Mut zugesprochen hat und mir die Zeit zugestanden hat, die ich brauchte. Danke dafür.

Supplement

The following tables list sequence variants of *POR*, *CYP1A2, CYP2D6* and *CYP2C8* in HepaRG and "Upcyte Hepatocyte" (batches 122-129-138 and 653-03) cells.

Supplemental table 1: *POR* sequence variants in HepaRG and "Upcyte Hepatocytes" (batches 122-129-138 and 653-03). In bold: SNPs as annotated on human Cytochrome P450 (CYP) Allele Nomenclature Website (https://www.pharmvar.org/).

Position	SNP, variant	Reference	HepaRG	122-129-138	653-03
Exon 4	rs369667255	G	G,A	G	G
Intron 8	rs2286821	C	C,T	C,T	C,T
Intron 8	rs55783084	C	C	C	C,T
Intron 9	rs3815455, **830 C>T**	C	C,T	C,T	C,T
Intron 9	rs41301394, **831C>T**	C	C,T	C	C
Intron 10	rs4732515	T	C	T	T
Intron 10	rs4732516	C	G	C	C
Intron 13	rs6961174	G	A	A	A
Intron 13	rs2302429, **1399 G>A**	G	G,A	G	G,A
Intron 13	rs2302431	T	C	C	C
Intron 13	rs2302432	G	T	T	T
Exon 13	rs2228104, **1455 T>C**	T	C	C	C
Exon 13	rs1057868, **1508C>T (A503V)**	C	C,T	C,T	C,T
Exon 13	rs372404067	A	A	A	A,T
Exon 14	rs782756315	C	C	C	C,T
Exon 14	rs1057870	G	G,A	G	G,A
Exon 16	rs17685, **2349 G>A**	G	G,A		

Supplemental table 2: *CYP1A2* sequence variants in HepaRG and "Upcyte Hepatocytes" (batches 122-129-138 and 653-03). In bold: SNPs as annotated on Human Cytochrome P450 (CYP) Allele Nomenclature Website (https://www.pharmvar.org/).

| Position	SNP, variant	Reference	HepaRG
Intron 1	rs762551, **-163 C>A**	C	C,A
Intron 2	rs34264399	G	G,A
Intron 4	rs2472304, **2159G>A**	G	G,A
Intron 5	rs1465142342	C	C,T
Intron 5	rs558851424	C	C,T

Supplemental table 3: *CYP2D6* **sequence variants in HepaRG and "Upcyte Hepatocytes"** (batches 122-129-138 and 653-03).
In bold: SNPs as annotated on Human Cytochrome P450 (CYP) Allele Nomenclature Website (https://www.pharmvar.org/).

| Position	SNP, variant	Reference	HepaRG	122-129-138	653-03
Promoter	rs1080985, **-1584 C>G**	C	C	C	G
Promoter	rs59099247, **-1298G>A**	G	G	G,A	G
Promoter	rs28735595, **-1235A>G**	A	A	G	A,G
Promoter	rs28624811, **-740C>T**	C	C,T	T	T
Promoter	rs28633410, **-678G>A**	G	A,G	A,G	A
Promoter	-7, not annotated	A	A	A	A,G
Promoter	-3, not annotated	A	A	A	A,G
Exon 1	rs769258, **31G>A**	G	G	G	G,A
Exon 1	rs28371696	G	G,C	G,C	G,C
Exon 1	rs146558635	C	C,G	C	C,G
Exon 1	rs139638916	C	C,G	C,G	C,G
Exon 1	142, not annotated	A	A	A	A,G
Exon 1	rs1223156470	G	G,A	G,A	G,A
Exon 1	rs1399750031	G	G,C	G,C	G,C
Intron 1	**Intron 1 conversion**	G, C, C, T, GA, A	G/C, C/A, C/G, T/C, GA/CC, A/G	G/C, C/A, C/G, T/C, GA/CC, A/G	C, A, G, C, CC, G
Intron 1	298 not annotated	G	G	G	T,G
Intron 1	rs28371699, **310G>T**	G	G,T	T	T
Intron 1	rs1349821007	C	C	C	C,T
Intron 1	rs546029764	A	A	A	A,G
Intron 1	rs28371701, **746 G>C**	C	C,G	G	G
Intron 1	rs28371702, **843 T>G**	T	T,G	G	G
Exon 3	rs376636053	T	T	T,C	T
Exon 3	rs184023369, **1661G>C**	G	G,C	C	C
Intron 5	rs5030656, **2615_2617delAAG**		DelAAG/ AAG	AAG	AAG
Exon 6	rs16947, **2850C>T (R296C)**	C	C/T	T	T
Exon 6	rs753667915	G	G/A	A	A
Exon 6	2911, not annotated	C	C,G	C	C
Exon 6	rs200234159	T	T,A	T	T
Intron 6	rs28371725, **2988G>A**	G	G	G,A	G
Intron 7	rs1985842, **3384A>C**	A	A,C	C	C
Intron 7	rs28371730, **3584G>A**	G	G,A	A	A
Intron 7	rs4987144, **3790C>T**	C	C,T	T	T
Exon 9	rs1135840, **4180G>C**	G	G,C	C	C
Enhancer	rs5758550	C	C,T	T	C
Enhancer	rs133333	C	C,T	T	C

Supplemental table 4: *CYP2C8* sequence variants in HepaRG and "Upcyte Hepatocytes" (batches 122-129-138 and 653-03). In bold: SNPs as annotated on Human Cytochrome P450 (CYP) Allele Nomenclature Website (https://www.pharmvar.org/).

Position	SNP, variant	Reference	HepaRG
Promoter	rs35811264	TTTTTTTTT	delT
Promoter	rs1557044	C	A
Promoter	rs11572064	C	T
Promoter	rs372775254	ATATATAT	delAT
Promoter	rs7912549	G	A
Intron 2	rs2275622	A	G
Exon 3	rs11572080, **416G > T (R139L)**	C>A / C>T	A
Intron 3	rs11572082	G	C
Intron 8	rs2275620	T	A
Exon 8	rs10509681, **1196A>G (R399L)**	T>C	G

The following figures show full length blots for Figure 18 and Figure 24.
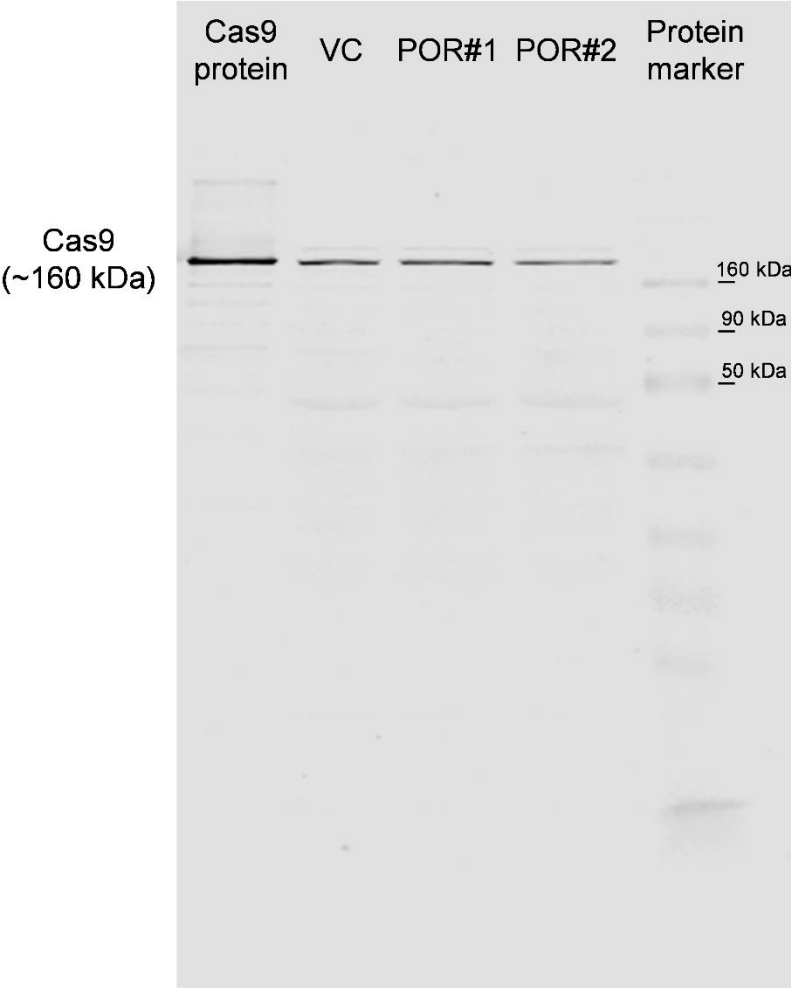
Supplementary figure 1: Full length blot of Figure 18, B: Western blot analysis of Cas9 expression in lysates of undifferentiated HepaRG^{VC}, HepaRG$^{-POR\#1}$ and HepaRG$^{-POR\#4}$, Cas9 protein as positive control.
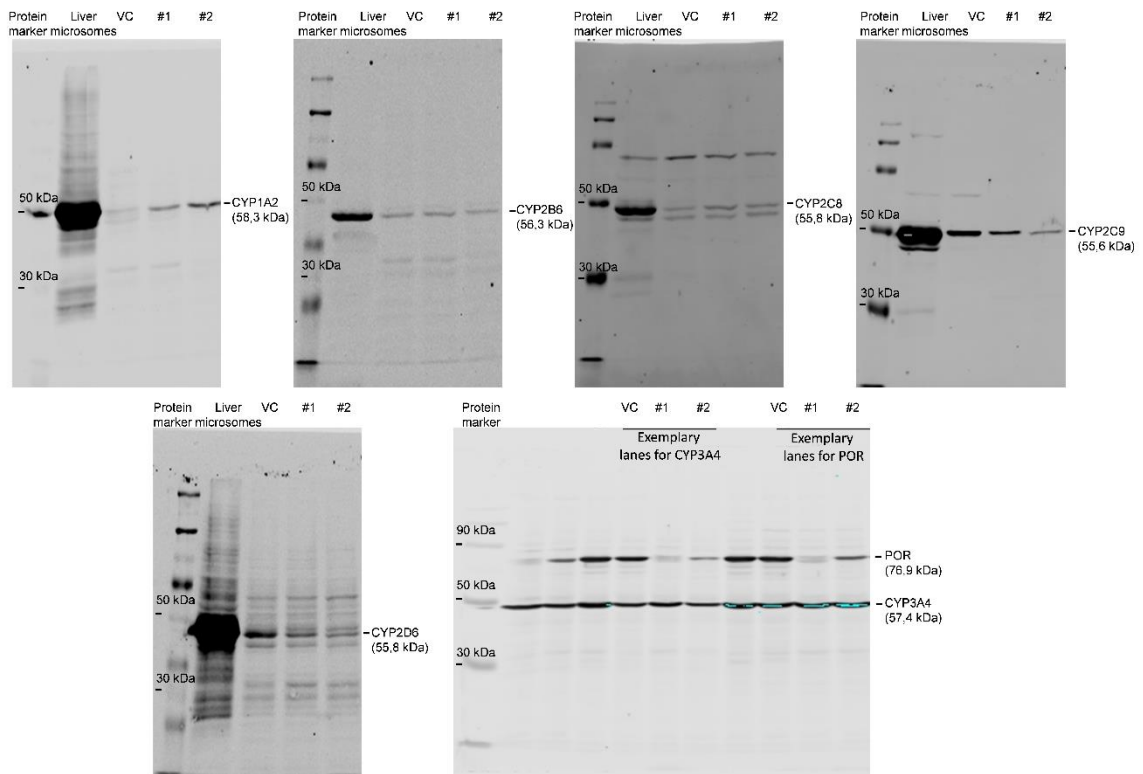
Supplementary figure 2: Full length blot of Figure 24: Exemplary western blots of microsomal fractions of HepaRG cells transduced with vector control (VC) or sgRNAs POR#1 or POR#4 after differentiation for three weeks.